The Dissertation Committee for Benjamin M. Trettel
certifies that this is the approved version of the following dissertation:

Turbulent jet breakup: theory and data

Committee:

Ofodike A. Ezekoye, Supervisor

David B. Goldstein

Matthew J. Hall

Yue (Stanley) Ling

Robert D. Moser

Turbulent jet breakup: theory and data

by

Benjamin M. Trettel

DISSERTATION

Presented to the Faculty of the Graduate School of

The University of Texas at Austin

in Partial Fulfillment

of the Requirements

for the Degree of

DOCTOR OF PHILOSOPHY

The University of Texas at Austin

August 2020

Acknowledgments

It is unlikely that I will be able to remember everyone who contributed to this work, so accept my sincere apologies if I have neglected your contribution.

Turbulent jet breakup: theory and data

Benjamin M. Trettel, Ph.D.

The University of Texas at Austin, 2020

Supervisor: Ofodike A. Ezekoye

Understanding the breakup of turbulent liquid jets is important for many applications including spray combustion, fire suppression, and water jet cutting. Turbulent jet breakup models are rarely fully predictive, and typically require re-calibration to experimental data for different cases. In this work the existing models for turbulent jet breakup are reviewed, highlighting the successes and shortcomings of existing and new approaches. A critical shortcoming of most existing models is the neglect of a measure of the strength of the turbulence like the turbulence intensity. New models are developed to address this shortcoming and others. Existing and new models are compared against a large experimental compilation, primarily from the archival literature. Because the physical mechanisms causing breakup can vary, a new regime diagram was developed in this work, allowing the breakup regime and consequently how to model a particular jet to be determined. Problems common in the validation of turbulent jet breakup models are detailed. A model for the turbulence intensity at the outlet of a nozzle is developed. Finally, a theoretical model is developed and validated for the range of a large firefighting water jet including the effects of jet breakup and air entrainment.

Table of Contents

List of Tables

List of Figures

Glossary

Variables

A_d droplet projected area

a coefficient defined in the trajectory theory by equation 7.72

b coefficient defined in the trajectory theory by equation 7.73

c nozzle contraction ratio, $c \equiv A_{in}/A_0 = (d_{in}/d_0)^2$; see figure 6.1

C_d drag coefficient

$C_d^* \equiv \dfrac{3}{2} \dfrac{C_d}{\rho_\ell/\rho_g} \dfrac{Fr_0}{D_{max}/d_0} (1-\alpha)^2$ reduced drag coefficient (equation 7.11)

$C_d^\circ \equiv C_d^* Fr_0$ alternative reduced drag coefficient used for brevity in some cases (equation 7.43)

C_K Kolmogorov inertial range spectra constant

C_ϵ dissipation model coefficient defined through $\Lambda \equiv C_\varepsilon \dfrac{k^{3/2}}{\varepsilon}$

D droplet diameter

DF droplet formation

D_{ij} characteristic droplet diameter, defined in equation 2.1

d pipe, nozzle, jet, etc. diameter, e.g., d_0 is the nozzle outlet (inner) diameter (lowercase d); see figures 2.1 and 6.1

$E(\kappa)$ isotropic energy spectrum function

F force, e.g., F_σ is the capillary force

$\mathrm{Fr}_0 \equiv \dfrac{\overline{U}_0^2}{g d_0}$ nozzle Froude number

$\mathrm{Fr}_{h_0} \equiv \dfrac{\overline{U}_0^2}{g h_0}$ (firing) height Froude number

f Darcy friction factor

$f(D)$ droplet diameter probability distribution function (number, not volume)

$f_{\mathrm{t}}(x, y)$ surface water distribution function; see figure 7.2

$f_{\mathrm{v}}(v)$ velocity fluctuation probability distribution function

h_0 firing height; see figure 7.2

$H = \dfrac{\overline{U}_0^2}{2g}$ maximum possible height (dragless case) in vertical jet theory

h maximum obtained height (including drag) in vertical jet theory

$h^* \equiv \dfrac{C_{\mathrm{d}}^* h}{d_0}$ h-star, a nondimensionalization of the jet height

$k \equiv \frac{1}{2}(u'^2 + v'^2 + w'^2)$ turbulent kinetic energy; also:

k rank of the dimensional matrix

$\overline{k}$ plane averaged turbulent kinetic energy

L_0 nozzle orifice length; see figure 6.1

ℓ eddy length scale; $\ell \equiv 2\pi/\kappa$

$\ell_{\mathrm{K}} \equiv C_{\ell_{\mathrm{K}}} \left(\dfrac{\nu_\ell^3}{\varepsilon} \right)^{1/4}$ liquid Kolmogorov length scale

$\ell_\sigma \equiv C_{\ell_\sigma} \left(\dfrac{\sigma^3}{\rho_\ell^2 \varepsilon^2} \right)^{1/5}$ liquid phase Hinze length scale (also known as the Kolmogorov critical radius)

$\dot{m}$ mass flow rate

$\dot{m}''$ mass flux (mass flow rate per unit area), e.g., used in § 5.2.6

m_{d} droplet mass

N number of dimensional terms

n number of dimensionless terms

$\mathrm{Oh}_{mn} \equiv \dfrac{\mu_m}{\sqrt{\rho_m \sigma d_n}} \equiv \dfrac{\mathrm{We}_{mn}^{1/2}}{\mathrm{Re}_{mn}}$ Ohnesorge number for fluid m at location n, e.g., $\mathrm{Oh}_{\ell 0} \equiv \dfrac{\mu_\ell}{\sqrt{\rho_\ell \sigma d_0}}$

P perimeter, e.g., of a jet with diameter d_{j}: P_{j} (capital P), or probability

p pressure (lowercase p)

r radial coordinate

r_0 nozzle outlet radius (= $d_0/2$)

R range of a water jet; see figure 7.2

$R^* \equiv \dfrac{C_{\mathrm{d}}^* R}{d_0}$ R-star, a nondimensionalization of the range

R^2 coefficient of determination

$\mathrm{Re}_{mn} \equiv \dfrac{\langle U_n \rangle d_n}{\nu_m}$ Reynolds number for fluid m at location n; e.g.: $\mathrm{Re}_{\ell 0} \equiv \dfrac{\overline{U}_0 d_0}{\nu_\ell}$

$\mathrm{Re}_D \equiv \dfrac{UD}{\nu_{\mathrm{g}}}$ droplet Reynolds number for a droplet of diameter D

$\mathrm{Re}_{\ell 0,\mathrm{crit}}$ a "critical" Reynolds number corresponding to the boundary between two breakup regimes

$\mathrm{Re}_{\ell 0,\mathrm{trans}}$ nozzle critical Reynolds number where turbulence transition begins

$\mathrm{Re}_{\ell 0,\mathrm{turb}}$ nozzle critical Reynolds number where full turbulence is established

$\mathrm{Re}_{\ell x,\mathrm{trans}} \equiv \dfrac{\overline{U}_0 x_{\mathrm{trans}}}{\nu_\ell}$ jet critical Reynolds number used to determine transition location

x_{trans}

SA surface area of a droplet

t_b breakup time

$\mathrm{Tu} \equiv \sqrt{\dfrac{2k}{3\langle U \rangle}}$ net turbulence intensity with average velocity $\langle U \rangle$ for all components

U instantaneous velocity in the x direction

$\langle u_\mathrm{d} \rangle$ average axial droplet velocity

U_b velocity of the jet in the x direction at the breakup point

U_d velocity of a droplet in the x direction

$U_\mathrm{d}^* \equiv U_\mathrm{d}/\overline{U}_0$ dimensionless velocity of a droplet in the x direction

$\vec{U}_\mathrm{g}$ vector for the velocity of the entrained air near a droplet

U_j velocity of the jet core in the x direction

$\langle U \rangle$ ensemble or time averaged velocity in the x direction

$u \equiv U - \langle U \rangle$ velocity fluctuation in the x direction

$u' \equiv \sqrt{\langle u^2 \rangle}$ turbulent RMS velocity in the x direction

V instantaneous velocity in the r or y direction

V_b velocity of the jet in the y direction at the breakup point

V_d velocity of a droplet in the y direction

$V_\mathrm{d}^* \equiv V_\mathrm{d}/\overline{U}_0$ dimensionless velocity of a droplet in the y direction

V_j velocity of the jet core in the y direction

$v \equiv V - \langle V \rangle$ velocity fluctuation in the r direction

$v' \equiv \sqrt{\langle v^2 \rangle}$ turbulent RMS velocity in r direction

$\overline{v'}$ "plane averaged" radial RMS velocity

v_{K} Kolmogorov velocity scale

$v_\sigma \equiv C_{v_\sigma} \left(\dfrac{\sigma \varepsilon}{\rho_\ell} \right)^{1/5}$ Hinze velocity scale

Ψ volume of a droplet

W instantaneous velocity in the ϕ direction

$\mathrm{W}(z)$ Lambert W function; see equation 7.65

$w \equiv W - \langle W \rangle$ velocity fluctuation in the ϕ direction

$w' \equiv \sqrt{\langle w^2 \rangle}$ turbulent RMS velocity in the ϕ direction

$\mathrm{We}_{mn} \equiv \dfrac{\rho_m \langle U_n \rangle^2 d_n}{\sigma}$ Weber number for fluid m at location n; e.g.: $\mathrm{We}_{\ell 0} \equiv \dfrac{\rho_\ell \overline{U}_0^2 d_0}{\sigma}$

$\mathrm{We}_{\ell 0,\mathrm{crit}}$ a "critical" Weber number corresponding to the boundary between two breakup regimes

X_{b} jet breakup location in x (different coordinates than $\langle x_{\mathrm{b}} \rangle$; used in trajectory theory)

X_{d} x component of the trajectory of a droplet

$X_{\mathrm{d}}^* \equiv X_{\mathrm{d}}/(\overline{U}_0^2/g)$ dimensionless x component of the trajectory of a droplet

X_{j} x component of the trajectory of a jet core

x coordinate for horizontal direction aligned with the jet in Cartesian coordinates; longitudinal coordinate in cylindrical coordinates

x_{b} instantaneous breakup length

$\langle x_{\mathrm{b}} \rangle$ average breakup length; see figure 2.1

xxv

x_i instantaneous breakup onset location

$\langle x_i \rangle$ average breakup onset location; see figure 2.1

x_{trans} location of turbulence transition on jet

Y_b jet breakup location in y

Y_d y component of the trajectory of a droplet

$Y_d^* \equiv Y_d/(\overline{U}_0^2/g)$ dimensionless y component of the trajectory of a droplet

Y_j y component of the trajectory of a jet core

α power law probability distribution (negative) exponent, i.e., $f_v(v) = C_f v^{-\alpha}$;

α entrainment coefficient ($\vec{U}_g \equiv \alpha \vec{U}_d$)

α velocity profile kinetic energy coefficient (equation B.12)

δ free surface perturbation amplitude

δ_0 initial disturbance level

ϵ Levi-Civita symbol

ε turbulent dissipation rate

$\eta_R \equiv \dfrac{Rg}{\overline{U}_0^2}\sqrt{\dfrac{\text{Fr}_{h_0}}{\text{Fr}_{h_0}+2}}$ range efficiency (equation 7.32)

$\eta_h \equiv \dfrac{2gh}{\overline{U}_0^2}$ height efficiency (equation 7.5)

$\widehat{\eta}$ a collection of terms including the range efficiency, defined in equation 7.61

θ_0 firing angle; see figure 7.2

θ_i spray angle; see figure 2.1

κ wavenumber; e.g., in chapter 5, $\kappa \equiv 2\pi/\ell$

Λ integral scale of turbulence

λ wavelength

μ_m dynamic viscosity of fluid m

ν_m kinematic viscosity of fluid m

ρ_m mass density of fluid m

σ surface tension of liquid phase in the gas of interest

$\tau \equiv t/(\overline{U}_0/g)$ dimensionless time used in trajectory theory

ϕ azimuth

ω growth rate

ω_{m} growth rate of most unstable mode

Subscripts

0 at nozzle outlet

b breakup (e.g., breakup length $\langle x_{\mathrm{b}} \rangle$)

crit when turbulence transition first starts; sometimes used interchangeably with "turb" as
    defined below

d droplet quantity (e.g., v_{d} is a droplet velocity)

FD fully developed

i at breakup onset location

in for nozzle inlet

j jet value, e.g., $d_\text{j}(x)$ is the diameter of the jet core at x

g using gas properties

K Kolmogorov scale (e.g., ℓ_K is the Kolmogorov length scale, and v_K is the Kolmogorov velocity scale)

ℓ using liquid properties

m most unstable mode

max maximum value

min minimum value

opt optimal value with respect to a particular variable, e.g., R_opt is the range at the optimal firing angle θ_i

turb when fully turbulent conditions are established, e.g., Re_turb (hydrodynamic regime, not spatial flow development)

σ capillary value (e.g., p_σ is the capillary pressure), or Hinze scale (e.g., ℓ_σ is the Hinze length scale, and v_σ is the Hinze velocity scale)

Other notation and comments

Bars over variables (e.g., $\overline{U}_0$) indicates spatial averaging. Note that I will deviate from the explicit interpretation of this for the turbulence intensity: $\overline{\text{Tu}} \not\equiv \overline{\left(\dfrac{U'_\text{net}}{\langle U \rangle}\right)}$, rather

$\overline{\text{Tu}} \equiv \sqrt{\dfrac{2\overline{k}}{3\langle U \rangle^2}}$. This is done as the latter appears in conservation equations.

Ensemble averaging of quantities is denoted with brackets (e.g., $\langle U \rangle$).

Quantities which are both ensemble and space averaged are denoted with only a single bar for brevity, e.g., $\langle \overline{U}_0 \rangle = \overline{U}_0$.

Instantaneous quantities are denoted with lower case, i.e., the standard Reynolds decomposition is $U = \langle U \rangle + u$. Some quantities will not follow the capitalization convention, e.g., v_σ is the Hinze velocity scale.

Some root mean squared (RMS) quantities are denoted with a prime ($\prime$) when customary, i.e., $u' \equiv \sqrt{\langle u^2 \rangle}$. However, other quantities will be written more explicitly or as a standard deviation (σ).

An exception to the prime notation is $\dot{m}''$, where the primes here imply that this term refers to the mass transfer rate per unit area.

Named dimensionless quantities are not italicized, e.g., Re.

The natural (base e) logarithm is denoted with ln.

Conditional averages are denoted $\langle X \mid Y \rangle$, where X is the random variable of interest and Y is the condition.

Citations frequently include the page number and column for multi-column works. The column is identified through the abbreviations L, C, or R, e.g., the right column of page 9 is "9R".

Several "critical" dimensionless numbers will appear in this work. A critical number is where the transition to a bordering regime occurs. For clarity, several different types of critical dimensionless numbers are defined. The subscript "crit" will be used for a *breakup* regime boundary. The subscript "turb" will be used to indicate the full development of turbulence, e.g., the critical *nozzle* Reynolds number is $\mathrm{Re}_{\ell 0,\mathrm{turb}}$, where the flow at the nozzle outlet is turbulent. Similarly, a critical *jet* Reynolds number will be written as $\mathrm{Re}_{\ell x,\mathrm{trans}}$. See the list of variables for precise definitions of these terms.

Chapter 1

Introduction

1.1 Goals

This dissertation has two goals. The first is to develop models for the breakup of turbulent liquid jets. The second goal is to develop a model for the trajectory of a large firefighting water jet. The two problems are strongly coupled, and the second goal motivates the first. See figure 1.1 for a flow chart showing the connections between the two problems and which chapters address which components of each problem. Also see figure 1.2 for an illustration of a water jet breaking up due to turbulence.

This dissertation was intended to be more heavily focused on the second problem, however, experimental difficulties described in § 9.4 combined with time constraints prevented that work from being completed in time.

1.2 Outline of dissertation

Chapter 2 is an introduction to the turbulent liquid jet breakup problem. Coverage includes definitions and past models of jet breakup. It may be helpful to skim chapter 3 before chapter 2 as the two are coupled.

Chapter 3 discusses the different varieties of jet breakup, termed "regimes" in the literature. Identifying the regime of a liquid jet is necessary to determine the physical mechanisms causing breakup and consequently how to model the jet. A more accurate regime diagram is developed using a large compilation of breakup length data combined with theory where the data is sparse. Improvements in the regime diagram include a new regime, the addition of the nozzle critical Reynolds number and the turbulence intensity as
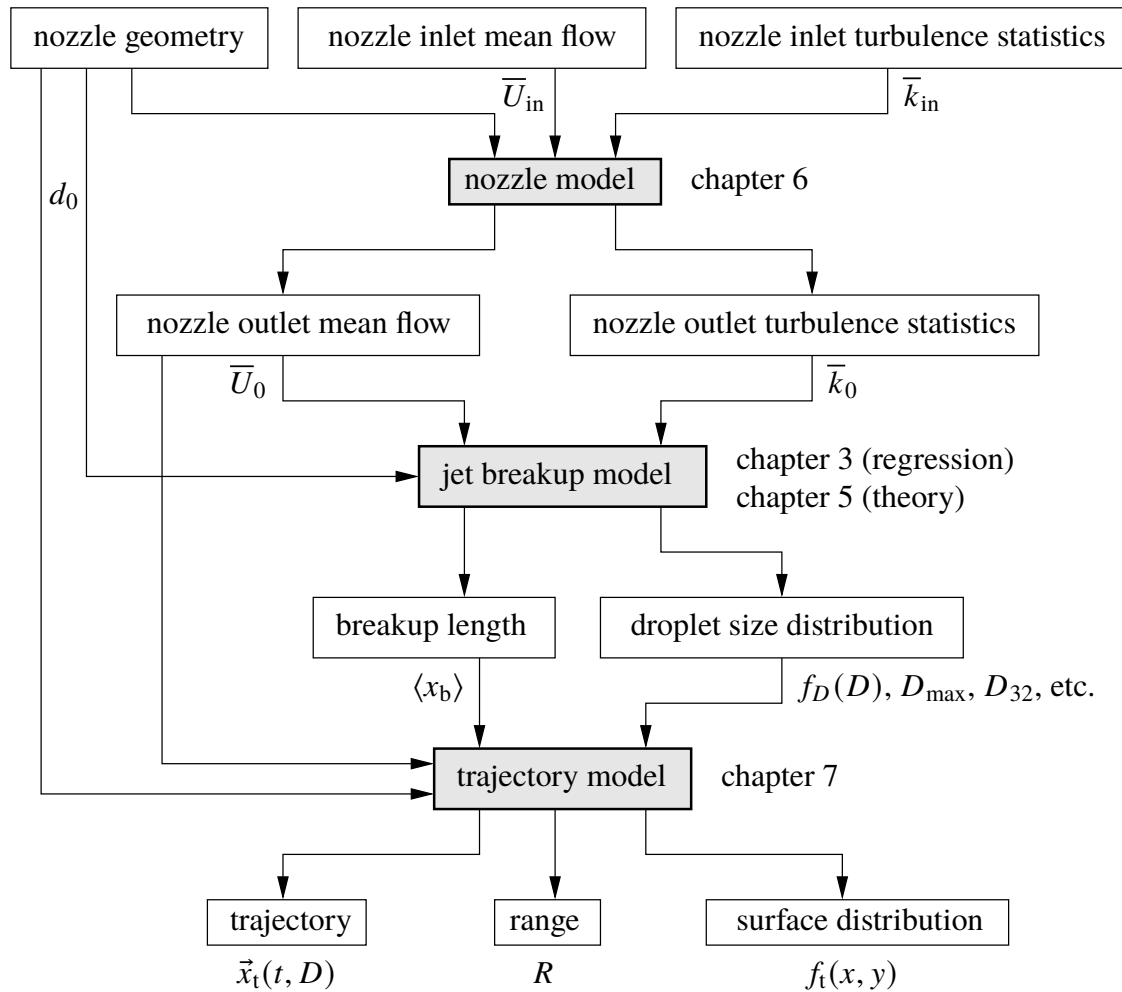
nozzle geometry | nozzle inlet mean flow | nozzle inlet turbulence statistics

$\overline{U}_{\text{in}}$ $\overline{k}_{\text{in}}$

d_0

nozzle model   chapter 6

nozzle outlet mean flow | nozzle outlet turbulence statistics

$\overline{U}_0$ $\overline{k}_0$

jet breakup model   chapter 3 (regression)
chapter 5 (theory)

breakup length | droplet size distribution

$\langle x_{\text{b}} \rangle$ $f_D(D), D_{\max}, D_{32}$, etc.

trajectory model   chapter 7

trajectory | range | surface distribution

$\vec{x}_{\text{t}}(t, D)$ R $f_{\text{t}}(x, y)$

Figure 1.1: Flow chart showing the main variables involved in the trajectory problem as a whole, and the chapters which cover each part. "Variables" which are essentially constant in the water jet trajectory problem such as the fluid properties are neglected here.

Figure 1.2: Large fire fighting water jet. Fire equipment and staffing courtesy of the Cedar Park, TX, Fire Department. Photo by Kevin Lee.

variables, and the recognition that how the regimes change with increasing velocity (i.e., Rayleigh to first wind-induced to second wind-induced to atomization) is not universal. Chapter 3 also contains a summary of the large data compilation used in this work.

Chapter 4 details model validation problems relevant to turbulent jet breakup. If a model's predictions are within the experimental uncertainty, then the model is deemed "validated". Three problems common in jet breakup model validation are identified that can make the apparent validation of a model actually an illusion: 1. important variables being omitted or guessed in experiments and models, 2. confounding between independent variables, that is, two variables changing simultaneously, making determining cause and effect impossible, and 3. testing only combinations of submodels and not each submodel in isolation. To avoid these problems and others, validation guidelines are developed.

Chapter 5 describes the *conditional damped random surface velocity* (CDRSV) theory of turbulent jet breakup. CDRSV theory is contrasted with other phenomenological theories and compared against the available experimental data. Ultimately it is concluded that while CDRSV has advantages over other previous theories/models, none of the theoretical models considered are trustworthy enough to be used for predictions.

Chapter 6 is motivated by the fact that the nozzle geometry affects the turbulence in the jet. In this chapter I critically evaluate a popular model of nozzle turbulence, showing that the model is highly inaccurate. A better model is developed through the use of a turbulent extension of the Bernoulli equation, showing a connection between flow losses and turbulence modeling that was implied by the earlier incorrect model.

3

Chapter 7 describes an analytical model of water jet trajectory and range which includes both the effects of the jet breakup length and air entrainment. Typically trajectories are obtained through *numerical* integration of the equations of motion. Instead, in this chapter the "flat fire" approximation is used so that the equations can be solved *analytically*. The theory is favorably compared against previous experimental data using measured breakup lengths from Theobald [The81].

Chapter 8 is a summary of important new results in this dissertation, as a convenience to the reader.

Chapter 9 is a discussion of several possible avenues for future research on the topics of this dissertation.

Appendix A contains a brief summary of some limited experiments conducted for this dissertation. These experiments were *intended* to measure the range and surface water distribution of water jets, however, for various reasons the trajectory data (far-field) was determined to be unreliable for those purposes (due mainly to wind). However, the near-field was unaffected by these problems and consequently this limited source of data was used for chapter 3.

Appendix B is a commentary on the variables relevant to turbulent jet breakup, combined with a dimensional analysis of the problem. Unfortunately, many previous dimensional analyses have missed important variables like the turbulence intensity. A discussion of velocity profile effects is included, focusing on how one method of characterizing these effects is mistaken.

Chapter 2

Review of turbulent jet breakup theories[1]

2.1 Introduction

The main goal of this chapters 2 through 6 is to develop models for the breakup of a statistically steady high Weber number turbulent liquid jet injected into a low density quiescent environment. This chapter reviews previous jet breakup models as this is the first part of the larger water jet trajectory problem. In this work, the model is intended to apply when the breakup is caused primarily by the turbulent velocity fluctuations at the free surface, i.e., in the turbulent surface breakup regime, commonly but inaccurately called the "second wind-induced regime" (chapter 3). I call the model developed in chapter 5 the conditional damped random surface velocity (CDRSV) model. Additional models for other conditions are also developed in this work.

The breakup of liquid jets under these conditions appears in many applications like fire protection and fuel sprays. Solving this relatively simpler case is necessary to solve more complex cases involving additional physics. In chapter 5, I neglect the effects of the transition to turbulence on the jet (as in the case under study the jet is turbulent at the nozzle outlet — a discussion of transition effects is in chapter 3), velocity profile relaxation or boundary layer effects, cavitation[2], swirl, and any aerodynamic (gas-phase) effects (e.g., the atomization regime, or gas co- or cross-flows). Cavitation and aerodynamic effects are more important in fuel spray problems.

---

[1]This chapter is modified from the introduction and review sections of a paper submitted to Atomization and Sprays [Tre20a]. I am the sole author.

[2]According to Stahl et al. [Sta+05], cavitation is generally accepted to influence jet breakup through increased turbulence intensity. But cavitation could also cause the flow to detach from the nozzle orifice walls, which can increase the breakup length [Hir00].

While there have been many previous models of turbulent jet breakup (to be reviewed in this chapter), none of the lower computational cost models are regarded as truly predictive. This is caused primarily by the assumptions and approximations inherent in the models. One important but neglected aspect of the validation of these models is the effect of turbulence, particularly through a measure of the strength of the turbulence like the turbulence intensity. As will be discussed, it is well accepted that the turbulence intensity of the jet is a major factor in the breakup of the jet. Yet relatively few models even *consider* the turbulence intensity as a factor. And merely considering the turbulence intensity in a model is insufficient — the model must be validated against experimental data with appreciable turbulence intensity variation. This work uses a relatively new experimental database with appreciable turbulence intensity variation ($\overline{\mathrm{Tu}}_0$ varies from 4.9% to 12.7%). There are many models which consider turbulence intensity, but in ways which are incorrect, as will be discussed. Many models fail to even capture the qualitative trends as the turbulence intensity varies, much less match the data quantitatively.

The reader of this dissertation is assumed to have a basic understanding of turbulent flows. I recommend that the interested reader without this background read an introductory turbulence book like Pope's *Turbulent Flows* [Pop00].

2.2 Quantities of interest, independent variables, and nomenclature

Figure 2.1 shows a slice through the center of a statistically steady ensemble averaged circular liquid jet ejected from left to right into a quiescent gas. The nozzle outlet plane is denoted with 0, e.g., the nozzle outlet diameter is d_0. The x axis starts at the center of the nozzle outlet plane and is oriented with the jet's bulk velocity ($\overline{U}_0$). The r axis extends radially from the center. The quantities of interest are the average droplet diameter at formation (D_{ij}, e.g., D_{32} for the Sauter mean diameter), average droplet radial velocity at formation ($\langle v_\mathrm{d} \rangle$), average breakup length ($\langle x_\mathrm{b} \rangle$), average breakup onset location ($\langle x_\mathrm{i} \rangle$), and average (full) spray angle (θ_i). I will typically drop the phrase "average" for the quantity of interest. Bars denote spatial averages, and angle brackets denote ensemble averages.

In this work the Reynolds number is $\text{Re}_{ij} \equiv \overline{U}_j d_j / \nu_i$ for location j (0 for nozzle outlet) and fluid i (l for liquid, g for gas), e.g., for the liquid phase at the nozzle outlet $\text{Re}_{\ell 0} \equiv \overline{U}_0 d_0 / \nu_\ell$. The Weber number is $\text{We}_{ij} \equiv \rho_i \overline{U}_j^2 d_j / \sigma$, e.g., for the liquid phase at the nozzle outlet $\text{We}_{\ell 0} \equiv \rho_\ell \overline{U}_0^2 d_0 / \sigma$. The Ohnesorge number can be found given the Reynolds and Weber numbers: $\text{Oh}_{\ell 0} \equiv \text{We}_{\ell 0}^{1/2} / \text{Re}_{\ell 0}$. $u' \equiv \langle (U - \langle U \rangle)^2 \rangle^{1/2}$ and $v' \equiv \langle (V - \langle V \rangle)^2 \rangle^{1/2}$ are the RMS velocities in x and r. $k \equiv (u'^2 + v'^2 + w'^2)/2$ is the turbulent kinetic energy. For simplicity, plane averaged turbulence intensities are used. The spatially averaged *equivalent isotropic* ($u' = v' = w'$) RMS velocity is defined as $\overline{u'_j} \equiv (2\overline{k}_j/3)^{1/2}$, not averaging over u'_j directly. This allows the turbulence intensity to be defined as $\overline{\text{Tu}}_j^2 \equiv (\overline{u'_j}/\overline{U}_j)^2 \equiv 2\overline{k}_j/(3\overline{U}_j^2)$, which is advantageous in transport equations — like $\overline{U}_0$ can be used in mass conservation equations, $\overline{k}$ can be used in turbulence transport equations — see chapter 6. More simply, $\overline{\text{Tu}}_0$ is the plane averaged turbulence intensity at the nozzle outlet. The dissipation ($\overline{\varepsilon}_j$) model also uses $\overline{k}_j$. The integral length scale is Λ, and does not have a bar for simplicity as it is not a well known quantity in turbulent jet breakup[3], so whether an average or local value is taken is of little importance. These simplifications can be relaxed in future works, but for the moment they are deemed acceptable given that free turbulent flows tend to become more homogeneous downstream, and that little information is available on the spatial variation of these quantities. It is well accepted that the turbulent kinetic energy peaks near the edge of the jet. A plane homogeneous approximation will be bad in many situations, however, it is a reasonable first approximation.

The average droplet diameter D_{ij} is a diameter which is representative of the spray in some sense. This can be defined in multiple ways by choosing i and j:

$$D_{ij} \equiv \left(\frac{\int_0^\infty D^i f(D) \, \mathrm{d}D}{\int_0^\infty D^j f(D) \, \mathrm{d}D} \right)^{1/(i-j)} . \tag{2.1}$$

where $f(D)$ is the droplet size distribution function. While this definition may seem

---

[3]In the data compilation of this work, the pipe radial integral scale measured by Powe [Pow70, figs. 83–85, 159–161, 232–233] closest to the wall is used, interpolated in the friction factor for rough pipes. Note that the integral scales given by Robertson, Burkhart, and Martin [RBM65, fig. 40] seem far more variable than and inconsistent with Powe, which suggests to me that the integral scale in a pipe flow is not well known.
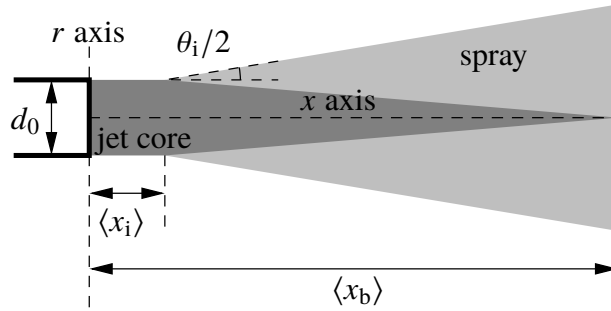
Figure 2.1: Jet breakup variables labeled on a schematic liquid jet. d_0 is the nozzle outlet diameter, $\langle x_i \rangle$ is the average breakup onset location, θ_i is the spray angle, and $\langle x_b \rangle$ is the breakup length.

arbitrary at first, various choices of i and j have different physical meanings. For example, the arithmetic mean diameter is D_{10}. The volume or mass mean diameter, D_{30}, is the diameter of a droplet which has the same volume or mass as the spray as a whole. Similarly, the Sauter mean diameter, D_{32}, is the diameter of a droplet with the same surface area to volume ratio as the spray as a whole.

The average droplet velocity is more clear than the average diameter: it is the average velocity of droplets at a particular location. The average droplet velocity *at formation* from the jet is termed $\langle v_d \rangle$ in this work.

The average breakup length $\langle x_b \rangle$ (typically breakup length for short) is defined as the time-averaged distance from the nozzle where the diameter of the jet core reduces to zero. This typically is found from images or electrical conductivity measurements, which return consistent results. This is demonstrated by the excellent fit ($R^2 = 0.958$ for 193 data points) of regressions like equation 3.28, sourced from both electrical conductivity and quantitative imaging measurements of the average breakup length..

The average breakup onset location $\langle x_i \rangle$ (again, typically breakup onset location for short) is defined as the time-averaged distance from the nozzle where breakup first occurs. This is typically measured using imaging techniques.

As has been highlighted by Reitz and Bracco [RB86, p. 234–235], at low speeds (the "Rayleigh regime"), the jet breaks up at a single point (i.e., everywhere in a particular cross

8

section), so $\langle x_i \rangle = \langle x_b \rangle$. At higher speeds these two diverge, so that surface breakup can be initiated at a certain distance but the jet core does not end until much farther downstream. Note that some researchers will call $\langle x_i \rangle$ the "breakup length". I am using the term "onset location" following the work of Wu and Faeth [WF95].

The spray angle θ_i is roughly defined as the angle produced by the outermost droplets of the spray region at the breakup onset location. Unfortunately there is no standard precise definition of this quantity despite its ubiquity, and consequently there is a large spread in the existing data for the spray angle. See § 4.2 for details.

Note that while figure 2.1 shows the spray cone and jet core as linearly changing over x, this does not necessarily represent the actual shape of the jet.

2.3 Turbulence effects on breakup

A focus of this chapter is on the effect of turbulence properties like the turbulence intensity on the breakup of liquid jets. This is motivated by common fire hose nozzle design guidelines emphasizing the negative effect of turbulence on the performance of water jet systems [RHM52, p. 1150; Oeh58, p. 9; MM74, p. 14; HT85]. While this effect is present in other applications as well, e.g., fuel sprays, it does not appear to have received the same level of attention. A few experiments have clearly shown that many quantities of interest are sensitive to the turbulence intensity, e.g., the effect of the increasing turbulence intensity typically decreases droplet size [Bog48; DCT05], increases spray angle [Skr66; EF87], and decreases breakup length [Kus69; EME80; ME80]. Kusui [Kus69] also showed a turbulence intensity effect on the transition to the atomization regime. Most quantities of interest show a turbulence intensity dependence in turbulent jet breakup to my knowledge.

As discussed in § 4.3, the turbulence intensity is the most natural way to measure the strength of the turbulence, but unfortunately the turbulence intensity is rarely estimated in experiments or considered in models. Frequently, the turbulence intensity is assumed to be roughly constant or a function of only the Reynolds number, making it unnecessary in models. The Reynolds number is often seen as a measure of "how turbulent" a flow is, but

9

this is mistaken. Contrary to what most expect, in fully developed smooth pipe flow, $\overline{\mathrm{Tu}}$ *decreases* as $\mathrm{Re}_{\ell 0}$ increases — see § 4.3. Nozzles do not necessarily have monotonically increasing or decreasing trends in the turbulence intensity [Leb19, figs. 2–4]. For a particular nozzle, the nozzle outlet turbulence intensity ($\overline{\mathrm{Tu}}_0$) is a function of $\mathrm{Re}_{\ell 0}$ and the nozzle inlet turbulence intensity ($\overline{\mathrm{Tu}}_{\mathrm{in}}$). Different nozzles have different trends, so both variables are needed.

	year	type	D_{ij}	$\langle v_\mathrm{d} \rangle$	$\langle x_\mathrm{i} \rangle$	$\langle x_\mathrm{b} \rangle$	θ_i
Rayleigh [Ray78]	1878	stability	●			●	
Weber [Web19]	1931	stability	●			●	
Natanzon [Nat18]	1938	phenomenological	●	●	○	○	●
Taylor and Ranz [Tay58; Ran58; RD64]	1940	stability	●		○	●	●
Bogdanovich [Bog48]	1948	phenomenological	●				
Sitkei [Sit63]	1959	phenomenological	●	○			●
Inoue [Ino63]	1963	phenomenological	●				
Skrebkov [Skr66]	1963	phenomenological	●	●			●
Lebedev [Leb19]	1977	phenomenological	●				
Huh et al. [HLK98; HG91]	1991	phenomenological	●	○			●
Wu et al. [WTF92; WF95; Sal02]	1992	phenomenological	●	○	●	●	
Beale and Reitz [BR99]	1999	stability	●			●	○
Som and Aggarwal [SA10]	2010	hybrid	●				
Schmitz [Sch11]	2011	phenomenological	●				
Kerstein et al. [KMO17]	2017	phenomenological	●		●		
Magnotti [Mag+17; Mag17]	2017	hybrid	●				
Movaghar et al. [Mov+17]	2017	phenomenological	●		●	●	
chapter 5	2018	phenomenological	●	●	●	●	●

Table 2.1: Classification of and quantities of interest in selected jet breakup models, with a focus on phenomenological models.
●, explicit; ○, implicit

2.4   Types of turbulent jet breakup models

Broadly, there are two approaches for modeling turbulent jet breakup. These approaches are not necessarily mutually exclusive, and can be viewed as two different ways of describing the same phenomena. The first approach analyzes the stability of the Navier-Stokes equations as applied to a liquid jet. This approach is called "stability theory" in this work. The second approach does not start with the Navier-Stokes equations, and instead assumes that turbulent jet breakup is described through a simplified model of the larger physics. Models taking the second approach are called "phenomenological" in this work. Some models are hybrids of the two approaches, applying stability theory where it works and phenomenological theory where stability theory fails, e.g., Som and Aggarwal [SA10] and Magnotti [Mag17]. Table 2.1 summarizes the quantities of interest in many past models and classifies the models.

Stability theory has dominated jet breakup modeling from the early work of Rayleigh [Ray78] to the popular KH-RT breakup model [BR99]. Stability theory has proved accurate at low Reynolds and Weber numbers, i.e., in the "Rayleigh" regime(more details on regimes are in chapter 3), but has not demonstrated accuracy in other regimes. The alternative phenomenological approach has been rising in popularity due to the shortcomings of stability theory in turbulent regimes. However, phenomenological theories so far have failed to accurately predict all relevant scalings, though they can overcome other shortcomings of existing stability theories (to be discussed) and may be preferred for that reason alone.

A third approach to modeling turbulent jet breakup is detailed computation, whether RANS, LES, DNS, or another approach. RANS models like the ELSA model of Demoulin et al. [Dem+07] tend to treat the liquid and gas phases as an Eulerian continuum with the ability to create Lagrangian droplets when certain criteria are met[4]. LES and DNS models involve less modeling, but have much higher computational costs. However, given the high computational costs associated with these approaches, low-order models will continue to be

---

[4]It is worth highlighting a shortcoming of existing RANS models like ELSA: These models do not distinguish between jet and droplet breakup. The two have different physics and it is not correct to model the two identically. This type of problem in general is discussed more in § 4.5.

used for the foreseeable future and consequently will be the focus of this work. A review of previous research on low-order models, much of which is presently obscure, follows. Note that this is not a rejection of computation — the results of DNS studies *will* be used as appropriate to help construct low-order models in a manner similar to experimental results, but DNS itself is not used *as a model* in this work.

2.5 Have any turbulent jet breakup models been truly validated?

Before describing the models and their *qualitative* features, it is worth describing in general how successful these models are *quantitatively*. This would show some of the strengths and weaknesses of each model, which will be elaborated on later. Existing turbulent jet breakup models are not validated in general in my view due to inadequacies in the validation data and tests, despite frequent claims to the contrary. While jet breakup in the laminar Rayleigh regime has had good success in modeling, the history of the validation of turbulent jet breakup has many examples of researchers trying to fit a square peg in a round hole. I am not going to claim success until a model fits the data with little or no special pleading.

Consider table 2.2, which summarizes how well the most popular turbulent jet breakup models and the models developed in this work (CDRSV) perform when compared against the data compilation for the turbulent surface breakup regime used in this work. Also included are comparisons against power law regressions made in chapter 3. This data compilation is described in chapter 4, and is much more difficult for models to match because it has much more data and also has appreciable variation in the turbulence intensity, unlike most data sets used for validation of turbulent jet breakup models.

Each model has a single coefficient taking the calibrated values on the left. The coefficient of determination (R^2), a measure of how well a model fits the data, is on the right, and higher R^2 is better. The R^2 values for the power law regressions (last row) should be higher than the R^2 values for the other models because the power law regressions are more general. However, note that because the power law regressions are linear regressions made in log coordinates (e.g, $\log \text{We}_{\ell 0}$), the R^2 value in true coordinates (e.g., $\text{We}_{\ell 0}$) may

have a different ordering. This is why some of the power law regression R^2 values are lower than the theory R^2 values in table 2.2 — they are actually higher in log coordinates.

The most popular model, KH-RT, is frequently *misapplied* to the turbulent surface breakup regime, as this model is designed for cases where aerodynamic influence is strong (the atomization regime). Consequently, the model performs consistently poorly in this regime, having negative R^2 values for all quantities of interest. Similarly, all *theoretical* models for the spray angle have negative R^2 values, indicating uniformly bad performance on this quantity of interest. The droplet size model of Huh, Lee, and Koo [HLK98] has a value of R^2 of zero *by definition* as it proposes that the droplet size is proportional to the integral scale. Given the lack of existing data, is assumed that the integral scale is proportional to the nozzle diameter, so in effect D_{32}/d_0 is a constant in the model of Huh, Lee, and Koo. Constants have R^2 values of zero by definition, and in this case a constant is not a good model for other reasons, as will be discussed.

Models for the breakup length tend to have mixed success at best. The Faeth group model has a slightly better R^2 value than that developed in this work, despite the fact that it has no turbulence intensity variation. This is likely because the Faeth group model has a Weber number exponent closer to that of the empirical regression ($\langle x_\mathrm{b} \rangle / d_0 \overset{\propto}{\sim} \mathrm{We}_{\ell 0}^{1/3}$ in the regression). Unfortunately no turbulent jet breakup model I am aware of has the correct scaling of the breakup length with the liquid Weber number.

Some models have better success. The droplet size model of the Faeth group (to be discussed) has the same scaling as the model developed in this work and has a respectable R^2 value. Similarly, calibrated breakup length models from the Faeth group and this work also have respectable R^2 values. The breakup onset location model developed in this work performs significantly better than that of the Faeth group, however.

2.6 Stability theory

Linear stability theory has been used since the 19th century to understand the transition to turbulence [Tho71; Hel68]. The basic equation for hydrodynamic stability

	coefficients				R^2			
	D_{ij}	$\langle x_i \rangle$	$\langle x_b \rangle$	θ_i	D_{ij}	$\langle x_i \rangle$	$\langle x_b \rangle$	θ_i
Faeth	0.522	1.63	1.45	—	0.730	0.513	0.766	—
Huh	0.0127	—	—	0.310	0.00	—	—	−0.0738
KH-RT	0.0275	—	7.78	2.28	−0.300	—	−2.38	−2.30
CDRSV	0.522	20.4	5.62	0.584	0.730	0.905	0.719	−0.889
regression	—	—	—	—	0.712	0.758	0.958	0.983

Table 2.2: Calibrated model coefficients for multiple models and associated coefficients of determination (R^2).

(in turbulence) is called the Orr-Sommerfeld equation. Linear stability theory examines how a linearized system evolves in time based on a constant background flow with small perturbations added to it. This section is an overview of stability theory based jet breakup models without details of the derivation, highlighting typically ignored weaknesses of stability theory as applied to turbulent jet breakup. The focus is on linear stability theories, however, it is worth noting that most of the mentioned issues apply equally well to non-linear stability theories.

2.6.1 Popular stability theory based models

Reitz and Bracco [RB82; RB86] note that many popular linear stability theory based models can be understood as simplifications of a general "dispersion relation" for liquid jets:

$$
\omega^2 + 2\nu_\ell \kappa^2 \omega \left(\frac{I_1'(\kappa r_0)}{I_0(\kappa r_0)} - \frac{2\kappa l}{\kappa^2 + l^2} \frac{I_1(\kappa r_0)}{I_0(\kappa r_0)} \frac{I_1'(l r_0)}{I_1(l r_0)} \right)
$$
$$
= \frac{\sigma \kappa}{\rho_\ell r_0^2} (1 - r_0^2 \kappa^2) \left(\frac{l^2 - \kappa^2}{l^2 + \kappa^2} \right) \frac{I_1(\kappa a)}{I_0(\kappa r_0)}
$$
$$
+ \frac{\rho_g}{\rho_\ell} \left(\overline{U}_0 - \frac{i\omega}{\kappa} \right)^2 \kappa^2 \left(\frac{l^2 - \kappa^2}{l^2 + \kappa^2} \right) \frac{I_1(\kappa r_0) K_0(\kappa r_0)}{I_0(\kappa r_0) K_1(\kappa r_0)}, \tag{2.2}
$$

where ω is the "growth rate", a measure of how quickly a disturbance of wavenumber κ grows, $r_0 \equiv d_0/2$ is the nozzle outlet radius, I_n are nth order modified Bessel function of

the first kind, K_n are nth order Bessel functions of the second kind, the primes indicate differentiation, and $l^2 \equiv \kappa^2 + \omega/\nu_\ell$.

Equation 2.2 can be simplified into various limiting forms for different scenarios and solved analytically to obtain the growth rate ω for a particular wavenumber κ, or the full equation could be solved numerically. Traditional linear stability theories then *assume* that the most unstable mode (i.e., largest ω, denoted ω_m) is responsible for all breakup of the jet.

Rayleigh [Ray78] in 1878 developed the first stability analysis of liquid jets. The analysis assumed the jet was inviscid jet and in a vacuum. Rayleigh hypothesized that the most unstable mode would dominate over all others, and numerically calculated the wavelength ($\lambda \equiv 2\pi/\kappa$) of this mode as

$$\lambda_m = 4.51 d_0. \tag{2.3}$$

If a cylinder of length λ_m with diameter d_0 forms a spherical droplet, it has a diameter of [LM17, p. 25L]

$$D = 1.89 d_0. \tag{2.4}$$

Similarly, the breakup length can be computed in Rayleigh's theory. A brief derivation of the breakup length here can be instructive, following McCarthy and Molloy [MM74, p. 2R]. The amplitude of the perturbation of the radial location of the free surface of the jet traditionally evolves according to

$$\delta = \delta_0 \exp(\omega_m t), \tag{2.5}$$

so the radial location of the free surface is

$$r = d_0/2 + \delta \cos(\kappa_m x), \tag{2.6}$$

where κ_m is the wavenumber associated with λ_m, δ is the amplitude of the free surface perturbation, and δ_0 is "initial disturbance level". The initial disturbance level is simply how disturbed the free surface is at time 0 at $x = 0$. The breakup length can be found by

16

locating where the jet diameter decreases to zero. This is approximately true when the disturbance amplitude grows to $d_0/2$. Consequently, in Rayleigh's theory

$$\omega_{\rm m} = 0.97 \left(\frac{\sigma}{\rho_\ell d_0^3} \right)^{1/2}, \tag{2.7}$$

which can be used to find an equation for the breakup time $t_{\rm b}$,

$$\frac{d_0}{2} = \delta_0 \exp \left[0.97 \left(\frac{\sigma}{\rho_\ell d_0^3} \right)^{1/2} t_{\rm b} \right]. \tag{2.8}$$

The breakup time can be converted into a length through the convective velocity $\overline{U}_0$ to find $t_{\rm b} \equiv \langle x_{\rm b} \rangle / \overline{U}_0$. Now equation 2.8 can be rearranged to state

$$\frac{\langle x_{\rm b} \rangle}{d_0} = 1.03 \ln \left(\frac{d_0}{2\delta_0} \right) {\rm We}_{\ell 0}^{1/2}. \tag{2.9}$$

Weber [Web19] in 1931 developed a theory for low-speed viscous jets. In this theory the most unstable wavelength is [Web19, p. 23; LM17, p. 27L]

$$\lambda_{\rm m} = \sqrt{2} \pi d_0 \sqrt{1 + 3{\rm Oh}_{\ell 0}}, \tag{2.10}$$

where the Ohnesorge number is ${\rm Oh}_{\ell 0} \equiv \mu_\ell / \sqrt{\rho_\ell \sigma d_0}$. The corresponding droplet diameter is found to be

$$D = \left(\frac{3\sqrt{2}}{2} \pi \sqrt{1 + 3{\rm Oh}_{\ell 0}} \right)^{1/3} d_0, \tag{2.11}$$

by, again, setting as equivalent the volume of a droplet of diameter D and a cylinder of length $\lambda_{\rm m}$ with diameter d_0.

The breakup length in Weber's theory is [Web19, p. 24; MM74, p. 4L]

$$\frac{\langle x_{\rm b} \rangle}{d_0} = \ln \left(\frac{d_0}{2\delta_0} \right) \left({\rm We}_{\ell 0}^{1/2} + 3 \frac{{\rm We}_{\ell 0}}{{\rm Re}_{\ell 0}} \right). \tag{2.12}$$

Experience has shown that Weber's theory is reasonable for low Weber number jets

in general (see § 3.4.4).

Another popular early theory was developed by Taylor [Tay58] in 1940 and later extended by Ranz [Ran58] and Ranz and Dreier [RD64]. Reitz [Rei78, p. 134] calculated a droplet diameter consistent with Taylor's theory:

$$D = \frac{4\pi B_1 \sigma \lambda_{\mathrm{m}}^*}{\rho_{\mathrm{g}} \overline{U}_0^2},$$ (2.13)

where B_1 is a model constant and λ_{m}^* is a dimensionless wavelength for the most unstable mode, defined as

$$\lambda_{\mathrm{m}}^* = \frac{\rho_{\mathrm{g}} \overline{U}_0^2}{\sigma \kappa_{\mathrm{m}}}.$$ (2.14)

For $\dfrac{\rho_\ell}{\rho_{\mathrm{g}}} \left(\dfrac{\mathrm{Re}_{\ell 0}}{\mathrm{We}_{\ell 0}} \right)^2 \gg 1$, λ_{m}^* asymptotically approaches $3/2$.

Similarly, for the breakup length in the same limit, Taylor's theory states that [Rei78, p. 135]

$$\frac{\langle x_{\mathrm{b}} \rangle}{d_0} = B_4 \sqrt{\frac{\rho_\ell}{\rho_{\mathrm{g}}}},$$ (2.15)

where B_4 is a model constant. Equation 2.15 has proved popular in predicting the breakup length in the atomization regime, though my own regression analysis detailed later in this chapter suggests the scaling with $\rho_\ell/\rho_{\mathrm{g}}$ may be incorrect. Also, the coefficient is known to take wildly varying values, suggesting that the model is not predictive, as discussed in the next section.

In the context of Taylor's theory, Ranz and Dreier [RD64, p. 59R] suggested that the spray angle can be modeled as

$$\tan \left(\frac{\theta_{\mathrm{i}}}{2} \right) \propto \frac{\omega_{\mathrm{m}} \lambda_{\mathrm{m}}}{\overline{U}_0}$$ (2.16)

This result applies for linear stability theory in general and can be used with other models.

In 1987, rather than analytically solving limiting cases of the dispersion relation, Reitz [Rei87] solved the dispersion relation numerically and fitted algebraic equations to it. Changing the notation to match that used in this dissertation, the curve fits for the maximum

growth rate ω_{m} and the associated wavelength λ_{m} are

$$\frac{\lambda_{\mathrm{m}}}{d_0} = \frac{18.04(1 + 0.54\mathrm{Oh}_{\ell 0}^{1/2})\left[1 + 0.4\left(\frac{\mathrm{We}_{\ell 0}}{\mathrm{Re}_{\ell 0}}\sqrt{\frac{\rho_{\mathrm{g}}}{\rho_\ell}}\right)^{0.7}\right]}{\left[1 + 0.27\left(\mathrm{We}_{\ell 0}\frac{\rho_{\mathrm{g}}}{\rho_\ell}\right)^{1.67}\right]^{0.6}}, \tag{2.17}$$

$$\omega_{\mathrm{m}}\left(\frac{\rho_\ell d_0^3}{\sigma}\right)^{1/2} = \frac{0.96 + 0.38\left(\mathrm{We}_{\ell 0}\frac{\rho_{\mathrm{g}}}{\rho_\ell}\right)^{1.5}}{(1 + \sqrt{2}\mathrm{Oh}_{\ell 0})\left[1 + 1.4\left(\frac{\mathrm{We}_{\ell 0}}{\mathrm{Re}_{\ell 0}}\sqrt{\frac{\rho_{\mathrm{g}}}{\rho_\ell}}\right)^{0.6}\right]}. \tag{2.18}$$

These equations fit the numerical solutions well in the ranges $0 \leq \mathrm{Oh}_{\ell 0} \leq \sqrt{2}/2$, $\rho_\ell/\rho_{\mathrm{g}} > 10$, and $0 \leq \mathrm{We}_{\mathrm{g}0} < 2000$.

Equation 2.17 is used as a component of the popular KH-RT model [BR99], where the droplet size of an atomizing liquid "blob" is calculated as

$$D = 2B_0\lambda_{\mathrm{m}}, \tag{2.19}$$

where B_0 is a constant (presumably universal as the wavelengths should be directly proportional to the droplet size in this theory) which is 0.61. While in principle a breakup length can be calculated with ω_{m} from equation 2.18, in practice the Ohnesorge number is assumed to be zero and the gas phase Weber number is assumed to be high, leading to simplified expressions for λ_{m} and ω_{m}. Under these approximations Beale [Bea99, pp. 94–95] finds that

$$\frac{\langle x_{\mathrm{b}}\rangle}{d_0} = \frac{B_1}{2}\sqrt{\frac{\rho_\ell}{\rho_{\mathrm{g}}}}, \tag{2.20}$$

which is identical to the result for Taylor's theory, equation 2.15

19

2.6.2 Shortcomings of stability theory

Often, the flow exiting a nozzle is turbulent, yet stability theories tend to assume that the flow is initially laminar with only small free surface perturbations (no velocity perturbations). Turbulence influences the breakup of the jet, but how should turbulence properties be included in stability analyses?

Inclusion of turbulence properties via model coefficients. In stability theory, various model coefficients can vary greatly. For example, in the previously mentioned KH-RT model, one of the coefficients, B_1, takes calibrated values ranging from 1.73 to 40 [Nin07, p. 14]. This has made some researchers conclude that the KH-RT model is not predictive [MG17, p. 34L]. A widely varying model coefficient suggests that there may be missing variables in the theory.

To be more specific, stability theories offer no clear mechanism by which $\overline{\text{Tu}}_0$ can be incorporated into the theory beyond the "initial disturbance level" or another similar model coefficient. The physical meaning of this term is unfortunately vague, and how it scales with $\overline{\text{Tu}}_0$ would at least require additional theoretical work. This fact was unfortunately realized slowly. Phinney [Phi72] noted that earlier research tended to assume that the initial disturbance level was constant, and suggested instead that the initial disturbance level be considered as a variable. Chen and Davis [CD64, p. 191] recommended a study of how the initial disturbance level relates to turbulence quantities at the nozzle outlet, though no such study was ever undertaken to my knowledge. Lin and Reitz [LR98, p. 92] note that the initial disturbance level depends on the nozzle geometry, as diesel and water jet cutting systems operate at similar pressures, yet the breakup length for diesel jets is short while that for water jet cutting jets is long. When studying diesel sprays, Reitz and Bracco [RB82] discuss how the initial disturbance level changes based on several different nozzle geometries tested, and gives in an earlier work [Rei78, p. 133] an empirical regression for a model coefficient, A, as a function of the nozzle aspect ratio (L_0/d_0):

$$A = 3.0 + \frac{L_0/d_0}{3.6}.$$

(2.21)

This model coefficient is higher for more disturbed flow. This equation is only valid for $L_0/d_0 < 10$, as the amount of disturbances to the flow should saturate as the flow develops, but the regression suggests that it continues to increase regardless of how developed the flow is.

The earliest attempt I am aware of to predict the initial disturbance level in Weber's theory was by Lenz [Len67, p. 14], who argued that molecular vibrations cause the initial disturbance at low velocities. Andrews [And93, p. 38] also argued that the e^N method of turbulence transition prediction by Mack [Mac77, §4.3] could be used to estimate the initial disturbance level including turbulence intensity effects. However, this would be purely empirical if done as Mack did because N is an empirically determined function of the turbulence intensity.

Assuming that stability analysis still works when the flow is turbulent at the nozzle outlet, an energy flux argument similar to that of Moallemi, Li, and Mehravaran [MLM16] can be used to suggest that in Weber's theory the initial disturbance level is a function of the turbulence intensity. Weber [Web19, p. 17] notes that the disturbance at the nozzle outlet takes the form of a cosine function in time:

$$\delta(x = 0) = \delta_0 \cos\left(\frac{2\overline{U}_0 t}{d_0}\right). \tag{2.22}$$

The functional dependency of δ, i.e., $(x = 0)$ will be dropped in this section for brevity. The disturbance is imposed as a perturbation of the jet radius, with a uniform velocity profile equal to $\overline{U}_0$. Consequently, the perturbed jet has additional energy as a result of being larger.

Equating the flow of disturbance energy $e_0(r)$ to the average flow of disturbance energy returns

$$\int_{A_0} e_0(r) \rho_\ell \overline{U}_0 \vec{i} \cdot \widehat{n} \, \mathrm{d}A = \left\langle \int_{A_\delta} \tfrac{1}{2} \overline{U}_0^2 \rho_\ell \overline{U}_0 \vec{i} \cdot \widehat{n} \, \mathrm{d}A \right\rangle, \tag{2.23}$$

where $A_0 \equiv \frac{\pi}{4} d_0^2$ is the nozzle orifice cross-sectional area, $\widehat{n} = \vec{i}$ is the nozzle orifice normal vector, A_δ is the area of the jet added due to δ (i.e., from $r = d_0/2$ to $r = d_0/2 + \delta$). The disturbance energy here could be just the turbulent kinetic energy $k_0(r)$, though I will take

$e_0(r) = k_0(r) + e \cdot \frac{1}{2}\overline{U}_0^2$ as there may be other sources of instability energy. The coefficient e is non-dimensional by construction.

Simplifying the integrals returns

$$\rho_\ell \overline{U}_0 \underbrace{\int_{A_0} e_0(r)\, dA}_{\overline{e}_0 A_0} = \rho_\ell \overline{U}_0 \cdot \tfrac{1}{2}\overline{U}_0^2 \left\langle \int_{A_\delta} dA \right\rangle, \tag{2.24}$$

where $\overline{e}_0$ is a plane-averaged energy. This can be more explicitly written as

$$\overline{e}_0 \cdot \tfrac{\pi}{4} d_0^2 = \tfrac{1}{2}\overline{U}_0^2 \cdot 2\pi \left\langle \int_{d_0/2}^{d_0/2+\delta} r\, dr \right\rangle. \tag{2.25}$$

Simplifying again and evaluating the integral returns

$$\overline{e}_0 \cdot \tfrac{1}{4} d_0^2 = \tfrac{1}{2}\overline{U}_0^2 \left\langle \left[\left(\frac{d_0}{2} + \delta \right)^2 - \left(\frac{d_0}{2} \right)^2 \right] \right\rangle, \tag{2.26}$$

$$= \tfrac{1}{2}\overline{U}_0^2 \left(\frac{d_0}{2} \right)^2 \left\langle \left[\left(1 + \frac{2\delta}{d_0} \right)^2 - 1 \right] \right\rangle. \tag{2.27}$$

In the limit of small disturbances, the binomial approximation returns

$$\overline{e}_0 \cdot \tfrac{1}{4} d_0^2 = \tfrac{1}{2}\overline{U}_0^2 \left(\frac{d_0}{2} \right)^2 \left\langle \left[\cancel{1} + \frac{2\delta}{d_0} - \cancel{1} + \ldots \right] \right\rangle, \tag{2.28}$$

$$\approx \tfrac{1}{2}\overline{U}_0^2 d_0 \underbrace{\langle \delta \rangle}_{\delta_0}. \tag{2.29}$$

The average disturbance level at the nozzle is $\langle \delta(x = 0) \rangle = \delta_0$ as can be seen from equation 2.22. Consequently, if I further assume that $e = 0$ so that only turbulence influences the initial disturbance and note that $\overline{k}_0 \equiv \tfrac{3}{2}\overline{u'}_0^2$, I can express the initial disturbance level as a function of only the turbulence intensity (using a plane averaged turbulent kinetic energy):

$$\frac{\delta_0}{d_0} = \tfrac{3}{4}\overline{\mathrm{Tu}}_0^2. \tag{2.30}$$

22

Unfortunately, this equation is a poor fit to the data in the turbulent Rayleigh regime (where it presumably applies as Weber's theory is for the Rayleigh regime), over-predicting the breakup length.

§ 3.4.8 develops a model for an equivalent initial disturbance level which performs better in the turbulent Rayleigh regime than equation 2.30:

$$\ln\left(\frac{d_0}{2\delta_0}\right) = \text{arccsch}\left(C_v \overline{\text{Tu}}_0 \text{We}_{\ell 0}^{1/2}\right), \tag{3.23}$$

where arccsch is the inverse hyperbolic cosecant function. Equation 3.23 with $C_v = 0.0615$ is an excellent fit to the available data (31 data points, $R^2 = 0.961$), indicating that modeling the coefficients in stability theory can be viable. However, there are no stability theory coefficient models with similar success in the turbulent surface breakup or atomization regimes.

Additionally, changing the initial disturbance level alone typically can not change the characteristic droplet sizes. The droplet size in *linear* stability theories is independent of the initial disturbance level — see equation 2.19. So even if the initial disturbance level increases as turbulence intensity increases, the decrease in droplet size observed experimentally as turbulence intensity increases [Bog48; DCT05] can not be reproduced. In *non-linear* stability theories the wavelength of the most unstable mode (and consequently, droplet sizes) depends on the initial disturbance level, possibly remedying this situation. The only study I am aware of to examine the effect of the initial disturbance level on the wavelength of the most unstable mode is by Wang [Wan68, p. 312, eqn. 91]. Using equation 3.23, it can be shown that Wang's correction term causes the droplet size to decrease in the turbulent Rayleigh regime. It is difficult to evaluate the accuracy of Wang's theory as the small parameter used in the perturbation analysis is not clearly defined. In the Rayleigh regime in general, the droplet size appears to be insensitive to the initial disturbance level § 3.4.8, though possibly Wang's correction is negligible. In other turbulent regimes the non-linear correction may not be negligible.

As it turns out, modeling the coefficients alone is sufficient for the turbulent Rayleigh regime likely because in this regime the most unstable mode approximation (to be discussed)

is valid, the droplet size appears to be roughly independent of the initial disturbance level, and the effect of the turbulence is felt by the jet primarily near the nozzle exit where the initial disturbance level is set (see § 3.4.8). These characteristics do not extend to other regimes.

In other turbulent regimes, the conclusion is that model parameters like the initial disturbance level are largely empirical at present. If a change is made to a nozzle design, it is typically not possible to estimate the effect on the model coefficients. This contrasts strongly with the phenomenological approach, where a nozzle model can easily be used as an input to a jet breakup model due to the turbulence intensity being explicitly considered.

Inclusion of turbulence properties via uncertainty propagation. Several previous researchers have proposed that existing stability analyses can be used if fluctuations in input quantities (e.g., turbulent velocity fluctuations) are used to generate distributions of output quantities like the breakup length [Laf77] or droplet size [SSS99; BS02]. This approach is promising, however, existing implementations have major flaws which must be addressed.

From a model validation perspective, past researchers using this approach have not characterized the input quantities (turbulent velocity fluctuations, again, in our case). This left past researchers unable to evaluate the success of these models more than qualitatively, which has been noted by Babinsky and Sojka [BS02, pp. 326–327], proponents of this approach. Fortunately, today we have the information to properly evaluate these models. To use Lafrance [Laf77] as an example, Lafrance use the stability analysis of Rayleigh and a random nondimensional initial disturbance level to calibrate the RMS nondimensional initial disturbance level to data from Phinney [Phi73]. Lafrance suggests this RMS nondimensional initial disturbance level can be interpreted as a RMS turbulent velocity (presumably a turbulence intensity). The value found, 0.8%, was called "reasonable" by Lafrance, but is actually roughly an order of magnitude too low — see § 4.3. Mere assertion is not enough; comparison with unambiguous experimental data is absolutely necessary. The failure of the approach of Lafrance is due to the shortcomings of the model used, not the idea that

fluctuations need to be taken into account. Similar criticism also applies to the approach taken by Sovani, Sojka, and Sivathanu [SSS99].

The most significant shortcoming of this approach is that it ignores the fact that velocity fluctuations can appreciably change the mean quantities and do not mainly widen the distributions. Higher turbulence levels typically decrease the breakup length, however, this is not reflected in Lafrance's analysis. Lafrance treated the initial disturbance level and turbulence intensity as independent, when in reality the two are coupled. The mean breakup length in Lafrance's model does not decrease as the turbulence level increases, in contradiction to experimental evidence. The same problem is also demonstrated through characteristic droplet sizes in typical linear stability theories being independent of the initial disturbance level as previously mentioned. In the droplet size case, making the initial disturbance level fluctuate would have no influence at all on the droplet size. The fluctuations are more than just uncertainties to be propagated.

Schmid [Sch07, p. 149] states that stochasticity has two effects on stability in general:

1. the response of a *deterministic* system disturbed by an external stochastic process, and

2. the *modification* of the system when it is disturbed by an external stochastic process.

Existing models consider only the first effect, but the second effect is very important in turbulent jet breakup as well. To my knowledge at present no stability-theory-based turbulent jet breakup model (outside of the turbulent Rayleigh regime) considers the second effect. How to incorporate the second effect in stability theory for turbulent jet breakup in general is an open problem. It is possible that combination with an initial disturbance model like equation 3.23 will *partly* account for the second effect. However, as the droplet size in linear stability theory is independent of the initial disturbance level, this approach will only be partial. As previously mentioned, a non-linear theory considering the effect of the initial disturbance level on the breakup process may be *necessary* to take into account the second effect. Still, at present it is not clear if a non-linear theory is *sufficient* to consider the second effect.

25

Inclusion of turbulence properties via using a turbulent viscosity or by analyzing the stability of the RANS equations. Chen and Davis [CD64, pp. 190–191] hypothesized that Weber's theory could be used if a turbulent viscosity were used in place of a molecular viscosity. Unfortunately, Chen and Davis found that this assumption did not agree with their experimental data. Use of a turbulent viscosity instead of a molecular viscosity in stability analysis seems unlikely to account for turbulence properties in turbulent jet breakup. Turbulent viscosities are much higher than molecular viscosities. Increased viscosity tends to stabilize liquid jets according to Weber's theory (see the Reynolds number effect in equation 2.12), but in experiments increased turbulence levels, which would increase turbulent viscosity, tend to destabilize liquid jets.

The physical reasons for using a turbulent viscosity instead of the molecular viscosity are not clear. If stability analysis is performed on the RANS equations with a turbulent viscosity model, then neglecting the molecular viscosity, the results will be identical to classical stability theory, albeit with a turbulent viscosity instead of a molecular viscosity. Indeed, Sauerwein [Sau20] analyzed the stability of the RANS equations in a case similar to that of Rayleigh without using a turbulent viscosity model and obtained similar incorrect results: higher turbulence levels led to more stable jets.

The simplest explanation for the failure is that the breakup stability of the RANS equations is not the same as the breakup stability of a turbulent flow. The perturbations that lead to breakup, even in the Rayleigh case, would seem to be averaged out in a RANS stability approach, leading to a more stable jet.

Assumption that the most unstable mode dominates. The vast majority of previous stability analyses assume that a single wavelength dominates the breakup process. This seems implausible in a broadband phenomena like turbulence. Measurements of surface waves on high Weber number turbulent liquid jets confirm that the breakup process is broadband [AS68, fig. 19; CD64, fig. 12]. Similarly, droplet size distributions in high Weber number turbulent jet breakup tend to be highly polydisperse, not essentially monodisperse as would be expected if a single wavelength dominated. More recently, Agarwal and Trujillo

[AT18, pp. 11R–12L] note that in a configuration like typical fuel sprays, the most unstable mode acts primarily to cause breakup of the surface, but the jet core itself is broken up by a different mode downstream. In the laminar and turbulent Rayleigh regimes, the most unstable mode dominance hypothesis appears reasonable. But its success in those regime does not imply this hypothesis is valid in other regimes.

Consideration of more than one wavelength is necessary to model high Weber number turbulent jet breakup. To my knowledge there have been few attempts to consider more than one disturbance wavelength. Lemberskii and Ferber [LF73] propose using the dispersion relationship to calculate a droplet size probability density function. Lemberskii and Ferber assume that the initial disturbance level is independent of the wavenumber. Yi and Reitz [YR04] later independently developed a computational model considering multiple different initial disturbances. This is an essentially empirical way to determine the initial disturbance level given a particular turbulent disturbance. Unfortunately, Yi and Reitz [YR04, eqn. 22] estimated the nozzle turbulent kinetic energy with a nozzle turbulence model that I showed to be extremely inaccurate chapter 6. Yi and Reitz also did not consider the possibility that the stochasticity changes the dispersion relationship, like all other precious stochastic models I am aware of. The works of Lemberskii and Ferber and Yi and Reitz are pioneering, but ultimately too flawed to justify using as-is.

Other assumptions made in stability analyses.   Agarwal and Trujillo [AT18] criticize some of the assumptions involved in linear stability theory. In particular, the DNS results of Agarwal and Trujillo show that at high Weber numbers, the non-linear term neglected in the analysis can have significant effects more than 4 nozzle diameters downstream of the nozzle outlet. Agarwal and Trujillo also showed that the Fourier decomposition used in stability analysis quickly becomes a poor approximation because the free-surface is multiple-valued.

Additionally, the vast majority of existing linear stability theories assume that the disturbances are axisymmetric. This assumption is questionable at best — Yang [Yan92, p. 681] notes that if axisymmetry were correct then rings would break off from the jet, not droplets. Still, Lin and Reitz [LR98, p. 101] still believe that axisymmetric disturbances

27

dominate, noting that the growth rate of the axisymmetric disturbances is typically higher than the growth rate for asymmetric disturbances. Lin and Reitz suggest that breakup of the rings into droplets may explain the observation of droplets, but again, droplets are observed to be formed directly from the jet, not rings, so this explanation is implausible. The simplest explanation for why asymmetric disturbances appear in turbulent jet breakup in practice is that the turbulence spectra leads to asymmetric initial disturbances.

Overall assessment of stability theory for turbulent jet breakup. Stability-theory-based models have so far produced results which are implausible with respect to the effect of turbulence intensity. Adding turbulence intensity to stability theories is not trivial. Simple fixes can not solve this problem — substantially new models are needed but do not appear forthcoming. While there are several plausible avenues for research in stability theory, ultimately the alternative phenomenological approach was deemed more plausible for developing simple models for turbulent jet breakup as this approach makes avoiding the shortcomings of stability theory easier.

2.7   Phenomenological models

In contrast to stability theory models, "phenomenological models" are not based on the Navier-Stokes equations, and instead assume a certain simplified physical process is occurring. I borrow the word "phenomenological" in this context from Wu, Tseng, and Faeth [WTF92] and others in the Faeth research group. These models may be developed in mechanistic ways, considering for example an energy or force balance which leads to droplet formation provided certain criteria are met. They also could be developed in heuristic ways like scaling arguments.

It is tempting to think that stability-theory-based models are inherently more credible than phenomenological models, as they are based on the Navier-Stokes equations, which are considered reliable. However, the assumptions and approximations inherent in present stability-theory-based models make these models arguably no more credible than
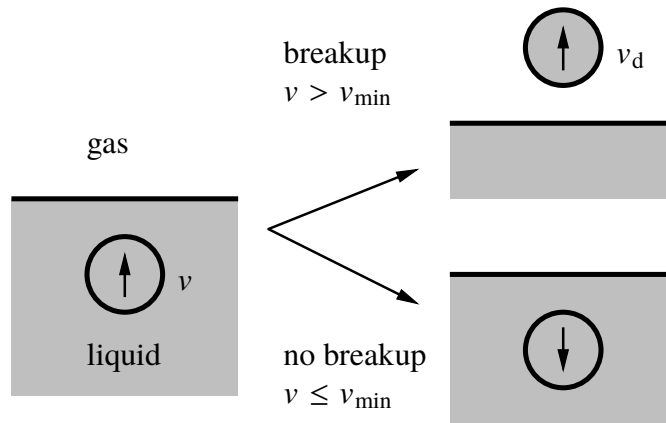
Figure 2.2: There are two possibilities when a turbulent event occurs at the free surface: breakup (top right) and no breakup (bottom right), depending on whether the velocity fluctuation exceeds the critical velocity v_{min} which could be a function of the length scale associated with the fluctuation.

phenomenological models. As has been discussed, these assumptions and approximations are not easily avoided. Further, phenomenological models do not necessarily abandon first principles. Phenomenological models instead choose simplified first principles. The inaccuracy, like in stability theory, comes from the assumptions and approximations.

There are many phenomenological models in the literature. To reduce the scope of this review, only models with turbulence intensity dependence are considered. The turbulence intensity can be more easily incorporated into a phenomenological model than a stability theory model due to the flexibility of construction of a phenomenological model. However, this review should not give the impression that most phenomenological models consider turbulence intensity, as few do. Additionally, in contrast to the stability theory section, some brief derivations of these models will be given as appropriate to give the reader an understanding of how these models work. For detailed derivations, the reader is referred to the original works like before.

It seems obvious that turbulent fluctuations normal to the free surface, i.e., in the radial direction, can perforate the surface and form droplets. An illustration of this process is shown in figure 2.2. This idea has a long history, dating back to the 1937 study of Schweitzer [Sch37, pp. 518–519], and independently rediscovered many times since then.

I'll term this the "radial velocity fluctuation hypothesis". Breakup through this mechanism has been observed in the photographic experiments of Hoyt et al. [Hoy+88, pp. 359–360] and Wu, Tseng, and Faeth [WTF92], and also the DNS study of Desjardins and Pitsch [DP10a].

Natanzon [Nat18] developed the earliest quantitative theory of turbulent jet breakup I am aware of in 1938. Natanzon applied the maximum entropy principle[5] with a kinetic energy constraint using k to find the droplet diameter (number) distribution

$$f(D) = \left(0.210 \frac{\rho_\ell \overline{k}_0}{\sigma}\right)^{13} D^{12} \exp\left[-0.0943 \left(\frac{\rho_\ell \overline{k}_0 D}{\sigma}\right)^2\right] \qquad (2.31)$$

and the mass mean diameter

$$D_{30} = 8.45 \frac{\sigma}{\rho_\ell \overline{k}_0}, \qquad (2.32)$$

which can be expressed in dimensionless variables:

$$\frac{D_{30}}{d_0} = 12.68 \text{We}_{\ell 0}^{-1} \overline{\text{Tu}}_0^{-2}, \qquad (2.33)$$

Bogdanovich [Bog48, pp. 122–123] developed an energy balance argument for an (unspecified) average droplet diameter. This argument proved popular in Eastern Bloc countries during the Cold War [Sit63, pp. 3–5; Leb19], and similar arguments (both inspired by and independent of Bogdanovich) were also made by researchers outside of the Eastern Bloc [Fri65, p. 61; Ino63, pp. 16.103–16.105]. The simplest form of this argument examines

---

[5]Natanzon did this about 50 years before the maximum entropy principle was popularized for droplet size distribution prediction. See Dumouchel [Dum09] for a review of the maximum entropy principle applied to droplet size distribution estimation. It is also interesting to note that one of the pioneers of maximum entropy for droplets, Sellens, discusses in his MS thesis and PhD dissertation how to extend the maximum entropy principle to turbulent jet breakup [Sel85, p. 80; Sel87, pp. 86–87], though Sellens made no such extension subsequently. The recent work of Hosseinalipour et al. [Hos+16] is the only work other than that of Natanzon I've seen to use turbulent kinetic energy with the maximum entropy principle to predict droplet size.

To be clear, the use of the maximum entropy principle by itself does not make a model phenomenological. The maximum entropy principle has been combined with stability analysis in the past [CD96; ML99; Kim+03; Mov+11]. What determines the type of a maximum entropy model is how the constraints are developed: if they are developed with stability theory, it's a stability theory model. If they are purely phenomenological, it's a phenomenological model.

the formation of a single spherical droplet of volume $V = \frac{\pi}{6}D^3$ and surface area $SA = \pi D^2$ at the free surface. When inside of the jet, the "droplet" has turbulent kinetic energy $\overline{k}_0$ (i.e., the same value as at the nozzle, plane averaged). All of this turbulent energy is consequently converted into surface energy, i.e.:

$$\rho_\ell \overline{k}_0 V = \sigma SA. \tag{2.34}$$

Then, substituting in the definitions of the volume and surface area of a spherical droplet, the droplet diameter obtained is

$$D = 6\frac{\sigma}{\rho_\ell \overline{k}_0}, \tag{2.35}$$

or in dimensionless variables

$$\frac{D}{d_0} = 9We_{\ell 0}^{-1}\overline{Tu}_0^{-2}, \tag{2.36}$$

which is the same scaling Natanzon found for D_{30}. Lebedev [Leb19] changes the constant to a model coefficient. Sitkei [Sit63] modifies the argument to add a term for viscous dissipation. This class of arguments is flawed, however, as the eddies interacting with the free surface do not all have the same kinetic energy as represented by $\overline{k}_0$.

Wu, Tseng, and Faeth [WTF92] avoided this issue through an energy balance argument combined with inertial range scaling to estimate D_{32} for the *initial* droplets, that is the Sauter mean diameter of the first droplets formed downstream of the nozzle. The difference in this argument is that instead of using the full turbulent kinetic energy $\overline{k}_0$, the turbulence spectrum is introduced as the energy appropriate for an "eddy" of size ℓ which is assumed to be in the inertial range[6]. Wu, Tseng, and Faeth convert the isotropic energy spectrum into an equivalent velocity[7]. Then, merely assuming proportionality rather than strict equality, Wu, Tseng, and Faeth state that the surface energy is proportional to the eddy

---

[6]While Wu, Tseng, and Faeth do not discuss the possibility of selecting $\overline{k}_0$ instead of the energy spectrum, this dichotomy is not unique to this work as it was discussed previously by Borghi [Bor96, p. 11].

[7]The original work by Wu, Tseng, and Faeth is vague on what this spectral velocity is. The reader is referred to § 5.2.3 of this dissertation for more details on this.

energy:

$$\frac{\pi \rho_\ell \ell^3 v^2}{12} \propto \pi \ell^2 \sigma \tag{2.37}$$

and apply the result below which follows from the inertial range spectrum

$$v \propto \overline{v_0'} \left(\frac{\ell}{\Lambda_0} \right)^{1/3}, \tag{2.38}$$

where Λ_0 is the turbulent integral scale at the nozzle outlet.

Wu, Tseng, and Faeth then assume that $D_{32} \propto \ell$ to obtain the following scaling:

$$\frac{D_{32}}{d_0} \propto \overline{\mathrm{Tu}_0}^{-6/5} \mathrm{We}_{\ell 0}^{-3/5} \left(\frac{\Lambda_0}{d_0} \right)^{2/5}, \tag{2.39}$$

where I am using a different notation than Wu, Tseng, and Faeth which has changed the form of the equation. The use of a spectral energy rather than the full turbulent kinetic energy appreciably changes the form of the droplet size equation.

Broadly, the simple arguments by Bogdanovich and Wu, Tseng, and Faeth have three problems:

1. the arguments assume that to obtain an average output (e.g., D_{32}), one can replace input quantities with their averages (or a "representative" value). However, this is only true for linear equations and is often false for non-linear equations (e.g., the RANS closure problem),

2. the arguments do not justify which characteristic diameter (D_{ij}) is appropriate, and

3. the arguments assume that all turbulent surface fluctuations will form droplets.

If strict energy conservation is followed, these arguments assume that the droplets have zero velocity at formation because all input energy (e.g., turbulent kinetic energy) is used to create new free surface. The use of empirical coefficients instead of those implied by strict energy conservation by Lebedev [Leb19] and Wu, Tseng, and Faeth [WTF92] avoids this issue, though I am not sure that these researchers were aware of this. Ultimately, it

would be better to follow strict energy conservation and model the distribution of turbulent energy into surface energy and droplet kinetic energy as I do in chapter 5.

Fortunately, Natanzon's theory does not have the first two problems or the droplet velocity problem, as the droplets are assigned velocities through maximum entropy as well, and averages are computed directly from a distribution function rather than assumed to be of a certain form. However, as before, having a model for droplet velocity would be preferably to merely using the maximum entropy principle to assign droplet velocities.

Recently, Schmitz [Sch11] developed a computational extension of the ideas of Wu, Tseng, and Faeth [WTF92] with a more general turbulence spectrum. This allows computation of the full droplet size distribution, avoiding the issue of which characteristic droplet size the model predicts.

The computational KH-RT model [BR99] mentioned in the stability theory section has seen many improvements over the years. One notable recent *phenomenological* improvement by Magnotti [Mag+17; Mag17] to the model has been the incorporation of a droplet diameter model from Wu, Tseng, and Faeth [WTF92, eqn. 14]. The model is a hybrid of the stability and phenomenological approaches, picking the approach that works best in different regimes. Ignoring cavitation and droplet/secondary breakup, Magnotti's model essentially switches between the stability theory "KH" model for the atomization regime to the phenomenological model by Wu, Tseng, and Faeth outside of the atomization regime. One major criticism of Magnotti's model is that it does not consider the effect of turbulence intensity as currently implemented.

Another computational approach is one-dimensional turbulence [Mov+17], abbreviated ODT. ODT is based on random mixing events in a simplified one-dimensional (transverse) domain that moves at the local (constant) convection velocity $\overline{U}_0$. When the mixing event causes liquid to no longer be attached to the core, breakup occurs. The accuracy of ODT for turbulent jet breakup has not yet been fully demonstrated to my knowledge; the model appears capable of predicting jet breakup lengths reasonably well, though droplet size appears to have some issues downstream, possibly due to a change in the mechanism of droplet formation from surface breakup to column (Rayleigh) breakup. I also

am concerned that the spatial grid resolution would impact the estimation of the smallest droplets. ODT is also considerably more complex and computationally expensive than the model proposed by Schmitz [Sch11].

The CDRSV model developed in chapter 5 of this dissertation is based on energy balance ideas, like in many previous models, however, averages are computed explicitly to make clear which characteristic droplet size is implied by the argument. This model also considers the fact that not all turbulent surface fluctuations will lead to droplet formation, which is essential for the prediction of quantities like the spray angle and droplet radial velocity.

Separate from energy balance arguments, Skrebkov [Skr66] and Huh, Lee, and Koo [HLK98] assume that a characteristic droplet diameter is proportional to the integral scale Λ:

$$D \propto \Lambda. \tag{2.40}$$

This does not avoid the previously mentioned problems. And, as the integral scale is the largest turbulent scale, this selection seems plausible for only the largest droplet diameter. Still, the model of Huh, Lee, and Koo has proved popular, being developed further into in part of the hybrid model of Som and Aggarwal [SA10][8].

The previous discussion in this section focused mainly on droplet size, which is the primary concern of most previous researchers, however, other quantities of interest may also be computed with phenomenological approaches.

Natanzon [Nat18, p. 6] assumed all breakup occurs at the nozzle outlet, so $\langle x_{\mathrm{b}} \rangle = 0$. Wu and Faeth [WF95, p. 2916R] assumed the jet core ends where the local Sauter mean droplet diameter increases to the local jet diameter, returning

$$\frac{\langle x_{\mathrm{b}} \rangle}{d_0} = C_c \mathrm{We}_{\ell 0}^{1/2}, \tag{2.41}$$

which is identical to Weber's theory at high Reynolds number (equation 2.12). As discussed

---

[8]The model of Som and Aggarwal itself was developed further into the model of Magnotti [Mag17] after replacing the turbulent breakup model of Huh, Lee, and Koo with that of Wu, Tseng, and Faeth [WTF92].

in § 3.4.10, the $\mathrm{We}_{\ell 0}^{1/2}$ scaling is not appropriate for liquid jets in the turbulent surface breakup regime or the atomization regime. This model also has no dependence on the turbulence intensity, making it implausible as-is.

The approach of Wu and Faeth does not directly predict where the jet core ends. In contrast, I take a more direct approach in chapter 5 by estimating the surface mass flux to find where the jet core ends on average.

In contrast, Tsyapko [Tsy19b, p. 13] used a jet geometry model to relate $\langle x_{\mathrm{b}} \rangle$ to θ_{i}, obtaining a result which can be written as

$$\frac{\langle x_{\mathrm{b}} \rangle}{d_0} = \frac{\overline{x}_{\mathrm{n}}}{2} \left(a_0 \sqrt{\frac{\rho_{\mathrm{g}}}{\rho_\ell}} + c_{\mathrm{n}} \mathrm{Re} + A_1 \mathrm{Tu} \right)^{-1},$$

where $\overline{x}_{\mathrm{n}}$, a_0, c_{n} and A_1 are model coefficients. While this is a function of the turbulence intensity, it is not a function of the Weber number, which makes it implausible.

The experiments of Wu, Tseng, and Faeth [WTF92, p. 305] suggest that $\langle v_{\mathrm{d}} \rangle$ may scale with the radial turbulent RMS velocity v'. Natanzon [Nat18], Tsyapko [Tsy19a], and Huh, Lee, and Koo [HLK98] developed spray angle θ_{i} models with this assumption. In the limit of high $\rho_\ell / \rho_{\mathrm{g}}$, the model of Huh, Lee, and Koo is

$$\tan \left(\frac{\theta_{\mathrm{i}}}{2} \right) = C_{\theta_{\mathrm{i}}} \overline{\mathrm{Tu}}_0, \tag{2.42}$$

where $C_{\theta_{\mathrm{i}}}$ is a model constant. Rather than assuming this scaling, Skrebkov [Skr66] used a energy balance including v' to determine $\langle v_{\mathrm{d}} \rangle$ and θ_{i}. I use a force balance in chapter 5.

Wu, Tseng, and Faeth [WTF92] and Kerstein, Movaghar, and Oevermann [KMO17] estimate the breakup onset location $\langle x_{\mathrm{i}} \rangle$ by finding the time required for breakup to occur, but they estimate this time differently. Wu, Tseng, and Faeth [WTF92, eqn. 10] find that

$$\frac{\langle x_{\mathrm{i}} \rangle}{d_0} = C_{\langle x_{\mathrm{i}} \rangle} \overline{\mathrm{Tu}}_0^{-9/5} \mathrm{We}_{\ell 0}^{-2/5}. \tag{2.43}$$

Kerstein, Movaghar, and Oevermann [KMO17, eqn. 2.5] instead find that

$$\frac{\langle x_i \rangle}{d_0} \propto \text{We}_{\ell 0}^{-1} \text{Re}_{\ell 0}^{1/4}. \tag{2.44}$$

Kerstein, Movaghar, and Oevermann is more consistent with the data. My model in chapter 5 is similar to that of Kerstein, Movaghar, and Oevermann, however, it has a more detailed justification and replaces the $\text{Re}_{\ell 0}$ dependence with a $\overline{\text{Tu}}_0$ dependence.

Chapter 3

Reevaluating the jet breakup regime diagram[1]

3.1 Introduction

Liquid jets break up through many mechanisms, and most mechanisms must be modeled differently. Even focusing solely on the case of the breakup of circular Newtonian jets injected into still low density ratio environments without considering cavitation, compressibility, evaporation, or combustion, there are many varieties of jet breakup. This is the case considered in this work[2]. Which "regime" a jet is in depends on factors including but not limited to the Reynolds number, Weber number, the liquid-gas density ratio, and the turbulence intensity.

Accurately determining the regime is necessary for both research on and design of systems in liquid jet breakup. Engineers often apply models applicable only in a particular regime to an inappropriate regime. Researchers may decide they want to study a particular regime, and consult a regime diagram to determine where to place their study. Frequently, the study is placed in a regime different from that intended. Similarly, when an engineer designs a spray system, they may target a particular regime for its breakup properties. For example, in fuel sprays smaller droplet sizes and breakup lengths are advantageous, while in fire hoses and water jet cutting larger droplet sizes and breakup lengths are advantageous. If the description of the breakup in a particular regime is inaccurate, an engineer may target the wrong regime. And if the regime diagram is inaccurate, an engineer can target the

---

[1]This chapter is slightly modified from a paper submitted to Atomization and Sprays [Tre20c]. I am the sole author.

[2]A complementary study focusing on non-Newtonian viscoelastic jets was published nearly simultaneously with this one [BS20].

correct regime but place the system in the wrong regime. All of these problems are avoided through a more accurate regime diagram and understanding of each regime.

Conventionally, the regime of a liquid jet has been determined through *qualitative* comparison of the appearance of the jet against prototypical jet images in the literature, e.g., Lin and Reitz [LR98, fig. 1]. Classification of images has also been used to produce regime diagrams which allow determination of the regime given variables like the jet Reynolds and Ohnesorge numbers. Unfortunately jets in several regimes appear superficially similar (e.g., the "second wind-induced" and "atomization" regimes), despite differing in terms of *quantitative* characteristics like the trend in the breakup length curve, as will be discussed. Frequently the superficial similarity of some regimes causes qualitative visual classification to be inaccurate. For this reason, quantitative characteristics are preferred when classifying regimes.

Regime diagrams are also typically constructed from relatively little data, lacking the resolution needed to precisely determine the boundaries of each regime. This problem is avoided in this work through a large compilation of data from the open literature and a small amount of new data (1.5% of the compilation) — see § 3.4.1. Additionally, this data compilation specifically included only cases with known turbulence intensity, a measure of the strength of the turbulence, to be defined shortly. The influence of this variable on jet breakup in general is typically only hypothesized, and rarely validated against experimental data with appreciable turbulence intensity variation.

In this section I'll first discuss the most popular regime diagram as of this writing (figure 3.2) in § 3.2, then detail problems with this regime diagram in § 3.3. After that, in § 3.4 I will discuss a largely new regime diagram (figure 3.3) which is much more accurate than any previous diagram for the cases of interest in this work. A reader interested only in the new regime diagram can skip to § 3.4 if desired.

3.2 Previous regime diagrams

The conventional regimes are [LR98, p. 88; BL09, pp. 507–509; LM17, pp. 26–28]:

1. Dripping regime — Breakup is driven by gravity, producing relatively large droplets.[3]

2. Rayleigh regime — Breakup due to a surface-tension-driven instability resulting in droplets larger than the nozzle outlet diameter but of the same order of magnitude ($D \approx 1.89d_0$). The breakup length increases with increasing jet velocity in this regime.

3. First wind-induced regime — Convention states that the droplet diameters are on the order of the nozzle outlet diameter [LR98, fig. 1], however, I challenge this view later in this chapter — see the end of § 3.4.6. Similarly, the breakup onset location is conventionally stated as many diameters from the orifice, but this is not necessarily true either. However, previous researchers did correctly understand that the breakup length decreases with increasing jet velocity in this regime [Rei78, p. 165, fig. 1.1].

4. Second wind-induced regime — The droplet diameters are smaller than the nozzle outlet diameter. The average breakup onset location is not negligible, but can be small. The breakup length increases following a power law with increasing jet velocity.

5. Atomization regime — The droplet diameters are much smaller than the nozzle outlet diameter. Frequently, in the atomization regime breakup is claimed to start at the nozzle outlet (i.e., $\langle x_i \rangle = 0$), though this is probably not true as will be discussed in § 3.3.8. In this work I instead suggest that the breakup onset location is small. In the absence of cavitation and compressibility effects, the breakup length plateaus as the jet velocity is increased.

These regime names have slowly changed since the early works of Haenlein [Hae32] and Ohnesorge [Ohn19]. The names for qualitative visual regimes and quantitative breakup length regimes can differ. For example, Lefebvre and McDonell [LM17, figs. 2.9, 2.10, 2.13] have three different regime diagrams, two based on qualitative criteria with different regime names (one archaic, the other state-of-the-art), and another based on quantitative breakup

---

[3]Depending on the orientation and design of the nozzle, a "teapot effect" regime could be observed between dripping and full jetting/"Rayleigh" [Reb66].

length data with completely different regime names. The qualitative and quantitative regimes have been unified by some in the past so that a qualitative description of jets in a regime has an associated quantitative behavior [Rei78, p. 165, fig. 1.1]. In this work, a unified regime diagram is proposed such that the quantitative and qualitative classifications are consistent, as shown in § 3.4.12. Some regime names will also be changed to be more consistent with the physical mechanisms present in each regime.

Reitz [Rei78, pp. 4-9] has a detailed discussion of earlier research into the boundaries of the breakup regimes, which for the most part remains current — Reitz's work continues to be cited by more recent reviews [CR96; LR98; BL09; LM17]. Several criteria have been proposed, to be discussed shortly. These criteria have not been treated as unimpeachable, but they are treated as accurate enough to use for the planning of experiments in a particular regime.

A summary of selected past regime studies is in table 3.1. The first regime diagram was due to Ohnesorge [Ohn19] in 1936 and is reproduced in figure 3.1. By computing the nozzle Reynolds number $\text{Re}_{\ell 0}$ and also what today is called the Ohnesorge number $\text{Oh}_{\ell 0} \equiv \mu_\ell/(\rho_\ell \sigma d_0)$., an engineer can determine the regime by the location of the point in figure 3.1 (with some caveats; the nozzle and liquid-gas density ratio need to be similar to Ohnesorge's). While some modifications to Ohnesorge's diagram have been made since 1936, nearly the same regime diagram is used today as can be seen in the recent book of Lefebvre and McDonell [LM17, figs. 2.9, 2.10].

The Ohnesorge number is independent of the velocity, which means that in these coordinates, increasing the velocity only changes the Reynolds number. Alternative coordinates (including the one I propose) lack this property, but the advantages gained from switching coordinates outweigh this small benefit. Regime boundary equations are typically constant gas or liquid Weber numbers (as physical arguments often suggest), so it would be simpler to create a plot in terms of the Weber and Reynolds numbers, as I do in figure 3.2. In this plot, an engineer needs to only compute one number (the Weber number) rather than two (the Ohnesorge and Reynolds numbers) to determine which regime a jet is in. A similar plot has been made by Faeth [Fae91, fig. 2] previously.

Some studies in table 3.1 focused on a single regime boundary rather than a complete diagram [Mie55; GM66; Kus69; SS75; MD01]. The majority of previous studies classified regimes based on qualitative evaluation of images (9 out of 13 considered). The majority of previous studies also only considered a relatively small amount of data, e.g., 8 out of 13 studies considered had less than 100 data points in total, making their regime diagrams based on rather sparse data. For that reason, as much quantitative data as possible was compiled to construct the new regime diagram in this work. As shown in table 3.1, this work uses roughly an order of magnitude more data than any previous study. This gives the new regime diagram much more resolution and also range than previous regime diagrams. The ranges of the Reynolds number and Weber number of each study and this work are given in table 3.1; this work is as broad as possible given the data quality guidelines developed in chapter 4.

Rough pipe data from Kusui [Kus69] was used to determine the variation of the atomization regime boundary with the turbulence intensity. The turbulence intensity varied appreciably in only a few additional previous studies. The estimation of the turbulence intensity will be discussed later using equation 4.1. In this study the turbulence intensity ranges from 4.9% to 12.7%.
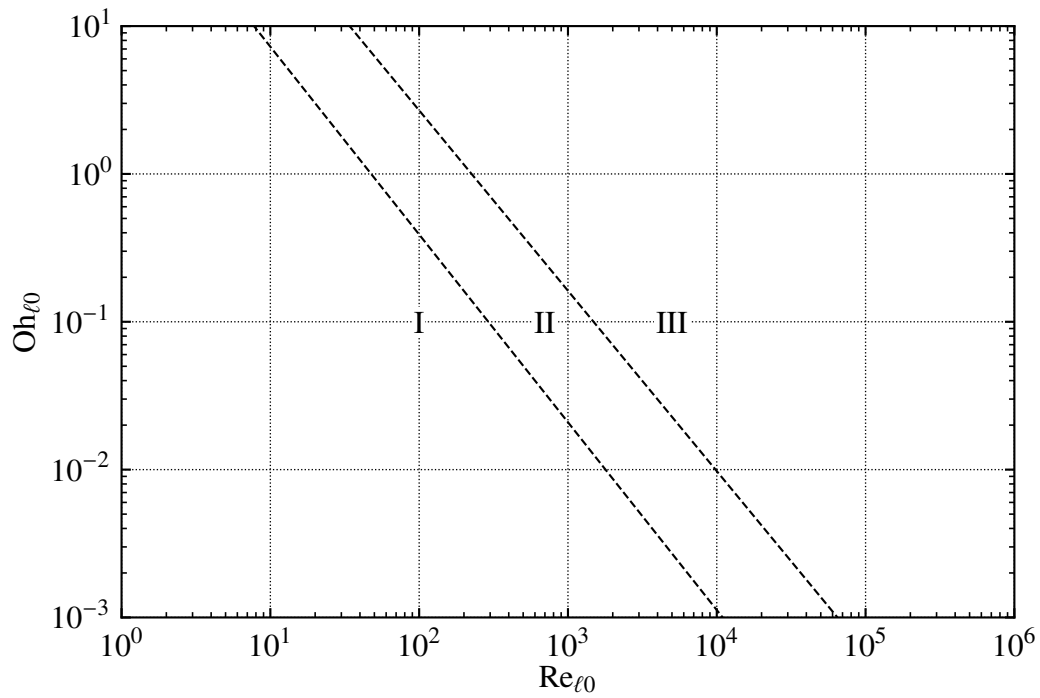
Figure 3.1: A reproduction of the regime diagram of Ohnesorge [Ohn19], using Roman numerals for the regime names. Lines approximating Ohnesorge's from Threlfall-Holmes [Thr09, p. 215].
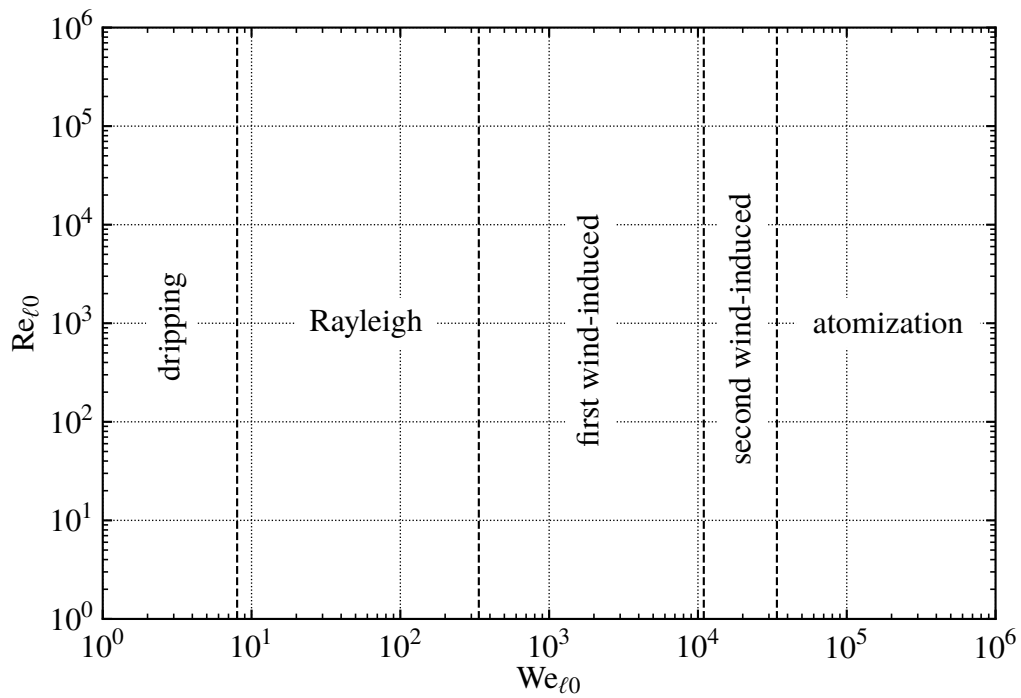
Figure 3.2: The most popular regime diagram in liquid Weber number and liquid Reynolds number coordinates for liquid water injected into atmospheric air at 25 °C. These coordinates are preferred over those used in figure 3.1 because they simplify the regime diagram. Note that in this regime diagram, 3 of 4 of the regime boundaries will move if the liquid-gas density ratio is changed.

	images	$\langle x_{\mathrm{b}} \rangle$	total	$\mathrm{Re}_{\ell 0}$ range	$\mathrm{We}_{\ell 0}$ range	$\overline{\mathrm{Tu}}_0$ range
Haenlein [Hae32]	24	0	24	2.3×10^0 to 4.2×10^4	1.4×10^2 to 1.4×10^5	—
Ohnesorge [Ohn19]	63	0	63	2.2×10^0 to 6.1×10^4	6.5×10^{-3} to 3.5×10^5	—
Littaye [Lit42, fig. 47]	52	0	52	6.5×10^2 to 6.0×10^3	8.3×10^0 to 9.6×10^2	—
Miesse [Mie55, fig. 8]	66	0	66	0.9×10^4 to 33.4×10^4	5.9×10^3 to 9.6×10^5	—
Ranz [Ran56, pp. 61–62]	0	0	0	—	—	—
Grant and Middleman [GM66]	26	127	132	2.6×10^1 to 4.6×10^4	7.2×10^0 to 1.2×10^5	6.3% to 8.7%
Kusui [Kus69]	0	158	158	2.2×10^4 to 2.3×10^5	2.9×10^3 to 5.1×10^4	6.1% to 12.7%
Sterling and Sleicher [SS75]	0	106	106	1.8×10^2 to 2.4×10^4	4.5×10^0 to 1.3×10^4	—
Torda [Tor73, fig. 14]	12	0	12	2.9×10^2 to 1.4×10^3	5.7×10^1 to 1.7×10^4	—
Reitz [Rei78, pp. 133–137]	67	0	67	3.3×10^0 to 4.8×10^4	3.4×10^3 to 8.4×10^4	—
Wu et al. [WMF95, fig. 7]	110	0	110	6.2×10^2 to 6.2×10^5	—	—
Malot and Dumouchel [MD01]	0	41	41	6.6×10^2 to 3.4×10^3	1.7×10^1 to 9.6×10^4	—
Tang and Masutani [TM03]	75	0	75	1.2×10^0 to 3.2×10^5	1.8×10^{-1} to 2.4×10^4	—
Schillaci et al. [Sch+19]	11	0	11	1.9×10^2 to 2.0×10^3	5.0×10^2 to 1.1×10^5	—
This work	120	1100	1194	1.5×10^1 to 7.3×10^5	2.0×10^0 to 4.1×10^5	4.9% to 12.7%

Table 3.1: Summary of data used to classify regimes in selected studies. "Images" refers to the number of data points where the regimes were determined based on images. Similarly, $\langle x_{\mathrm{b}} \rangle$ refers to the number of data points where the regime was determined from breakup length measurements. Some data points have had regimes determined both ways, so the total does not equal the sum of the two. The remaining columns are the ranges of critical independent variables.

3.3 Issues with previous regime diagrams

Figures 3.1 and 3.2 have many issues, the most significant of which will be detailed in this subsection.

3.3.1 Little data justifying most of the boundaries

The most egregious problem with the most commonly used boundaries as represented in figure 3.2 is how little data they are based on. 3 out of 4 of the regime boundaries in figure 3.2 come from Ranz [Ran56, p. 61]:

$$\text{dripping if} \quad \text{We}_{\ell 0} < 8 \tag{3.1}$$

$$\text{Rayleigh if} \quad \text{We}_{g0} < 0.4 \quad \text{and We}_{\ell 0} > 8 \tag{3.2}$$

$$\text{first wind-induced if} \quad 0.4 < \text{We}_{g0} < 13 \tag{3.3}$$

$$\text{second wind-induced if} \quad 13 < \text{We}_{g0}. \tag{3.4}$$

These boundaries are purely theoretical. There is no comparison of the boundaries against experimental data in Ranz's report — see table 3.1. The derivations are missing from Ranz's report, but they appear to be based on simple scaling arguments using assumed physical mechanisms. Some of these assumptions end up being poor. For example, the assumption that the transition to the second wind-induced regime is caused by the influence of ambient gas is found to be false in § 3.3.3 and § 3.4.10 of this work. (Note that Ranz calls the second wind-induced regime atomization — a distinction between the two regimes was not made until later.) While the accuracy of these boundaries could be worse, they are appreciably less accurate than the new boundaries developed in this work.

3.3.2 The most common atomization regime boundary was miscalculated

The most popular atomization regime boundary criteria is $\text{We}_{g0,\text{crit}} = 40.3$, and this boundary is used in figure 3.2. This boundary was developed from a functional form proposed by Littaye [Lit44] that was fitted by Miesse [Mie55, p. 1697L] to regime data

classified visually. The criteria was not written as $\mathrm{We}_{g0,\mathrm{crit}} = 40.3$ until the work of Reitz [Rei78, p. 8]. As noted by Etzold [Etz19, pp. 77–78], $\mathrm{We}_{g0,\mathrm{crit}} = 40.3$ is inconsistent with Miesse's original criteria, which can be written as $\sqrt{\mathrm{We}_{g0,\mathrm{crit}}/2} = 6.35$, or, $\mathrm{We}_{g0,\mathrm{crit}} = 80.6$. Reitz gives no derivation, but presumably the division by 2 was neglected.

Chigier and Reitz [CR96, p. 113] imply that this criteria was derived in a different way using an alternative regime boundary equation from Miesse [Mie55, p. 1698L]:

$$\mathrm{Oh}_{l0} = 100 \mathrm{Re}_{\ell 0}^{-0.92}. \tag{3.5}$$

Reitz [Rei78] and Chigier and Reitz [CR96] claim this equation is consistent with $\mathrm{We}_{g0,\mathrm{crit}} = 40.3$ because if $\mathrm{We}_{g0,\mathrm{crit}}$ is assumed to be constant then $\mathrm{We}_{g0,\mathrm{crit}} \equiv \rho_\ell \overline{U}_0^2 d_0 / \sigma$ can be rewritten as

$$\mathrm{Oh}_{l0} = \left(\mathrm{We}_{g0,\mathrm{crit}} \frac{\rho_\ell}{\rho_g} \right)^{1/2} \mathrm{Re}_{\ell 0}^{-1}, \tag{3.6}$$

so presumably $100 \approx \sqrt{\mathrm{We}_{g0,\mathrm{crit}}\rho_\ell/\rho_g}$. However, this implies a density ratio of $\rho_\ell/\rho_g \approx 248$, which is inconsistent with Miesse's experiment. Miesse used water in ambient air and liquid nitrogen in air [Mie55, p. 1694L]. Based on the numbers included in Miesse's paper, the density ratio for water in air was $\rho_\ell/\rho_g = 742$ and the density ratio for liquid nitrogen in air was $\rho_\ell/\rho_g = 671$. (Using instead $\mathrm{We}_{g0,\mathrm{crit}} = 80.6$ is even less accurate, implying that $\rho_\ell/\rho_g \approx 124$.) Using the density ratio for water in air returns $\mathrm{We}_{g0,\mathrm{crit}} = 12$. This is more consistent with Ranz [Ran56, p. 61], who proposes that $\mathrm{We}_{g0,\mathrm{crit}} = 13$ as the onset of atomization, although as stated previously, that limit was later associated with the onset of the second wind-induced regime.

In summary, the existing regime boundaries are either based on no data at all, or based on a miscalculation. This situation is unacceptable, and the heavily data-driven regime diagram developed here is intended to remedy this.

3.3.3 Regime names

In this work I use the phrase "turbulent surface breakup" instead of "second wind-

induced"[4], and the phrase "downstream transition" instead of "first wind-induced". The "wind-induced" regime names do not accurately describe the physical mechanisms involved. Many past researchers believe that breakup in these regimes is caused mainly by ambient gas effects [Rei78; LR98; Dum08, p. 376R], but my own analyses cast doubt on these assertions. To be more specific, in the "second wind-induced" (i.e., turbulent surface breakup) regime I find negligible influence of the ambient gas (see § 3.4.10 on the breakup length for the numbers), which makes the "wind-induced" name seem inappropriate. Breakup in this regime appears to be caused by the internal turbulence of the jet. Sallam [Sal02, p. 94] agrees with this assessment. The so-called "first wind-induced" regime appears to at least sometimes have a dependence on the ambient gas, though other factors like turbulence transition and velocity profile relaxation (both possibly influenced by the ambient environment) appear to be factors as well. However, without the second wind-induced regime, a regime called the first wind-induced regime seems misplaced, so I've chosen the name "downstream transition" instead. This name is tentative as I believe there are multiple regimes contained within the downstream transition regime; see § 3.4.6 for details.

3.3.4 Hydrodynamic regime at nozzle outlet

It is important to consider how the hydrodynamic regime (i.e., turbulent vs. laminar) of the flow at the nozzle outlet affects breakup regimes. One would expect turbulence transition to cause a change in the breakup regime. I first realized this after seeing that there was no turbulence transition in the nozzle in the original Ohnesorge diagram, figure 3.1. Based on the data I've compiled, which is limited to jets produced by long pipes, the transition from the downstream transition regime to the turbulent surface breakup regime appears to be caused by turbulence transition in the nozzle. This is most readily seen in the data of Grant and Middleman [GM66, fig. 11, p. 675R], who classified the nozzle outlet flow as laminar or turbulent. Unfortunately, the most popular regime diagram as expressed through figure 3.2 does not distinguish between jets which are turbulent or laminar at the nozzle outlet, despite the clear effects the hydrodynamic regime has on the jet breakup.

---

[4]Following Lightfoot [Lig09] who defines a "surface" mode of breakup that appears here.

In this work the new regime diagram has a critical Reynolds number for the start of transition inside the nozzle, $\text{Re}_{\ell 0,\text{trans}}$, and also a second critical Reynolds number for the establishment of fully turbulent flow inside the nozzle, $\text{Re}_{\ell 0,\text{turb}}$. The numbers used in figures 3.3 and 3.4 are 2300 and 4000, respectively. These will vary from system to system in difficult to predict ways, even for fully developed pipe flows [Mul11]. For simplicity, it is convenient to use a single nozzle critical Reynolds number, $\text{Re}_{\ell 0,\text{turb}}$. Because the nozzle critical Reynolds number can vary greatly, breakup regime diagrams must consider the nozzle critical Reynolds number as a variable. Reviewing the literature on the nozzle critical Reynolds number of nozzles and pipes is prudent. A compilation of values observed in the literature is given in table 3.2 and these values will be discussed. Laminar flows at the outlet of a converging nozzle have been observed at Reynolds numbers two orders of magnitude higher that those seen in pipe flows. For example, Hoyt and Taylor [HT77b, fig. 2] observed laminar flow at the outlet of a converging nozzle at $\text{Re}_{\ell 0} = 2 \times 10^5$. With that being said, the critical Reynolds number for a nozzle flow can be comparable to that of a pipe flow. For example, appreciable turbulence intensities were measured by Lebedev [Leb19] for a nozzle presumably like a diesel injector at Reynolds numbers of about 1×10^3. One can assume the nozzle was rough[5], as Tonkonogiy et al. [Ton+90] shows that the critical Reynolds number of a rough pipe can decrease below that of a smooth pipe:

$$\text{Re}_{\ell 0,\text{turb}} = \min\left[38 \left(\frac{\epsilon}{d_0} \right)^{-0.8} , \sim 2000 \right], \tag{3.7}$$

where ϵ is the height of the roughness elements used inTonkonogiy et al.'s experiments.

The nozzle critical Reynolds number is also a function of the nozzle length. van de Sande and Smith [vdSS76, pp. 220R–221L, eqn. 10][6] conducted experiments and constructed the following empirical regression for the nozzle critical Reynolds number as a

---

[5]Another possibility is that laminar flows could have appreciable turbulence intensities. Despite the name, the "turbulence intensity" is defined for any unsteady flow, not just turbulent flows. However, it seems unlikely that the turbulence intensity would be as high as it is in Lebedev's study.

[6]Note that Lefebvre and McDonell [LM17, p. 34L] introduce a typographical error into their version of this equation, changing the L_0 to a 1.

function of the dimensionless nozzle length L_0/d_0, valid for $1 \leq L_0/d_0 \leq 100$:

$$\mathrm{Re}_{\ell 0,\mathrm{turb}} = 1.2 \times 10^4 \left(\frac{L_0}{d_0}\right)^{-0.3}. \tag{3.8}$$

The contraction ratio of these experiments was very large ($d_\mathrm{in}/d_0 > 150$), so presumably the flow was stabilized due to relaminarization or turbulence reduction in the contraction [NS79; BP54]. With smaller contraction ratios, likely the nozzle critical Reynolds number is lower than implied by equation 3.8. Further, because equation 3.8 is a power law, the calculated nozzle critical Reynolds number will not saturate at large L_0/d_0 as one might expect when the flow becomes fully developed. Consequently, to predict the nozzle critical Reynolds number if the nozzle length is longer than $100d_0$ it is recommended to use $L_0/d_0 = 100$ instead of the actual nozzle length.

As a check on this equation, a regime plot of Wu, Miranda, and Faeth [WMF95, fig. 7] can be used to develop a very approximate nozzle critical Reynolds number equation ($\mathrm{Re}_{\ell 0,\mathrm{turb}} \approx 4.7 \times 10^4 (L_0/d_0)^{-0.22}$) which is similar to equation 3.8. Equation 3.8 is recommended over this latter equation due to the likely better accuracy. One difference is worth noting: Wu, Miranda, and Faeth do not observe turbulence at the nozzle outlet for $L_0/d_0 < 6$, but van de Sande and Smith do. The reason for this difference is unknown, and highlights the difficulty of predicting turbulence transition.

Interestingly, apparently all data in the classic regime study of Ohnesorge [Ohn19] was laminar at the nozzle outlet. This actually has major consequences for the regime diagram, which are discussed in § 3.4.6. It is possible that previous regime diagrams did not distinguish between laminar and turbulent flows because all flows observed were laminar at the nozzle outlet. This is not to say that initially laminar jets will never breakup up due to turbulence. These jets tend to transition to turbulence externally; they are merely *initially* laminar.

Some of the jet breakup data compiled in this work apparently had unusually high nozzle critical Reynolds numbers for pipe flows, i.e., for Sterling and Sleicher [SS75] and Eisenklam and Hooper [EH58], $\mathrm{Re}_{\ell 0,\mathrm{turb}} = O(10^4)$. These studies were neglected for that

reason, as they are inconsistent with other studies. It is not unheard of to have critical Reynolds numbers higher than those typical for pipe flows. Pfenninger [Pfe61] was able to increase $\mathrm{Re}_{\ell 0,\text{turb}}$ to $O(10^5)$ for a pipe by taking care to eliminate flow disturbances. Mullin [Mul11] notes that a high critical Reynolds number is a good measure of the quality of an experimental facility.

3.3.5   Turbulence intensity effects

Reitz [Rei78, p. 9] notes that the conventional regime boundaries do not correctly predict the regime in water jet cutting, where the jets appear to be considerably more stable and consequently in "earlier" regimes than the standard criteria would suggest. Reitz [Rei78, p. 9] attributes these violations to "nozzle geometry effects"[7]. The turbulence intensity can explain this discrepancy, as the turbulence intensity would be lower in cutting water jets than the fuel sprays typically studied. The more recent study of Tafreshi and Pourdeyhimi [TP03] shows another violation of the earlier regime boundaries likely due to turbulence intensity effects.

Existing regime diagrams suffer from poor reproducibility due to neglecting several turbulence related variables like the nozzle critical Reynolds number, jet critical Reynolds number, and turbulence intensity. General regime criteria need to take into account fundamental physics, and not be mere regressions which apply only to particular cases. Consequently, a goal of this work is to include the turbulence intensity as a variable wherever possible.[8]

---

[7]Nozzle geometry effects can not explain all of the discrepancies as changing the fluid can also cause discrepancies.

[8]Of course, turbulence intensity alone is not sufficient to fully characterize the turbulence, but this is a good starting point.

source	nozzle shape	L_0/d_0	d_{in}/d_0	$Re_{\ell 0,turb}$
Ohnesorge [Ohn19]	—	—	—	$> 6.1 \times 10^4$
Pfenninger [Pfe61]	tube, smooth inlet, cond.	246	4	$> 1 \times 10^5$
Grant [Gra65, tab. 5-1]	re-entrant tube	51 to 148	7.0 to 30.7	2.35×10^3 to 2.67×10^3
Lissenburg, Hinze, and Leijdens [LHL75]	tube with obstruction	10 to 40	1	$< 5 \times 10^3$
van de Sande and Smith [vdSS76]	tube with chamfered inlet	1 to 100	> 150	$1.2 \times 10^4 \left(\dfrac{L_0}{d_0}\right)^{-0.3}$
Hoyt and Taylor [HT77b, fig. 2]	conical with tube outlet	0.94	6.5	$> 2 \times 10^5$
Lebedev [Leb19]	"pin nozzle"	—	—	$O(10^3)$
Kent and Brown [KB83]	smooth & sudden inlets, cond.	4	4	$< 1.5 \times 10^4$
Hoyt and Taylor [HT79, noz. I]	convex	~ 0	7.6	$> 2 \times 10^5$
Tonkonogiy et al. [Ton+90]	rough tube	140 to 280	—	$\min\left[38\left(\dfrac{\epsilon}{d_0}\right)^{-0.8}, \sim 2000\right]$
Wu, Miranda, and Faeth [WMF95]	tube with smooth inlet	6 to 156	> 100	$\sim 4.7 \times 10^4 \left(\dfrac{L_0}{d_0}\right)^{-0.22}$

Table 3.2: Various critical Reynolds numbers for nozzles (and some pipes) from the literature in chronological order. Em-dashes mean that the values are unclear. ϵ is the height of the roughness elements in the pipe. If the source distinguished between when laminar flow ended and when turbulent flow became fully established, when turbulence was fully established was chosen. "Cond." refers to the use of flow conditioners upstream of the nozzle/pipe.

3.3.6 Qualitative vs. quantitative classification

As previously mentioned, regimes are typically defined in qualitative ways based on images or vague descriptions (e.g., see the appearance column of table 3.3). This is particularly problematic for the atomization regime, as it's superficially similar to the turbulent surface breakup regime, just more vigorous in some sense. Consequently, I use quantitative criteria to determine the regimes based on breakup length in table 3.3 (discussed earlier as well). In this work I also unify the visual and breakup length regimes so that each "breakup length" regime has an associated appearance. However, it may not be always possible to go the other direction, from the appearance to the regime, due to ambiguities in the appearance. Note that the choice of the breakup length as the quantity of interest does not imply that the breakup length is superior to other quantities for the purposes of classifying regimes — the breakup length merely is ubiquitous in the literature.

The next problem is partly caused by the superficiality of qualitative regime determination.

3.3.7 A missing regime and the varying regime progression

When a liquid jet is in the Rayleigh regime and the velocity is increased (all else equal), convention stipulates that the jet will eventually enter the downstream transition regime (again, previously called the first wind-induced regime). This is not necessarily true. The "regime progression" — that is, how the regimes change as the jet velocity increases — is not universal.

While the majority of jets previously studied will enter the downstream transition regime after "the" Rayleigh regime, some researchers have identified a *turbulent Rayleigh* regime that is different from the conventional *laminar Rayleigh* regime (see figure 3.5) and can follow the laminar Rayleigh regime instead of the downstream transition regime [AB51; Phi73; Laf+74; Phi75; vdSS76; SA81; MC94a; SDF02]. This regime is missing from the conventional Ohnesorge diagram. The turbulent Rayleigh regime is sometimes superficially visually similar to the downstream transition regime. The downstream transition regime

takes various forms — see figures 3.6 through 3.8. Compare figure 3.6, a jet early in the downstream transition regime, against figure 3.9, a jet in the turbulent Rayleigh regime. The two regimes appear to be visually similar to the laminar Rayleigh regime, although less regular.

However, the breakup length decreases as velocity increases in the downstream transition regime, but increases as velocity increases in the turbulent Rayleigh regime. Typically, the first wind-induced regime is defined as having a decreasing breakup length, e.g., by Reitz [Rei78, fig. 1.1] and Dumouchel [Dum08, fig. 1]. Many studies have examined the first peak in the breakup length curve, motivated by the downstream transition regime; see Dumouchel [Dum08, pp. 376–379] for a review of these studies. However, the breakup length can also peak due to turbulence transition in the nozzle ($\mathrm{Re}_{\ell 0} > \mathrm{Re}_{\ell 0,\mathrm{trans}}$). And once turbulent flow is established, the breakup length then will increase roughly proportional to $\mathrm{We}_{\ell 0}^{1/2} + 3\mathrm{We}_{\ell 0}/\mathrm{Re}_{\ell 0}$, just like in the laminar Rayleigh regime, albeit with a lower constant of proportionality — see § 3.4.8. As such, I define the downstream transition regime as laminar at the nozzle outlet, in contrast to previous researchers like Reitz [Rei78, p. 24]. The data compilation detailed in this work shows that the downstream transition regime only appears when the flow is laminar at the nozzle outlet.

Conflating the downstream transition and turbulent Rayleigh regimes is not uncommon. For example, Reitz [Rei78, pp. 24–25] suggests that the experiments of Phinney [Phi73] are in the downstream transition regime, but these experiments are actually largely in the turbulent Rayleigh regime. Similarly, Dumouchel [Dum08, p. 378] does not consider the turbulent Rayleigh regime as a possibility, rather, the downstream transition boundary Dumouchel uses in effect differentiates between the turbulent Rayleigh and downstream transition regimes.

The existence of the turbulent Rayleigh regime is just one example of how the regime progression is not universal. Examine the three diagonal lines in figure 3.4. The middle line is the "conventional" case, that is, where the jet transitions from the (laminar) Rayleigh regime to the downstream transition regime, then to the turbulent surface breakup regime (shown in figure 3.10), and then to the atomization regime. The trends in the breakup

length for this case are shown in figure 3.14. The "conventional" case is only one of several possibilities. A larger pipe nozzle with a low viscosity and high surface tension liquid (i.e., water) follows the path shown by the upper diagonal line in figure 3.4. This case never enters the downstream transition regime, as seen in figure 3.15. A more typical case is that seen for a lower surface tension liquid like gasoline with a smaller nozzle, corresponding to the lower diagonal line. This case, which is typical for fuel sprays, never enters the turbulent surface breakup regime, as seen in figure 3.16.

Another way in which the regime progression is not universal comes through the influence of the nozzle critical Reynolds number. This has been recognized by previous researchers. Eisenklam and Hooper [EH58, fig. 14] noticed that if they add a turbulence trip inside of their nozzle, they can avoid what they called "bursting breakup", which is a particularly violent form of breakup in the downstream transition regime (see figure 3.7 for an example). Similarly, Hoyt and Taylor [HT85] suggest moving turbulence transition inside of the nozzle, or in other words, decreasing the nozzle critical Reynolds number, to avoid very vigorous breakup (identical to "bursting breakup") apparently caused by external turbulence transition.

3.3.8 Breakup onset location in atomization

The atomization regime is sometimes defined as when the breakup onset location is very small, indistinguishable from zero [RB86, p. 235; LR98, p. 88, fig. 1]. This definition is unsatisfactory as the breakup onset location can also be small in the turbulent surface breakup regime. The breakup onset location theory in chapter 5 applies to both the turbulent surface breakup and atomization regimes. Consequently, I define the atomization regime based on more obvious quantitative criteria: the breakup length curve. I define the turbulent surface breakup regime as having an increasing power law behavior in the breakup length as a function of $We_{\ell 0}$ (i.e., $\langle x_b \rangle / d_0 \propto We_{\ell 0}^{1/3}$), and the atomization regime is defined as a plateau as $We_{\ell 0}$ increases, with all else constant and neglecting cavitation and compressibility effects (to be discussed in § 3.4.11).

3.3.9 Problems with other regime diagrams

Wu and Faeth [WF93] suggests that $\rho_\ell/\rho_g < 500$ is a reasonable criteria for the onset of aerodynamic effects, in this work called the atomization regime. Magnotti [Mag17] later suggested that $\rho_\ell/\rho_g < 300$ is a more accurate criteria for the onset of aerodynamic effects. Purely density ratio based criteria are not accurate, as increasing the bulk velocity alone can change the regime from turbulent surface breakup to atomization [Kus69; SDF02]. The differences in the boundaries observed by Wu and Faeth and Magnotti likely could be attributed to differences in the Weber numbers and turbulence intensities.[9]

Reitz developed a criteria for the onset of the atomization regime which is claimed to consider the effects of nozzle geometry [LR98, pp. 93–94]. The criteria uses a regression for a model parameter based on Reitz's experiments. The only nozzle geometric parameter used was the nozzle length-to-diameter ratio, L_0/d_0. This neglects the large impact that the contraction ratio d_{in}/d_0 can have as discussed in § 3.3.4. Rather than using nozzle geometry, the model would generalize better if nozzle outlet turbulence intensity and nozzle critical Reynolds number were used (and be further improved by the inclusion of other variables like the velocity profile, etc.).

---

[9]Wu and Faeth [WF93] and Magnotti [Mag17] also consider different types of atomization. This work does not examine the different types of atomization as the experiments in this dissertation were not conducted in the atomization regime.

new regime name	old regime name	$\langle x_{\mathrm{b}}\rangle/d_0$	D_{32}	appearance
dripping	dripping	$\underset{\sim}{\propto}\left(\dfrac{\mathrm{Fr}_0}{\mathrm{We}_{\ell 0}}\right)^{1/3}$	$O(d_0)$	slow formation of droplets at the nozzle outlet
laminar Rayleigh	Rayleigh	$\propto \mathrm{We}_{\ell 0}^{1/2} + 3\dfrac{\mathrm{We}_{\ell 0}}{\mathrm{Re}_{\underline{\ell 0}}}$	$O(d_0)$	symmetric breakup into large droplets
downstream transition	first wind-induced	decreasing with $\overline{U}_0$	varies	varies from Rayleigh-like to abrupt breakup
turbulent Rayleigh	—	$\propto \mathrm{We}_{\ell 0}^{1/2} + 3\dfrac{\mathrm{We}_{\ell 0}}{\mathrm{Re}_{\ell 0}}$	$O(d_0)$	similar to laminar Rayleigh, but turbulent
turbulent surface breakup	second wind-induced	$\underset{\sim}{\propto} \mathrm{We}_{\ell 0}^{1/3}$	$< d_0$	small surface disturbances causing breakup
(turbulent) atomization	atomization	$\underset{\sim}{\propto}\left(\dfrac{\rho_\ell}{\rho_{\mathrm{g}}}\right)^{C_\rho}$	$\ll d_0$	larger spray angle than turbulent surface breakup

Table 3.3: Summary of new regime names, old regime names, and the basic properties of each regime. Regimes which have names that start with "laminar" are laminar at the nozzle outlet, correspondingly, regimes which have names that start with "turbulent' are turbulent at the nozzle outlet.

3.4 Proposed regime diagram and information on each regime

Figure 3.3 is the proposed regime diagram. A sample of data for high liquid-gas density ratios and smooth pipe nozzles is shown in figure 3.4 to give a sense for how well these boundaries fit the data. In contrast with figure 3.3, which is for constant turbulence intensity, in figure 3.4 the turbulence intensity is a function of the Reynolds number, which is why some of the regime boundaries are not straight lines as they are in figure 3.3.

Individual regime boundaries were developed in various ways, using all data available for that boundary (i.e., not only high density ratio data as in figure 3.3), as described in the corresponding section for that boundary.

A warning: The proposed regime diagram is not meant to be used as presented to determine the regime. It is a *schematic* used to organize knowledge about the regimes. Regime determination is best done with the empirical equations developed in this work for each regime boundary. This is because the regime boundaries will move depending on the configuration. Figure 3.3 is only appropriate for pipe nozzles at high liquid-gas density ratios. Additionally, this regime diagram is not expected to be perfectly accurate, so engineers should check its prediction against the behavior of the jet (visual description and/or breakup length trend) to confirm the prediction.

3.4.1 Data compilation

The proposed regime diagram is based on a compilation of data available at GitHub [Tre20b]. The GitHub repository will contain the latest data, regime diagrams, and regressions as this data compilation is updated in the future. The description and motivations of the data compilation are described in detail in chapter 4 and will only be briefly described here. This data compilation uses "pipe jet" data, where the nozzle is simply a long pipe. Pipe jets were chosen for their ubiquity in the literature, their high reproducibility (due to fully developed flows being a universal state), and because the turbulence intensity can be determined for pipes given the friction factor. Data from 22 studies was compiled [AB51; BC55; EH58; CD64; Rup62; GM66; Kus69; PH70; Phi73;

Figure 3.3: Schematic regime diagram at low ambient densities *for illustration purposes only*. Do not use this plot to determine the regime. Regime boundaries are very approximate and apply only for a special case. More general regime boundary equations are given in the text. The nozzle critical Reynolds number will typically be an order of magnitude or more higher than in this plot, which is based on long pipe nozzles (fully developed pipe flow) that have atypically low critical Reynolds numbers — see table 3.2. Constant high density ratio ($\rho_\ell/\rho_g = 1000/1.2$) corresponding approximately to water-air at standard temperature and pressure. The dripping boundary is also for water-air systems. Turbulence intensity is 5%. Turbulent regime boundaries should vary with Reynolds number in a smooth pipe due to variation of turbulence intensity with the Reynolds number — see figure 3.4.

Figure 3.4: Regime diagram for smooth pipe nozzles with data and example lines showing the regime progression for three different cases. Transitional regimes removed for clarity. Data from Eisenklam and Hooper [EH58] and Sterling and Sleicher [SS75] removed due to abnormally high nozzle critical Reynolds numbers. 564 data points. In contrast with figure 3.3, the turbulence intensity is now a function of the Reynolds number (as is the case for a smooth pipe flow), and consequently the turbulent regime boundaries vary with Reynolds number. High density ratio data only ($\rho_\ell/\rho_g > 500$). Atomization regime boundary for $\rho_\ell/\rho_g = 1000/1.2$. Dripping regime boundary for n-dodecane.
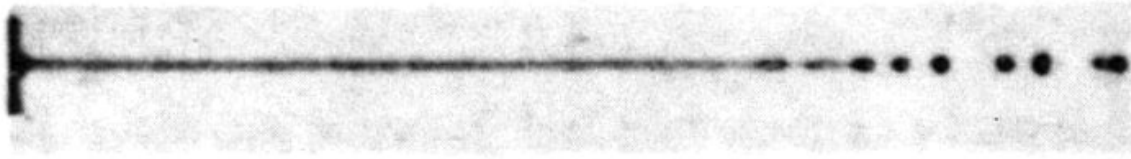
Figure 3.5: Image of a water jet in the laminar Rayleigh regime from Asset and Bales [AB51, fig. 1]. Note the breakup is caused by disturbances symmetric to the jet axis. Flow is from left to right. (Public domain image.)
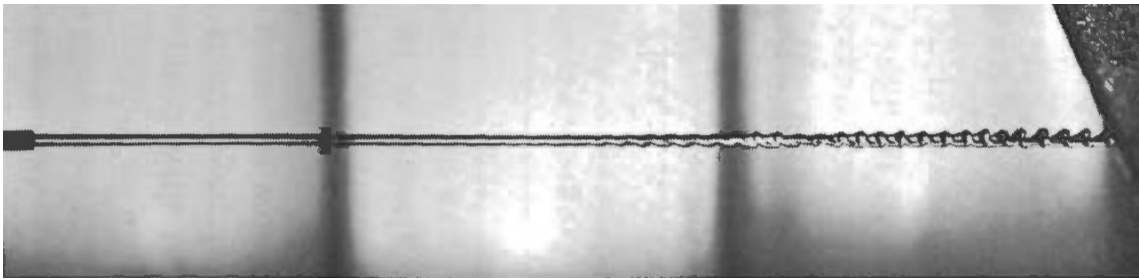
Figure 3.6: Image of a water jet early in the downstream transition regime from Rupe [Rup62, fig. 4c]. Flow is from left to right. (Image used under license.)
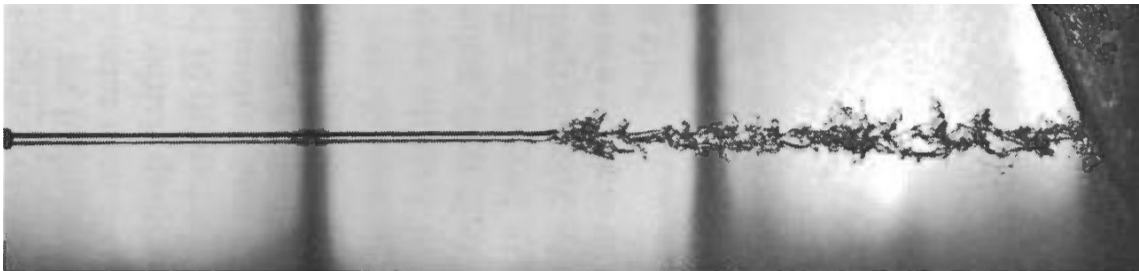
Figure 3.7: Image of a water jet late in the downstream transition regime from Rupe [Rup62, fig. 4d] which is atomization-like. Note that the breakup is much more vigorous than that seen in figure 3.6. Flow is from left to right. (Image used under license.)
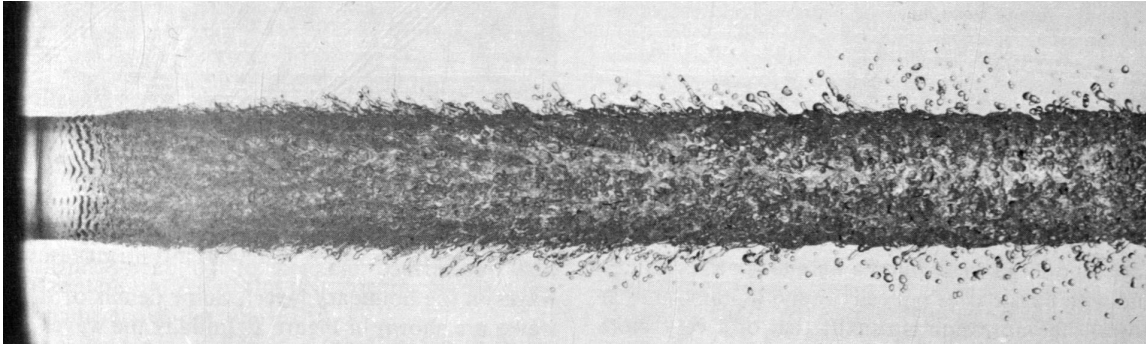
Figure 3.8: Image of a water jet in the downstream transition regime from Hoyt and Taylor [HT82, fig. 1]. Flow is from left to right. Here the breakup is more vigorous than that seen in figure 3.6, but less vigorous than figure 3.7. This jet is in a regime similar to the turbulent surface breakup regime. Unlike the other images, which use pipe nozzles, this for a nozzle with a length-to-diameter ratio (L_0/d_0) of 1. (Public domain image.)
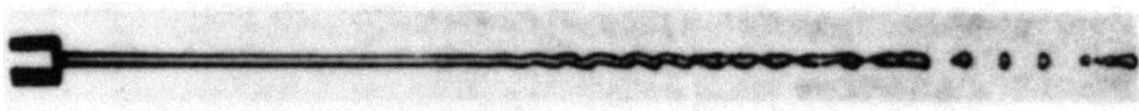
Figure 3.9: Image of a water jet in the turbulent Rayleigh regime from Asset and Bales [AB51, fig. 10]. Flow is from left to right. (Public domain image.)
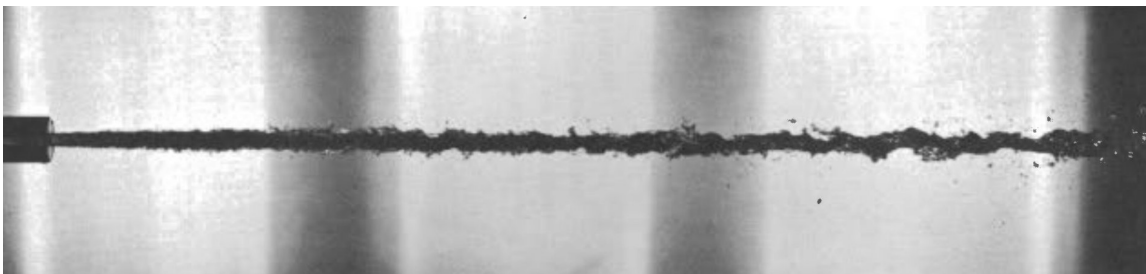
Figure 3.10: Image of a water jet in the turbulent surface breakup regime from Rupe [Rup62, fig. 15c]. Flow is from left to right. (Image used under license.)
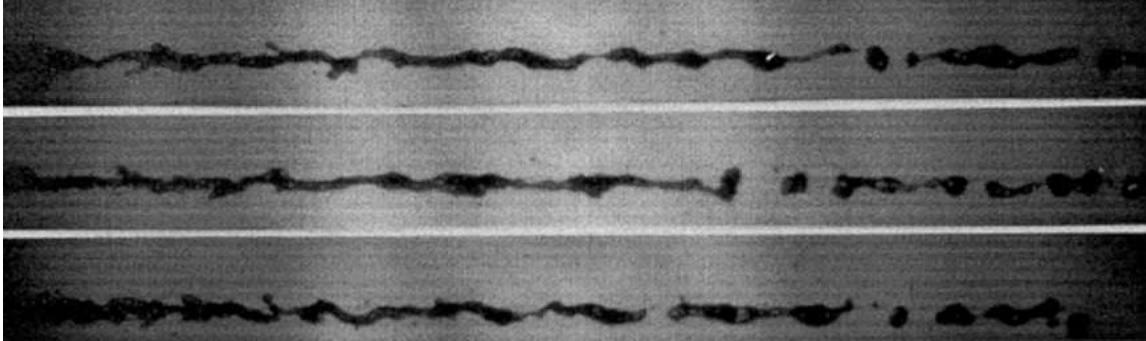
Figure 3.11: Downstream (near breakup length) image of a water jet in the turbulent surface breakup regime from Sallam, Dai, and Faeth [SDF02, fig. 3]. Flow is from left to right.
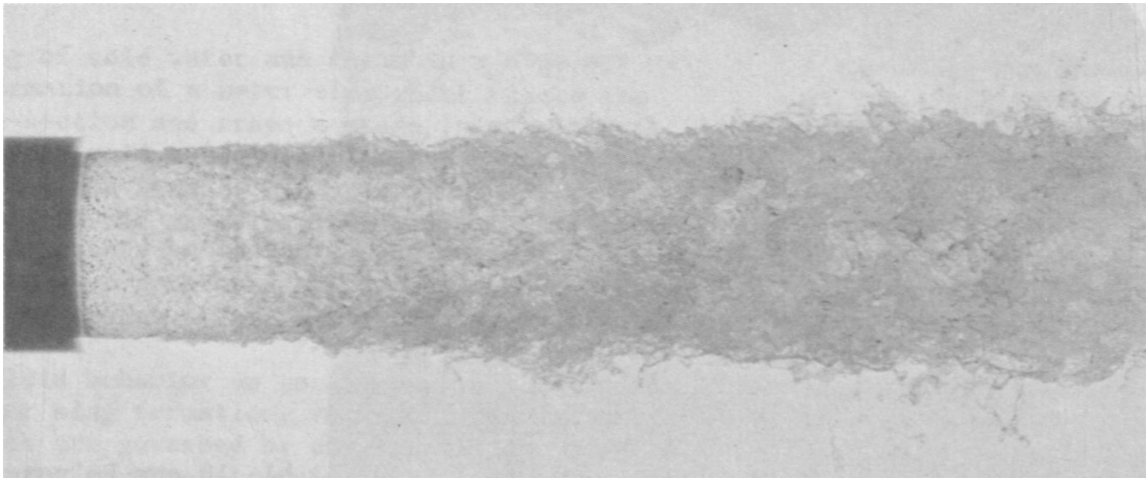
Figure 3.12: Near-nozzle image of a water jet believed to be in the atomization regime from Hoyt and Taylor [HT80, fig. 1a]. Flow is from left to right. Note the similarity to figure 3.10; determining if a jet is in the turbulent surface breakup or atomization regime based on visual characteristics alone is challenging. (Reprinted by license from the American Society of Mechanical Engineers.)
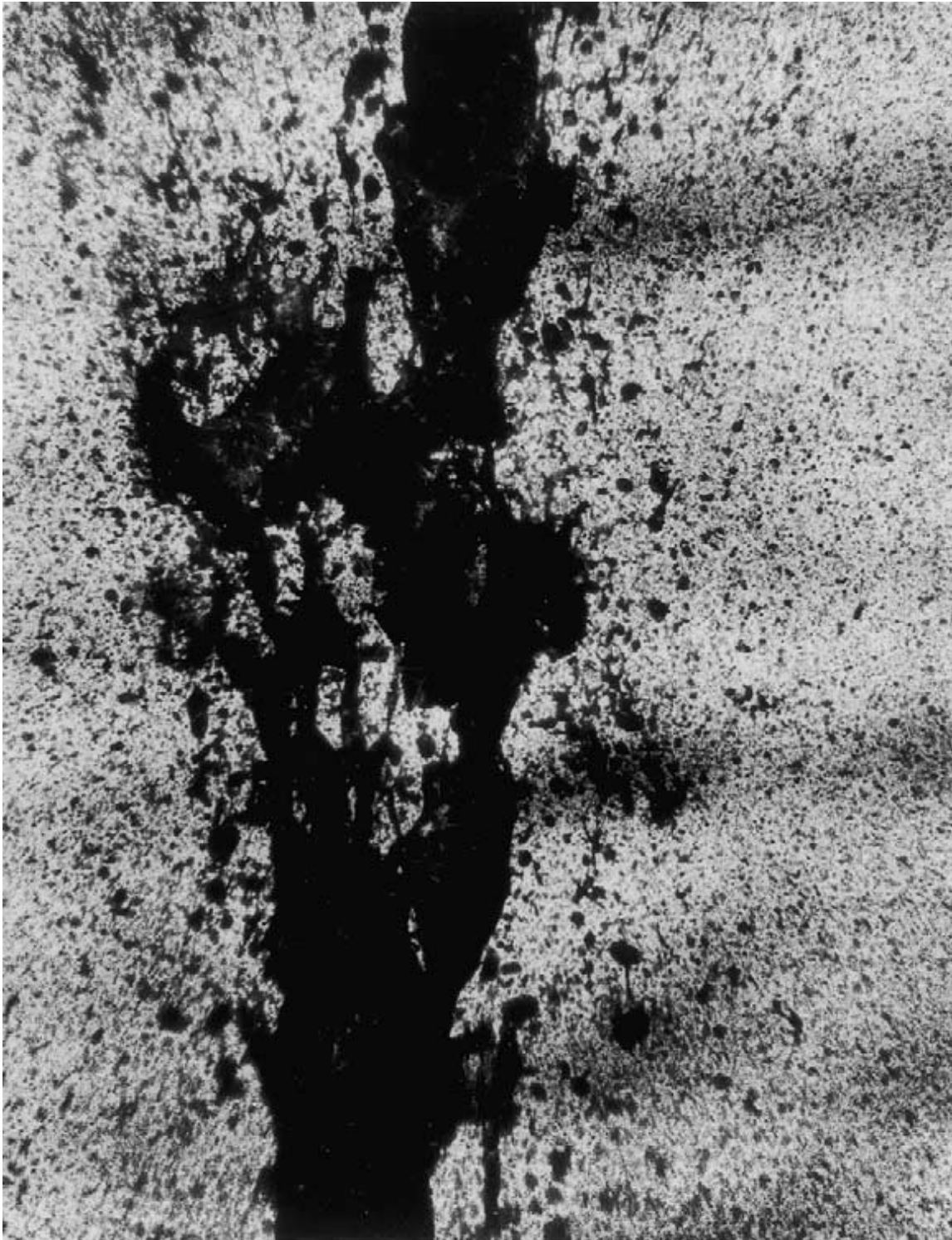
Figure 3.13: Downstream image of a water jet in the atomization regime from Sallam, Dai, and Faeth [SDF02, fig. 6]. Flow is from bottom to top.
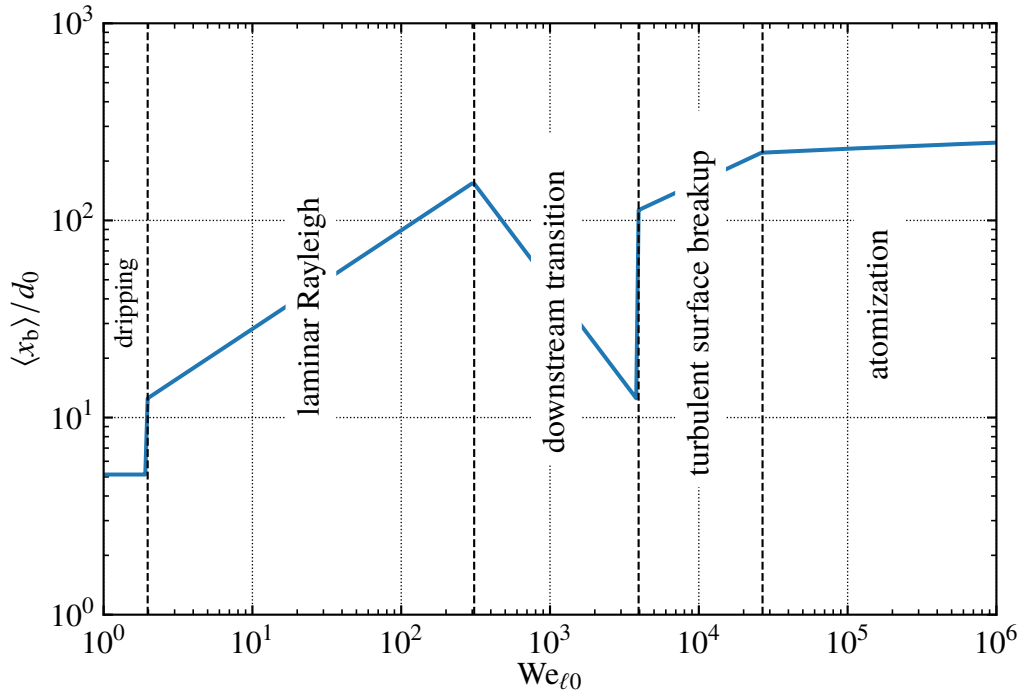
Figure 3.14: *Schematic* "stability curve" for the "conventional" pipe nozzle case in figure 3.4 (center diagonal line). Pure isopropyl alcohol for pipe nozzle with $d_0 = 1$ mm. Regressions for the breakup length $\langle x_b \rangle$ from the text are used in each marked regime above. Breakup lengths for the downstream transition regime are approximate, and the real stability curve will be smoother. Note that like in figure 3.4, the turbulence intensity $\overline{\mathrm{Tu}}_0$ and Reynolds number $\mathrm{Re}_{\ell 0}$ are changing as the Weber number $\mathrm{We}_{\ell 0}$ changes.
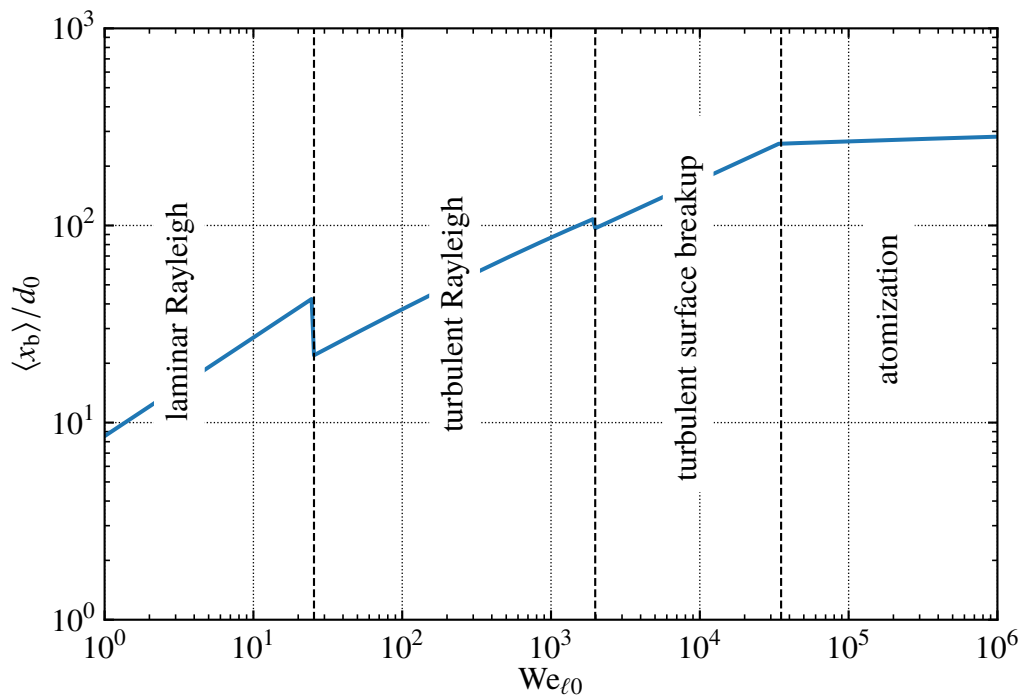
Figure 3.15: *Schematic* "stability curve" for the pipe nozzle $d_0 = 6$ mm, water case in figure 3.4 (top diagonal line). See figure 3.14 for details.
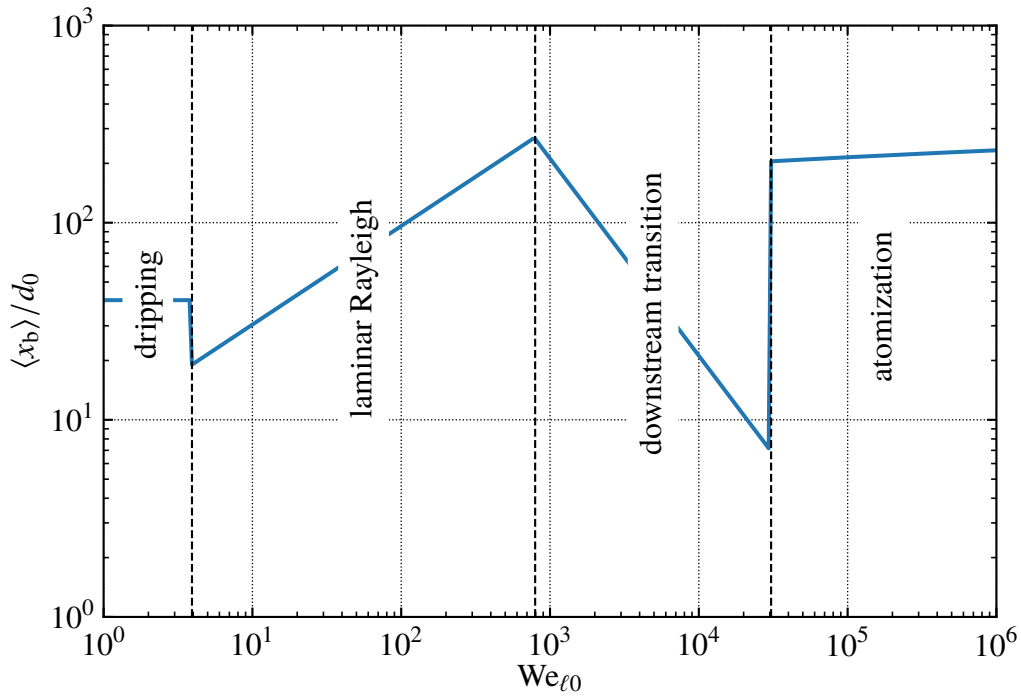
Figure 3.16: *Schematic* "stability curve" for the pipe nozzle $d_0 = 50$ μm, *n*-dodecane (similar to gasoline engine nozzle but with a lower $\mathrm{Re}_{\ell 0,\mathrm{turb}}$) case in figure 3.4 (bottom diagonal line). In an actual engine nozzle, the same regime progression will be seen as the order is preserved if the nozzle critical Reynolds number is increased. See figure 3.14 for other details.

Phi75; SS75; HT80; HT85; KM89b; Wu+83; SAH84; ASH85; Ruf90; WTF92; MC94a; SDF02]. To be clear, about 98.5% of the data in this compilation comes from the open literature and is not new to this work.

To limit the scope of the data compilation, only data where $\rho_\ell/\rho_\mathrm{g} > 1$ was included in the data compilation. It is likely that the regime diagram is appreciably different at low density ratios — the turbulent surface breakup regime for instance might completely cease to exist as the critical Weber number for atomization decreases with the density ratio.

3.4.2 Regimes and their physical mechanisms

More detailed descriptions and analysis of each regime follows, going from left to right in figure 3.3, starting with the regimes with flows that are laminar at the nozzle outlet and following with the regimes with flows that are turbulent at the nozzle outlet.

When applicable, regressions for the breakup length and other quantities of interest will be presented. In forthcoming chapters, I'll describe the data analysis and compilation process in detail, including information about the choice of the functional forms for the regressions (dimensional analysis, theory), and the philosophy and limitations of the data compilation process.

3.4.3 Dripping regime and transition to jetting

Grant and Middleman [GM66, fig. 1], McCarthy and Molloy [MM74, fig. 2], Dumouchel [Dum08, fig. 1], and Lefebvre and McDonell [LM17, fig. 2.13] suggest that the breakup length in the dripping regime increases considerably with velocity. This seems unlikely. While the breakup length has not been measured in the dripping regime to my knowledge, presumably it is roughly proportional to the droplet diameter. Assuming that the nozzle is very thin, the simple theory of Tate as described by Clanet and Lasheras [CL99, p. 308] suggests that approximately

$$D \propto \left(\frac{\sigma d_0}{\rho_\ell g}\right)^{1/3}.$$ (3.9)

If $\langle x_b \rangle \propto D$ in the dripping regime, then we might expect

$$\frac{\langle x_b \rangle}{d_0} \propto \left(\frac{\sigma}{\rho_\ell g d_0^2} \right)^{1/3} = \left(\frac{\mathrm{Fr}_0}{\mathrm{We}_{\ell 0}} \right)^{1/3}, \tag{3.10}$$

which does not vary with jet bulk velocity, $\overline{U}_0$. Possibly other effects will change this result, but likely the breakup length varies little with the jet bulk velocity in the dripping regime.

The transition from dripping to "jetting" (laminar Rayleigh regime) has been studied extensively in the past. Clanet and Lasheras [CL99] develop the following regime boundary for the end of dripping based on their theory and validate it with an extensive series of experiments:

$$\mathrm{We}_{\ell 0,\mathrm{crit}} = 4\frac{\mathrm{Bo}_{\mathrm{outer}}}{\mathrm{Bo}} \left[1 + K\mathrm{Bo}\mathrm{Bo}_{\mathrm{outer}} - ((1 + K\mathrm{Bo}\mathrm{Bo}_{\mathrm{outer}})^2 - 1)^{1/2} \right]^2, \tag{3.11}$$

where $\mathrm{Bo}^2 \equiv \rho_\ell g d_0^2/(2\sigma)$ and $\mathrm{Bo}_{\mathrm{outer}}^2 \equiv \rho_\ell g d_{\mathrm{outer}}^2/(2\sigma)$ define the Bond numbers for the inside and outside of the nozzle outlet (d_{outer} is the outer diameter), respectively, and K is a constant which equals 0.37 for water injected into air.

Equation 3.11 is plotted in figures 3.3 and 3.4 for water and n-dodecane, respectively, with $d_{\mathrm{outer}} = d_0$. Note that while Clanet and Lasheras's theory is valid in the high Reynolds number limit only, it is possible to calculate a Bond number consistent with the Reynolds and Weber numbers, as was done in these plots.

3.4.4 Laminar Rayleigh regime

A jet in the laminar Rayleigh regime is shown in figure 3.5. Weber's theory accurately describes the breakup of jets in this regime. To reiterate, the equation for the breakup length in Weber's theory is

$$\frac{\langle x_b \rangle}{d_0} = C_{\mathrm{LR}} \left(\mathrm{We}_{\ell 0}^{1/2} + 3\frac{\mathrm{We}_{\ell 0}}{\mathrm{Re}_{\ell 0}} \right). \tag{2.12}$$

The term C_{LR} is an empirical coefficient that applies only for the laminar Rayleigh case. In the turbulent Rayleigh case the notation C_{TR} will be used.

Based on limited data from Haenlein [Hae32], Weber [Web19, p. 24] recommends $C_{\mathrm{LR}} = 12$ for the laminar Rayleigh regime. Grant and Middleman [GM66, p. 673L] state that $C_{\mathrm{LR}} = 13.4$ fits their data better. Grant and Middleman further suggest that C_{LR} is a function of $\mathrm{Oh}_{\ell 0}$. However, Kroesser and Middleman [KM69, p. 385L] note that the variation in C_{LR} as a function of $\mathrm{Oh}_{\ell 0}$ is "so weak that it probably does not warrant detailed investigation". Along those lines, fitting data from multiple studies compiled in this work returns $C_{\mathrm{LR}} = 8.51$ (247 points, $R^2 = 0.942$). A comparison of the available data to the regression is in figure 3.17.

Weber's theory predicts that the size of the droplets in this regime is

$$D = \left(\frac{3\sqrt{2}}{2} \pi \sqrt{1 + 3\mathrm{Oh}_{\ell 0}} \right)^{1/3} d_0, \tag{2.11}$$

and this equation is generally regarded as accurate when satellite droplets are negligible.

3.4.5 Transition to the downstream transition regime

The conventional explanation for why the laminar Rayleigh regime ends and the downstream transition regime begins is that aerodynamic forces become significant in the downstream transition regime, however, this is only one of several possibilities as will be explained. Early models of the aerodynamic effects variety were developed by Weber [Web19] and Sterling and Sleicher [SS75]. A recent popular approach is by Dumouchel and co-workers, based around the idea that the transition to the downstream transition regime (and the turbulent Rayleigh regime) can be found through the use of an ad hoc effective gas density, ρ_{g}^* [Dum08, p. 378]. Malot and Dumouchel [MD01, p. 231] admit that there is no theoretical justification for ρ_{g}^* at the time of writing. The ρ_{g}^* approach is essentially empirical and does not apply beyond the cases tested. A more general approach is needed.

Suppose that transition to turbulence on the jet itself (rather than in the nozzle) causes the regime change. Working from that hypothesis, a simple model that fits the available pipe jet data can be derived. I'll start with the assumption that the jet transitions to turbulence when a critical Re_x value is reached, where x is the axial distance from the

69
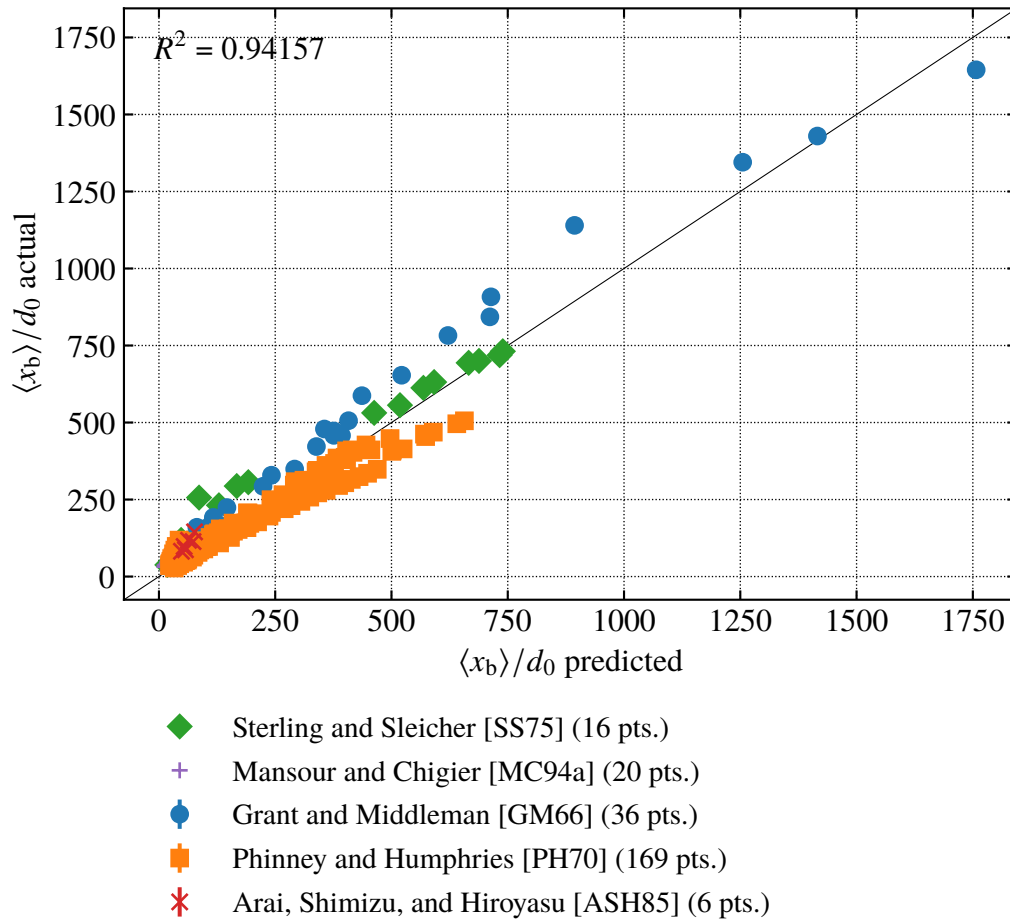
Figure 3.17: Comparison of the laminar Rayleigh breakup length estimated from equation 2.12 with $C_{\mathrm{LR}} = 8.51$ against experimental data.

nozzle — see figure 2.1. This suggests that the jet critical Reynolds number is

$$\mathrm{Re}_{\ell x,\mathrm{trans}} \equiv \frac{\overline{U}_0 x_{\mathrm{trans}}}{\nu_\ell}, \tag{3.12}$$

where x_{trans} is the location of transition. Critical Reynolds number models of transition distance are fairly primitive, but they are simple and to my knowledge they have not been used previously in jet breakup. Note that the *jet* critical Reynolds number differs from the *nozzle* critical Reynolds number, $\mathrm{Re}_{\ell 0,\mathrm{turb}}$. This jet critical Reynolds number presumably is influenced by disturbances present as the jet leaves the nozzle[10], the jet velocity profile, and the ambient gas, and for these reasons the model coefficients used here are not expected to be correct aside from the limiting case of pipe jets with high liquid-gas density ratios (high $\rho_\ell/\rho_\mathrm{g}$). It is also likely that factors which increase the nozzle critical Reynolds number, like reducing flow disturbances, also increase the jet critical Reynolds number.

Transition does not occur in the laminar Rayleigh case, so there $x_{\mathrm{trans}} > \langle x_\mathrm{b} \rangle_{\mathrm{LR}}$. When transition does occur, obviously $x_{\mathrm{trans}} < \langle x_\mathrm{b} \rangle_{\mathrm{LR}}$. The boundary between the laminar Rayleigh and downstream transition cases occurs *roughly* when the breakup length and the transition length are equal: $x_{\mathrm{trans}} = \langle x_\mathrm{b} \rangle_{\mathrm{LR}}$. This is only an approximate criteria for reasons which will be mentioned shortly. Using equation 2.12 for $\langle x_\mathrm{b} \rangle_{\mathrm{LR}}$, writing $x_{\mathrm{trans}} = \langle x_\mathrm{b} \rangle_{\mathrm{LR}}$ returns

$$\frac{\nu_\ell \mathrm{Re}_{\ell x,\mathrm{trans}}}{\overline{U}_0} = d_0 \cdot C_{\mathrm{LR}} \left(\mathrm{We}_{\ell 0}^{1/2} + 3 \frac{\mathrm{We}_{\ell 0}}{\mathrm{Re}_{\ell 0,\mathrm{crit}}} \right), \tag{3.13}$$

which can be rewritten as

$$\mathrm{Re}_{\ell 0,\mathrm{crit}} = \frac{\mathrm{Re}_{\ell x,\mathrm{trans}} - 3 C_{\mathrm{LR}} \mathrm{We}_{\ell 0}}{C_{\mathrm{LR}} \mathrm{We}_{\ell 0}^{1/2}}. \tag{3.14}$$

The jet critical Reynolds number $\mathrm{Re}_{\ell x,\mathrm{trans}}$ can be found in two different ways. The first is by measuring the transition distance on images, which returns $\mathrm{Re}_{\ell x,\mathrm{trans}} = 7.16 \times 10^4$ using 8 data points [Rup62; Gra65], with a range of 5.61×10^4 to 9.75×10^4. The second is by

---

[10]As mentioned in a footnote in § 3.3.4, even laminar jets have fluctuations, whose strength could presumably be measured with a turbulence intensity.

finding the implied value of $\mathrm{Re}_{\ell x,\mathrm{trans}}$ from equation 3.14, calculated for all data points in the compilation marked as in transition between the laminar Rayleigh and downstream transition regimes. The latter suggests that $\mathrm{Re}_{\ell x,\mathrm{trans}} = 1.75 \times 10^5$ using 79 data points [Gra65; PH70; Phi73; ASH85], with a range of 4.75×10^4 to 7.18×10^5.

While the two estimates differ by a factor of 2.44, there is broad overlap between their distributions. Consequently, the idea of a jet critical Reynolds number determining the regime transition is not discounted by the data. Additionally, the data compilation classifies each data point by breakup length trend, not the appearance of transition waves. The two are similar but not identical, and this is why $x_{\mathrm{trans}} = \langle x_{\mathrm{b}} \rangle_{\mathrm{LR}}$ is only approximate. When turbulence transition begins downstream (i.e., beyond $x_{\mathrm{trans}} = \langle x_{\mathrm{b}} \rangle_{\mathrm{LR}}$), the breakup length does not immediately start decreasing as velocity increases. In fact, with increasing velocity, all else equal, the breakup length will often continue to increase as the velocity increases before starting to decrease. Therefore, one should expect that the implied jet critical Reynolds number would be higher than the actual jet critical Reynolds number, as is observed. More advanced theories than that developed in this work could in principle determine where the breakup length peak occurs rather than where downstream turbulence transition occurs. Given that the implied jet critical Reynolds number has an order of magnitude more data and fits the regime data better, it is used in this work.

Equation 3.14 is plotted in figures 3.3 and 3.4. When the transition length x_{trans} is very large, it is unlikely that breakup will be observed in many applications, so despite the jet being strictly in the "downstream transition" regime it will appear to be in the laminar Rayleigh regime. For this reason, a line is drawn in the regime diagrams corresponding to when the transition length is 1000 nozzle diameters. Below that line the curve for the onset of the downstream transition regime is drawn lighter as the downstream transition regime will not be easily observed there.

3.4.6 Downstream transition regime

The defining qualitative (visual) characteristic of the downstream transition regime in this work is the flow (or at least the free surface) being laminar at the nozzle outlet,

transitioning to turbulence downstream. The defining quantitative characteristic for the downstream transition regime is the breakup length decreasing as the velocity increases. All images with breakup length data in the data compilation are consistent with these definitions — the caveat mentioned in § 3.4.5 does not appear in the present photos. While future work is needed, to the best of my knowledge for pipe jets the decrease in the breakup length coincides with downstream transition to turbulence.[11]

One non-obvious consequence of this categorization is that apparently none of the data of Ohnesorge (again, who made the earliest regime diagram) is strictly in the turbulent surface breakup or atomization regimes now. Describing breakup at the highest velocities tested, Ohnesorge [Ohn19, p. 4] states (translated into English) "The atomization process III starts suddenly. The jet shows a smooth surface in the immediate vicinity of the nozzle outlet with axisymmetric swellings, which degenerate into helical transverse displacements of increasing amplitude." Presumably the "smooth surface" refers to an initially laminar flow. The images provided in the journal article lack the resolution to show that the jet was initially laminar, so we only have Ohnesorge's word that the jet was initially laminar. Some recent DNS studies may confirm that the flow at the outlet of a fuel spray nozzle (presumably like the nozzle Ohnesorge used) is laminar [AT18, fig. 3; Tru+18, fig. 4], however, this could be an artifact of not specifying turbulent inflow boundary conditions, as neither paper discusses whether turbulence was injected into the computational domain at the inflows.

Note that just because the flow is initially laminar does not mean that the breakup is not vigorous. On the contrary, as Hoyt and Taylor [HT85] note, liquid jet flows which are initially laminar but transition downstream can have particularly vigorous breakup. Indeed, as can be seen in figures 3.14 and 3.16, the breakup length in the downstream transition regime can be lower than in the atomization regime. But not all downstream transition regime breakup is as vigorous. I propose that the "downstream transition regime" is actually

---

[11]Another possibility is that the boundary layer is laminar but the core of the flow is turbulent. Then, the spread of the turbulent region to the free surface can cause an apparent transition. Pipe jets, studied in this work, will not show this behavior as it typically occurs in a converging nozzle.

a class of regimes. One of these regimes is like the Rayleigh regime (see figure 3.6), another is like the turbulent surface breakup regime (see figure 3.8), and another is like the atomization regime (see figure 3.7)[12]. The turbulent surface breakup and atomization regimes as defined in this work could be viewed as merely fully turbulent versions of those regimes, while their corresponding regimes in the downstream transition class are merely transitional versions.

Unfortunately, because pipe nozzles have low critical Reynolds numbers, the downstream transition part of the $We_{\ell 0}$–$Re_{\ell 0}$ parameter space as seen in figure 3.4 is too small to easily distinguish between the different varieties of downstream transition breakup. Studies into the downstream transition regime in the future should use nozzles with higher nozzle critical Reynolds numbers for this reason.

From a modeling perspective, it is necessary to consider turbulence transition. The jet behaves differently before, during, and after transition. In principle, one could model the laminar-to-turbulent transition by changing the behavior of the jet (which could be the growth rate in a linear stability theory like that of Weber [Web19]) when the transition length x_{trans} is reached. This model contrasts strongly with the prevailing models in the literature. Typical models for this regime (those discussed in § 3.4.5) assume that the growth rate does not change as a disturbance propagates downstream. This is false in the downstream transition regime — see figure 3.7 for an example. In figure 3.7, the disturbance on the jet is small until it starts growing rapidly after what appears to be turbulence transition. Non-linear theories could avoid the constant growth rate approximation, however, it may be sufficient and easier to use a linear model with different behavior before and after transition and possibly a jump in the disturbance at transition. Presumably the turbulence intensity increases dramatically as the velocity increases in the downstream transition regime.

Given the present lack of accurate models for this regime, the breakup length model

---

[12]It is possible that the breakup observed in figure 3.7 is entirely independent of aerodynamic effects, which would make the mechanism different than atomization, or possibly there are multiple types of this vigorous breakup, some of which have aerodynamic influence and others which do not.

used for the downstream transition regime in figures 3.14 and 3.16 is

$$\frac{\langle x_\mathrm{b} \rangle}{d_0} \propto \mathrm{We}_{\ell 0}^{-1}, \tag{3.15}$$

with the constant of proportionality chosen by setting the breakup length of the laminar Rayleigh regime equal to equation 3.15 at the transition point. This model is simple and motivated by the observation of Etzold et al. [Etz+18] that at least sometimes in the downstream transition regime $\langle x_\mathrm{b} \rangle \propto \overline{U}_0^{-2}$.

The droplet size is similarly uncertain. Convention suggests a representative droplet sizes in this regime is comparable to the nozzle outlet diameter, but as can be seen in figures 3.6 and 3.7, the droplet size could vary from similar to on the order of the nozzle outlet diameter to smaller than the nozzle outlet diameter.

3.4.7 Transition to turbulence inside the nozzle

Depending on the location in the regime diagram, once transition is complete, transition to turbulence could decrease the breakup length (e.g., figure 3.15, transition from laminar to turbulent Rayleigh, as shown by Mansour and Chigier [MC94a, fig. 5]), or increase it (e.g., figures 3.14 and 3.16, transition from downstream transition to turbulent surface breakup or atomization, as suggested by Hoyt and Taylor [HT85]). The latter is because the downstream transition regime can be particularly unstable, as seen through it's decreasing breakup length with increasing velocity. Hoyt and Taylor [HT85] recommend that if one wants a more stable jet to bring turbulence transition inside of the nozzle if it is occurring outside of the nozzle. This seems counterintuitive if you believe that earlier transition is bad, but one way to rephrase this recommendation is to avoid the downstream transition regime if you want a stable jet. Even the atomization regime would be preferable in terms of the breakup length.

See § 3.3.4 for a discussion of the nozzle critical Reynolds number for turbulence.

3.4.8 Turbulent Rayleigh regime

As stated earlier, the turbulent Rayleigh regime appears similar to the Rayleigh regime, except that the jet is now turbulent at the nozzle outlet. An image of a jet in the turbulent Rayleigh regime is shown in figure 3.9. Compared against the laminar Rayleigh regime, the breakup in the turbulent Rayleigh regime is less regular, but large droplets are still being produced downstream like in the laminar Rayleigh regime. The turbulent Rayleigh regime follows Weber's theory for the breakup length (equation 2.12), with the Reynolds number variation neglected here as it is negligible at high Reynolds numbers:

$$\frac{\langle x_b \rangle}{d_0} = C_{TR} We_{\ell 0}^{1/2}. \tag{3.16}$$

The value of C_{TR} is lower than C_{LR}. Fitting a model with a constant value of C_{TR} to the available pipe jet data returns $C_{TR} = 2.79$, however, the R^2 value is only 0.641. The constant C_{TR} model has a lower R^2 value compared against the laminar case because C_{TR} varies appreciably with the liquid Weber number. It is anticipated that C_{TR} also varies with the turbulence intensity. The available pipe jet data has little variation in turbulence intensity, so the sensitivity to the turbulence intensity can not be determined from the data compilation in this work. This sensitivity will be estimated through a simple model.

Typically, free surface disturbance amplitudes are modeled as following exponential growth in temporal stability theory [Web19]:

$$\delta = \delta_0 \exp(\omega_m t), \tag{2.5}$$

where δ is the free surface radial perturbation amplitude, δ_0 is the initial disturbance level (dimension of length), ω_m is the growth rate of the disturbance, and t is the time since the jet exited the nozzle. This assumption implies that the coefficient on the breakup length (C_{LR} or C_{TR}, in the typical notation) is independent of the Weber number. This is incorrect in the turbulent Rayleigh case. By hypothesis, the initial free surface deformation in the turbulent Rayleigh case is zero — this would mean that $\delta_0 = 0$ and that $\delta = 0$ for all times in equation 2.5. However, equation 2.5 is only one of many possible solutions

to the stability problem, which differ in their *initial conditions*. This has been noted by previous researchers [GG08, p. 5]. Equation 2.5 suggests not only that the initial disturbance *amplitude* is δ_0 but also suggests there is a non-zero initial disturbance *velocity* δ_0'. The way the theory is typically presented implies that only an amplitude is set, but as δ is the solution of a second-order differential equation, two initial conditions are required. In the laminar Rayleigh case, velocity fluctuations are presumably small and the disturbance at the nozzle is likely caused by geometric imperfections. Using only an initial disturbance height seems reasonable in this case, i.e., $\delta_0 > 0$, $\delta_0' \approx 0$. Consequently the choice of equation 2.5 can be seen to be made more for convenience than realism in the laminar Rayleigh case[13]. For turbulent Rayleigh, however, velocity fluctuations are appreciable and geometric imperfections are relatively unimportant, so $\delta_0 \approx 0$ and $\delta_0' > 0$. Because the turbulence decays downstream in this regime [MC94b, fig. 18], the impact of turbulent velocity fluctuations at the surface is felt primarily near the nozzle, so it is reasonable to model the effect of the disturbances *only* in the initial condition in the turbulent Rayleigh regime — this is not expected to extend to other regimes.

To set both $\delta_0 = 0$ and $\delta_0' \neq 0$ requires at least two modes. For the inviscid case considered here, it can be shown that the most unstable mode's growth rate, ω_m, has a corresponding decay rate, $-\omega_\mathrm{m}$. The decay rate in the viscous case is not simply the negative of the growth rate. The inviscid case simplifies the math appreciably and is realistic for turbulent Rayleigh, so it will be used here. Now, instead of equation 2.5 the disturbance amplitude evolves according to

$$\delta = \delta_1 \exp(\omega_\mathrm{m} t) + \delta_2 \exp(-\omega_\mathrm{m} t), \tag{3.17}$$

where δ_1 and δ_2 are arbitrary constants. For the initial conditions $\delta_0 = 0$ and $\delta_0' \neq 0$,

---

[13]Performing the same analysis as in the turbulent Rayleigh case for the laminar Rayleigh case leads to $C_\mathrm{LR} = \operatorname{arcsech}\left(\dfrac{2\delta_0}{d_0}\right)$ instead of the typical $\ln\left(\dfrac{d_0}{2\delta_0}\right)$, where arcsech is the inverse hyperbolic secant function. Note that the arcsech result is for an inviscid jet but is expected to be reasonable for a viscous jet as well. If C_LR is constant than so is δ_0 regardless of whether arcsech or ln are used, though the implies values of δ_0 would differ.

equation 3.17 can be written in terms of the hyperbolic sine function:

$$\delta = \frac{\delta'_0}{\omega_{\text{m}}} \sinh(\omega_{\text{m}} t).$$

(3.18)

To find the breakup length from equation 3.18, find the time, t_{b}, where the surface disturbance amplitude grows to $d_0/2$. Approximately at that point the surface wave valleys will meet, leading to the breakup of the jet's core. The result is

$$\frac{\langle x_{\text{b}} \rangle}{d_0} = \text{arccsch}\left(\frac{2\delta'_0}{\overline{U}_0} \text{We}_{\ell 0}^{1/2}\right) \text{We}_{\ell 0}^{1/2},$$

(3.19)

which implies that

$$C_{\text{TR}} = \text{arccsch}\left(\frac{2\delta'_0}{\overline{U}_0} \text{We}_{\ell 0}^{1/2}\right),$$

(3.20)

where arccsch is the inverse hyperbolic cosecant function.

At this point a choice needs to be made for the initial disturbance velocity, δ'_0. By hypothesis, turbulent fluctuations cause the initial surface deformation. Considering C_{TR} to be an average over each realization. As δ is the *amplitude* of the waves, δ can not be negative. Consequently, to model the initial disturbance velocity I take the absolute value of the velocity fluctuation, so for a particular realization, $\delta'_0 = |v_0|$, where v_0 is the fluctuating radial velocity at the free surface near the nozzle outlet:

$$C_{\text{TR}} = \left\langle \text{arccsch}\left(\frac{2|v_0|}{\overline{U}_0} \text{We}_{\ell 0}^{1/2}\right) \right\rangle \approx \text{arccsch}\left(\frac{2\langle |v_0| \rangle}{\overline{U}_0} \text{We}_{\ell 0}^{1/2}\right).$$

(3.21)

Now, note that

$$\frac{\langle |v_0| \rangle}{\overline{U}_0} \propto \frac{v'_0}{\overline{U}_0} = \text{Tu}_0.$$

(3.22)

The selection $2\delta'_0 = C_v \overline{v'_0}$ leads to the model

$$C_{\text{TR}} = \text{arccsch}\left(C_v \overline{\text{Tu}}_0 \text{We}_{\ell 0}^{1/2}\right).$$

(3.23)

The pipe nozzle data from Phinney [Phi73; Phi75] and Sallam, Dai, and Faeth [SDF02]

appears to have consistent breakup lengths that can be used to calibrate the model for C_{TR}. Data from Mansour and Chigier [MC94a, pp. 597–598] was neglected due to inconsistencies with the other data, likely due to using a different definition of the breakup length that examined waves rather than the end of the jet's core [MC94a, p. 594][14]. Regression analysis on the consistent data suggests that $C_v = 0.0615$ (31 points, $R^2 = 0.961$). The fit with the data is excellent as can be seen in figure 3.18. The no-slip condition at the nozzle wall would suggest that the initial RMS radial velocity v'_0 is likely much smaller than $\overline{v'_0}$, so C_v is expected to be smaller than 1, consistent with the data.

Note that the experiments of Vliem [Vli75, p. 30] with obstructions placed in the nozzle suggest that the breakup length (and as a consequence, the initial disturbance level) in the turbulent Rayleigh regime varies within the measurement uncertainty as the *centerline* streamwise turbulence intensity increases by a factor of 2.1 from that of a smooth pipe. However, the centerline turbulence intensity is not representative of the *near-surface* turbulence intensity. The turbulence intensity peaks near the edge of the nozzle/jet. Lissenburg, Hinze, and Leijdens [LHL75] provides the turbulence intensity at the centerline and at $r/r_0 = 0.9$ for a system geometrically identical to that of Vliem's higher turbulence case at the same Reynolds number. The lower turbulence intensity case for comparison is a smooth pipe, and smooth pipe data from Loulou et al. [Lou+97, fig. 3.16] is at a Reynolds numbers similar to Vliem's experiment. At $r/r_0 = 0.9$, the turbulence intensity of the high turbulence case is only approximately 1.2 times that of a smooth pipe. Assuming that $\overline{\mathrm{Tu}_0}$ increases by the same factor, C_{TR} as calculated by equation 3.23 for the high turbulence intensity case is found to be 0.95 times its value for a corresponding smooth pipe nozzle. This is within the measurement uncertainty, so Vliem's results do not contradict the C_{TR} model presented in this work.

The droplet size in the turbulent Rayleigh regime is similar to that of the laminar

---

[14]Data from Mansour and Chigier [MC94a] was used for the laminar Rayleigh regime, however, as this data is consistent with that of other researchers despite the difference in definition. Mansour and Chigier [MC94a, p. 594] note that under their definition the laminar jet breakup length was unambiguous, but note difficulties with the turbulent jet breakup length, so ultimately their definition may not be appropriate for turbulent jets unlike the average definition used in this work.
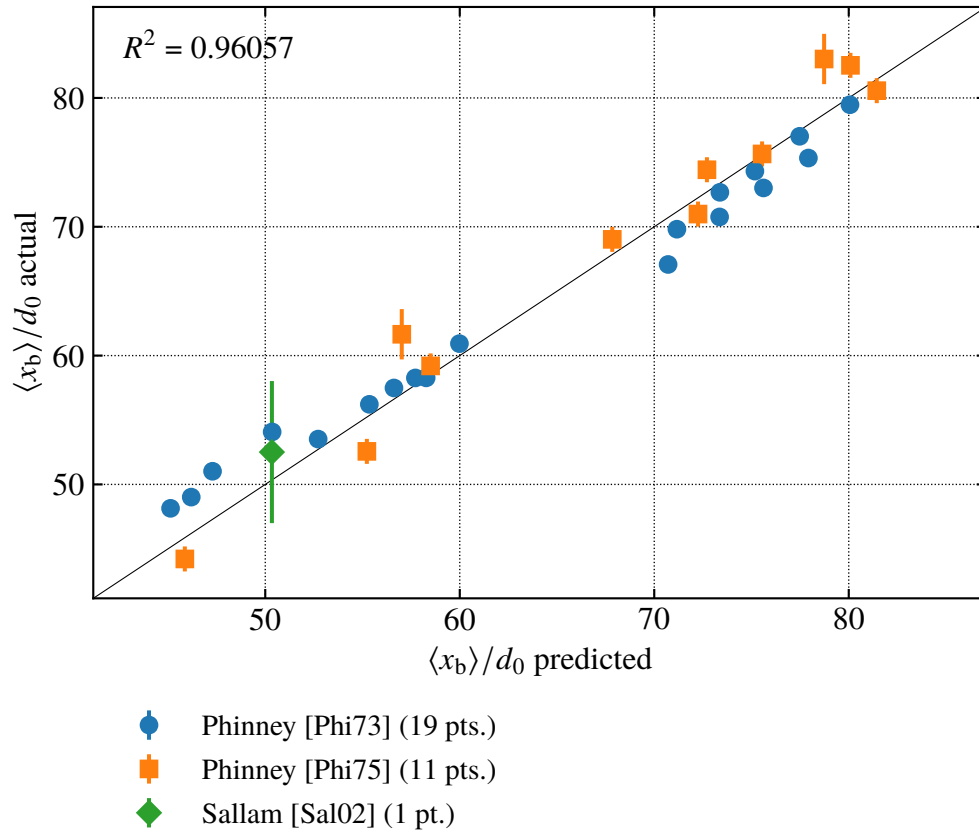
Figure 3.18: Comparison of the turbulent Rayleigh breakup length estimated from equation 2.12 with C_{TR} modeled with equation 3.23 against *selected* experimental data; see text for discussion.

Rayleigh regime (equation 2.11). Mansour and Chigier [MC94a, p. 600] note that the droplet size distribution is bimodal, with the fundamental peak at approximately $D = 2.4d_0$, near the value predicted by Weber's theory, and a second peak at $D = 0.5d_0$ for satellite droplets. Vliem [Vli75] gives a similar distribution function, albeit with much more frequent satellite droplets. The (fundamental peak) droplet size was not explicitly given by Vliem but was reported by Sterling and Abbott [SA81, p. I-4.6] as within 2% of Weber's theory in Vliem's experiments. The droplet size is expected to be independent of the turbulence intensity in the turbulent Rayleigh regime. This is because the droplet size in Weber's theory is independent of the initial disturbance level — see equation 2.11.

3.4.9   Transition from the turbulent Rayleigh regime to the turbulent surface breakup regime

The transition from the turbulent Rayleigh regime to the turbulent surface breakup regime is gradual, as both the Rayleigh (core breakup) and turbulent surface breakup mechanisms are present in both regimes. The difference is that the Rayleigh mechanism dominates in the turbulent Rayleigh regime, and correspondingly, turbulent fluctuations directly causing breakup at the free surface dominate in the turbulent surface breakup regime. One simple way to measure the relative strengths of each mechanism would be to compute the ratio of the average breakup onset location, $\langle x_i \rangle$, to the average breakup length in the turbulent Rayleigh regime, $\langle x_b \rangle$. In the turbulent Rayleigh regime, presumably a long distance is needed for turbulent surface breakup to start, hence, $\langle x_i \rangle \gg \langle x_b \rangle$. The opposite is true in the turbulent surface breakup regime. Setting the ratio of the average breakup onset location theory developed in chapter 5 (equation 5.11) and Weber's breakup length theory (equation 2.12) using C_{TR} from equation 3.23 to a critical value returns

$$\frac{\langle x_i \rangle}{\langle x_b \rangle} \propto \frac{\overline{\text{Tu}}_0^{-3} \text{We}_{\ell 0}^{-1}}{\text{arccsch}\left(C_v \overline{\text{Tu}}_0 \text{We}_{\ell 0}^{1/2}\right) \text{We}_{\ell 0}^{1/2}} \equiv \frac{1}{\widehat{C}_{\text{TR to TSB}}}. \tag{3.24}$$

The transition between the two regimes is defined here as a certain critical value of the ratio $\langle x_{\mathrm{i}} \rangle / \langle x_{\mathrm{b}} \rangle$. Rearranging this ratio returns

$$\widehat{C}_{\text{TR to TSB}} = \text{arccsch}\left(C_v \overline{\text{Tu}}_0 \text{We}_{\ell 0,\text{crit}}^{1/2} \right) \left(\overline{\text{Tu}}_0 \text{We}_{\ell 0,\text{crit}}^{1/2} \right)^3 , \tag{3.25}$$

where the Weber number has been labeled as the critical Weber number. This implies that $\overline{\text{Tu}}_0 \text{We}_{\ell 0,\text{crit}}^{1/2}$ is a constant, e.g.:

$$C_{\text{TR to TSB}} = \overline{\text{Tu}}_0 \text{We}_{\ell 0,\text{crit}}^{1/2}. \tag{3.26}$$

Written explicitly in terms of the critical Weber number, the equation

$$\text{We}_{\ell 0,\text{crit}} = 8 \overline{\text{Tu}}_0^{-2} \tag{3.27}$$

fits the limited available data.

3.4.10 Turbulent surface breakup regime

Breakup in the turbulent surface breakup regime is caused primarily by turbulent fluctuations perforating the free surface, as discussed in § 2.7. Figure 3.10 shows what a jet in the turbulent surface breakup regime looks like near the nozzle. The breakup here is rather vigorous, and the breakup is mainly at the free surface of the jet rather than of the core itself as in the turbulent Rayleigh regime. Farther downstream, as shown in figure 3.11, the jet core may fragment, but in a much more disordered way than seen in the turbulent Rayleigh regime.

A variety of regressions were developed for the turbulent surface breakup regime in this work. The most important, the breakup length regression, made use of data from Kusui [Kus69] with significant turbulence intensity variation ($5.4\% \leq \overline{\text{Tu}}_0 \leq 12.7\%$), among other studies. This regression is (193 points, $R^2 = 0.958$):

$$\frac{\langle x_{\mathrm{b}} \rangle}{d_0} = 3.61 \overline{\text{Tu}}_0^{-0.275} \text{We}_{\ell 0}^{0.334}. \tag{3.28}$$

The regression above neglected $Re_{\ell 0}$ and ρ_ℓ/ρ_g. Including $Re_{\ell 0}$ and ρ_ℓ/ρ_g, their exponents would be 0.0195 and 0.0171 respectively, nearly zero. This indicates that the influence of these variables is negligible in the turbulent surface breakup regime. The lack of a density ratio influence makes the earlier name for this regime, the "second wind-induced regime", a misnomer, as mentioned in § 3.3.3. For simplicity the Reynolds number and density ratio were removed from the regression.

Plots comparing equation 3.28 against experimental data are shown in figures 3.19 and 3.20. Note that the regression was made only against data with breakup lengths measured via electrical conductivity as the large uncertainties seen in the breakup length measurements based on images appreciably change the turbulence intensity exponent, and this change is likely spurious. However, the comparison is against all available breakup length data in the turbulent surface breakup regime.

The regression was cross-validated with non-pipe breakup length data [EME80; ME80], excluding points estimated to be in the atomization regime by equation 3.34. This alternative data set has lower turbulence intensity ($0.3\% \leq Tu_{c0} \leq 8.0\%$) than the turbulent surface breakup regime pipe jets in the database ($5.4\% \leq \overline{Tu}_0 \leq 12.7\%$)[15]. The fit between the regression and the alternative data is worse (79 points, $R^2 = 0.526$), but the error appears to be random — see figure 3.20 and compare against figure 3.19 for only pipe jets. The error possibly is due to variables not considered in the regression, e.g., the integral scale and the velocity profile. The error could also be due to Ervine, McKeogh, and Elsawy and McKeogh and Elsawy measuring centerline turbulence intensity (Tu_{c0}) rather than the plane average turbulence intensity ($\overline{Tu}_0$) that I use. Another possibility is that the uncertainty of the breakup length is large due to a low number of images used to establish the average — see § 4.2 for general uncertainty analysis of the breakup length. Likely all of these are

---

[15]While equation 3.27 suggests much of this data is in the turbulent Rayleigh regime, equation 3.27 fits data at the higher turbulence intensities mentioned previously, and may not apply for the low turbulence intensities in the alternative data. It is assumed that all of the alternative data is in the turbulent surface breakup regime, as the two experiments are similar and Ervine, McKeogh, and Elsawy [EME80, §23] suggests that the jets has "intense roughness" which made measuring the breakup length via images difficult. Jets in the turbulent Rayleigh regime are unlikely to be that rough.

factors. The general agreement suggests that the regression may be valid for $\overline{\mathrm{Tu}}_0$ outside its calibration data and consequently may be a useful model for non-pipe jets.

A regression was made for the spray angle in the turbulent surface breakup regime. Analysis of available data in either the turbulent surface breakup or atomization regimes suggests that the spray angle is far too noisy to naively use for regression purposes. This is likely due to the lack of standard definitions of the spray angle — see § 4.2 for a discussion of this problem. Additionally, the only study with spray angle data with appreciable turbulence intensity variation [Skr66] is in the atomization regime (according to equation 3.34), so it is not strictly possible to determine the sensitivity to the turbulence intensity for the spray angle in the turbulent surface breakup regime at the moment. However, a power law regression was applied to Skrebkov's data and it was assumed that the turbulence intensity exponent in the atomization regime is equal to that of the turbulent surface breakup regime. Then, with the prescribed turbulence intensity variation, another regression was made using only data from the Faeth group [Ruf90; Sal02], which appears to be less noisy and may have used a consistent definition, returning (5 points, $R^2 = 0.983$):

$$\tan\left(\frac{\theta_i}{2}\right) = 4.73 \times 10^{-4} \overline{\mathrm{Tu}}_0^{-0.827} \mathrm{We}_{\ell 0}^{0.621}. \tag{3.29}$$

Due to the sparsity of consistent data available for the spray angle and high match with the data, for brevity the predicted vs. actual plot is neglected.

Similarly, because there is no pipe jet data with appreciable turbulence intensity variation for $\langle x_i \rangle$, D_{32}, or $\langle v_d \rangle$, a regression analysis was done using composite variables including both the Weber number and the turbulence intensity as the theory in chapter 5 predicted they'll appear. For the breakup onset location, the regression is (52 points, $R^2 = 0.758$, predicted vs. actual plot in figure 3.21)

$$\frac{\langle x_i \rangle}{d_0} = 13.0 \left(\overline{\mathrm{Tu}}_0^3 \mathrm{We}_{\ell 0}\right)^{-0.915}. \tag{3.30}$$

For the Sauter mean diameter, only data at the breakup onset location had known turbulence intensities, so only data there was used in the regression. Because of confounding
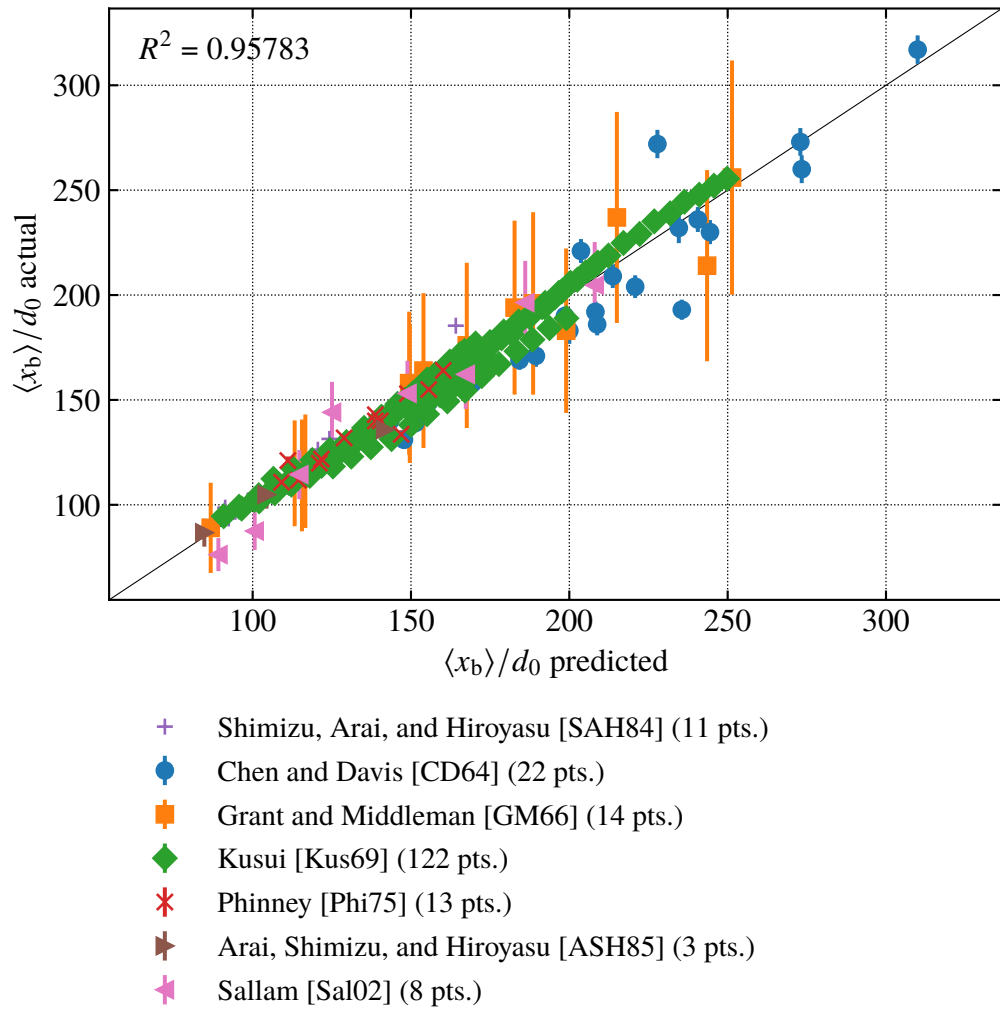
Figure 3.19: Comparison of the breakup length regression (equation 3.28) against experimental data with (estimated) uncertainties.
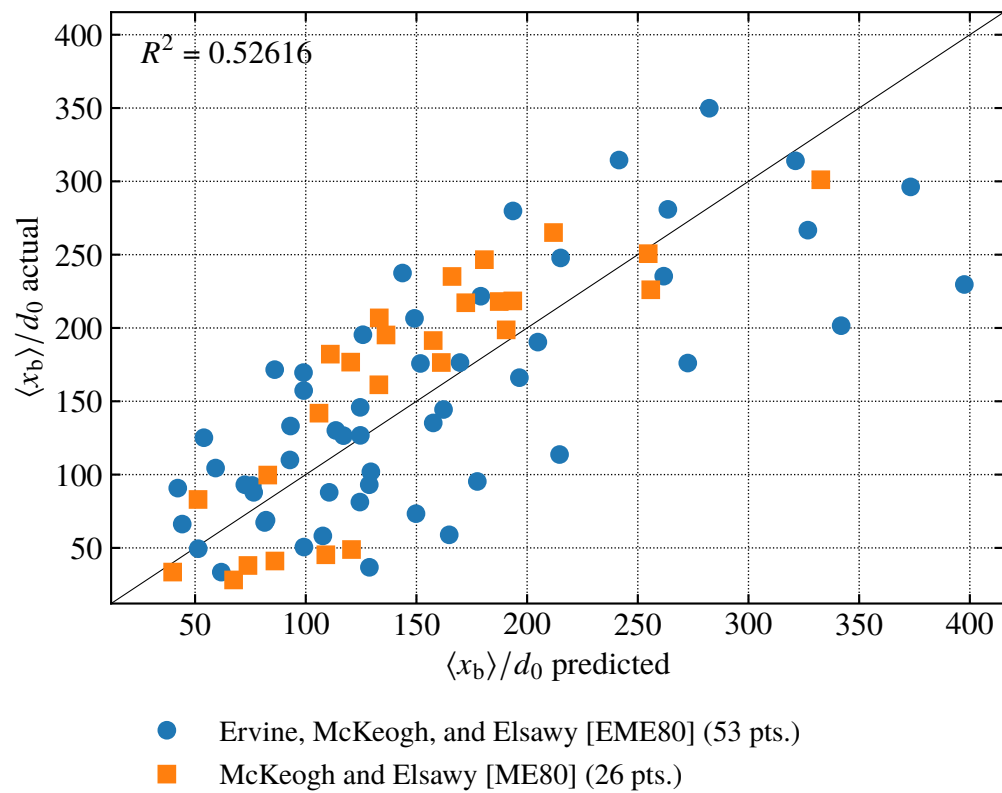
Figure 3.20: Comparison of the breakup length regression (equation 3.28) against alternative experimental data.
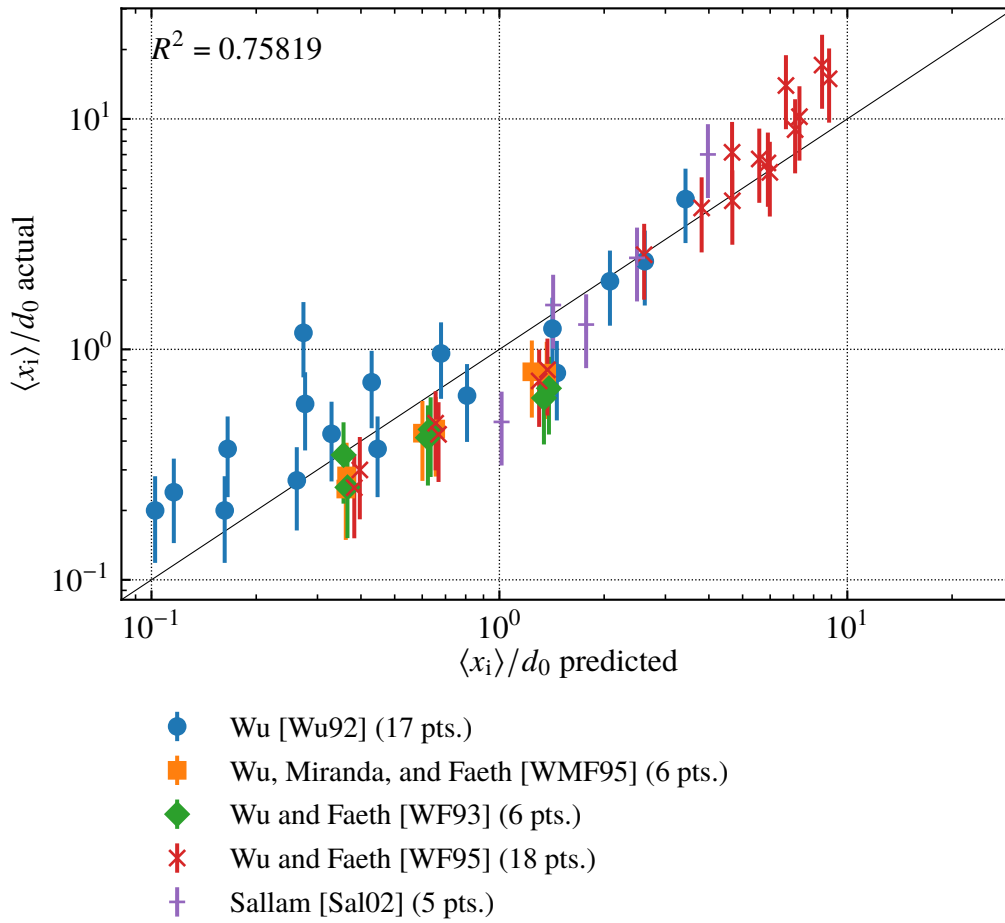
Figure 3.21: Comparison of the breakup onset location regression for the turbulent surface breakup regime (equation 3.30) against experimental data with uncertainties.
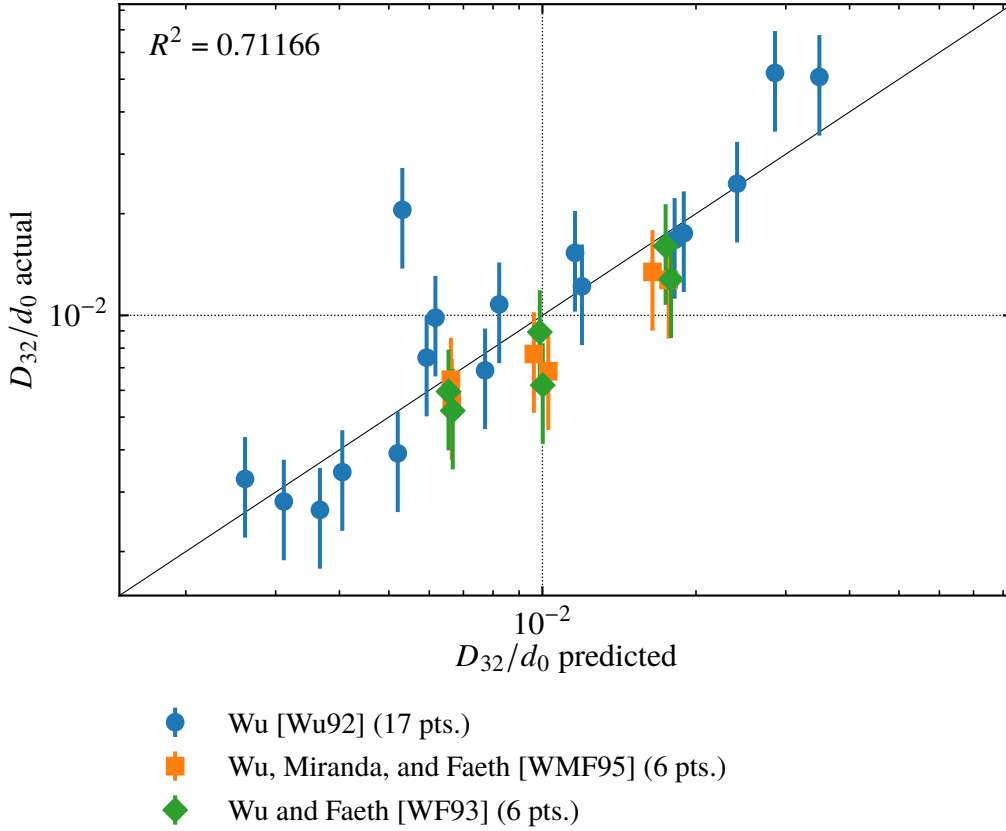
Figure 3.22: Comparison of the Sauter mean diameter regression for the turbulent surface breakup regime (equation 3.31) against experimental data with uncertainties.

between $\overline{\mathrm{Tu}}_0$ and $\mathrm{Re}_{\ell 0}$ I used solely the variable $\overline{\mathrm{Tu}}_0^2 \mathrm{We}_{\ell 0}$ in the regression analysis, consistent with CDRSV theory § 5.2.4. The regression is (29 points, $R^2 = 0.712$, predicted vs. actual plot in figure 3.22)

$$\frac{D_{32}}{d_0} = 0.564 \left(\overline{\mathrm{Tu}}_0^2 \mathrm{We}_{\ell 0} \right)^{-0.644} . \tag{3.31}$$

This regression includes only droplets formed at the breakup onset location and does not contain the large droplets formed downstream. As suggested by figure 3.10, the droplet sizes in the turbulent surface breakup regime are smaller than the nozzle outlet diameter as can be seen in figure 3.22.

And like the Sauter mean diameter, for the radial droplet velocity after formation,
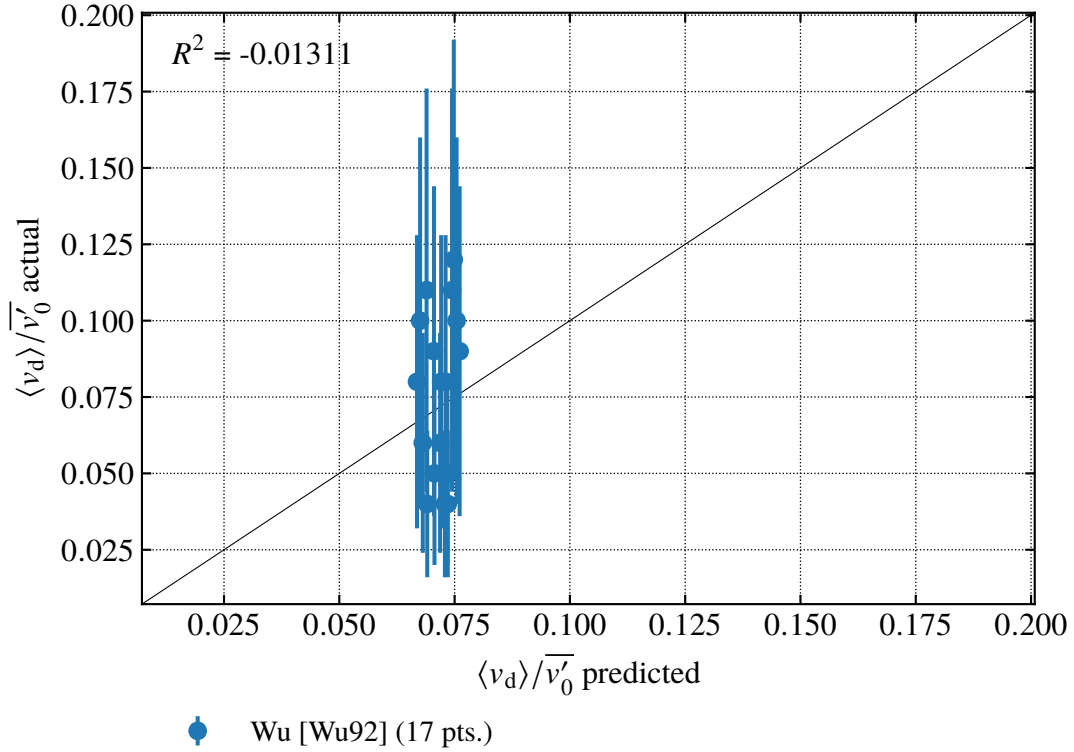
Figure 3.23: Comparison of the radial droplet velocity after formation regression for the turbulent surface breakup regime (equation 3.32) against experimental data with uncertainties.

only data at the breakup onset location had known turbulence intensities. As such, the regression is (17 points, $R^2 = -0.0131$, predicted vs. actual plot in figure 3.23)

$$\frac{\langle v_\mathrm{d} \rangle}{\overline{v'_0}} = 0.0582 \left(\overline{\mathrm{Tu}}_0^2 \mathrm{We}_{\ell 0} \right)^{0.0322} . \tag{3.32}$$

Note that the R^2 value for the droplet velocity is low because of the extremely high uncertainties in the data — 60% according to Wu [Wu92, p. 129]. See figure 3.23. It is unlikely *any* reasonable model would fit this data well because the data is largely random noise.

A comparison of these regressions to theory is in chapter 5.

3.4.11 Atomization regime and the transition from the turbulent surface breakup regime

A variety of mechanisms are factors in the atomization regime: turbulence, aerodynamic influence of the ambient gas (controlled by the density ratio), cavitation, the velocity profile, and compressibility. A near-nozzle image of a jet likely in the atomization regime is in figure 3.12. A downstream image is in figure 3.13. Note how the atomization regime is superficially identical to the turbulent surface breakup regime as shown in figure 3.10. This highlights the need for quantitative characteristics defining the atomization regime, in this case using the breakup length. Here I'll define atomization as a regime where the power law increase of the breakup length with the Weber number no longer applies. At low Mach numbers, the breakup length plateaus when the jet enters the atomization regime [Kus69; Sal02]. At higher Mach numbers the breakup length peaks before the plateau [SAH84; ASH85]. In this work, data at and surrounding the peak is classified as transitional between the turbulent surface breakup and atomization regimes.

Drawing a line in a regime diagram to get the boundary equation directly does not seem prudent as the data is sparse at high Weber and Reynolds numbers. Alternatively, given the different behaviors of the breakup length in the turbulent surface breakup and atomization regimes, finding the intersection of breakup length regressions for these regimes would return an equation for the boundary between these regimes. Unfortunately, if one limits the regression for the atomization regime to the available low Mach number ($\mathrm{Ma_g} < 0.3$) data for pipe jets, one can not distinguish between cavitation and density ratio effects. The cases with low $\rho_\ell/\rho_\mathrm{g}$ also have only sudden contraction entrances to the pipe, while the cases with high $\rho_\ell/\rho_\mathrm{g}$ have only smooth entrances to the pipe. Sudden contractions are more prone to cavitation [AKY06, fig. 3], which reduces the breakup length, just like low density ratios. Problems like this are called "confounding" and is discussed more in chapter 4.

Fitting the available data, shortcomings and all, returns the following equation for the breakup length in the atomization regime (11 points, $R^2 = 0.602$, $\rho_\ell/\rho_\mathrm{g}$ ranging from

29.4 to 882, predicted vs. actual plot in figure 3.24):

$$\frac{\langle x_b \rangle}{d_0} = 5.31 \overline{Tu}_0^{-0.568} \left(\frac{\rho_\ell}{\rho_g} \right)^{0.335}, \tag{3.33}$$

which implies the following turbulent surface breakup to atomization regime boundary:

$$We_{\ell 0,\mathrm{crit}} = 3.17 \overline{Tu}_0^{-0.876} \left(\frac{\rho_\ell}{\rho_g} \right)^{1.00}. \tag{3.34}$$

The density ratio exponent given above is accurate to 3 significant figures — it does not equal 1 exactly here. Note that equation 3.34 approximates a simple critical gas Weber number criteria:

$$We_{g0,\mathrm{crit}} = 3.17 \overline{Tu}_0^{-0.876}. \tag{3.35}$$

The use of a critical gas Weber number for atomization as suggested by Reitz [Rei78, p. 8] and discussed in § 3.3.2 appears reasonable given the limited amount of data available.

Further, the critical gas Weber number predicted by equation 3.34 for 5% turbulence and a density ratio of 1000/1.2 (approximating water and air) is 44.8, not far from the number 40.3 Reitz suggested in error. The simplest explanation for why Reitz's criteria ends up being accurate despite the miscalculation is coincidence combined with the fact that the data the criteria was based on did not look at quantitative characteristics like the breakup length. It likely corresponded to a different boundary, assuming it was not entirely spurious.

Finally, given the difficulty of distinguishing between the turbulent surface breakup and atomization regimes based on single images alone, a criteria was developed to allow the regime to be estimated based on the spray angle, independent of the Weber number. To develop this criteria, substitute the simplified atomization boundary equation (equation 3.35) into the equation for the spray angle in the turbulent surface breakup regime (equation 3.29) to obtain

$$\tan \left(\frac{\theta_i}{2} \right)_{\mathrm{crit}} = 9.69 \times 10^{-4} \left(\frac{\rho_\ell}{\rho_g} \right)^{0.621} \overline{Tu}_0^{-0.282}. \tag{3.36}$$
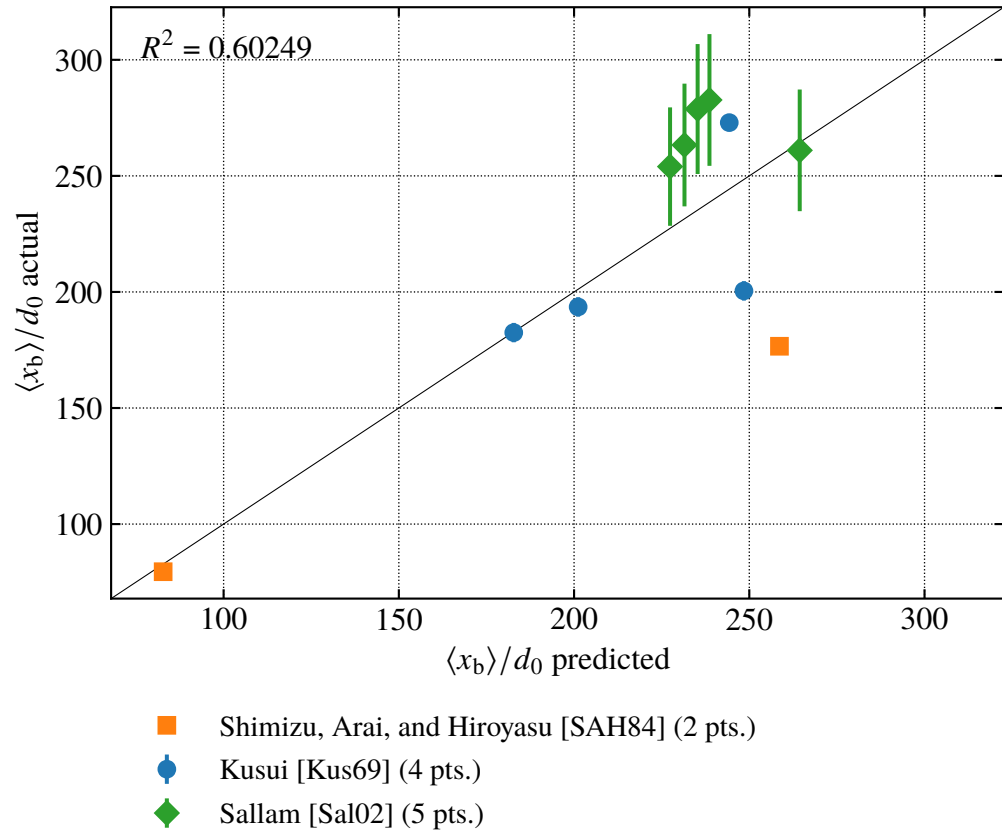
Figure 3.24: Comparison of the breakup length regression for the atomization regime (equation 3.33) against experimental data with (estimated) uncertainties.

In the data compilation, equation 3.36 was used to determine the regime for images where the regime was ambiguous between turbulent surface breakup and atomization, as the two are visually similar. The criteria used were as follows: For $\tan(\theta_i/2)/\tan(\theta_i/2)_{crit} \leq 0.5$, the regime was marked as turbulent surface breakup. For $0.5 < \tan(\theta_i/2)/\tan(\theta_i/2)_{crit} \leq 1.25$, the regime was marked as transitional between turbulent surface breakup and atomization. For $\tan(\theta_i/2)/\tan(\theta_i/2)_{crit} > 1.25$, the regime was marked as atomization.

A brief comment on droplet size in the atomization regime: Aerodynamic effects will enhance the formation of droplets by free surface turbulence, making the droplet sizes smaller than in the turbulent surface breakup regime. The reader is referred to the study of Wu and Faeth [WF93] for a detailed experimental treatment of these effects on the droplet size.

3.4.12 Universality of the regime diagram

The reader may be concerned that the new regime diagram applies only for the behavior of the jets in terms of breakup length, and not, for instance, for the visual appearance of the jet or for other quantities like the droplet size. A comparison of regime data classified visually and regime data classified by breakup lengths would be the clearest way to check whether visual and breakup length regimes are consistent. Compare figures 3.25 and 3.26 — no major differences appear aside from the fact that the visual data is more sparse.

Other quantities of interest were not studied in detail in this work, so it is possible that regimes classified with other quantities of interest are inconsistent with the new regime diagram.

An argument can be made for broad universality of the regime diagram: A change in the regime changes the physical mechanisms relevant to the problem. The behavior of each quantity of interest is determined by the physical mechanisms involved. Consequently, changing the regime should simultaneously change the behavior of multiple quantities of interest, making the regimes "universal". The most significant flaw to this argument is that even if true, some quantities of interest still do not change across regimes. For example, the

droplet size is similar in both the laminar and turbulent Rayleigh regimes. For that reason, regimes classified in terms of droplet sizes may not be able to distinguish between the two Rayleigh regimes.

There is one regime boundary where the visual appearance of the jet and the breakup length trend do not precisely match: the boundary between the laminar Rayleigh and downstream transition regimes. To summarize, the name "downstream transition" suggests that the regime starts when turbulence transition occurs downstream on the jet. However, as velocity increases, downstream turbulence transition occurs slightly before the peak in the breakup length used to demarcate the breakup length regimes. The practical difference between the two definitions is small. See § 3.4.5 for details.

Additional studies are needed to test how universal the regime diagram developed in this work is.

3.5   Conclusions

Liquid jets break up in 6 regimes recognized in this work: dripping, laminar Rayleigh, downstream transition, turbulent Rayleigh, turbulent surface breakup, and atomization. The turbulent Rayleigh regime has rarely been recognized due to the common but erroneous belief that as the velocity of a jet increases the jet first starts dripping, then enters the (conventionally laminar) Rayleigh regime, then enters the downstream transition regime, then enters the turbulent surface breakup regime, and then enters the atomization regime. This regime progression was shown to be only one of several possibilities. Jets with high Ohnesorge numbers may never enter the turbulent surface breakup regime and skip from downstream transition to atomization. Similarly, jets with low Ohnesorge numbers and low nozzle critical Reynolds numbers may never enter the downstream transition regime and instead enter the turbulent Rayleigh regime prior to the turbulent surface breakup regime.

The regime of a jet is typically determined through qualitative comparison against prototypical images of jets. This procedure was shown to be ambiguous, and instead regime classification based on quantitative characteristics like the breakup length was proposed.

94
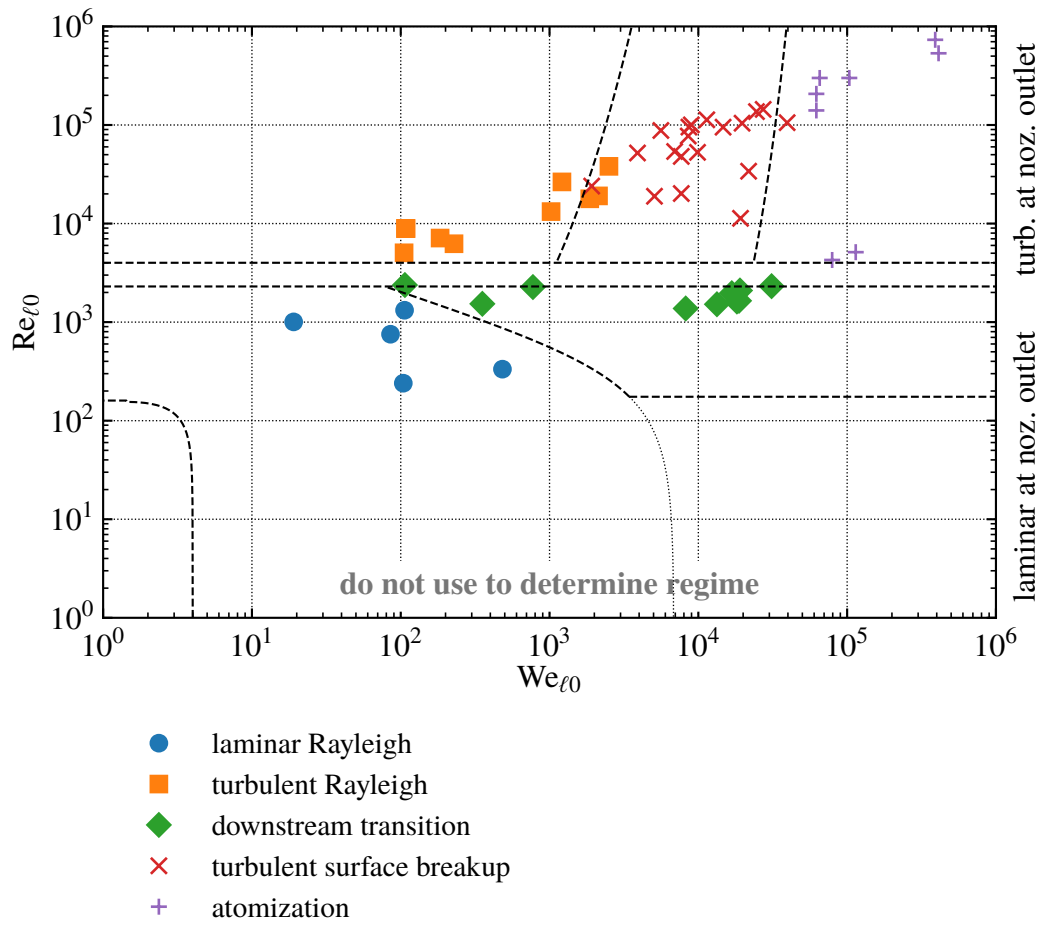
Figure 3.25: Regime diagram similar to figure 3.4 but including only data points where the regime was determined visually. 63 data points.
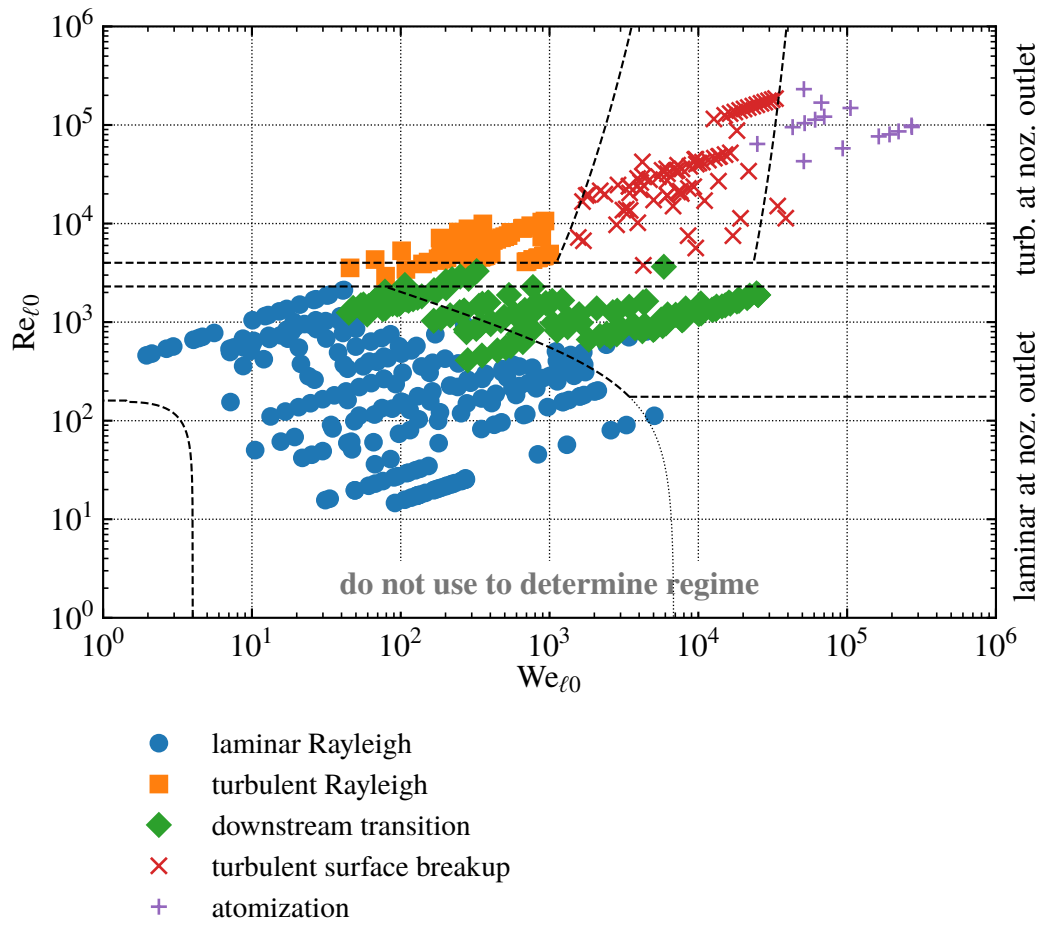
Figure 3.26: Regime diagram similar to figure 3.4 but including only data points where the regime was determined from breakup length measurements. 514 data points.

The critical Reynolds number for the onset of turbulence at the nozzle outlet is a factor typically neglected in regime diagrams, but is included in the new regime diagram in this work. The nozzle critical Reynolds number can vary by roughly two orders of magnitude in practice, and whether the jet is turbulent or laminar at the nozzle outlet can strongly influence how the jet breaks up.

The downstream transition regime itself appears to contain multiple other regimes similar each of the turbulent regimes, however, the available data makes studying the boundaries inside of the downstream transition regime difficult. This is due to the low nozzle critical Reynolds number in the data used in this study, which made the area in the $We_{\ell 0}$–$Re_{\ell 0}$ parameter space covered by the downstream transition regime too small to map the regime. New studies with higher and quantified nozzle critical Reynolds numbers are needed to study the downstream transition class of regimes.

The popular Ohnesorge diagram (figure 3.1) and more recent variations of it (figure 3.2) are inaccurate and should not be used. A *schematic* diagram (figure 3.3) is proposed as a replacement, though it must be emphasized that this diagram is merely a schematic which applies only for a special case. More general equations for the boundaries of each regime were given to determine the regime in more general cases.

Chapter 4

Improving the validation of turbulent jet breakup models[1]

Liquid jet breakup has been modeled in a wide variety of different ways since the theoretical study of liquid jets began in the 19th century. This chapter is not concerned with the precise modeling techniques used. Rather, the concern is how to evaluate the accuracy of models. The comparison of model predictions against experimental data is called "validation" [MO16]. If the comparison is a success, then the model is deemed "validated" and believed to accurately predict cases not yet measured. Often, models appear to work well in published works, but their accuracy is still regarded with suspicion. A goal is this chapter is to highlight some of the reasons why an apparently successful validation of a turbulent jet breakup model may actually be illusory.

While the precise criteria which determines whether a model has been validated is not trivial [MO16], for the purposes of this work I'll call a model validated if its estimates are within the error bounds (say, 95%) roughly as frequently as the error bound itself. In other words, roughly 95% of the model predictions need to be within the 95% intervals of the data. These model predictions are considered the most likely cases estimated by the model. Model uncertainty and multi-modal distributions are not considered in this work. This simplified approach is sufficient for this work because, as will be discussed in more detail, relatively few turbulent jet breakup experimental data sources have quantified uncertainty, many data sources which have quantified uncertainty have large uncertainties that are not difficult for models to stay within, and even if these data sources did have quantified and small uncertainties, it's still possible for a "bad" model to match the experimental data well

---

[1]This chapter is a revised and slightly modified version of paper originally published at the ILASS-Americas 2019 conference [Tre19a]. I am the sole author.

due to validation problems unrelated to uncertainty quantification.

These problems largely will be resolved through better and more comprehensive data. Consequently, for validating turbulent jet breakup models, I developed a large data compilation for turbulent jet breakup. This data compilation was specifically designed to be challenging and diagnostic for turbulent jet breakup models. A summary of the problems with existing data is in table 4.1. These problems are elaborated in this work. Ultimately, only 18 of the 44 (41.9%) experimental studies with the quantities of interest were used. 10 studies were neglected despite being acceptable because the data collected appeared to mainly duplicate already transcribed data. For reference, all studies considered are cited at the end of this sentence [Lit42; AB51; DM53; BC55; EH58; Pal62; Rup62; Skr66; CD64; MA66; GM66; Kus68; Kus69; PH70; Phi73; vdSan74; Yan74; Phi75; SS75; Baf77; KT78; Rei78; HT80; Baf82; HSA82; Ici82; Kim83; Wu+83; ASH85; DI85; DIL86; MTZ86; DY88; HA90; Ruf90; Kar+92; TRF92; WTF92; WF93; Hua+94; Man94; RN94; WF95; SDF02; MB04; Sal10; Ost10]. The studies used are cited at the end of this sentence [AB51; Skr66; CD64; GM66; Kus69; PH70; Phi73; Phi75; Rei78; HSA82; Kim83; Wu+83; ASH85; Ruf90; TRF92; WTF92; WF93; Man94; WF95; SDF02]. The individual breakdown of studies used for each quantity of interest is discussed in § 3.4.10.[2]

4.1 Disclaimer

Following Rider [Rid09], a disclaimer is warranted. I will use certain published papers as examples of poor model validation. *The issues identified in this work are not an indictment of the researchers. Instead, they show flaws in the accepted practices of the jet breakup community.* In this work, an accepted practice is defined as a practice which appears in the recent (and up-to-date) literature repeatedly or in papers which are widely accepted at present in the community. All of the research I cite was conducted in good faith to my knowledge. The problems I discuss are not obvious. In particular, confounding

---

[2]Note that this study was conducted before the regimes study (chapter 3), and consequently the list of studies used is slightly different. This work will be updated before journal publication.

description	number	percentage
total considered	47	—
acceptable, used	20	42.6%
acceptable, not used	10	23.3%
D_{32}	7	16.3%
$\langle v_\mathrm{d} \rangle$	1	2.3%
$\langle x_\mathrm{i} \rangle$	8	18.6%
$\langle x_\mathrm{b} \rangle$	16	34.0%
θ_i	7	16.3%
uncertainty quantification	18	41.9%
rough pipes	3	7.0%
far-field droplets	5	71.4% (of 7)
just-formed droplets	2	28.6% (of 7)
no QoI	4	—
ambiguous data	2	4.7%
curves, not data points	2	4.7%
inconsistencies found	2	7.0%
foreign language	3	7.0%

Table 4.1: Summary of reasons why studies were neglected from the data compilation. The numbers are the total number of studies fitting a criteria on the left. The percentage does not include studies which did not have any of the quantities of interest (QoIs). The percentage for droplet quantities is taken out of all studies which measured droplet quantities.

can be particularly challenging to identify. This study is by no means comprehensive, and reflects my own judgment about which validation problems are more pressing based on examination of a large fraction of the published literature on turbulent jet breakup at low atmospheric densities. Other regimes and other breakup problems may not suffer from the same issues or suffer from any major issue at all.

4.2 Uncertainty quantification

A minority of the data sources (41.9%; see table 4.1) considered in this work quantify uncertainty[3] [AB51; CD64; GM66; PH70; Phi73; Phi75; Rei78; Wu+83; DY88; TRF92;

---

[3]To determine whether a study had quantified uncertainty, I used a generous definition: If it was possible using data in the work and some mild assumptions, I considered the work to have quantified uncertainty.

WTF92; WF93; Man94; WF95; SDF02; Ost10]. When uncertainties are estimated, they are often large. For example, the percent error of the Sauter mean diameter measurements of Wu [Wu92, p. 139] was estimated as 33%. Large uncertainties make validation easier than it should be. New experiments with small, known uncertainties are needed for rigorous validation of turbulent jet breakup models.

There are established procedures for uncertainty quantification for droplet size [BD51b; Hei62; Smi71; Bus74; Sal02, p. 128]. There also appears to be a wide spread in spray angle data due to the sensitivity of the spray angle to its definition [KM00; Bal10, p. 114; Ara12, p. 12; RGP18], a problem which can only be solved by standardization of the definition of the spray angle[4].

Aside from a brief discussion by Osta [Ost10, p. 108] little has been written on uncertainty quantification for the breakup length, which is used for the examples in this section. There are two main methods to measure breakup length: electrical conductivity of the jet and photographic measurement of where the jet core ends. The electrical conductivity measurements define the breakup length as the point where the jet conducts electricity through itself 50% of time. Photographic measurement defines the breakup length as the average location of the end of the jet's core. Because the distribution of breakup location is highly symmetric, these two numbers are essentially equal [Phi73; YO78], and consequently I use the notation $\langle x_b \rangle$ for the breakup length irrespective of how it was measured. The two components of the uncertainty in this case are the measurement precision and the statistical error from taking a finite number of data points[5]. The electrical conductivity case is essentially taking a very large number of measurements, making the statistical component negligible, so the main source of uncertainty is the precision of the measurements. For photographic measurements, the main source of error is typically statistical. For turbulent jets this can be estimated using the fact that the standard deviation of the jet breakup location

---

[4]New experiments may be necessary to determine how to obtain roughly equivalent spray angles using different techniques, e.g., different thresholds for photographic or mass fraction measurements which result in approximately the same spray angles.

[5]A third component, transcription error from the conversion of data to graphical plots back to data, is more difficult to characterize and has not been included in this work. However, I intend to examine this in future work.

(σ_b) is well predicted by a constant coefficient of variation $C_{\sigma_b} \equiv \sigma_b/\langle x_b \rangle = 0.1291 \pm 0.0019$, as will be discussed in detail in § 7.3.1.2. This along with the t-distribution can be used to estimate the uncertainty in photographic measurements of the breakup length. The statistical error for photographic measurements tends to be rather large at the sample sizes used in the previous literature, a fact which has not been appreciated to my knowledge. This can be seen in figure 3.19; the large errors in the measurements of Grant [Gra65] are particularly noticeable[6]. It is likely that if the uncertainty were quantified in some of the earlier photographic breakup length measurements, the researchers would have conducted more trials to reduce the statistical error in their measurements. Electrical conductivity measurements are preferred, though in principle photographic measurements can have small statistical errors at larger sample sizes.

4.3   Omitted and qualitative independent variables

If a model does not include an important variable, it is intuitive that the model may perform poorly. The model may match its calibration data well, but be severely inaccurate in other situations where the neglected variable differs substantially from the values it took in the calibration data.

Unfortunately, this is often the case in turbulent jet breakup for an entire class of variables: turbulence quantities. It is uncontroversial that some measure of the "strength" of turbulence is a major factor in turbulent jet breakup, with the breakup being more severe for "stronger" turbulence [MM74, p. 14; BL09, p. 512; LM17, p. 72L]. The most natural measure of the strength of turbulence is the turbulence intensity, Tu[7].

---

[6]Neither Kusui [Kus69] or Arai, Shimizu, and Hiroyasu [ASH85] report measurement precision. These were estimated as 1 cm and 0.2 cm, respectively. Also, note that the R^2 value in the corner of figure 3.19 differs from that of table 4.2 because the table only uses the electrical conductivity measurements, neglecting the noisier photographic measurements of Chen and Davis [CD64] and Grant [Gra65]. This was necessary to obtain a clear turbulence intensity exponent in the regression procedure. The large error washed out any turbulence intensity effects.

[7]Many researchers believe that the Reynolds number ($\mathrm{Re}_{\ell 0} \equiv \overline{U}_0 d_0/\nu_\ell$) is the most natural measure of the strength of turbulence. The Reynolds number absolutely is a factor in turbulence, however, it will be shown later in this chapter that in the turbulent surface breakup regime, the breakup length is nearly insensitive to the

The turbulence intensity is not typically constant. Measurements of the turbulence intensity in large-scale air models of nozzles varied between roughly 4% and 11% for nozzles similar to diesel nozzles [Leb19, fig. 4] and roughly 4% and 13% for sudden and smooth contraction nozzles with orifice lengths of $L_0/d_0 = 4$ [KB83]. These measurements neglected cavitation, which presumably could increase the turbulence level further. In applications where particularly stable jets are desired, low turbulence intensities on the order of 1% are expected.

Unfortunately, the vast majority of previous liquid jet experiments did not characterize turbulence quantities. This was observed as early as the 1967 survey of Lapple, Henry, and Blake [LHB67, pp. 9–10] and unfortunately the situation has not changed since then. In 2010, Osta and Sallam [OS10, p. 945] note that turbulence quantities are still neglected in experiments, despite their importance. The neglect of turbulence quantities is understandable as turbulence measurements in free surface flows are difficult [GH08, p. 345]. With that being said, there have been several turbulent jet breakup studies which varied the turbulence intensity, often by avoiding the need for measurement of the turbulence level in a free surface flow. The 1948 study of Bogdanovich [Bog48] used large-scale air models of nozzles to get credible estimates of the turbulence intensity at the nozzle outlet. In 1963, Skrebkov [Skr66] used long pipes of varying roughness to control the turbulence intensity relatively precisely with a known relationship between the turbulence intensity in fully developed pipe flow and the friction factor. The first theoretical study to consider the turbulence intensity was made by Natanzon [Nat18] in 1938. Unfortunately these studies are little known, likely because they were originally written in Russian.[8]

The neglect of turbulence intensity was examined in a review of dimensional analysis of turbulent jet breakup in chapter B. Only 20% of the 45 studies considered the RMS velocity (and by extension, the turbulence intensity) in their dimensional analyses. A further 20% considered nozzle geometry as a factor, which could be considered a proxy

─────────────────────────

Reynolds number.

[8]Even the Russians seem to have forgotten about these studies now, citing instead mostly western sources recently.

for turbulence intensity (though not a good one; see the next section on confounding). As adding a variable is easy in dimensional analysis, this indicates that turbulence intensity effects are understudied in turbulent jet breakup in general.

The neglect of turbulence quantities presents major issues from a modeling perspective. The data can not be compared fairly against models because the turbulence intensity is now a free parameter. Its precise value is unknown, and it is frequently estimated at precisely where it needs to be to make the model work regardless of whether that value is credible. One example of this problem is breakup length model of Lafrance [Laf77], which uses an implausibly low value for the turbulence intensity (0.8% for fully developed smooth pipe flow, vs. about 5% in reality, depending on the Reynolds number) because that's what matches the data best. If a realistic value of the turbulence intensity were used, the model would not produce a realistic breakup length, suggesting that the model is miscalibrated. Another example is the breakup length model of Ervine, Falvey, and Withers [EFW97] which uses data from Miesse [Mie55][9] with an arbitrarily chosen turbulence intensity value of 3%, which, of course, fits the data very nicely. There is no reason to believe that choice is appropriate and possibly the model suffers from the same problem as Lafrance's model.

This problem is not limited to low-order models. The RANS model of Shirani, Jafari, and Ashgriz [SJA06, p. 1461L] uses an assumed turbulence intensity of 1% to model a jet which likely had a higher turbulence intensity.

The work of Wu [Wu92] also relies on estimates of the turbulence intensity implicitly as the turbulence intensity was assumed roughly constant. This hides the problem in empirically determined coefficients, which ultimately are functions of the turbulence intensity. By treating these coefficients are constants, the model assumes that the turbulence intensity is constant, limiting its ability to generalize. Being based on the work of Wu [Wu92], the recent model of Magnotti et al. [Mag+17] itself neglects the turbulence intensity, despite Magnotti and Genzale's criticism of the KH-RT model for not considering turbulence

---

[9]Ervine, Falvey, and Withers [EFW97] claim the data comes from Baron [Bar49], but this is not true as Baron mentions no experimental data. Miesse [Mie55, p. 1698L] used the correlation form of Baron with his own data. It appears that Ervine, Falvey, and Withers mistakenly believed the data was from Baron.

effects [MG17, p. 34L].

It's not even necessary to quantify a variable (even implicitly as in the coefficient case) to "validate" a model. Bergwerk [Ber59, p. 655] rejects the idea that turbulence can cause breakup because "turbulent velocity components [...] are hardly likely to be of sufficient magnitude" to cause breakup. However, Bergwerk did not quantify the magnitude of the turbulent velocity components or the velocity magnitude needed to cause breakup, making their argument simply an assertion.

Admittedly, the inverse problem of determining a model input from the outputs can often be perfectly valid. But it relies entirely on the model being validated with known values of the inputs. If the model was not validated with known values of the inputs, avoiding the issues mentioned in the previous paragraph, then there is little reason to be confident in the inversion. I don't believe that current models have been properly validated due to the issues mentioned in this chapter. And even if a model passed a series of good validation tests for turbulent jet breakup, I am not convinced that any present models (including the model I develop in chapter 5) are sufficiently trustworthy to be used for inverse modeling purposes. The parameter space explored by existing data is too small; I'd need to be confident outside of the ranges of the source data. If an inverse problem can be avoided entirely (through measurement, pre-existing data, etc.), avoiding inversion is obviously much preferred. In this work I intentionally only select data where this inverse problem can be avoided entirely.

Estimating the turbulent kinetic energy with a model seems prudent if measurement is difficult. Unfortunately, the popular nozzle turbulence model developed by Huh, Lee, and Koo [HLK98] as part of a larger spray model is in severe error when compared against experiment data, as I detailed in a chapter 6. For typical nozzle lengths ($L_0/d_0 \approx 4$), Huh, Lee, and Koo's model predicts turbulent kinetic energies which are more than an order of magnitude too high. Despite this severe error, the combined nozzle-spray model was successfully validated for predicting spray angles. This suggests either that the turbulence level of the jet is unimportant, which seems unlikely and contradicts the claims of Huh, Lee, and Koo, or it suggests that the spray model is mis-calibrated due to the poor estimates of the turbulence level. This type of problem (integration tests being insufficient) will be

discussed later in this chapter.

Qualitative trends are also not sufficient. There are many studies which compare jets with presumably "low" turbulence intensity produced by smooth and short nozzles against against jets of presumably "high" turbulence intensity produced by jets from longer nozzles. These studies can be used for only qualitative validation of models at best. For example, Reitz and Bracco [RB82, p. 1741L] reject the idea that turbulence alone could be responsible for jet breakup in a high density environment because the trend of a particular model coefficient as the nozzle length increases (presumably increasing the turbulence intensity) is the opposite of expectations if turbulence contributed to breakup[10]. A more recent example is the study of Osta et al. [Ost+12], which examined injectors of nozzle aspect ratios $L_0/d_0 = 10$ and $L_0/d_0 = 40$ as a proxy for turbulence level. Osta et al. conclude that the longer nozzle has a faster rate of breakup, but different models can predict that without getting the precise sensitivity to turbulence intensity correct because the nozzle length also changes the velocity profile, as will be discussed in the next section. Because qualitative trends are so easy to match, they are not sufficient for validation.

The conclusion from these examples is that if a variable is not *empirically* quantified, it can be used to "validate" essentially any model or "confirm" any hypothesis.

From an experimental perspective, neglecting important variables also means that an experiment could be less reproducible. A later experimentalist could try to reproduce the experiment but be unable to, and have no way to verify that their setup is producing the same jets. Aside from fully developed pipe flows, the turbulence intensity at the outlet of an internal flow component is a function of the inlet turbulence intensity. Consequently, even using the same nozzles and same upstream pipework may not be sufficient for reproducibility. The inflows to the test system must also be standardized.

Given that fully developed turbulent pipe flows have a universal and well-understood state, they make an excellent basis for experimentation. "Pipe" nozzles are the de facto

---

[10]This also commits the fallacy of assuming that the model is true such that the model coefficients are meaningful. It would be better to instead plot the quantity of interest (not the model coefficient) as a function of nozzle length if one is going to use nozzle length as a proxy for turbulence intensity.

standard nozzle for basic turbulent jet breakup research. The friction factor f of a long pipe is strongly correlated with the averaged turbulence intensity $\overline{\text{Tu}}_0$ of the flow:

$$\overline{\text{Tu}}_{\text{FD}} = 0.366 f^{0.459}. \tag{4.1}$$

See figure 4.1. Consequently, the turbulence intensity of any pipe nozzle can be estimated[11]. The data compilation I made was restricted solely to pipe nozzles for this reason. Even if the researchers did not measure the turbulence intensity, it can still be credibly estimated if they used a pipe nozzle. This regression was produced through compilation of experimental data for both rough and smooth pipes, selecting only studies which measured all three velocity components [Lau54; San55; RBM65; Pat68; Gow69; Pow70; Law71] (17 points, 9 smooth, 8 rough). The power law has an R^2 value of 0.9753. Neglecting measurement error, the exponent with 95% error is 0.4587 ± 0.0401. On the subject of uncertainty, Rosler and Prieto [RP68] conducted an interesting experiment, showing that even for an identical pipe (to keep relative roughness constant) the turbulence intensities can vary by about 15% between water and air at the same Reynolds number. This may be a rough indication of the accuracy of this turbulence intensity estimation method.

The scaling $\overline{\text{Tu}} \propto f^{1/2}$ would follow from the assumption that $k^{1/2} \propto u_\tau$. This scaling has been suggested by Skrebkov [Skr66, p. 143][12] for radial RMS velocities near the pipe wall, Bourke et al. [Bou+68, p. 63, fig. 9.3] for centerline axial RMS velocities, Kim and Mills [KM89a, p. 1072L] and Bhunia and Lienhard [BL94, p. 341] for RMS velocities in pipe flows in general, and Yakhot, Bailey, and Smits [YBS10] for a plane averaged axial turbulence intensity. Yakhot, Bailey, and Smits propose that the relationship between $\overline{\text{Tu}}$ and f may be more complicated for $\text{Re}_{\ell 0} < 1 \times 10^5$ (or possibly 1×10^4 due to idiosyncrasies of their experimental facility; see Yakhot, Bailey, and Smits [YBS10, p. 69]).

One further observation from the regression is that the Blasius friction factor law for smooth pipes, $f = 0.316 \, \text{Re}^{-1/4}$, suggests that $\overline{\text{Tu}}_{\text{FD}}$ decreases as $\text{Re} \equiv \overline{U} d / \nu$ increases,

---

[11]When the friction factor of the pipe was not available, the regression from Incropera et al. [Inc+06, p. 490, eqn. 8.21] was used.

[12]Who cited Minskii [Min52, p. 133, eqn. 4.34], who in turn cited Velikanov [Vel46, p. 338, eqn. 10].
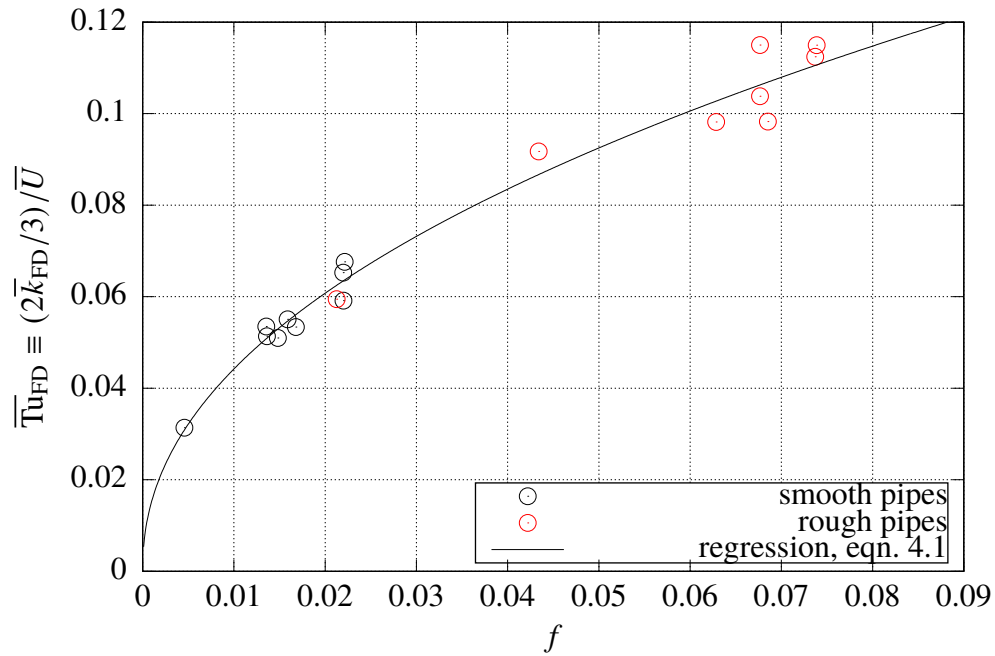
Figure 4.1: Experimental measurements of $\overline{\overline{\text{Tu}}}_{\text{FD}}$ as a function of the pipe friction factor, using only experiments where profiles of all three RMS velocity components (u', v', and w') are available. Also plotted is a regression.

contrary to what many expect. This trend is consistent with the experimental measurements of axial turbulence intensity at the centerline [San55, p. 35, fig. 15].

For smooth pipes with turbulent flows, the friction factor is a relatively weak function of the Reynolds number. The previously mentioned study by Skrebkov [Skr66] used pipes of varying roughness to change the turbulence intensity independent of the Reynolds number. Unfortunately, as can be seen in table 4.1, only 3 studies I am aware of used rough pipes [Skr66; Kus69; Kim83], so there is very little data with appreciable variation in turbulence intensity. This variation in turbulence intensity is much wider than is typical and provides a strong challenge to turbulent jet breakup models.

With this being said, pipe nozzles are not a panacea. Pipe nozzles are a poor choice for studying low turbulence intensity scenarios as a smooth pipe has a turbulence intensity of roughly 5%, while some nozzles designed to produce highly stable jets may have turbulence intensities below 1%. The critical Reynolds number of a pipe jet is on the order of 2000,

	all	$\mathrm{We}_{\ell 0}$	$\mathrm{We}_{\ell 0}, \overline{\mathrm{Tu}}_0$	$\mathrm{Re}_{\ell 0}$
C_{b}	3.52	7.87	3.61	10.3
C_{Tu}	−0.278	0.00	−0.275	0.00
C_{We}	0.321	0.321	0.334	0.00
C_{Re}	0.0120	0.00	0.00	0.246
R^2	0.956	0.855	0.958	0.457

Table 4.2: Table showing the effects of using different variables in a regression analysis for the breakup length, $\langle x_{\mathrm{b}} \rangle$. All the available electrical conductivity data fitting the data quality guidelines is used. The regression equation is the same as in table 4.3. Regression equation: $\langle x_{\mathrm{b}} \rangle / d_0 = C_{\mathrm{b}} \overline{\mathrm{Tu}}_0^{C_{\mathrm{Tu}}} \mathrm{We}_{\ell 0}^{C_{\mathrm{We}}} \mathrm{Re}_{\ell 0}^{C_{\mathrm{Re}}}$. Total number of data points: 193.

	all	$\mathrm{We}_{\ell 0}$	$\mathrm{We}_{\ell 0}, \overline{\mathrm{Tu}}_0$	$\mathrm{Re}_{\ell 0}$
C_{b}	1.16	4.49	9.87×10^4	5.02
C_{Tu}	−0.431	0.00	3.42	0.00
C_{We}	0.295	0.389	0.342	0.00
C_{Re}	0.0938	0.00	0.00	0.320
R^2	0.998	0.989	0.998	0.910

Table 4.3: Table showing the effects of using different variables in a regression analysis for the breakup length, $\langle x_{\mathrm{b}} \rangle$. Only data from Kusui [Kus69] is used. Total number of data points: 29.

compared against 10^5 or higher in contracting nozzles as discussed in § 3.3.4. Consequently, given a pipe jet that is turbulent at the nozzle outlet, it is possible that a contracting nozzle jet at the same Weber and Reynolds numbers will be laminar at the nozzle outlet. Care must also be taken to have a smooth outlet to separate the effects of imperfections in the orifice and turbulence intensity [RHM52, p. 1162; CD64, p. 179; PH70, p. 6].

If pipe nozzles are found to be inadequate in the future, there are other established ways of varying the turbulence intensity worth considering [SC96, p. 291R].[13]

When the turbulence intensity can be taken into account, the accuracy of a turbulent jet breakup model is improved. The results of regression analysis of breakup length data

---

[13]While not used in the regression analysis in this chapter, the integral scale is estimated using the data of Powe [Pow70] as discussed in footnote 3 on page 7.

under various conditions is shown in table 4.2. The regression equation

$$\frac{\langle x_b \rangle}{d_0} = C_b \overline{\mathrm{Tu}}_0^{C_{\mathrm{Tu}}} \mathrm{We}_{\ell 0}^{C_{\mathrm{We}}} \mathrm{Re}_{\ell 0}^{C_{\mathrm{Re}}} \tag{4.2}$$

is fitted to 149 data points from 7 different studies, as shown in figure 3.19[14]. These studies all used long pipes which produce fully developed turbulent flow as their nozzles. The data has been limited to the turbulent surface breakup regime where a power law for breakup length has been shown to hold. The study of Kusui [Kus69] had varying roughness which allows the turbulence intensity to vary from about 5% for a smooth pipe to about 13% for a very rough pipe as can be seen in figure 4.3[15] This variation in turbulence intensity is much wider than is typical and provides a strong challenge to turbulent jet breakup models.

The columns of table 4.2 indicate which of the 3 variables ($\mathrm{We}_{\ell 0}$, $\mathrm{Re}_{\ell 0}$, and $\overline{\mathrm{Tu}}_0$) are considered. The left column lists the exponents of the regression equation. The bottom row is R^2, a simple measure of how well the model matches the data[16]. Higher R^2 values indicate a better fit, with 1 being the maximum. Comparing the $\mathrm{We}_{\ell 0}$ and $\mathrm{We}_{\ell 0}$, $\overline{\mathrm{Tu}}_0$ cases shows that including the turbulence intensity in the model does appreciably improve the accuracy, increasing R^2 from 0.855 to 0.958. Adding $\mathrm{Re}_{\ell 0}$ only offers no improvement with an R^2 value of 0.956[17], indicating that the turbulence intensity is indeed more important than the Reynolds number in the turbulent surface breakup regime. As will be discussed in the next section, any apparent (small) Reynolds number effect may actually be a turbulence intensity effect due to confounding.

Lastly, I want to emphasize that taking into account some measure of the strength

---

[14]The data is fitted to only electrical measurements of breakup length because the photographic measurements are too noisy. However, the R^2 values are computed for all of the data, 193 points.

[15]Unfortunately Kusui [Kus69] had a moderate length smooth section after their rough pipe, which complicated the estimation of the turbulence intensity. The turbulence intensity was estimated as if the length of the short section was zero. This selection was found to be most consistent with breakup length data from non-pipe nozzles, as shown in figure 3.20. New experiments without this issue are needed.

[16]In the introduction, I had recommended examining how frequently the model estimates are within the error bounds of the data instead. R^2 implicitly assumes that the data has no uncertainty, and is chosen here for simplicity.

[17]The R^2 value is reduced slightly due to the fact that the regression is done in log coordinates but the R^2 values are taken in true coordinates, as discussed in § 2.5.

of the turbulence like the turbulence intensity is not sufficient. Likely other variables are factors, as discussed in appendix B. Additionally, only a measure of the *bulk* turbulence intensity was used in this work; the turbulence intensity profile likely is a factor as well.

4.4   Confounding and spurious correlation

Confounding between variables occurs when one can not differentiate between the effects of changing one variable and the effects of changing another. If two independent variables are changed at once, it is impossible to know the relative contributions each independent variable to the change seen in the dependent variable. Any change seen could have been due to one variable, the other, or both. The vast majority of previous turbulent jet breakup experiments considered in this work suffered from confounding between variables, making data analysis ambiguous unless steps are taken to avoid the confounding. Unfortunately, that was done infrequently for the confounding between $\mathrm{We}_{\ell 0}$ and $\mathrm{Re}_{\ell 0}$, rarely for the confounding between $\mathrm{Re}_{\ell 0}$ and $\overline{\mathrm{Tu}}_0$, and rarely for the confounding between the velocity profile and $\overline{\mathrm{Tu}}_0$. The difficulty of distinguishing between $\mathrm{We}_{\ell 0}$ and $\mathrm{Re}_{\ell 0}$ effects in jet breakup experiments was first noted by Asset and Bales [AB51, p. 2] in 1951, later independently noted by Dodu [Dod59; Dod60] in 1959, but appears to have received little attention since.

The most obvious example of confounding in turbulent jet breakup is between the Reynolds number $\mathrm{Re}_{\ell 0} \equiv \overline{U}_0 d_0 / \nu_\ell$ and the Weber number $\mathrm{We}_{\ell 0} \equiv \rho_\ell \overline{U}_0^2 d_0 / \sigma$. For most experiments, the researcher runs a series of tests with a particular nozzle and fluid, varying only the pressure. This, in turn, varies the jet bulk velocity, $\overline{U}_0$. Changing only the jet bulk velocity changes both the Weber and Reynolds numbers at the same time. See figure 4.2; the apparent lines come from different experimental trials using the same nozzle and fluid.[18]

Again, if two variables are changed simultaneously, it's impossible to attribute the effects seen to either variable unambiguously. Perhaps the jet is insensitive to changes in

---

[18] The earliest example of a $\mathrm{We}_{\ell 0}$-$\mathrm{Re}_{\ell 0}$ plot that I am aware of is due to Dodu [Dod59, p. 500, fig. 4] in 1959.

the Reynolds number as long as the Reynolds number is high enough to establish turbulent flow[19]. Then, all of the changes seen would be due solely to the Weber number changes. However, that can not be determined from a single nozzle with a single fluid. One must use different nozzle outlet diameters and/or fluids to break the correlation between $\mathrm{We}_{\ell 0}$ and $\mathrm{Re}_{\ell 0}$. This is what I did by compiling data from many different diameter nozzles and fluids, as can be seen in figure 4.2. Breaking the confounding requires varying the nozzle diameter and the fluid (to change the viscosity and/or surface tension).

Less obvious is the confounding between $\mathrm{Re}_{\ell 0}$ and $\overline{\mathrm{Tu}}_0$. For a particular nozzle geometry and surface roughness, the Reynolds number at the nozzle outlet determines the turbulence intensity at the nozzle outlet. The relationship between the two is not universal [Leb19], but is known for long pipe nozzles, as discussed previously. This confounding can be seen in figure 4.3. The confounding between the velocity profile and $\overline{\mathrm{Tu}}_0$ was also discussed in § B.6.

Confounding is often caused by nondimensionalization, as it is in the $\mathrm{We}_{\ell 0}$ and $\mathrm{Re}_{\ell 0}$ case. Dimensionless variables frequently have common dimensional variables. Even if all of the dimensional variables were uncorrelated, there may now exist a correlation between the dimensionless variables. A subset of this issue has been discussed extensively in the dimensional analysis literature as "spurious correlation" [Mer98]. However, spurious correlation is only a consequence of a particular type of confounding. In spurious correlation, the dependent (output) dimensionless variables contain dimensional variables in common with the independent (input, not statistically independent) dimensionless variables. In contrast, confounding is more general, and applies between independent variables.

Estimates of the correlation between variables with common terms can be computed assuming that the dimensional variables are uncorrelated [Mer98]. The correlation between dimensionless variables often should be considered when quantifying uncertainty, as typical approaches assume that all variables are uncorrelated[20].

---

[19]For convenience, when I write "independent of $\mathrm{Re}_{\ell 0}$", I mean "independent of $\mathrm{Re}_{\ell 0}$ provided it is high enough that the hydrodynamic flow regime is turbulent".

[20]Note that even if the dimensional variable in common between two dimensionless terms were held

To be clear, the confounding seen in turbulent jet breakup is not necessarily caused by nondimensionalization. For example, while the dimensionless velocity profile and turbulence intensity both have the average velocity $\overline{U}_0$ in common, confounding can still occur in cases where $\overline{U}_0$ is held constant, as it roughly is in many experiments. The confounding is actually an artifact of how some experiments are conducted. Multiple variables change as the nozzle aspect ratio L_0/d_0 is changed, where L_0 is the nozzle orifice length: 1. the velocity profile changes (and consequently, the boundary layer thickness increases); 2. the flow can transition from laminar to turbulent; 3. the turbulent kinetic energy typically increases (as would the magnitude of the Reynolds shear stress); 4. swirl decays; and 5. the flow could have separated at the nozzle inlet but reattach further downstream. Consequently, if one uses L_0/d_0 as a proxy for any of the 5 mentioned effects, one can not distinguish between these effects. A similar problem causes confounding between the turbulence intensity $\overline{\mathrm{Tu}}_0$ and Reynolds number $\mathrm{Re}_{\ell 0}$, as for smooth pipe nozzles the turbulence intensity is only a function of the Reynolds number. If one variable is a function of the other only, then regardless of the composition of those variables (i.e., into dimensional terms), they will be highly correlated. The type of confounding caused specifically by nondimensionalization is, however, the cause of confounding between $\mathrm{We}_{\ell 0}$ and $\mathrm{Re}_{\ell 0}$.

4.4.1 Avoiding confounding

Confounding in general is best avoided by covering the relevant parameter spaces relatively completely. This could be accomplished through factorial experimental designs. Factorial experiments appear to be rare in turbulent jet breakup; I am aware of only the studies of Ruiz and Chigier [RC87; RC90; RC91]. The researcher is also required to not miss any important variables. This work is limited by existing experiments in this regard. For turbulent jet breakup, existing data can avoid confounding only for the breakup length, because the parameter spaces are widely sampled enough in that case. To detect confounding, check parameter space plots (e.g., figures 4.2 and 4.3) for correlations between different variables. If these are seen, then cover the parameter space more comprehensively

---

constant experimentally, the errors would still be correlated.
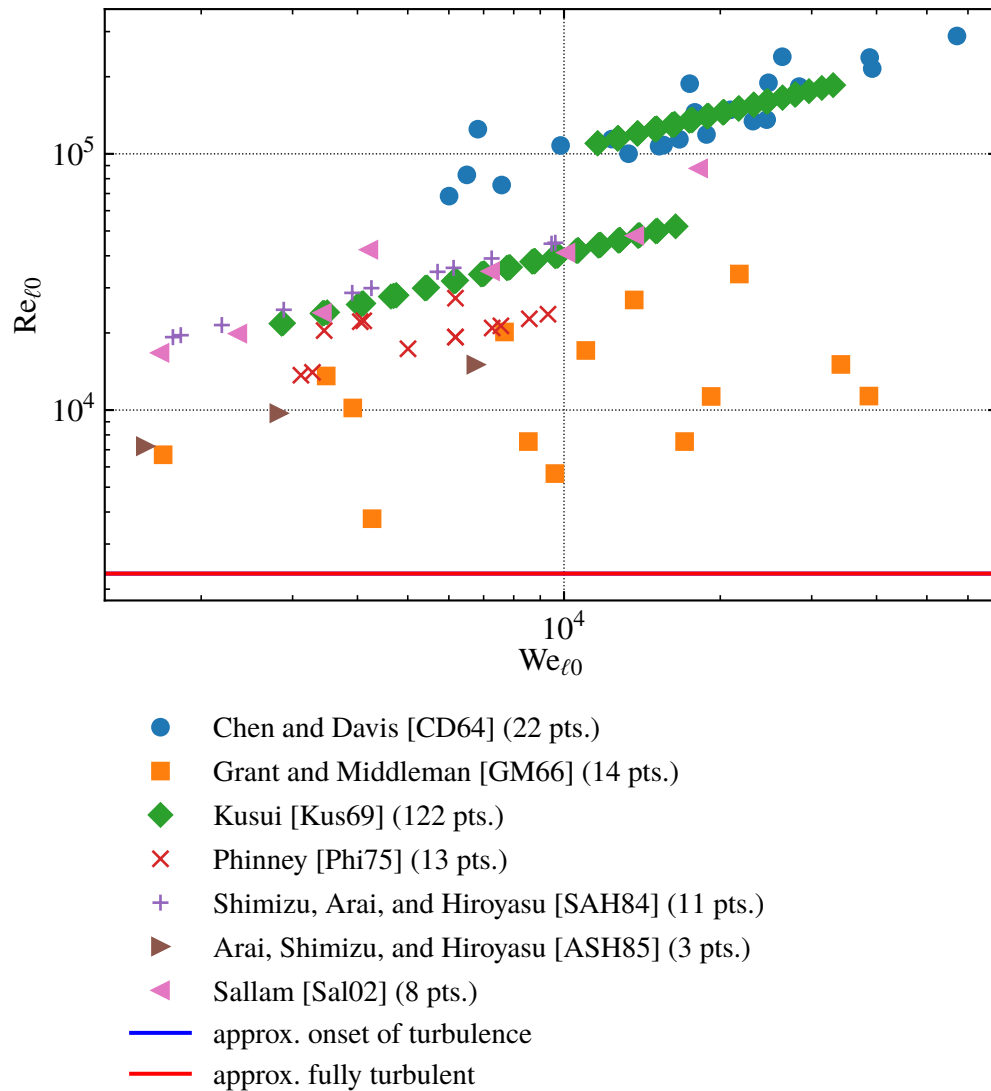
Figure 4.2: Parameter space of the breakup length showing the confounding between $We_{\ell 0}$ and $Re_{\ell 0}$ for pipes of a constant diameter with the same fluid. In the legend, the lines for the onset and full development of turbulence refer to turbulence *in the nozzle* rather than downstream on the jet.
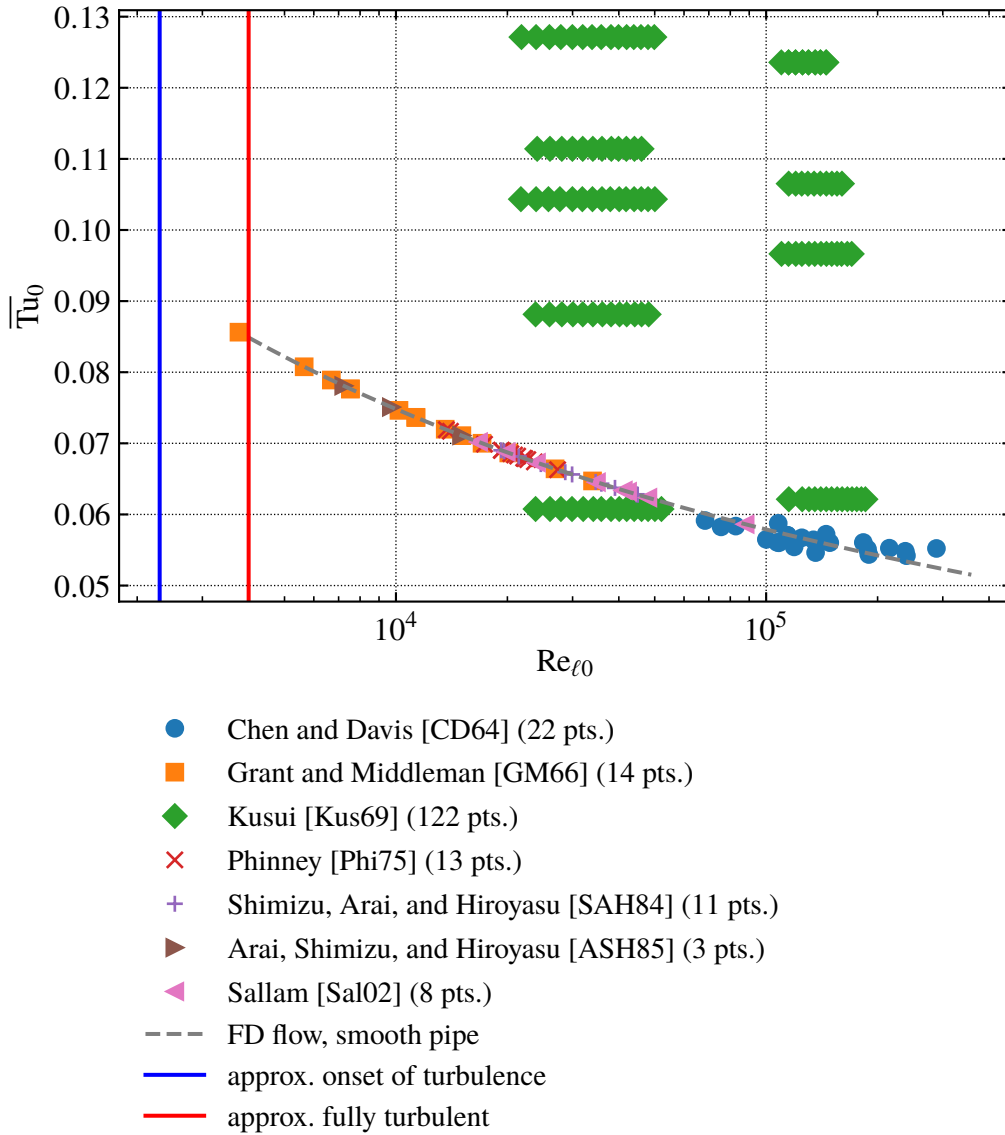
Figure 4.3: Parameter space of the breakup length showing confounding between $\mathrm{Re}_{\ell 0}$ and $\overline{\mathrm{Tu}}_0$ for smooth pipes. The jump at $\mathrm{Re}_{\ell 0} \approx 2 \times 10^4$ is an artifact of the use of a piecewise friction factor equation.

by changing the experimental conditions or looking for new data in different parts of the parameter space. As previously mentioned for the $\mathrm{We}_{\ell 0}$ and $\mathrm{Re}_{\ell 0}$ case, this may require changing the nozzle diameter and fluid.

4.4.2 Consequences of confounding

The potential consequences of confounding can be seen in tables 4.2 and 4.3. These tables show the results of regression analyses of breakup length data under various conditions. As previously discussed, table 4.2 shows the effect of using different variables in a regression analysis. Table 4.3 shows the effect of using different variables in a regression analysis *of confounded data*. Due to the confounding between $\mathrm{We}_{\ell 0}$ and $\mathrm{Re}_{\ell 0}$, and also $\mathrm{Re}_{\ell 0}$ and $\overline{\mathrm{Tu}}_0$, is is impossible to say whether the observed trends are due to changes in any of those three variables in the confounded case. Indeed, the R^2 values for three out of four conditions considered are nearly 1 in this case, and the remaining Reynolds number only condition is still very high. Any model can appear to work well here. Confounding between the Reynolds number and turbulence intensity occurs in most turbulent jet breakup experiments. And confounding between the Weber and Reynolds numbers is not uncommon either. As can be seen in figure 4.2, only 2 experimental studies (Grant and Middleman [GM66] and Kusui [Kus69]) out of 7 considered avoided confounding by using different nozzle diameters and/or fluids to cover the parameter space more widely. Compiling data in this case helped avoid confounding, but just adding data is not a solution to confounding. The data must avoid a correlation between the two variables of interest to avoid confounding.

Confounding may help explain why so many regressions in turbulent jet breakup seem to be contradictory[21]. For the breakup length, many different functional dependencies have been used. A small sample can give the reader an idea of the variety. Miesse [Mie55, p. 1698] proposed

$$\frac{\langle x_{\mathrm{b}} \rangle}{d_0} = 538 \mathrm{We}_{\ell 0}^{0.5} \mathrm{Re}_{\ell 0}^{-0.625}. \tag{4.3}$$

---

[21]The contradictions likely can be partly explained by differences in regimes as well.

Grant and Middleman [GM66, p. 184] suggested

$$\frac{\langle x_{\mathrm{b}} \rangle}{d_0} = 8.51 \mathrm{We}_{\ell 0}^{0.32}. \tag{4.4}$$

Wu and Faeth [WF95, p. 2917L] suggested a similar form using a data compilation including data from Grant and Middleman. Shavlovsky [Sha72, p. A6-82] offered

$$\frac{\langle x_{\mathrm{b}} \rangle}{d_0} = A - 68 \times 10^{-6} \mathrm{Re}_{\ell 0}, \tag{4.5}$$

where $A \approx 85$ to 112. Finally, De Jarlais, Ishii, and Linehan [DIL86, p. 87R] obtained the best fit equation

$$\frac{\langle x_{\mathrm{b}} \rangle}{d_0} = 480 \mathrm{We}_{\ell 0}^{0.5} \mathrm{Re}_{\ell 0}^{-0.53}. \tag{4.6}$$

Some researchers try both Weber and Reynolds numbers, while some prefer just one of either. It is possible that each of these expressions does in fact fit the source data well, but confounding makes the precise functional dependency more difficult to identify. Considering confounding, the data most closely matches the general form first proposed by Grant and Middleman [GM66], albeit with a turbulence intensity modification.[22]

The data presented here does not clearly eliminate a Reynolds number dependence, rather, it merely shows that any Reynolds number dependence on the breakup length in the turbulent surface breakup regime is weak. If I assume that the experimental data has no uncertainty and neglect the (presumably small) effects of confounding, then using the standard error for the coefficient in the case where all three variables are considered (table 4.2) I find that $C_{\mathrm{Re}_{\ell 0}} = 0.0120 \pm 0.0004$ (95% interval). This does not overlap with zero, though it might if the uncertainty in the experimental data is considered. Future work will examine if there still is some confounding between $\mathrm{Re}_{\ell 0}$ and $\overline{\mathrm{Tu}}_0$ which might make $C_{\mathrm{Re}_{\ell 0}}$ statistically indistinguishable from zero.

---

[22]On this note, McCarthy and Molloy [MM74, p. 7R] suggest that equation 4.4 "can scarcely be regarded as any more than a relation between $\langle x_{\mathrm{b}} \rangle / d_0$ and $\overline{U}_0$". Clearly, McCarthy and Molloy are aware of the dangers of viewing these regressions as more than relationships between the physical variable being varied and the physical variable being measured. Determining the precise relationship in terms of dimensionless variables is challenging. Unfortunately, McCarthy and Molloy appear to recommend instead equation 4.3, which is found in this work to be spurious.

4.5 Integration tests are necessary but not sufficient

Another common problem is the use of easily measured quantities which include droplet breakup (secondary breakup), droplet coalescence, and droplet transport to "validate" models which only predict primary[23] breakup quantities like the droplet diameter at formation. For simplicity I'll call measurements which include secondary breakup, droplet coalescence, and droplet transport "far-field" measurements. Kastengren et al. [Kas+17, p. 132L] rightfully note that "simply comparing modeled to measured droplet size in the far-field is insufficient to validate the physical breakup model; data in the "near-field" are needed, since this is the region in which primary breakup actually occurs." Magnotti and Genzale [MG17, p. 34L] have also expressed skepticism about the usefulness of far-field measurements.

Converting between near-field and far-field quantities now requires additional droplet breakup, coalescence, and transport models. As such, this attempt at validation does not test the primary breakup model directly. Now a validation failure could mean a failure of either the droplet breakup model, the droplet coalescence model, the droplet transport model, the primary breakup model, or any combination of the four. The result is ambiguous, making the models difficult to falsify. And a validation success does not necessarily mean that the primary breakup model is correct, as the droplet breakup and coalescence models could hypothetically compensate for problems in the primary breakup model in a way which makes each model wrong when taken in isolation. This possibility becomes much more likely when one considers that these models are usually tuned to the data.

For this reason, it is strongly preferred to validate each model individually (like a "unit test") in addition to the "integration test" for all of the submodels in combination. In software testing, a unit test tests a specific part of a software. An integration test tests the combination of the parts of the software. The same terminology can be applied to testing models in isolation vs. testing the larger collection of models. Similar terminology has been adopted in model validation previously [Obe01, pp. 37L-38R].

---

[23]"Primary" breakup and "jet" breakup are identical.

In the droplet diameter measurement case there is one additional subtlety that is often missed in the literature. It is not *strictly* correct to merely compare predictions of primary breakup droplet diameters to droplet measurements in the near-field, that is, droplet measurements at a particular location. One must measure only droplets which were just formed from the jet, that is, droplets formed through primary breakup without any other influences. I'll call these "just-formed" droplets for brevity. The measurements of the Faeth group (e.g. Wu, Tseng, and Faeth [WTF92], Wu, Miranda, and Faeth [WMF95], and Wu and Faeth [WF93]) are the only which I am aware of for just-formed droplets. These measurements are more difficult and limited than either near-field or far-field measurements, as they require analyzing many photographs of the breakup process to select only just-formed droplets. Photography is unfortunately limited in the near-field due to the density of the spray in many situations. Fortunately, new DNS data analysis techniques are being developed to obtain size distributions for just-formed droplets [RO19], however, this processed DNS data is not available as of this writing.

It is possible that the distribution of near-field droplets is similar to the distribution of just-formed droplets. If true, this would greatly simplify experimentation while maintaining rigor. To my knowledge, this hypothesis has yet to be validated. The easiest way to test the hypothesis would be to measure droplet diameters in the near-field in a case directly comparable to data collected by the Faeth group.

Several sources of data were neglected in my data compilation because only far-field quantities were measured. Of the 7 pipe jet studies with droplet diameter measurements, only 2 had droplets in the near-field. Both were measurements of just-formed droplets. The non-pipe data of Bogdanovich [Bog48] and Dumouchel, Cousin, and Triballier [DCT05] includes turbulent kinetic energy at the nozzle outlet, however, the droplet diameter measurements are in the far-field, making these data sources less attractive for validation.

The insufficiency of integration tests also was previously mentioned in the case of the combined nozzle turbulence and jet breakup models of Huh, Lee, and Koo [HLK98]. The nozzle turbulence model is in severe error, making one of the inputs of the spray model far off where it should be, likely making the model poorly calibrated for the true turbulence

119

intensity despite the apparent validation of the model.

4.6 Other common model validation problems

4.6.1 Apples-to-oranges comparisons

Strictly speaking, it is incorrect to naively combine data from nozzles of different geometries, but this is still frequently done in liquid jet breakup research. If not all the important variables are quantified, to properly combine data a researcher needs to be confident that the variables which are not quantified do not vary much, and as such can not have a major influence on the results. This is difficult to do in jet breakup research in general. Assuming that one has the turbulence intensity, for example, that is not sufficient to fully characterize the turbulence. One would need at the very least some measure of the integral scales. However, integral scale measurements are even more rare than turbulence intensity measurements. Consequently, when compiling data, for the moment it would be useful to know that the integral scales are roughly fixed and consequently will not be affecting the results appreciably. This may be true for pipe jets and is another reason to prefer pipes as nozzles. Earlier in this dissertation I compared against data from non-pipe nozzles and found deviations — see § 3.4.10. The prime suspects for the error are of course variables which I have no estimates for, such as the integral scales.

To give some examples of this problem, consider the breakup length model of Gorokhovski [Gor01] in 2001. The breakup length is plotted as a function of the square root of the density ratio $\sqrt{\rho_\ell/\rho_g}$ in figure 4.4. Gorokhovski would have had to selected a Weber and Reynolds number for this plot based on their model (if not other variables like turbulence intensity not considered in the model). This selection was not discussed in the paper, and it seems unlikely that the Weber and Reynolds numbers match the experimental data cited (Lee and Spencer [LS33] and Hoyt and Taylor [HT77b]). Consequently, this appears to be an apples-to-oranges comparison. The problem is actually worse than it appears at first glance, as neither Lee and Spencer [LS33] or Hoyt and Taylor [HT77b] report what is most commonly known as breakup length. Their studies are photographic and

do not report enough photos to allow for estimation of the breakup length. Gorokhovski's model computes the breakup length, but it is not being compared against the breakup length. And, finally, the fit between the model and data is not particularly good. Possibly Hoyt and Taylor's single data point fits poorly due to the apples-to-oranges comparison. Gorokhovski does not discuss this discrepancy, but characterizes the fit as "satisfactory", though the lack of uncertainty quantification makes how adequate the fit is difficult to determine.

This problem was not isolated to Gorokhovski's model. Over a decade later in 2017, Movaghar et al. [Mov+17] used a very similar plot to validate their turbulent jet breakup model. See figure 4.5. Movaghar et al.'s model was calibrated on pipe nozzles, so it seems inappropriate for the model to match data from different nozzles without mention of changing the turbulence intensity, which is a factor in Movaghar et al.'s model. This second example shows that these poor validation practices have been accepted as sufficient for the past 20 years.

4.6.2   Validation against only a small amount of data when more is available

The examples from Gorokhovski [Gor01] and Movaghar et al. [Mov+17] demonstrate another common issue: Validation against a small amount of data. Gorokhovski [Gor01] compared against a total of 5 data points. For the density ratio effect, Movaghar et al. [Mov+17] used only 4 of the previous data points. Fortunately, Movaghar et al. [Mov+17] used the data compilation of Wu and Faeth [WF95] for validation of their breakup length model at low atmospheric densities (high ρ_ℓ/ρ_g). Aside from the Faeth group, data compilation is rare.

As previously mentioned, turbulence intensity is frequently neglected. Comparison against data where the turbulence intensity varies over the range expected in practice is necessary to validate turbulent jet breakup models. Aside from my CDRSV model (chapter 5)[Tre20a], Skrebkov's model [Skr66]'s, and Bogdanovich's scaling model [Bog48], I am not aware of comparison of a model against data with varying turbulence intensity[24].

---

[24]The regression model of Dumouchel, Cousin, and Triballier [DCT05] is worth mentioning at this point,

More data, as long as it does not duplicate existing data or contribute to confounding, typically challenges a model. Jet breakup has been studied for over a century. While many of the early experimental studies are of poor quality by modern standards, studies from the 1950s through now are generally worth consideration. Validation is best done with as much data as possible to identify as many faults with a model as possible.

4.6.3 Not measuring the most typical quantity of interest

Considering only pipe jets, 4 studies were neglected because the QoIs were not measured at all [BC55; Rup62; MA66; HT80]. These studies tended to be old and were often qualitative (e.g. Hoyt and Taylor [HT80]) or focused on different QoIs than I do.

Considering non-pipe jets, another problem appeared. Some researchers used an alternative QoI which is analogous to but not the same as another common QoI. As an example, the DNS study of Salvador et al. [Sal+18, fig. 7] has a plot of axial mass concentration. It is reasonable to believe this is analogous to the breakup length, but the two are not directly comparable. There is no reason why the time-averaged or 50th percentile breakup length could not have been measured from the same DNS data that produced the axial mass concentration plot.

These issues would be reduced by adoption of standard quantities of interest. In this chapter I focus on the most commonly measured quantities of interest (see figure 2.1), which I believe are physically meaningful and useful.

4.7 Data presentation issues

4.7.1 Ambiguous data

Spray angle data from Van de Sande and Smith [VS73, fig. 3] was neglected due to the data being presented ambiguously. Parts of other studies were neglected for ambiguity as well. For example, to my knowledge it is not possible to determine the Reynolds number,

---

but it is not a phenomenological model like the others mentioned.

Weber number, etc., from the regime data presented by the study of Kusui [Kus69]. This is because the data was only plotted in coordinates that did not allow the Reynolds number and Weber number to be determined independently.

This problem is likely to persist due to space considerations in journals. However, in the future it is strongly recommended to include tabulated raw data (in primitive variables, e.g., $\overline{U}_0$, d_0, and ν_ℓ rather than $Re_{\ell 0}$) in reports and dissertations. Posting raw data online is also highly recommended in addition. To increase the probability of the data being available in the future, both are recommended.

To identify whether something is ambiguous in the data, it is recommended that someone else reproduce some basic plots of the data given the tabulated or digitized version.

On a related note, 2 studies were neglected from the data compilation because they presented curves for experimental data rather than data points [Pal62; MTZ86]. These studies were neglected because it is impossible to determine which precise points were tested from a curve.

4.7.2 Data neglected due to inconsistency with others

A few data sources were neglected due to inconsistency with other data sources deemed reliable.

Breakup onset location ($\langle x_i \rangle$) measurements from Eisenklam and Hooper [EH58] and Reitz [Rei78] were neglected because they were inconsistent with other measurements[25]. Possibly this is due to the use of small sample sizes, making the error in the mean very large.

Breakup length measurements for fluid II from Phinney [Phi73, p. 695, fig. 3] were neglected because the surface tension for fluid II appears to be much lower than seems possible for salt water.

---

[25]Because the spray angle from Reitz [Rei78] was used, this study does not count towards the count of inconsistent studies.
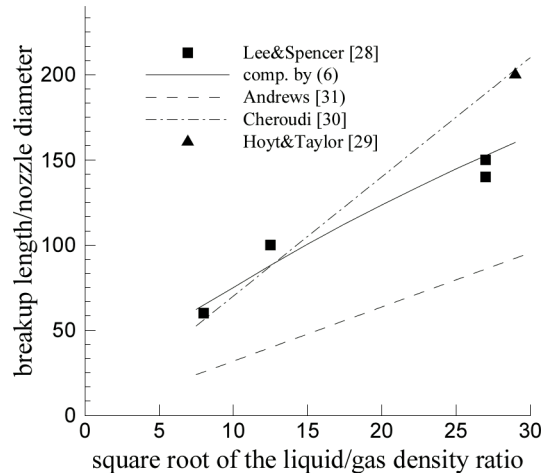
Figure 4.4: Breakup length as a function of the square root of the density ratio from Gorokhovski [Gor01, fig. 2].

4.7.3 Foreign language

3 studies were neglected because they were written in a foreign language and did not appear to contain useful data [Lit42; Baf77; Baf82]. While foreign language does not disqualify a study[26], if a foreign language study does not appear to contain valuable data from a superficial examination, I did not deem it important enough to examine further. It is possible that these studies do contain useful data that is obscured by the language barrier.

4.8 Conclusions

Improving the validation of turbulent jet breakup models requires not only changes to how models are validated but also new experimental data that is more challenging for model validation. Consequently recommendations are made for both modelers and experimentalists/computationalists. These guidelines are designed to address issues specifically in turbulent jet breakup, and they complement existing validation guidelines [Obe01].

---

[26]I published English translations of Russian papers by Natanzon [Nat18], Lebedev [Leb19], and Tsyapko [Tsy19b; Tsy19a] using Google Translate (I do not know Russian), so the language barrier is not impenetrable.
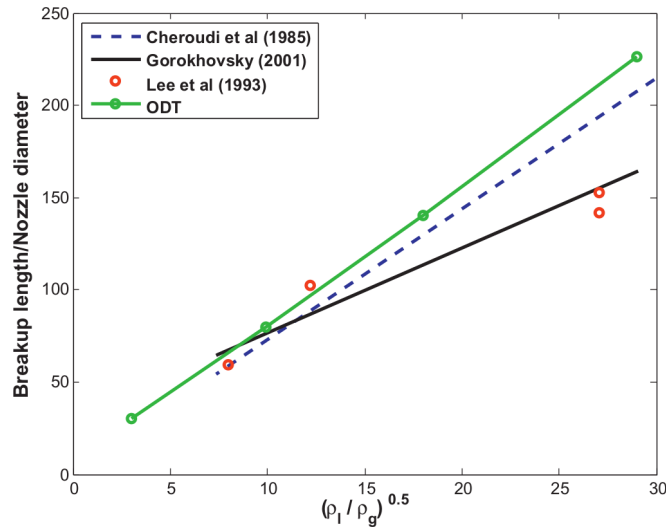
Figure 4.5: Breakup length as a function of the square root of the density ratio from Movaghar et al. [Mov+17, fig. 7]. Plot clearly based on Gorokhovski [Gor01, fig. 2].

4.8.1 Recommendations for model developers

1. Compile as much data as possible. Actively look for data that fills in gaps in your parameter spaces (e.g., figure 4.2) and avoids confounding.

2. Consider the uncertainty of the source data. If necessary, neglect data which is too uncertain.

3. Consider turbulence intensity in new models, as it is an important variable in turbulent jet breakup that is frequently neglected.

4. For primary breakup droplet diameter and velocity models, it is necessary to compare against primary breakup data, i.e., data on the diameter and velocity of droplets just-formed from the jet. Far-field measurements are discouraged. Near-field measurements may be acceptable, but they need to be compared against just-formed measurements to check that they are similar.

5. Match all variables ($We_{\ell 0}$, $Re_{\ell 0}$, $\overline{Tu}_0$, etc.) when comparing model estimates to data. And ensure that the model estimate is for the same quantity as the data. Otherwise the comparisons are invalid; they would be apples-to-oranges comparisons.

4.8.2 Recommendations for experimentalists and computationalists

1. Estimate uncertainty for every measurement.

2. Measure or estimate turbulence intensity at the very least, if not other turbulence quantities (integral scale, Reynolds stress).

3. If turbulence intensity will not be measured, use a standardized setup where the turbulence intensity can be credibly estimated. "Pipe" nozzles which produce fully developed turbulent flow are one way to do this. If the pipes are roughened and the friction factor of the pipe is measured, then the turbulence intensity can be credibly estimated.

4. Cover the $We_{\ell 0}$-$Re_{\ell 0}$ and $Re_{\ell 0}$-$\overline{Tu}_0$ parameter spaces well enough to avoid confounding. Don't use nozzle orifice length as a proxy for turbulence level or the velocity profile.

5. Measure common quantities of interest: droplet diameter distribution $f(D)$ or Sauter mean diameter D_{32}, average droplet velocity at formation $\langle v_d \rangle$, average breakup onset location $\langle x_i \rangle$, average breakup length $\langle x_b \rangle$, and spray angle θ_i. Other quantities of interest may be useful in specific applications.

6. For quantities without clear standard definitions (e.g., the spray angle), define the quantity in a precise way. Preferably this definition does not require expensive equipment. For the spray angle the standard could be a specific threshold for photographic or mass fraction measurements.

7. Distinguish between quantities of interest which depend on only primary breakup and those which include other effects. For testing primary breakup models, it is better to measure the diameters of droplets "just-formed" from the jet. If only near-field measurements are possible, replicate one of the papers with just-formed droplets and compare the near-field and just-formed measurements. If the two are close, then near-field is an acceptable proxy for just-formed measurements.

8. Release raw data with each publication. Both online publication of raw data and including tabulated data in dissertations are recommended. Ensure that the data is archived in a repository which is likely to be available for a long time in the future, for example, a university data repository.

Chapter 5

Conditional damped random surface velocity model of turbulent jet breakup[1]

5.1 Introduction

In this chapter I develop a theory for the breakup of a statistically steady high (liquid) Weber number turbulent liquid jet injected into a low density quiescent environment without cavitation. The present theory is intended to apply when the breakup is caused primarily by the interactions of the free surface and turbulent fluctuations, i.e., in the turbulent surface breakup regime, previously but erroneously called the "second wind-induced regime". I call this model the conditional damped random surface velocity (CDRSV) model. Fire hose jets are in the turbulent surface breakup regime, and I believe models for the turbulent surface breakup regime are an appropriate starting point for modeling the atomization regime as the two regimes are similar.

The model is comparable or superior to previous analytical models, though ultimately the accuracy is insufficient for applications. This model should be viewed as progress towards a statistical theory of turbulent jet breakup rather than the final word on the subject. Better estimates can be found from regressions developed from the large experimental database I compiled, described in chapter 3 and repeated in this chapter. Also, for convenience, an illustration of the quantities of interest found in this chapter is in figure 2.1.

---

[1]This chapter is modified from the second half of a paper submitted to Atomization and Sprays [Tre20a]. I am the sole author.
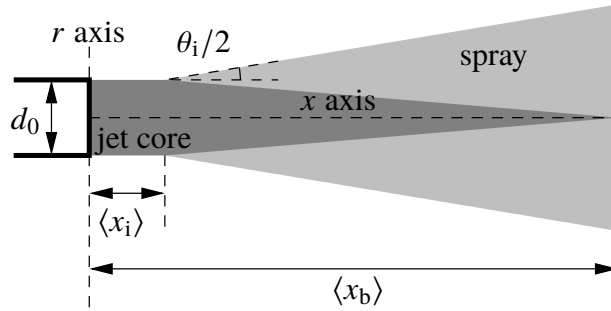
Figure 2.1: Jet breakup variables labeled on a schematic liquid jet. d_0 is the nozzle outlet diameter, $\langle x_i \rangle$ is the average breakup onset location, θ_i is the spray angle, and $\langle x_b \rangle$ is the breakup length.

5.2 CDRSV model development

Only data in the "turbulent surface breakup" regime is used in this work. In this regime the breakup is caused by turbulence with negligible aerodynamic effects — see § 3.4.10.

5.2.1 Turbulence evolution in liquid jets

Understanding how turbulence quantities (k and Λ) evolve spatially in the jet is required to develop models of the breakup of the entire jet. Kim [Kim83, p. 23] and Huh, Lee, and Koo [HLK98, p. 458] used turbulence models to estimate the decay of turbulence in the jet. Experiments show that turbulence in a liquid jet decays at the centerline initially [MC94b, p. 3390]. However, shear at the jet surface causes production of turbulence, such that k can increase. As droplets are formed at the free surface, using solely decay is not necessarily correct if production is significant. The measurements of Mansour and Chigier [MC94b, p. 3389] suggest that k at the jet boundary grows slowly downstream. This is inconsistent with the measurements of Wolf, Incropera, and Viskanta [WIV95, p. 402L], which suggest that k only decays at the boundary. Given the complexity of turbulence modeling, I will use the approximation of Wu, Tseng, and Faeth [WTF92, p. 308]: k and Λ do not vary downstream. The turbulence will also be approximated as homogeneous in the radial and angular directions and isotropic. Spatial averaged $\overline{k}$ will approximate the k profile. In reality, k peaks near the free surface, becoming more homogeneous downstream.

129

5.2.2 Simplified example of CDRSV theory
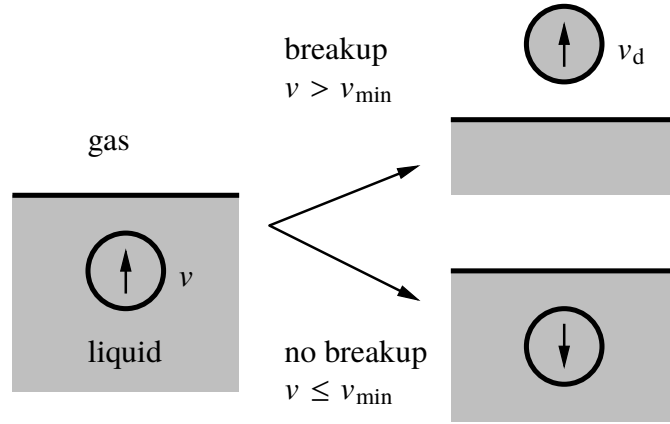
Figure 2.2: There are two possibilities when a turbulent event occurs at the free surface: breakup (top right) and no breakup (bottom right), depending on whether the velocity fluctuation exceeds the critical velocity v_{min} which could be a function of the length scale associated with the fluctuation.

Jet breakup models often *assume* that the average radial droplet velocity at formation is proportional to the turbulent RMS velocity, $\langle v_d \rangle \propto v'$ [Nat18, p. 38; WTF92, p. 305; HLK98, p. 460]. CDRSV theory can easily mathematically derive this result and predict the constant of proportionality.

Consider an eddy with radial velocity v approaching the free surface as seen in figure 2.2. Additionally assume that the free surface returns to a straight line once all interactions with eddies are complete and that no more than one eddy interacts with the free surface at any time. The velocity fluctuations at the free surface are assumed to be accurately described by a Gaussian probability density function (Gaussian PDF for short).

In this example, the free surface presents no obstacle to the eddy, i.e., the surface tension is zero and there is no "damping". So $v_d = v$. Or, in words, the droplet velocity equals the fluctuation velocity. A droplet is formed if the droplet velocity is greater than zero, i.e., $v_d > 0$, so if $v > v_{min} = 0$ in this case — v_{min} will not be zero in the more complex cases considered later in this chapter. I abbreviate this condition as DF (droplet formation).
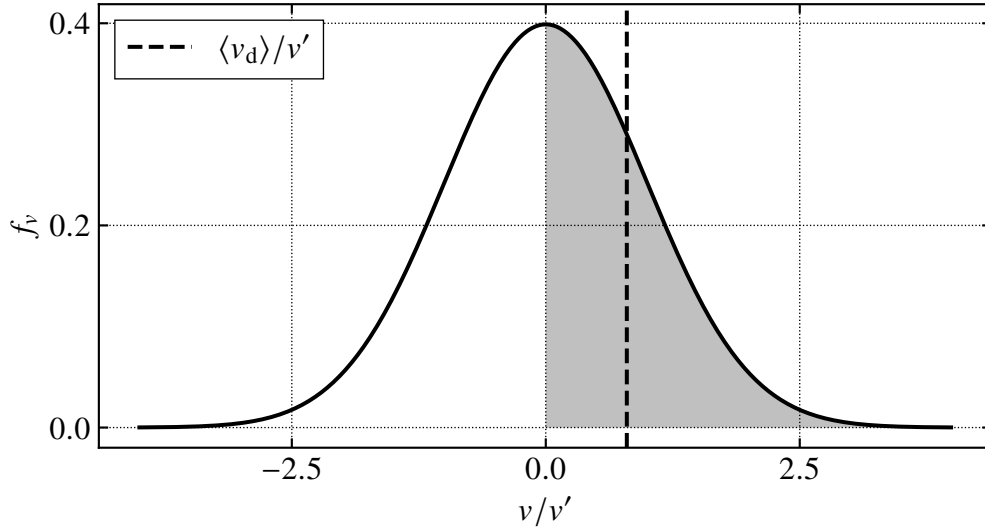
Figure 5.1: A Gaussian velocity probability density function, with the fluctuations that can lead to breakup shaded. The vertical dashed line is the average velocity fluctuation which causes breakup, which in the simplified model is the same as the average radial droplet velocity, $\langle v_d \rangle$.

The term DF will be dropped if redundant.

$$\langle v_d \rangle = \langle v_d \mid \text{DF} \rangle = \langle v \mid \text{DF} \rangle = \int_{v_{\min}}^{\infty} v \cdot \underbrace{\left(\frac{f_v(v)}{\int_{v_{\min}}^{\infty} f_v(v)\, dv} \right)}_{\text{conditional density}} dv$$

$$= \int_{0}^{\infty} \frac{2v}{\sqrt{2\pi v'^2}} \exp\left(-\frac{v^2}{2v'^2} \right) dv = \sqrt{\frac{2}{\pi}} v'$$

Without conditioning, $\langle v_d \rangle = 0$. With the $v > 0$ condition, the average radial droplet velocity has to be greater than zero. Graphically, the effect of the conditioning can be see in figure 5.1. The shaped portion of the Gaussian PDF is the part conditioned on. The average of the conditioned portion is given by the red vertical line. Obviously, by excluding all fluctuations in the negative direction, the average droplet velocity must move to greater than zero, as the math shows. This basic procedure can be applied to calculate various quantities of interest in turbulent jet breakup, not just the droplet radial velocity.

5.2.3 Droplet radial velocity v_d for a particular eddy and the Hinze scales — the damping

A model of the droplet formation process considering surface tension is needed. Consider a random turbulent velocity fluctuation v (mean zero) at the free surface at time 0 (so $\tilde{v}(t=0) = v$). A droplet forms if the radial velocity $\tilde{v}(t) > 0$ when a droplet detachment condition is met. Surface tension opposes/damps the turbulent fluctuations. This force $F_\sigma = A \cdot p_\sigma$ where A is the cross-sectional area of the surface perturbation and $p_\sigma = 2\sigma/R$ is the capillary pressure, where R is the radius of curvature. I assume that the surface perturbations are spherical, with a radius of curvature R equal to the distance δ the eddy penetrates outside the free surface (see figure 5.2). Multiplying by an arbitrary constant, I find that $F_\sigma = 2\pi C_F \sigma \delta$. I assume that the eddy has a diameter proportional to $\ell \equiv 2\pi/\kappa$, where κ is the wavenumber of the turbulence associated with the velocity fluctuation v. (Note that despite the eddy's nominal diameter being ℓ, I select the radius of curvature as δ for simplicity.) The eddy's mass then is $C_{\forall}\rho_\ell \pi \ell^3/6$, with another arbitrary constant. The equations of motion of the eddy as it penetrates the surface are

$$\frac{\mathrm{d}\delta}{\mathrm{d}t} = \tilde{v} \quad \text{and} \quad -2\pi C_F \sigma \delta = C_{\forall}\rho_\ell \frac{\pi}{6}\ell^3 \frac{\mathrm{d}\tilde{v}}{\mathrm{d}t}, \tag{5.1}$$

which have the solutions

$$\delta = v t_R \sin\left(\frac{t}{t_R}\right), \quad \tilde{v} = v \cos\left(\frac{t}{t_R}\right), \quad \text{where} \quad t_R^2 \equiv \frac{C_{\forall}\rho_\ell \ell^3}{12 C_F \sigma}. \tag{5.2}$$

If it is assumed that the droplet detaches after traveling a distance $\delta = C_{\text{lig}}\ell$ ($C_{\text{lig}} \gtrsim 2$, so that detachment occurs when the lower end of the ligament is beyond the original free surface location), then the breakup time t_b can be found and the droplet velocity at detachment ($v_d = \tilde{v}(t = t_b)$) is:

$$\frac{t_b}{t_R} = \sin^{-1}\left(\frac{C_{\text{lig}}\ell}{v t_R}\right) \quad \text{and} \quad \frac{v_d}{v} = \sqrt{1 - \frac{12 C_{\text{lig}}^2 C_F}{C_{\forall}} \frac{\sigma}{\rho_\ell v^2 \ell}} = \sqrt{1 - \frac{\mathrm{We_{T,crit}}}{\mathrm{We_T}}}. \tag{5.3}$$

This model is oversimplified, but it has the desired features. The last term is an
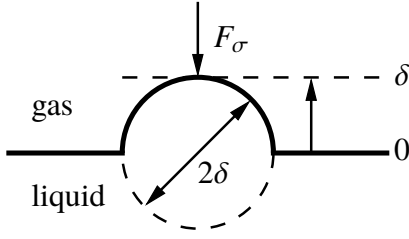
Figure 5.2: Eddy penetrating surface.

inverse eddy Weber number, $\mathrm{We_T} \equiv \rho_\ell v^2 \ell / \sigma$. Droplet formation ($v_d > 0$) requires that $\mathrm{We_T} > \mathrm{We_{T,crit}} \equiv 12 C_{\mathrm{lig}}^2 C_F / C_V$. As such, minimum scales for droplet formation exist. An arbitrary eddy velocity v can be related to a corresponding eddy wavenumber κ with $v = \sqrt{\kappa E(\kappa)}$ [Hin75, p. 222]. If I assume that the minimum scales are in the inertial range and apply $v = \sqrt{\kappa E(\kappa)}$ to the inertial range spectrum $E(\kappa) = C_K \varepsilon^{2/3} \kappa^{-5/3}$, I find that $\ell = 2\pi v^3 / (C_K^{1/2} \varepsilon)$. Note that $C_K = 1.5$ is recommended by Pope [Pop00, p. 231]. From there I can calculate the Hinze scales [Kol91; Hin55], the smallest for which droplet formation can occur ($v_d = 0$):

$$v_\sigma \equiv \underbrace{\left(\frac{\mathrm{We_{T,crit}}}{2\pi} \right)^{1/5}}_{C_{v_\sigma}} \left(\frac{\sigma \varepsilon}{\rho_\ell} \right)^{1/5} \qquad \text{and} \qquad \ell_\sigma \equiv \underbrace{\left(\frac{2\pi C_{v_\sigma}^3}{C_K^{1/2}} \right)^{1/5}}_{C_{\ell_\sigma}} \left(\frac{\sigma^3}{\rho_\ell^3 \varepsilon^2} \right)^{1/5}. \qquad (5.4)$$

The velocity v_σ is the minimum for droplets to form *if surface tension dominates*. At high Weber numbers v_σ may decrease below v_K, the Kolmogorov velocity scale [Pop00, p. 185], and in that case v_K will be the minimum. I use the term v_{min} for whichever minimum applies. Because not all fluctuations produce droplets, the ensemble averages I calculate will be conditioned on droplet formation, abbreviated DF. The condition notation will be dropped for terms which imply breakup occurs, e.g., $\langle v_d \mid \mathrm{DF} \rangle$ would be redundant. Additionally, I'll use $v_{min} = v_\sigma$ for simplicity in this chapter. Analogous expressions for $v_{min} = v_K$ are easily found.

I am unaware of data capable of validating the minimum droplet velocity and diameter estimates. The smallest droplet observed by Wu [Wu83, p. 36] was 3 μm in

diameter ($< 0.5 \ \mu$m uncertainty, $\rho_\ell / \rho_\mathrm{g} < 40$, likely in the atomization regime), but insufficient detail was provided to estimate ℓ_σ or ℓ_K, the Kolmogorov length scale [Pop00, p. 185], for this case. The smallest droplets measured by Wu, Tseng, and Faeth [WTF92, p. 307] ($\rho_\ell / \rho_\mathrm{g} > 500$) were said to be much larger than ℓ_K in the turbulent surface breakup regime. The DNS study of McCaslin and Desjardins [MD15, p. 5, fig. 2b] suggests that surface perturbations are suppressed for scales smaller than ℓ_σ if $\ell_\sigma > \ell_\mathrm{K}$. Also, note that while the DNS study of Ling et al. [Lin+19] suggests that the Hinze scale is larger than the smallest observed droplets, this study is not in the turbulent surface breakup regime studied here, as that work has very strong shear that is absent in the problem studied in this work.

5.2.4   Sauter mean diameter, D_{32}, and average droplet radial velocity, $\langle v_\mathrm{d} \rangle$

Wu, Tseng, and Faeth [WTF92, p. 312] assume that D_{32} scales with a representative length (in the terminology used here, $D_{32} \propto \langle \ell \mid \mathrm{DF} \rangle$), however, I will not assume this. D_{32} is controlled by the surface energy, not the size of the eddies directly. Energy conservation suggests (assuming the process is adiabatic and neglecting rotational and other energies):

$$\tfrac{1}{2} \rho_\ell \mathcal{V} \left[\left(\overline{U}_0 + u \right)^2 + v^2 + w^2 \right] = \sigma SA + \tfrac{1}{2} \rho_\ell \mathcal{V} \left(u_\mathrm{d}^2 + v_\mathrm{d}^2 + w_\mathrm{d}^2 \right), \tag{5.5}$$

or simplified:

$$\sigma \frac{SA}{\mathcal{V}} = \tfrac{1}{2} \rho_\ell \left(v^2 - v_\mathrm{d}^2 \right), \tag{5.6}$$

where in the first equation the left side is before breakup and the right side is after breakup. I assumed that only one droplet is formed per eddy event. The eddy/droplet has volume $\mathcal{V}$, and the formed droplet has surface area SA. The model also implicitly assumes that v_d and droplet diameter D are perfectly correlated. For simplicity I assume that the r direction is always normal to the liquid surface, accurate for large $\langle x_\mathrm{b} \rangle / d_0$. Like v ($= \tilde{v}(t = 0)$ as before), u and w are turbulent velocity fluctuations with mean zero defined in the streamwise and angular directions, respectively. The mean velocities in the radial and angular directions are zero. (If the jet is decelerating, there is a mean $\overline{V}$ as well, however, I neglect this as I assume aerodynamic drag is negligible.) I assume that the free surface does not affect

streamwise or angular velocities such that $u_d \equiv \overline{U}_0 + u$ and $w_d \equiv w$. These cancel with the input energy, leaving the surface area to volume ratio to be determined by the energy left over from the damping. Now, I apply the conditional average and the model for v_d (equation 5.3), and note that by hypothesis $\langle SA/\mathcal{V} \rangle \approx \langle SA \rangle / \langle \mathcal{V} \rangle = 6/D_{32}$:

$$\sigma \left\langle \frac{SA}{\mathcal{V}} \right\rangle = \tfrac{1}{2}\rho_\ell \left\langle v^2 - v_d^2 \,\middle|\, \mathrm{DF} \right\rangle = \tfrac{1}{2}\rho_\ell \mathrm{We_{T,crit}} \left\langle \frac{v^2}{\mathrm{We_T}} \,\middle|\, \mathrm{DF} \right\rangle, \tag{5.7}$$

which returns

$$D_{32} = \frac{12}{\mathrm{We_{T,crit}}} \left\langle \ell^{-1} \,\middle|\, \mathrm{DF} \right\rangle^{-1}. \tag{5.8}$$

Contrary to what one might expect, D_{32} is proportional to the *harmonic mean* $\left\langle \ell^{-1} \,\middle|\, \mathrm{DF} \right\rangle^{-1}$, not the *arithmetic mean* $\langle \ell \mid \mathrm{DF} \rangle$. The two terms are the same to first-order, but not identical. This term is unclosed, so it requires a model.

The concept of an "eddy" in this work will be clarified. The length ℓ associated with a particular velocity fluctuation v is ambiguous. The energy spectrum as used by Wu and Faeth [WF95, p. 2916] can relate v and ℓ, but this is only a heuristic. More than one "eddy" can contribute to velocity fluctuations at a particular location. Smaller lengths likely have only one eddy contribution, making the idea behind the Hinze scales reasonable. Larger velocity fluctuations may involve more than one eddy, making the spectrum heuristic incorrect. I'll use the functional form of the average to inform the choice of the model. For D_{32} specifically, I'll use the inertial range spectrum, as the average is more strongly influenced by the smallest scales. Averages controlled by larger scales require a different length scale specification. The inertial range spectrum with the dissipation model $\overline{\varepsilon}_0 = C_\varepsilon \overline{k}_0^{3/2}/\Lambda_0$ suggests $D_{32} \propto \left\langle v^{-3} \,\middle|\, \mathrm{DF} \right\rangle$, which can be computed with a prescribed PDF. The value $C_\varepsilon = 0.43$ is recommended by Pope [Pop00, p. 244].

To maintain analytical tractability, a power law velocity PDF ($f_v(v) = Cv^{-\alpha}$) will be used. A Gaussian PDF would be more realistic, but will be used in future work to keep this work simple. Both are compared in figure 5.3. Generally $\left\langle v^\beta \,\middle|\, v > v_{\min} \right\rangle \propto \overline{v'}^\beta f_v(v_{\min}/\overline{v'})$, implying $\langle v_d \rangle \propto \overline{v'}$ as hypothesized by Wu, Tseng, and Faeth [WTF92, p. 305], but for power law PDFs $\left\langle v^\beta \,\middle|\, v > v_{\min} \right\rangle \propto v_{\min}^\beta$ with no $\overline{v'}$ dependence. (Again, DF means $v > v_{\min}$ here.)
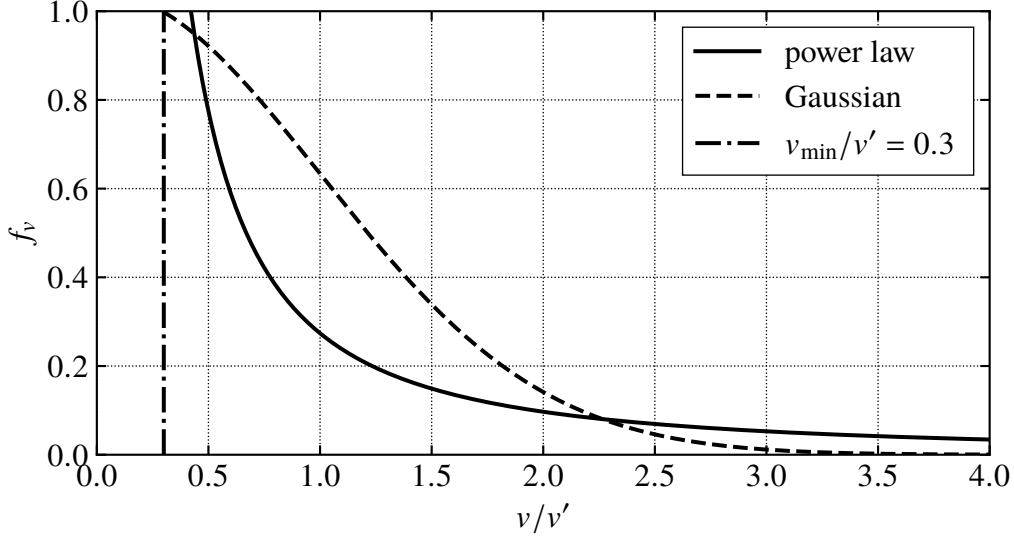
Figure 5.3: A comparison of Gaussian and power law probability density functions for the tails of the velocity fluctuations. Both are conditioned on $v > v_{\min} = 0.3v'$.

Using a power law PDF, I find that $\langle v^{-3} \,|\, v > v_{\min} \rangle = (\alpha - 1)v_{\min}^{-3}/(\alpha - 2)$. To compute D_{32}, I start with equation 5.8, then use the inertial range spectrum to eliminate ℓ, substitute in the dissipation and $\langle v^{-3} \,|\, v > v_{\min} \rangle$ models, and choose $v_{\min} = v_\sigma$ (equation 5.4) to find

$$
\begin{aligned}
\frac{D_{32}}{d_0} &= \frac{24\pi}{\mathrm{We_{T,crit}}} \frac{\langle v^{-3} \,|\, v > v_{\min} \rangle}{C_{\mathrm{K}}^{1/2}\varepsilon} \\
&= \frac{24\pi}{\mathrm{We_{T,crit}}} \frac{\alpha - 2}{\alpha - 1} \left(\frac{v_\sigma}{\overline{v_0'}} \right)^3 \frac{\Lambda_0}{d_0} \\
&= C_{D_{32}} \overline{\mathrm{Tu}_0}^{-6/5} \mathrm{We}_{\ell 0}^{-3/5} \left(\frac{\Lambda_0}{d_0} \right)^{2/5}.
\end{aligned}
\tag{5.9}
$$

which has a similar scaling to Wu, Tseng, and Faeth [WTF92, p. 308] for the initial value of D_{32}, despite the difference in the definition (see equation 2.39). This is a consequence of the power law PDF. Alternative choices could make how $\langle \ell \,|\, \mathrm{DF} \rangle$ and $\langle \ell^{-1} \,|\, \mathrm{DF} \rangle^{-1}$ scale differ. To find the average droplet velocity $\langle v_{\mathrm{d}} \rangle$ I start with equation 5.3 and apply an approach similar to that for D_{32}, noting that $\langle v^{-5} \,|\, v > v_{\min} \rangle = (\alpha - 1)v_{\min}^{-5}/(\alpha + 4)$ for a

136

power law PDF. I find that

$$
\begin{aligned}
\frac{\langle v_{\mathrm{d}} \rangle}{\overline{v_0'}} &\approx \frac{\langle v \mid \mathrm{DF} \rangle}{\overline{v_0'}} \left\langle 1 - \mathrm{We}_{\mathrm{T,crit}} \frac{\sigma}{\rho_\ell v^2 \ell} \,\middle|\, \mathrm{DF} \right\rangle^{1/2} \\
&= \frac{v_{\min}}{\overline{v_0'}} \left(\frac{\alpha - 1}{\alpha - 2} \right) \left(1 - C_{\mathrm{K}}^{1/2} \frac{\alpha - 1}{\alpha + 4} \right)^{1/2} \\
&= C_{v_{\mathrm{d}}} \overline{\mathrm{Tu}}_0^{-2/5} \left(\mathrm{We}_{\ell 0} \frac{\Lambda_0}{d_0} \right)^{-1/5}.
\end{aligned}
\tag{5.10}
$$

The theory will now be calibrated against experimental data. Only initial droplet diameter and velocity measurements are compared because the constant k and Λ approximations may be inaccurate downstream. For initial D_{32}, three data sources are available [WTF92; WMF95; WF93]. For initial droplet radial velocity, I use data from Wu, Tseng, and Faeth [WTF92, p. 305]. None of these sources have rough tubes, so the data has almost no variation in $\overline{\mathrm{Tu}}_0$. Fitting the data, the coefficient $C_{D_{32}} = 0.522$ (29 points, $R^2 = 0.730$) and the coefficient $C_{v_{\mathrm{d}}} = 0.254$ (17 points, $R^2 = -0.625$). Figure 5.4 shows a comparison of the D_{32} theory against the data. The measurement error in $\langle v_{\mathrm{d}} \rangle$ is large — 60% according to Wu [Wu92, p. 129] — making a close fit impossible for any reasonable model. Given the small variation in $\overline{\mathrm{Tu}}_0$ for the data, for the moment the most that can be said is that the theory is not inconsistent with the data for $\langle v_{\mathrm{d}} \rangle$. Due to the high measurement error and consequential poor fit, no plot comparing the $\langle v_{\mathrm{d}} \rangle$ theory and the data is presented.

Similar procedures can find other diameters. The mass mean diameter has the same average mass as the ensemble averaged spray at that location, so $\langle m_{\mathrm{d}} \rangle = \rho_\ell \pi D_{30}^3 / 6$. Consistent with the model used to find v_{d}, $\langle m_{\mathrm{d}} \rangle = \left\langle C_V \rho_\ell \pi \ell^3 / 6 \,\middle|\, \mathrm{DF} \right\rangle$, so $D_{30} = C_V \left\langle \ell^3 \,\middle|\, \mathrm{DF} \right\rangle^{1/3}$ (a *cubic mean*). This term is more strongly influenced by the larger scales than D_{32}.

5.2.5 Average breakup onset location, $\langle x_{\mathrm{i}} \rangle$

I define the breakup onset location as the average distance eddies travel from the nozzle outlet in the time it takes for breakup to occur: $\langle x_{\mathrm{i}} \rangle \equiv \left\langle (\overline{U}_0 + \overline{u_0'}) t_{\mathrm{b},0} \,\middle|\, \mathrm{DF} \right\rangle \approx$
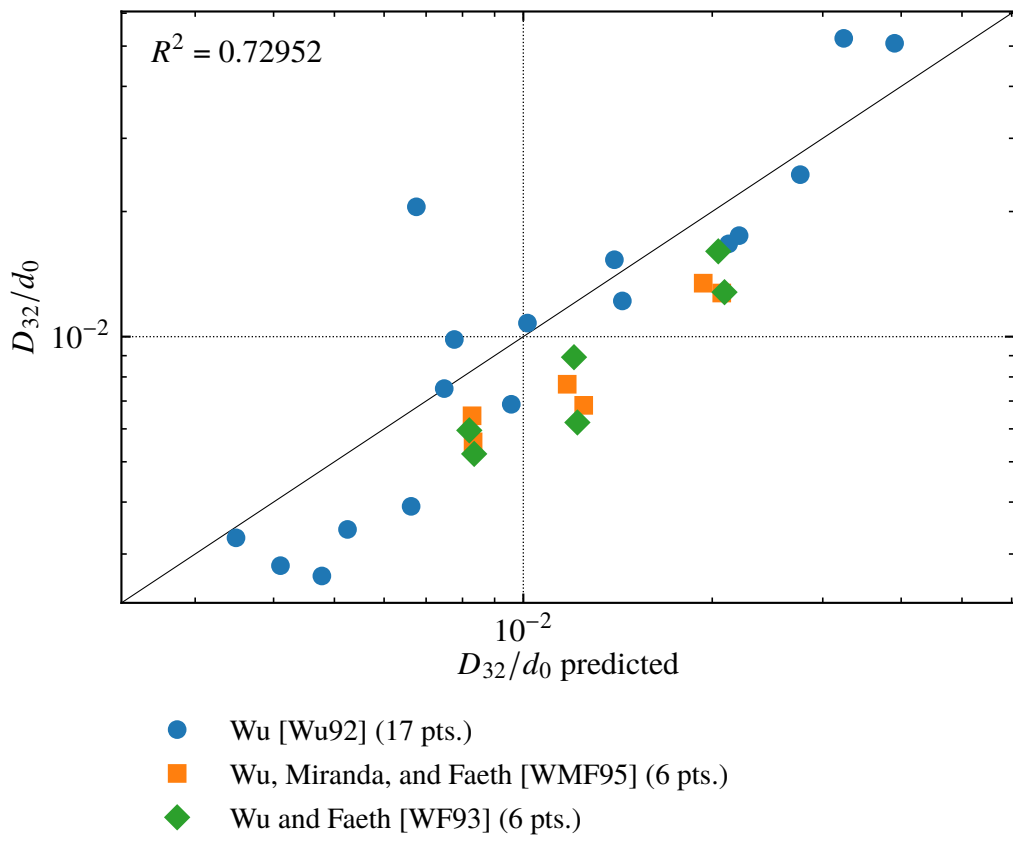
Figure 5.4: Comparison of the D_{32} theory (equation 5.9) against experimental data.

$\overline{U}_0 \langle t_{b,0} \rangle$ assuming that $\langle uv \rangle$ is small (because u and v are correlated) and that $t_{b,0}$ is small (or else an integral with a random integrand would need to be computed). To second-order $t_b = C_{lig}\ell/v$ (see equation 5.3) so $\langle t_{b,0} \rangle \propto \langle \ell/v \mid DF \rangle$, which is difficult to model. The term is not influenced by the smallest scales as much as D_{32}. As such, I assume that the conditioning has little effect. By hypothesis, the parameters influencing the breakup time are σ (N/m), ρ_ℓ (kg/m^3), and $\overline{v'_0}$ (m/s), from which a unique time scale can be formed: $\langle t_{b,0} \rangle \propto \sigma/(\rho_\ell \overline{v'_0}^3)$, leading to

$$\frac{\langle x_i \rangle}{d_0} = \frac{\overline{U}_0 \langle t_{b,0} \rangle}{d_0} = \frac{C_{lig}\overline{U}_0}{d_0}\left\langle \frac{\ell}{v} \,\middle|\, DF \right\rangle = C_{x_i}\frac{\overline{U}_0 \sigma}{d_0 \rho_\ell \overline{v'_0}^3}$$

$$= C_{x_i}\left(\frac{\overline{U}_0}{\overline{v'_0}}\right)^3 \frac{\sigma}{d_0 \rho_\ell \overline{U}_0^2} = C_{x_i}\overline{Tu}_0^{-3}We_{\ell 0}^{-1}. \tag{5.11}$$

This result is equivalent that of Kerstein, Movaghar, and Oevermann [KMO17] if one replaces their $u_{\tau,0}$ with $\overline{v'_0}$. Their model would have no $Re_{\ell 0}$ dependence with this modification. The $\overline{v'_0} \propto u_{\tau,0}$ scaling implies $\overline{Tu}_0 \propto \sqrt{f}$, similar to the regression for fully developed pipe flows ($\overline{Tu}_0 \propto f^{0.4587}$, equation 4.1). This scaling is consistent with multiple physical pictures, not just the boundary layer scaling described by Kerstein, Movaghar, and Oevermann. The available pipe jet data is unfortunately not able to distinguish between the two theories. Fitting the theory to the data returns $C_{x_i} = 20.4$ (52 data points, $R^2 = 0.905$). A comparison of the theory and experimental data is in figure 5.5.

5.2.6 Average breakup length, $\langle x_b \rangle$

To determine the breakup length, I first calculate the average surface mass flux of droplets from the jet, $\langle \dot{m}'' \rangle$. I decompose the surface into waves of wavenumbers $\kappa \propto 1/\ell$ in the streamwise and angular directions. I assume droplets are formed with frequency v/ℓ and mass proportional to $\rho_\ell \ell^3$. I ensemble average to determine $\langle \dot{m}'' \rangle$:

$$\langle \dot{m}'' \rangle = C_m \left\langle \frac{1}{\ell}\frac{1}{\ell}\frac{v}{\ell}\rho_\ell \ell^3 \,\middle|\, DF \right\rangle = C_m \rho_\ell \langle v \mid DF \rangle, \tag{5.12}$$
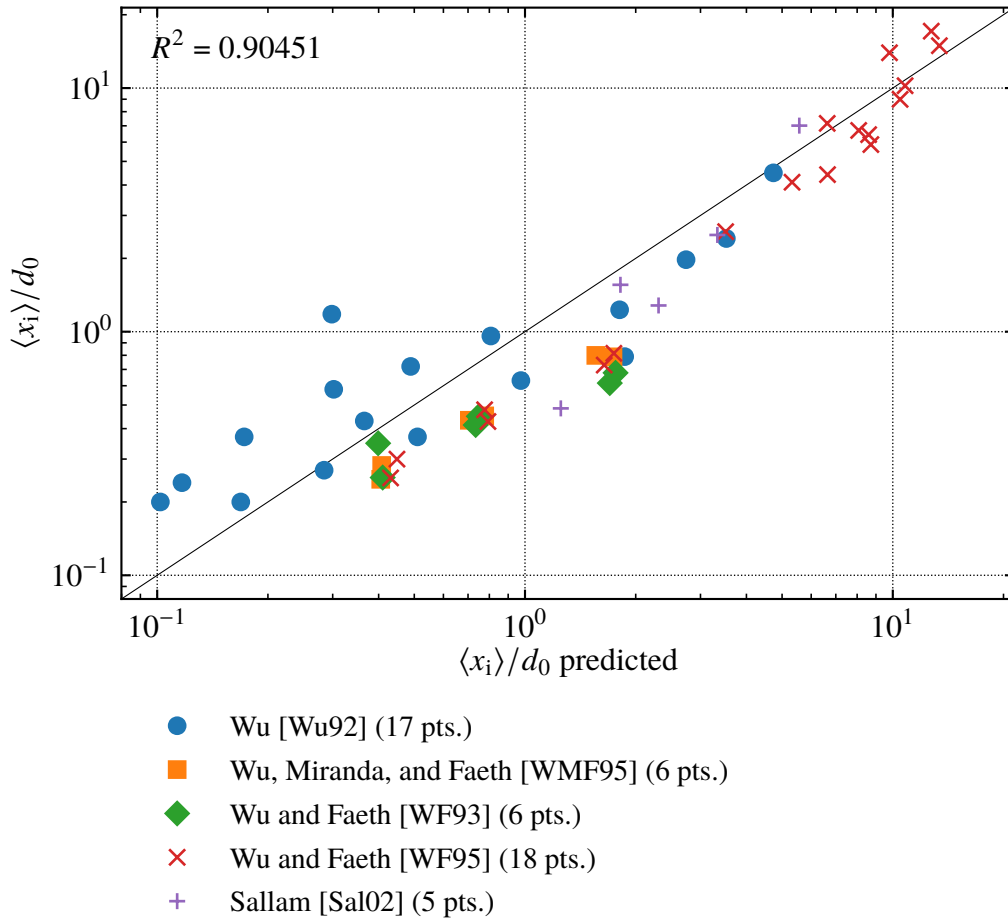
Figure 5.5: Comparison of the $\langle x_i \rangle$ theory (equation 5.11) against experimental data.

which is constant downstream because I take k and Λ as constant. Similarly, the dimension-less quantity

$$\frac{\langle \dot{m}'' \rangle}{\rho_\ell \langle v_{\mathrm{d}} \rangle} = \frac{\langle \dot{m}'' \rangle}{C_{v_{\mathrm{d}}} \rho_\ell \langle v \mid \mathrm{DF} \rangle} = \frac{C_{\mathrm{m}}}{C_{v_{\mathrm{d}}}}, \tag{5.13}$$

a constant. But the experiments of Sallam, Dai, and Faeth [SDF02, fig. 10] show that this quantity increases with x from $O(10^{-2})$ to $O(1)$. Consequently the model is not correct. The inaccuracy could be due to the $\langle \dot{m}'' \rangle$ model, $\langle v_{\mathrm{d}} \rangle$ model, or both.

For simplicity, I assume that $\langle x_{\mathrm{i}} \rangle = 0$ for the derivation of $\langle x_{\mathrm{b}} \rangle$. Otherwise, a delay differential equation would be required to account for the delay between an eddy impacting the surface and droplet formation. After applying mass conservation for a particular realization of the jet to a differential element, I find that

$$\frac{\mathrm{d}(\rho_\ell A(x) \overline{U}_0)}{\mathrm{d}x} = -P(x)\dot{m}'', \tag{5.14}$$

or after rearrangement and averaging

$$\frac{\mathrm{d}\langle d_{\mathrm{j}} \rangle}{\mathrm{d}x} = -\frac{2\langle \dot{m}'' \rangle}{\rho_\ell \overline{U}_0}, \tag{5.15}$$

where $\overline{U}_0$ is the (constant) jet convection velocity, the jet is assumed to have a circular cross section, $d_{\mathrm{j}}(x)$ is the diameter of the jet at x, $A(x) = \pi d_{\mathrm{j}}^2/4$ is the cross sectional area, and $P(x) = \pi d_{\mathrm{j}}$ is the perimeter. Consistent with how $\langle x_{\mathrm{b}} \rangle$ is measured, I define x_{b} with $d_{\mathrm{j}}(x_{\mathrm{b}}) \equiv 0$, so to first-order $\langle d_{\mathrm{j}}(\langle x_{\mathrm{b}} \rangle) \rangle = 0$. Solving equation 5.15 for $\langle x_{\mathrm{b}} \rangle$ with the $\langle d_{\mathrm{j}}(\langle x_{\mathrm{b}} \rangle) \rangle = 0$ approximation using the $\langle \dot{m}'' \rangle$ model (equation 5.12), I obtain

$$\frac{\langle x_{\mathrm{b}} \rangle}{d_0} = \frac{\rho_\ell \overline{U}_0}{2\langle \dot{m}'' \rangle} = \frac{\overline{U}_0}{2C_{\mathrm{m}}\langle v \mid \mathrm{DF} \rangle} = \frac{(\alpha - 2)}{2C_{\mathrm{m}}(\alpha - 1)} \frac{\overline{U}_0}{v_{\mathrm{min}}}$$
$$= \frac{(\alpha - 2)\overline{U}_0}{2C_{\mathrm{m}}(\alpha - 1)} \left(\frac{\rho_\ell}{\sigma \overline{\varepsilon}_0} \right)^{1/5} = C_{x_{\mathrm{b}}} \overline{\mathrm{Tu}}_0^{-3/5} \left(\mathrm{We}_{\ell 0} \frac{\Lambda_0}{d_0} \right)^{1/5}, \tag{5.16}$$

where I applied the result for a power law PDF, $\langle v \mid \mathrm{DF} \rangle = \langle v \mid v > v_{\mathrm{min}} \rangle = (\alpha - 1)v_{\mathrm{min}}/(\alpha - 2)$, and also chose $v_{\mathrm{min}} = v_\sigma$ (equation 5.4). The theory was fitted to the data, returning $C_{x_{\mathrm{b}}} = 5.62$ (193 data points, $R^2 = 0.719$). The theory and experimental data is

compared in figure 5.6.

In the case of the breakup length, comparison against an empirical regression is worthwhile. The power law regression for the turbulent surface breakup regime developed earlier is ($R^2 = 0.958$):

$$\frac{\langle x_\text{b} \rangle}{d_0} = 3.61 \overline{\text{Tu}}_0^{-0.275} \text{We}_{\ell 0}^{0.334}. \tag{3.28}$$

The signs of the $\overline{\text{Tu}}_0$ and $\text{We}_{\ell 0}$ exponents are correct, but the magnitudes are in error. The most likely cause of the error may be the model for $\langle \dot{m}'' \rangle$, as use of the $\langle \dot{m}'' \rangle$ correlation from Sallam, Dai, and Faeth [SDF02, p. 446] for the turbulent surface breakup regime, $\langle \dot{m}'' \rangle / (\rho_\ell \langle v_\text{d} \rangle) \propto x / [\Lambda_0 (\text{We}_{\ell 0} \Lambda_0 / d_0)^{1/2}]$, returns $\langle x_\text{b} \rangle / d_0 \propto \overline{\text{Tu}}_0^{-3/10} \text{We}_{\ell 0}^{3/10}$. This suggests that the breakup length in the turbulent surface breakup regime is controlled mainly by turbulent primary breakup at the free surface rather than the Rayleigh mechanism, which breaks up the entire jet core.

5.2.7 Spray angle, θ_i

Similar to previous works [Nat18, p. 38; Skr66, p. 144; HLK98, p. 460], I define the spray angle through $\tan \theta_\text{i}/2 \propto \langle v_\text{d}/u_\text{d} \rangle$ (at $x = \langle x_\text{i} \rangle$). In other words, the spray angle is determined through simple geometry via the ratio of the radial to streamwise droplet velocities. The spray angle is a maximum angle rather than an average angle, as the observed boundary of the spray is the maximum extent of the spray, so the spray angle is not written as an average. However, it is assumed that the maximum is proportional to the average, similar to Markov's inequality.

As $u_\text{d} = \overline{U}_0 + u$, then $\langle u_\text{d} \rangle \neq \overline{U}_0$ because there is an additional term with the correlation $\langle uv \rangle$. I assume this effect is negligible as I did for $\langle x_\text{i} \rangle$, so $\langle u_\text{d} \rangle = \overline{U}_0$. Then $\tan \theta_\text{i}/2 = C_{\theta_\text{i}} \langle v_\text{d} \rangle / \overline{U}_0$, so

$$\tan \left(\frac{\theta_\text{i}}{2} \right) = C_{\theta_\text{i}} \frac{\overline{v'_0}}{\overline{U}_0} \overline{\text{Tu}}_0^{-2/5} \left(\text{We}_{\ell 0} \frac{\Lambda_0}{d_0} \right)^{-1/5} = C_{\theta_\text{i}} \overline{\text{Tu}}_0^{3/5} \left(\text{We}_{\ell 0} \frac{\Lambda_0}{d_0} \right)^{-1/5}, \tag{5.17}$$

Fitting the theory against the experimental data returns $C_{\theta_\text{i}} = 0.584$ (5 data points,
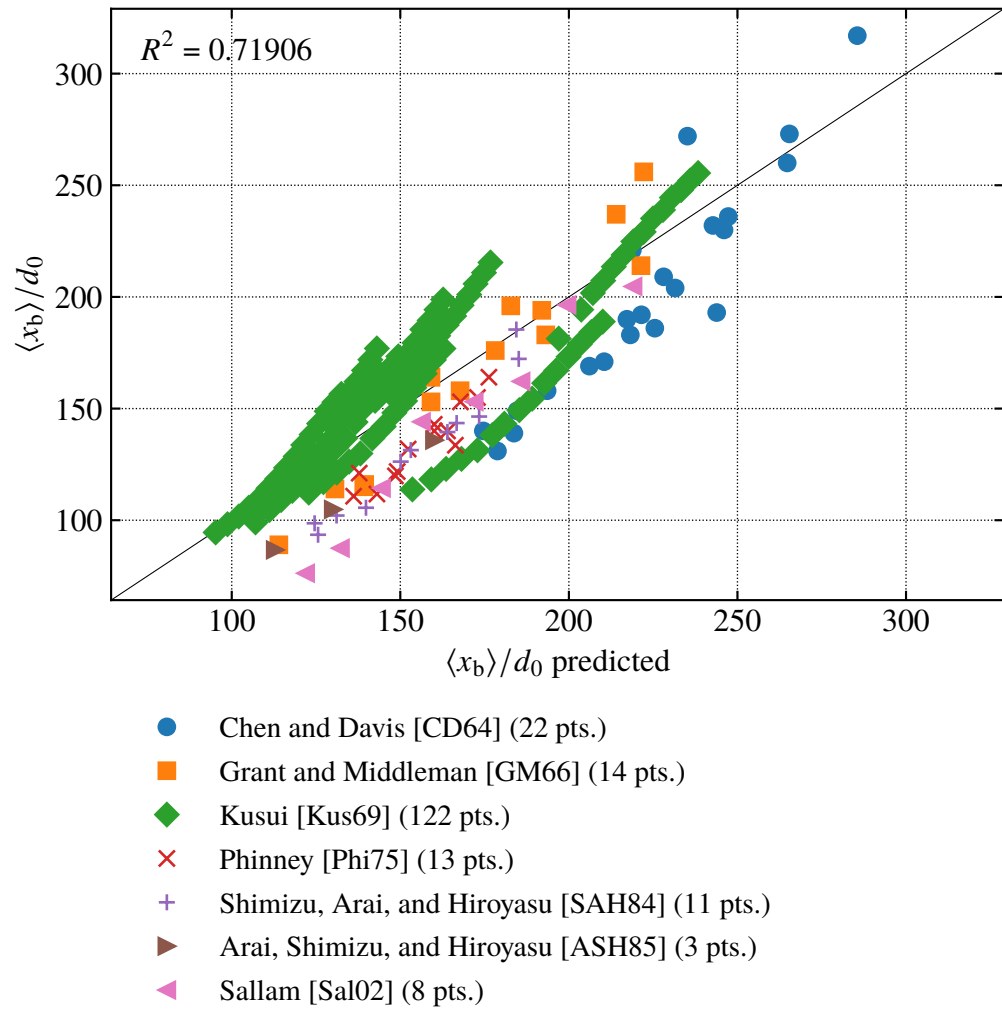
Figure 5.6: Comparison of the $\langle x_b \rangle$ theory (equation 5.16) against experimental data.

$R^2 = -0.889$). As shown in table 2.2, all models tested in this work fit the spray angle data very poorly. It is worth examining a more general regression of the data to see what causes the poor fit.

As mentioned in § 3.4.10, the available spray angle data in the turbulent surface breakup regime was very noisy and lacked appreciable turbulence intensity variation. Consequently, a regression was made from two studies from the Faeth group [Ruf90; Sal02] which were less noisy, likely due to using a more consistent definition of the spray angle ($R^2 = 0.983$):

$$\tan\left(\frac{\theta_i}{2}\right) = 4.73 \times 10^{-4}\overline{\text{Tu}}_0^{0.827}\text{We}_{\ell 0}^{0.621}. \tag{3.29}$$

See § 3.4.10 for more detail on this regression. One major source of the poor fit is the variation with the Weber number. In CDRSV theory, $\tan\theta_i/2$ decreases with $\text{We}_{\ell 0}$, contrary to the regression. The only model I am aware of where $\tan\theta_i/2$ increases with $\text{We}_{\ell 0}$ is that of Skrebkov [Skr66, p. 145], who suggests that $(\tan\theta_i/2)^2 = \overline{\text{Tu}}_0^2 + 12C\rho_g/\rho_\ell - 12/(D\text{We}_{\ell 0})$ for high $\text{Re}_{\ell 0}$. The model of Huh, Lee, and Koo [HLK98] has no $\text{We}_{\ell 0}$ variation at all. The model of Tsyapko [Tsy19a] is similar to Huh, Lee, and Koo's, except for the addition of a term such that $\tan\theta_i/2$ is linear in $\text{Re}_{\ell 0}$. This is more correct, as both $\text{Re}_{\ell 0}$ and $\text{We}_{\ell 0}^{1/2}$ scale with $\overline{U}_0$, but ultimately $\text{Re}_{\ell 0}$ is not $\text{We}_{\ell 0}$. Why CDRSV theory obtains the wrong scaling with the Weber number for the spray angle is unclear at present.

5.3 Conclusions

Conventional stability theory has, so far, failed to work in the turbulent surface breakup regime. Phenomenological theories like that developed in this work appear to have more promise due to their flexibility. However, future stability theories may completely supplant phenomenological theories if the issues identified in this work are solved.

Jet breakup does not occur for all surface fluctuations, so it is inappropriate for a model to imply that it does. Conditional averages must be computed to account for this feature of turbulent jet breakup.

While excellent agreement between current CDRSV theory and measurements was

found for D_{32} and $\langle x_i \rangle$, the theory has only modest success for $\langle x_b \rangle$, and none for θ_i — see table 2.2. Ultimately no theory for turbulent jet breakup has been fully validated, in part due to the failures of these theories with existing data, and also because $\overline{Tu}_0$ varies little in existing data. Alternative modeling choices might improve accuracy.

One possible avenue for improvement is using a more general turbulence spectrum like Schmitz [Sch11] rather than the Kolmogorov inertial range spectrum. This would likely require a computational model, which is why this approach was not used in this work. This work focused on the issues of the *definitions* of quantities of interest and *analytical* modeling rather than *detailed* modeling of each quantity of interest.

Another way to improve CDRSV theory would be to use a more accurate velocity probability density function function. A Gaussian probability density function would be more accurate. A Gaussian PDF was used in an example in § 5.2.2, and the theory can easily be extended to use Gaussian PDFs.

Chapter 6

Estimating turbulent kinetic energy and dissipation with internal flow loss coefficients[1]

6.1 Introduction and background

The turbulent kinetic energy (or equivalently, the turbulence intensity) must be known to use models of turbulent jet breakup as developed in chapter 5. Unfortunately, the turbulent kinetic energy at the outlet of a nozzle is typically unknown. Prior to this work, turbulent kinetic energy in internal flow systems can typically be found only through computational fluid dynamics (CFD), because measuring turbulence quantities in internal flows is usually difficult. Reynolds averaged CFD of single components is presently tractable, but computationally expensive. Accurate CFD of complex piping systems in practice is difficult, if not prohibitively expensive. Further, one source of error in CFD is the specification of inlet turbulent kinetic energy and dissipation boundary conditions. Given these concerns, there is a need for a computationally tractable methodology to predict turbulent kinetic energy in internal flows.

There's also an interest in extending the Bernoulli equation to more general contexts. There are two approaches to generalization. The first approach is to find paths other than streamlines where the Bernoulli integral is constant under more general conditions, e.g., in viscous flows. Brutyan, Golubkin, and Krapivskiy [BGK89] identify such paths for general steady viscous flows. The second approach is to determine how the Bernoulli integral varies along streamlines under more general conditions. Typically, this is only done for internal flows. Grose [Gro83] and Synolakis and Badeer [SB89] develop viscous corrections to

---

[1]This chapter is a revision of a paper originally published at the ILASS-Americas 2018 conference [Tre18]. I am the sole author.

the Bernoulli equation. A more common approach adds a term for energy "lost" along the flow path in internal flows. The equation has been called the "mechanical energy balance", the "engineering Bernoulli equation", or the "extended Bernoulli equation". The models for the lost energy are $\Delta p = \zeta \cdot \frac{1}{2}\overline{U}^2$ for pipe fittings ("minor loss") and valves and $\Delta p = (f\, L/d) \cdot \frac{1}{2}\overline{U}^2$ for pipe segments ("major loss"). The lost energy is attributed to viscous dissipation by Panton [Pan13, p. 133] and Bird, Lightfoot, and Stewart [BLS02, p. 204]. However, these derivations of the loss term are only valid for steady flows, precluding the possibility of anything one would call turbulence. Pope [Pop00, p. 125] notes that the (laminar) mean flow dissipation term the previously studies highlight is generally negligible. Consequently, how the lost energy is distributed in a turbulent flow is unclear. A relationship between the loss and turbulence quantities like the turbulent kinetic energy and dissipation exists, and it will be detailed in this paper.

Past researchers have attempted to relate flow losses to turbulence quantities, without clear success. Most previous theories modeled turbulence reduction by screens as a function of the loss coefficient of the screen. Loehrke and Nagib [LN72, p. 5] suggested that the theories disagree with the data because the theories treat the screen as only a turbulence suppression device, and do not include any way for turbulence to be generated. Examining both screens and honeycombs, Scheiman and Brooks [SB81] agree with that conclusion. Groth and Johansson [GJ88] made the same suggestion and showed experimentally that the turbulence intensities immediately downstream of the screen are higher than that upstream of the screen, but the turbulence decays further downstream of the screen. Groth and Johansson's measurements show that both turbulence generation and dissipation are factors.

For modeling screen turbulence, Baines and Petersen [BP51, p. 471R] proposed an equation similar the Bernoulli equation along a streamline with additional terms for turbulent kinetic energy and dissipation. No derivation was provided. The equation was justified by stating it represents energy conservation, however, this is implausible as there are no terms for energy transfer between streamlines. No link between this equation and flow losses was made. Focusing on more general hydraulic resistances, Nikitin and Nikitina [NN80] developed models for the maximum RMS pressure p' using the friction factor
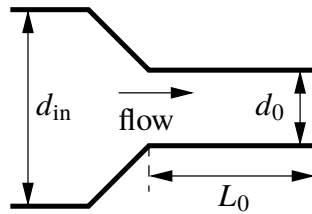
Figure 6.1: Schematic nozzle geometry.

or loss coefficient in pipe and general hydraulic resistances. Nikitin and Nikitina used dimensional analysis, not energy conservation, to determine p', and the equations developed are valid only if the inlets have negligible turbulence.

In an attempt to justify ad-hoc Bernoulli-like equations including turbulent kinetic energy like that proposed by Baines and Petersen, Rouse [Rou62] in 1960 derived a turbulent form of the Bernoulli equation. Later in 1964, independent of Rouse, Birkhoff [Bir64, p. 71] derived a similar equation under a one-dimensional duct flow approximation. The equation given by Rouse is not well suited for turbulence modeling as it does not contain $\overline{k}$ directly, and the equation given by Birkhoff likely is inaccurate due to the one-dimensional duct flow approximation. In these works no attempts at turbulence modeling were made to create practical simple models for internal flow turbulence. A better equation directly containing $\overline{k}$ was proposed by Liu, Xue, and Fan [LXF13, p. 914], however, no derivation is provided and the relationship with the turbulent dissipation is not clear.

Independent from the attempts to model turbulence through screens or general hydraulic resistances, researchers interested in liquid jet breakup developed simplified models to estimate turbulent kinetic energy at the outlet of a nozzle. Early models were developed by Natanzon [Nat18, pp. 18–29], Tsyapko [Tsy19a], and Jackson [Jac83, p. 111]. Another early researcher, Harmon [Har53, p. 110], used the nozzle frame mentioned in appendix B, combining both the nozzle and jet rather than focusing specifically on the nozzle as I do here. More notable than any of these, however, is the model of Huh, Lee, and Koo [HG91; HLK98] (abbreviated as "Huh's model" here). In Huh's model, the turbulent
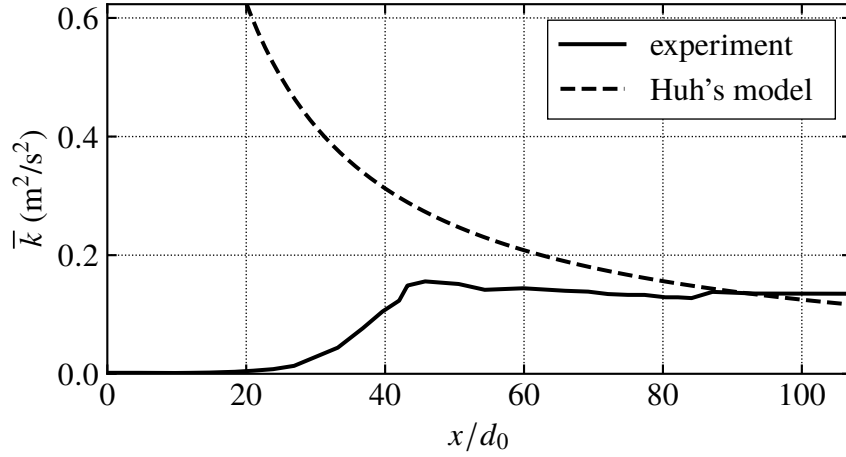
Figure 6.2: A comparison of the model of [HLK98] (equation 6.1) against an experimental data series compiled by Klein [Kle81].

kinetic energy at the nozzle outlet can be estimated with the equation

$$\overline{k}_0 = \frac{\overline{U}_0^2}{8L_0/d_0} \left[\frac{1}{C_{\mathrm{d}}^2} - \zeta_{\mathrm{c}} - \left(1 - c^{-2}\right) \right] \tag{6.1}$$

where $\overline{k}_0$ is the plane averaged turbulent kinetic energy at the nozzle outlet, $\overline{U}_0$ is the bulk (plane averaged) velocity through the nozzle orifice, L_0 is the nozzle orifice length, d_0 is the nozzle orifice diameter, C_{d} is the discharge coefficient of the nozzle, ζ_{c} is the contraction loss coefficient, and $c \equiv A_{\mathrm{in}}/A_0 = (d_{\mathrm{in}}/d_0)^2$ is the area contraction ratio of the nozzle. See figure 6.1 for an illustration of a conical nozzle with a cylindrical orifice using the previous notation.

This model has two major problems evident by inspection. First, in this model the nozzle *outlet* turbulent kinetic energy is not a function of the nozzle *inlet* turbulent kinetic energy. This is inconsistent with the evidence that strong turbulent kinetic energy at the nozzle inlet can affect the stability of a liquid jet [EME80; ME80]. Second, this equation implies that turbulent kinetic energy grows arbitrarily large as L_0/d_0 decreases to zero, and that turbulent kinetic energy goes to zero as L_0/d_0 grows arbitrarily large. Both are false — see figure 6.2. Klein [Kle81, p. 246, fig. 3] reviews past measurements of turbulent kinetic

energy as a function of development length. For small L_0/d_0, k approaches the inlet value, and as L_0/d_0 increases to infinity (i.e., the flow becomes fully developed), k goes to a value determined by the friction factor for fully developed flow. The latter value is independent of the inlet turbulent kinetic energy. Further, if k grew arbitrarily large as L_0/d_0 decreased, this would violate energy conservation. k increasing would also imply that the stability of a liquid jet would be worse for shorter nozzles, but typically the opposite is true [ASH85].

These problems are caused by an error made in the derivation of equation 6.1. Huh, Lee, and Koo use a force balance in an attempt to relate the turbulent kinetic energy to the pressure drop across the nozzle orifice. Presumably the "turbulent stress" used in the model is the Reynolds shear stress ($\langle uv \rangle$ if one divides by the liquid density), but this is not the same as the turbulent kinetic energy (k), what is desired in the model. The model implicitly assumes the two are the same or at least proportional. One can relate $\langle uv \rangle$ to the turbulent kinetic energy via the stress-intensity ratio, $|\langle uv \rangle/k|$, found to be about 0.3 in many shear flows [DP10b, pp. 116, 121, 126, 138]. However, this option is not viable, as using wall friction requires taking the force balance at the orifice walls. Both $\langle uv \rangle$ and k are zero at smooth walls due to the no-slip and no-penetration conditions [Pop00, p. 269]. The stress at a smooth wall comes entirely from the viscous component[2]. Finally, the constant stress-intensity ratio approximation is not particularly accurate [Als78].

Further, $\overline{k}$ is determined solely by the nozzle orifice walls in Huh's model, explaining why inlet turbulent kinetic energy does not factor into the model. In addition to ignoring the effect of inlet $\overline{k}$, this implies that the contraction does not change the turbulent kinetic energy. The effects of contractions on turbulent kinetic energy and anisotropy are well known [BP54; RH76; HGH05]. Rapid distortion theory (RDT) can model these effects.

The failures of previous models prompted the development of a more rigorous approach which also uses empirical loss coefficients.

---

[2]The wall stress is not entirely viscous in the special case of rough walls, but in this case one would still need to know the viscous component of the wall stress to determine the Reynolds stress. The viscous component is not generally known. The link between the plane average value of $\langle uv \rangle$ (to find $\overline{k}$) and the value of $\langle uv \rangle$ at the wall is also unclear. There is no simple link between τ_{w} and $\overline{k}$ even for rough pipes. In the remainder of this paper, I assume that all fluctuations are zero at the wall.

6.2 Derivation of the turbulent Bernoulli equation and relationship between loss and turbulence quantities

I start with a standard derivation of the Bernoulli theorem, albeit from the Reynolds averaged equations rather than the instantaneous equations. I depart from the standard derivation when I take the new term for the work done by the Reynolds stress, and decompose that term into the production of turbulent kinetic energy and a turbulent flux. This returns an equation including terms for energy transfer between streamlines. Algebraic manipulation and integration over the volume of the internal flow path returns a relationship between flow losses, k, and ε. For brevity, the ensemble mean velocity in the Reynolds decomposition will be denoted with a capital U_i rather than $\langle U_i \rangle$, and the fluctuating terms will be denoted with lowercase u_i.

6.2.1 Differential turbulent Bernoulli equation for a streamline

Start with the Reynolds averaged Navier-Stokes equations in Stokes form and consider the statistically stationary case (no change in the mean with time) [Pop00, p. 23, p. 86]:

$$\frac{\partial U_i}{\partial t} + \frac{\partial \frac{1}{2} U_j U_j}{\partial x_i} - \epsilon_{ijk} U_j \omega_k = -\frac{1}{\rho} \frac{\partial P}{\partial x_i} + \nu \frac{\partial^2 U_i}{\partial x_j \partial x_j} - \frac{\partial \langle u_i u_j \rangle}{\partial x_j} . \tag{6.2}$$

Rewrite the previous equation so that only $\epsilon_{ijk} U_j \omega_k$ is on one side, and the remaining terms are on the other:

$$\epsilon_{ijk} U_j \omega_k = \frac{\partial}{\partial x_i} \left(\frac{1}{2} U_j U_j + \frac{P}{\rho} \right) + \frac{\partial \langle u_i u_j \rangle}{\partial x_j} - \nu \frac{\partial^2 U_i}{\partial x_j \partial x_j} . \tag{6.3}$$

Consider a vector s_i which is in the direction of a streamline[3] at a point in space. Multiply the previous equation by a differential element of this vector:

$$\epsilon_{ijk} U_j \omega_k \, \mathrm{d}s_i = \frac{\partial}{\partial x_i} \left(\frac{1}{2} U_j U_j + \frac{P}{\rho} \right) \mathrm{d}s_i + \left(\frac{\partial \langle u_i u_j \rangle}{\partial x_j} - \nu \frac{\partial^2 U_i}{\partial x_j \partial x_j} \right) \mathrm{d}s_i. \tag{6.4}$$

---

[3]By "streamline" in this context, I mean a *streamline of the mean flow*.

The cross product term has no component in the direction of U_i, which is the same as s_i, so $\epsilon_{ijk}U_j\omega_k\,\mathrm{d}s_i$ is zero. Note that the local differential length element along a streamline can be related to the local time-averaged velocity vector by $\mathrm{d}s_i = U_i\,\mathrm{d}t$. This is done for the Reynolds stress term only:

$$0 = \frac{\partial}{\partial x_i}\left(\tfrac{1}{2}U_jU_j + \frac{P}{\rho}\right)\mathrm{d}s_i - \nu\,\frac{\partial^2 U_i}{\partial x_j\partial x_j}\,\mathrm{d}s_i + U_i\,\frac{\partial\langle u_iu_j\rangle}{\partial x_j}\,\mathrm{d}t. \qquad (6.5)$$

Now, note that the following decomposition is a consequence of the product rule:

$$U_i\,\frac{\partial\langle u_iu_j\rangle}{\partial x_j} = \frac{\partial U_i\langle u_iu_j\rangle}{\partial x_j} \underbrace{-\langle u_iu_j\rangle\,\frac{\partial U_i}{\partial x_j}}_{\text{production}}. \qquad (6.6)$$

The second term is recognized as the production of turbulent kinetic energy. Rearranging the transport equation for the turbulent kinetic energy [DP10b, p. 49] to solve for the production of turbulent kinetic energy, and substituting that result into the previous equation returns

$$U_i\,\frac{\partial\langle u_iu_j\rangle}{\partial x_i} = U_i\,\frac{\partial k}{\partial x_i} + \underbrace{\nu\left\langle\frac{\partial u_i}{\partial x_j}\,\frac{\partial u_j}{\partial x_i}\right\rangle}_{\varepsilon}$$

$$+ \frac{1}{2}\,\frac{\partial\langle u_ju_iu_i\rangle}{\partial x_j} - \nu\,\frac{\partial^2 k}{\partial x_i\partial x_i} + \frac{\partial U_i\langle u_iu_j\rangle}{\partial x_j} - \frac{1}{\rho}\,\frac{\partial\langle u_ip\rangle}{\partial x_i}. \qquad (6.7)$$

The previous equation can be used to see how turbulent kinetic energy changes along a streamline. Aside from the first and third terms, everything else is between streamlines. Later, when I average over the projected area of the pipe, the other terms go to zero at the walls as there is no transfer between the pipe and the walls due to the no-slip and no-penetration boundary conditions. These terms may need to be kept for inlets and outlets, however.

Substituting the result from equation 6.7 into equation 6.5 returns (after application

of $U_i = \mathrm{d}s_i/\mathrm{d}t$ to the turbulent kinetic energy derivative and some rearrangement)

$$
0 = \frac{\partial}{\partial x_i} \left(\tfrac{1}{2} U_j U_j + \frac{P}{\rho} + k \right) \mathrm{d}s_i - \nu \frac{\partial^2 U_i}{\partial x_j \partial x_j} \, \mathrm{d}s_i
$$
$$
+ \left[\varepsilon + \frac{1}{2} \frac{\partial \langle u_j u_i u_i \rangle}{\partial x_j} - \nu \frac{\partial^2 k}{\partial x_i \partial x_i} + \frac{\partial U_i \langle u_i u_j \rangle}{\partial x_j} - \frac{1}{\rho} \frac{\partial \langle u_i p \rangle}{\partial x_i} \right] \mathrm{d}t. \qquad (6.8)
$$

6.2.2 Turbulent Bernoulli equation for a streamtube with no-slip and no-penetration boundary conditions

Equation 6.8 is valid along a particular streamline, but there are many terms which need to be modeled, limiting its utility. Consequently, I seek to develop a version for a streamtube applicable in internal flows where there are no-slip and no-penetration boundary conditions, like the "extended Bernoulli equation". Multiply all terms by $\rho \, U_l \, n_l \, \mathrm{d}A$. n_l is a unit vector which is normal to the integration area $\mathrm{d}A$. The overall area integrated over is, for example, the cross sectional area of a pipe or pipe fitting.

$$
0 = \rho \, U_l \, n_l \, \mathrm{d}A \frac{\partial}{\partial x_i} \left(\tfrac{1}{2} U_j U_j + \frac{P}{\rho} + k \right) \mathrm{d}s_i - \rho \, \nu \, U_l \, n_l \, \mathrm{d}A \frac{\partial^2 U_i}{\partial x_j \partial x_j} \, \mathrm{d}s_i
$$
$$
+ \rho \, U_l \, n_l \, \mathrm{d}A \left[\varepsilon + \frac{1}{2} \frac{\partial \langle u_j u_i u_i \rangle}{\partial x_j} - \nu \frac{\partial^2 k}{\partial x_i \partial x_i} + \frac{\partial U_i \langle u_i u_j \rangle}{\partial x_j} - \frac{1}{\rho} \frac{\partial \langle u_i p \rangle}{\partial x_i} \right] \mathrm{d}t. \quad (6.9)
$$

For the first term, note that $\dfrac{\partial}{\partial x_i} (\cdots) \, \mathrm{d}s_i$ is the change in the quantity inside of the parentheses along a streamline, so it can be written as $d(\cdots)$. For the second term, note that $\mathrm{d}s_i = t_i \, \mathrm{d}s$, where t_i is a unit vector tangent to the streamline. For the third term, note that $\mathrm{d}t = \mathrm{d}s/\sqrt{U_m U_m}$, where s is the arclength of the streamline. These changes result in

$$
0 = \rho \, U_l \, n_l d \left(\tfrac{1}{2} U_j U_j + \frac{P}{\rho} + k \right) \mathrm{d}A - \rho \, \nu \, U_l \, n_l \, t_i \frac{\partial^2 U_i}{\partial x_j \partial x_j} \, \mathrm{d}s \, \mathrm{d}A
$$
$$
+ \frac{\rho \, U_l \, n_l}{\sqrt{U_m U_m}} \left[\varepsilon + \frac{1}{2} \frac{\partial \langle u_j u_i u_i \rangle}{\partial x_j} - \nu \frac{\partial^2 k}{\partial x_i \partial x_i} + \frac{\partial U_i \langle u_i u_j \rangle}{\partial x_j} - \frac{1}{\rho} \frac{\partial \langle u_i p \rangle}{\partial x_i} \right] \mathrm{d}s \, \mathrm{d}A.
$$
$$
(6.10)
$$

The previous result is simplified by noting that $U_l / \sqrt{U_m U_m} = t_i$:

$$0 = \rho\, U_l\, n_l d \left(\tfrac{1}{2} U_j U_j + \frac{P}{\rho} + k \right) \mathrm{d}A - \rho\, v\, U_l\, n_l\, t_i\, \frac{\partial^2 U_i}{\partial x_j \partial x_j}\, \mathrm{d}s\, \mathrm{d}A$$

$$+ \rho\, t_l\, n_l \left[\varepsilon + \frac{1}{2} \frac{\partial \langle u_j u_i u_i \rangle}{\partial x_j} - v \frac{\partial^2 k}{\partial x_i \partial x_i} + \frac{\partial U_i \langle u_i u_j \rangle}{\partial x_j} - \frac{1}{\rho} \frac{\partial \langle u_i p \rangle}{\partial x_i} \right] \mathrm{d}s\, \mathrm{d}A. \quad (6.11)$$

Now, I make the approximation $t_l n_l = 1$, which means that the streamlines are normal to the surface on each end of the streamtube. This is not satisfied in internal flows aside from long straight stretches of pipe, but it is approximately satisfied. A consequence of this approximation is that $U_i n_i = \sqrt{U_i U_i} \equiv U$. After this, I have

$$0 = \rho\, U d \left(\tfrac{1}{2} U_j U_j + \frac{P}{\rho} + k \right) \mathrm{d}A - \rho v U_i \frac{\partial^2 U_i}{\partial x_j \partial x_j}\, \mathrm{d}s\, \mathrm{d}A$$

$$+ \rho \left[\varepsilon + \frac{1}{2} \frac{\partial \langle u_j u_i u_i \rangle}{\partial x_j} - v \frac{\partial^2 k}{\partial x_i \partial x_i} + \frac{\partial U_i \langle u_i u_j \rangle}{\partial x_j} - \frac{1}{\rho} \frac{\partial \langle u_i p \rangle}{\partial x_i} \right] \mathrm{d}s\, \mathrm{d}A. \quad (6.12)$$

The viscous mean flow term can be decomposed as below, which follows from the product rule:

$$v U_i \frac{\partial^2 U_i}{\partial x_j \partial x_j} = v \frac{\partial}{\partial x_j} \left(U_i \frac{\partial U_i}{\partial x_j} \right) - v \underbrace{\left(\frac{\partial U_i}{\partial x_j} \right) \left(\frac{\partial U_i}{\partial x_j} \right)}_{\varepsilon_m}. \quad (6.13)$$

The second term is the dissipation due to the mean flow, ε_m, as defined by Pope [Pop00, p. 124]. Applying this decomposition to equation 6.12 and simplifying the result returns

$$0 = \rho\, U d \left(\tfrac{1}{2} U_j U_j + \frac{P}{\rho} + k \right) \mathrm{d}A + \rho \left[\varepsilon_m + \varepsilon - v \frac{\partial}{\partial x_j} \left(U_i \frac{\partial U_i}{\partial x_j} \right) \right.$$

$$\left. + \frac{1}{2} \frac{\partial \langle u_j u_i u_i \rangle}{\partial x_j} - v \frac{\partial^2 k}{\partial x_i \partial x_i} + \frac{\partial U_i \langle u_i u_j \rangle}{\partial x_j} - \frac{1}{\rho} \frac{\partial \langle u_i p \rangle}{\partial x_i} \right] \mathrm{d}s\, \mathrm{d}A. \quad (6.14)$$

Now integrate equation 6.14 over the volume of the streamtube, note that $\mathrm{d}s\, \mathrm{d}A \equiv \mathrm{d}V$,

154

and use the kinetic energy coefficient α [Ben80, p. 218][4], defined in § B.6:

$$0 = \dot{m} \left[\frac{\alpha \overline{U}^2}{2} + \frac{\overline{P}}{\rho} + \overline{k} \right]_1^2 + \rho \int_{CS} \int_s \left[\varepsilon_m + \varepsilon - \nu \frac{\partial}{\partial x_j} \left(U_i \frac{\partial U_i}{\partial x_j} \right) \right.$$

$$\left. + \frac{1}{2} \frac{\partial \langle u_j u_i u_i \rangle}{\partial x_j} - \nu \frac{\partial^2 k}{\partial x_i \partial x_i} + \frac{\partial U_i \langle u_i u_j \rangle}{\partial x_j} - \frac{1}{\rho} \frac{\partial \langle u_i p \rangle}{\partial x_i} \right] d\Psi. \qquad (6.15)$$

The averaging in the first term is averaging in the area normal to the streamlines, e.g., in a pipe flow under the approximation previously mentioned, this is the plane of the pipe. All of the terms in the second term aside from the dissipation terms go to zero *at the walls* after applying the divergence theorem, and applying the no-slip and no-penetration boundary conditions (U_i and u_i are zero at the boundaries). (If it is unclear, $\frac{\partial k}{\partial n} = 0$ at the wall due to k's quadratic dependence on the velocity, where n is the normal direction to the wall [Pop00, p.284].) Unfortunately, the divergence theorem does not help at the inlet and outlet of the streamtube, as the terms of interest are not necessarily zero. However, as a hypothesis they may be zero or otherwise small compared against the others, or possibly well modeled similarly to the dissipation. The validity of this approximation may depend on where the control volume ends. Under this approximation the turbulent Bernoulli equation is

$$0 = \left[\frac{\alpha \overline{U}^2}{2} + \frac{\overline{P}}{\rho} + \overline{k} \right]_1^2 + \frac{\rho}{\dot{m}} \int_\Psi (\varepsilon_m + \varepsilon) \, d\Psi. \qquad (6.16)$$

The deviation from the typical Bernoulli equation is generally called "loss":

$$\text{loss} = \sum \zeta \cdot \tfrac{1}{2} \overline{U}^2 = \Delta \overline{k} + \frac{\rho}{\dot{m}} \int_\Psi (\varepsilon_m + \varepsilon) \, d\Psi. \qquad (6.17)$$

The energy "loss" is decomposed into three components:

1. $\Delta \overline{k}$, which is mean flow energy converted into turbulent kinetic energy,

---

[4] $1 \le \alpha \le 2$. If all velocities are forward then $\alpha = 1$ for only a uniform velocity profile, and $\alpha = 2$ for only a parabolic velocity profile.

2. $(\rho/\dot{m}) \int_V \varepsilon_m \, \mathrm{d}V$, which is energy dissipated by the mean flow, and

3. $(\rho/\dot{m}) \int_V \varepsilon \, \mathrm{d}V$, which is energy dissipated by turbulence.

To reiterate a point made earlier, Panton [Pan13, p. 133] and Bird, Lightfoot, and Stewart [BLS02, p. 204] only include the term with ε_m, which Pope [Pop00, p. 125] notes is generally negligible in turbulent flows.

6.2.3 Differential loss decomposition for pipe flows

A differential version of the energy loss decomposition for pipe flows can be useful. Recognize that in a pipe flow $\zeta \equiv \int_0^x (f(s)/d) \, \mathrm{d}s$. Consequently, the loss can be written as (integrating from point 0 to point x)

$$\left(\int_0^x \frac{f(s)}{d} \, \mathrm{d}s \right) \cdot \tfrac{1}{2}\overline{U}^2 = \overline{k}(x) - \overline{k}_0 + \frac{\rho}{\dot{m}} \int_0^x A(s)(\overline{\varepsilon_m + \varepsilon}) \, \mathrm{d}s. \tag{6.18}$$

Differentiating this expression with respect to x returns

$$\frac{\mathrm{d}}{\mathrm{d}x}\left(\int_0^x \frac{f(s)}{d} \, \mathrm{d}s \right) \cdot \tfrac{1}{2}\overline{U}^2 = \frac{\mathrm{d}\overline{k}}{\mathrm{d}x} - \cancel{\frac{\mathrm{d}\overline{k}_0}{\mathrm{d}x}} + \frac{\rho}{\dot{m}} \frac{\mathrm{d}}{\mathrm{d}x} \int_0^x A(s)(\overline{\varepsilon_m + \varepsilon}) \, \mathrm{d}s, \text{ and finally}$$

$$\frac{f(x)\overline{U}^2}{2d} = \frac{\mathrm{d}\overline{k}(x)}{\mathrm{d}x} + \frac{\rho A(x)}{\dot{m}} \overline{(\varepsilon_m(x) + \varepsilon(x))}. \tag{6.19}$$

6.3 Turbulence modeling

Equation 6.17 is simple, but even with a known loss coefficient, k and ε can not be uniquely determined. A turbulence model is needed to estimate quantities of interest. Two simple models are detailed. To reiterate, I am neglecting certain terms for simplicity. Future works should relax these approximations.

6.3.1 Dissipation fraction model

When modeling individual piping components, e.g., valves and fittings, the easiest model would simply assume a certain fraction of the loss energy is dissipated. Presumably

156

typical values of this "dissipation fraction" could be tabulated alongside loss coefficients if it proves to be relatively universal for classes of valve and fitting geometries. Following equation 6.17, I define the dissipation fraction as

$$\alpha_\varepsilon \equiv \frac{(\rho/\dot{m}) \int_V (\varepsilon_m + \varepsilon)\, dV}{\zeta \cdot \frac{1}{2}\overline{U}^2} \quad \text{which implies} \quad \Delta \overline{k} = \sum (1 - \alpha_\varepsilon) \cdot \zeta \cdot \tfrac{1}{2}\overline{U}^2. \quad (6.20)$$

α_ε can be assumed constant for a pipe system component. Note that α_ε is only bounded below by zero. There is no obvious upper bound to the amount of dissipation. In some circumstances, e.g., where turbulence reduction is desired, the amount of dissipation will exceed $\zeta \cdot \frac{1}{2}\overline{U}^2$, causing $\Delta \overline{k}$ to be negative and α_ε to be greater than one.

6.3.2 Dissipation scaling model

A common scaling used to estimate turbulence dissipation is $\varepsilon = C_\varepsilon k^{3/2}/\Lambda$, where Λ is the integral length scale [Pop00, p. 244]. Assuming that the integral length scale is proportional to a characteristic diameter, for example, the pipe diameter, the volume averaged dissipation can be modeled as $\overline{\varepsilon_m + \varepsilon} = C_\varepsilon \overline{k}^{3/2}/d$. This leads to the following equation for $\Delta \overline{k}$ if $\overline{k}$ in the dissipation model is taken as the inlet value, $\overline{k}_1$, which simplifies the computation:

$$\zeta \cdot \tfrac{1}{2}\overline{U}^2 = \overline{k}_2 - \overline{k}_1 + \frac{C_\varepsilon V_c \rho}{\dot{m} d}\overline{k}_1^{3/2}, \quad (6.21)$$

for a single flow resistance between 1 and 2, where V_c is the characteristic volume of the component. Unlike the dissipation fraction approach, it is impossible to solve for the overall increase in the turbulent kinetic energy with a simple sum. The model requires solving for $\overline{k}$ at each node in a pipe system.

6.4 Models for specific internal flow situations

6.4.1 Fully developed pipe flow

Equation 6.19 can be applied to the case of fully developed pipe flow. Here $\dfrac{dk}{dx} = 0$ and f is also a constant, independent of the location. The dissipation scaling model leads to

157

the equation[5]

$$\frac{f\overline{U}^2}{2d} = \frac{C_\varepsilon \rho A}{\dot{m}d}\overline{k}_{\mathrm{FD}}^{3/2}, \quad \text{or,} \quad \overline{k}_{\mathrm{FD}} = \overline{U}^2\left(\frac{f}{2C_\varepsilon}\right)^{2/3} \tag{6.22}$$

which implies

$$\overline{\mathrm{Tu}}_{\mathrm{FD}} \equiv \frac{\sqrt{2\overline{k}_{\mathrm{FD}}/3}}{\overline{U}} = \sqrt{\frac{2}{3}}\left(\frac{f}{2C_\varepsilon}\right)^{1/3}. \tag{6.23}$$

To test this theory, an experimental database for both rough and smooth pipes was compiled, selecting only studies which measured all three velocity components [Lau54; San55; RBM65; Pat68; Gow69; Pow70; Law71] (17 points, 9 smooth, 8 rough). Fitting the theory with least squares returns $\overline{\mathrm{Tu}}_{\mathrm{FD}} = 0.246f^{1/3}$ ($R^2 = 0.909$). Fitting a general power law returns $\overline{\mathrm{Tu}}_{\mathrm{FD}} = 0.366f^{0.459}$ ($R^2 = 0.975$) — see figure 4.1 for a comparison with the data. Neglecting measurement error, the exponent with 95% error is 0.4587 ± 0.0401. The scaling $\overline{\mathrm{Tu}} \propto f^{1/3}$ is not consistent with this. A power closer to $1/2$ seems justified. The scaling $\overline{\mathrm{Tu}} \propto f^{1/2}$ would follow from the assumption that $k^{1/2} \propto u_\tau$. This discrepancy is likely due to the neglect of many terms when constructing the model. It is interesting to note that the power is between the two theories.

One further observation from the correlation is that the Blasius friction factor law for smooth pipes, $f = 0.316\,\mathrm{Re}^{-1/4}$, suggests that $\overline{\mathrm{Tu}}_{\mathrm{FD}}$ decreases as $\mathrm{Re} \equiv \overline{U}_0 d/\nu$ increases, contrary to what many expect. This trend is consistent with experimental measurements at the centerline [San55, p. 35, fig. 15].

6.4.2 Contracting nozzle

Contractions followed by cylindrical segments (e.g., figure 6.1) are the typical nozzle geometry in turbulent jet breakup. To offer an alternative to Huh's inaccurate model, I will apply RDT to the contraction and equation 6.19 to the cylindrical segment. Batchelor and

---

[5]The plane averaged turbulence intensity defined as $\overline{\mathrm{Tu}} \equiv \sqrt{2\overline{k}/3}/\overline{U}$, not averaging over $u'/\overline{U}$ as one might expect. Rather than plane averaging the turbulence intensity directly, a new turbulence intensity is formed from the plane averaged turbulent kinetic energy per the definition of the turbulence intensity. This is done so that $\overline{\mathrm{Tu}}^2 \propto \overline{k}$, which is convenient for energy conservation.
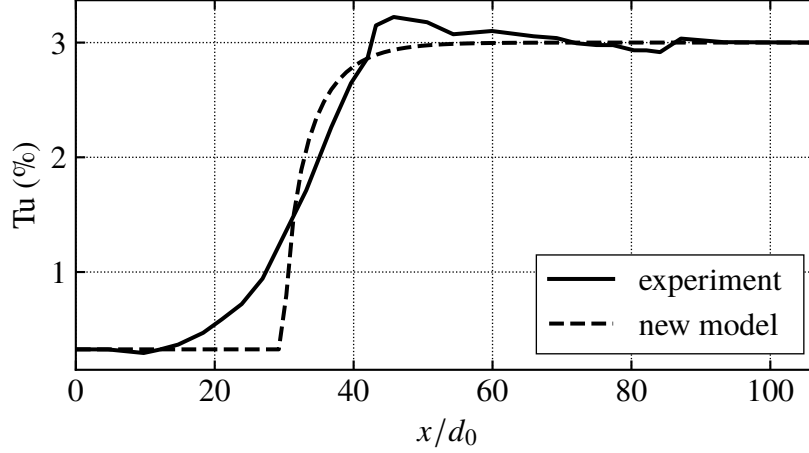
Figure 6.3: A comparison of the nozzle turbulence model developed in this work (equation 6.25) against an experimental data series compiled by Klein [Kle81].

Proudman [BP54, p. 94, equation 4.6] develop an approximation to RDT for contractions, accurate if $c \gtrsim 2$. Typically in internal flows $u' > v' \approx w'$. If I assume that $v' = w'$, then the anisotropies $b_{22} = b_{33} = b$ [Pop00, p. 360]. For isotropic turbulence $b = 0$, and for fully developed pipe flows $b \approx -1/8$. I can then compute the overall turbulence intensity at the end of the contraction:

$$\overline{Tu}_c^2 = \frac{3}{4}\left(\frac{\overline{Tu}_{in}}{c}\right)^2 \left[\frac{\left(\frac{1}{3} - 2b\right)[\ln(4c^3) - 1]}{c^2} + 2\left(b + \frac{1}{3}\right)c\right], \tag{6.24}$$

where $\overline{Tu}_{in}$ is the turbulence intensity at the nozzle inlet and $\overline{Tu}_c$ is the turbulence intensity at the end of the contraction. Using equation 6.19 for the nozzle orifice with the linearization $\overline{k}^{3/2} \approx \overline{k} \cdot \overline{k}_{FD}^{1/2}$, I estimate that

$$\overline{Tu}_0^2 = \overline{Tu}_{FD}^2 + \left(\overline{Tu}_c^2 - \overline{Tu}_{FD}^2\right)\exp\left(-\frac{3\overline{Tu}_{FD}^2}{f}\frac{L_0}{d_0}\right). \tag{6.25}$$

Equation 6.25 suggests that the turbulence intensity starts increasing immediately after the contraction, but this is unlikely. The flow in the contraction likely relaminarizes, so it needs to transition to turbulence inside the orifice before the model will apply. A model for

turbulence transition is needed. The simplest modification that can be made would be to subtract a transition length from L_0 in equation 6.25, i.e.:

$$\overline{\mathrm{Tu}}_0^2 = \overline{\mathrm{Tu}}_{\mathrm{FD}}^2 + \left(\overline{\mathrm{Tu}}_{\mathrm{c}}^2 - \overline{\mathrm{Tu}}_{\mathrm{FD}}^2\right) \exp\left(-\frac{3\overline{\mathrm{Tu}}_{\mathrm{FD}}^2}{f} \frac{L_0 - x_{\mathrm{trans}}}{d_0}\right), \tag{6.26}$$

where the inlet value of turbulence intensity is taken if $L_0 < x_{\mathrm{trans}}$.

There is little data available to validate equation 6.26. I am not aware of any nozzle turbulence experimental data where all of the model inputs (e.g., including inlet turbulence intensity, $\overline{\mathrm{Tu}}_{\mathrm{in}}$) are available. However, in contrast to Huh's model, this model is at least qualitatively correct in the limits of L_0/d_0.

Comparison with centerline (rather than plane average) turbulence intensity data compiled by Klein [Kle81, p. 246, fig. 3] (see figure 6.3) suggests that the model likely has the wrong concavity in $\overline{k}$ for small to moderate lengths after where transition starts, likely due to intermittency early after transition starts. (A value of $x_{\mathrm{trans}}/d_0 = 30$ was chosen arbitrarily for this plot; the uncertainty in the data does not justify a more complicated fitting procedure.) The intermittency likely could also explain why the slope in the model is higher than the slope in the experiment. Further theoretical developments are needed, and more detailed nozzle turbulence experiments are also needed to validate both the contraction and cylindrical segment parts of any nozzle turbulence model.

Despite these shortcomings, if a quick estimate for the turbulence intensity at the outlet of a nozzle is needed, equation 6.26 could provide that. One would need an accurate estimate of the transition length, as it is unclear how well the arbitrarily chosen value of $x_{\mathrm{trans}}/d_0 = 30$ would apply in other cases.

6.5 Estimation of inlet turbulent kinetic energy

Models of this variety typically require the inlet turbulent kinetic energy. There are a few possibilities to estimate this quantity: 1. Find the inlet turbulent kinetic energy from empirical measurements. 2. Select the inlet turbulent kinetic energy to match other
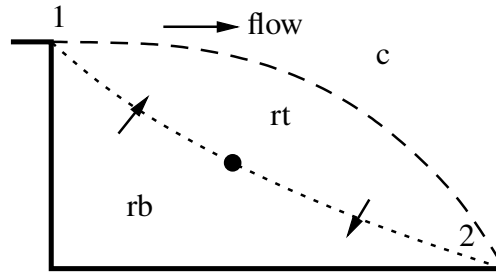
Figure 6.4: Recirculation zone.

measured quantities (less desirable). 3. Assume the flow is fully developed at the inlet. 4. Assume the inlet turbulent kinetic energy is zero, which may be acceptable for laminar or essentially quiescent entrances. 5. Use standardized tabulated empirical values of turbulent kinetic energy. At present, these tables do not exist, but it seems plausible that one could measure and compile values of turbulent kinetic energy at the outlet for pumps and other common starting points.

Appendix: The effect of recirculation zones

Earlier in this appendix, the side boundaries of the streamtube were assumed to be no-slip. This assumption is false when one or more recirculation zones appear in the flow. Briefly, I'll show that recirculation zones bounded outside by no-slip boundaries have the same effect as no-slip boundaries. In figure 6.4, the solid line is a no-slip boundary, the dashed line is the boundary (dividing streamline) of the central streamtube (denoted with c), the dotted line from the left corner (point 1) to the large dot is the inlet to the top of the recirculation zone (denoted with rt; also the outlet of the bottom of the recirculation zone, denoted with rb), and the dotted line from the large dot to the reattachment point (point 2) is the rt outlet (rb inlet). Equation 6.15 can be decomposed into $0 = \Delta_c + \int_{\text{in/out,c}} + \int_{\text{slip,c}} + \int_{\text{no-slip,c}}$ for c, $0 = \Delta_{\text{rt}} + \int_{\text{in/out,rt}} + \int_{\text{slip,rt}} + \int_{\text{no-slip,rt}}$ for rt, and $0 = \Delta_{\text{rb}} + \int_{\text{in/out,rb}} + \int_{\text{slip,rb}} + \int_{\text{no-slip,rb}}$ for rb. Δ are the conservative terms. The "in/out" integrals are the inlet and outlet integrals. The slip and no-slip integrals are the integrals over surfaces with slip and no-slip boundaries, respectively. The terms $\int_{\text{no-slip,rt}}$ and $\int_{\text{slip,rb}}$

161

equal zero by construction. Because rt and rb form a loop, $\Delta_{\mathrm{rt}} + \Delta_{\mathrm{rb}} = 0$. And because the inlet of rt equals the outlet of rb, and vice versa, $\int_{\mathrm{in/out,rt}} = -\int_{\mathrm{in/out,rb}}$. The central streamtube can be connected to rt by noting that $\int_{\mathrm{slip,c}} = -\int_{\mathrm{slip,rt}}$. Combining these and rearranging, I find that $0 = \Delta_{\mathrm{c}} + \int_{\mathrm{in/out,c}} + \int_{\mathrm{no\text{-}slip,c}} + \int_{\mathrm{no\text{-}slip,rb}}$ for the central streamtube, indicating that the recirculation zone is equivalent to the no-slip boundary on its periphery. If multiple recirculation zones separate the central streamtube from the no-slip boundary, this procedure can be repeated multiple times with the same result.

6.6 Conclusions

While Huh's model is inaccurate, relating $\overline{k}$ to the pressure drop in the nozzle is valid and has a long history. Unfortunately, no simple trick like a force balance at the orifice walls can allow one to avoid turbulence modeling. Using standard turbulence modeling approaches I developed equation 6.25, which can be used in place of Huh's model. However, equation 6.25 has not been validated. I recommend instead using CFD to determine $\overline{k}$ for now.

Chapter 7

Water jet trajectory theory[1]

7.1   Introduction

Predicting the trajectory and surface water distribution from a fire hose or fire monitor (as seen in figure 7.1) is difficult a priori. While models exist at present, their accuracy outside the range of their calibration data is questionable. For example, if a model is calibrated for a certain nozzle, it is unlikely that the model would be accurate for a different nozzle, even with an identical internal flow system upstream of the nozzle.

Given how critical time to extinguishment is to total property and life loss, more accurately predicting how long it will take for a water jet to extinguish a fire is essential to more accurately assess risk. The development of an accurate model of the trajectory of a water jet would help to more accurately estimated fire risk where fire hoses or fire monitors are used. The specific scenarios where water jets are used to suppress fire are varied, from first responders who apply hose streams, to deck-mounted fire monitors on boats used to fight fires on the deck or even outside the boat. Fire monitors mounted on towers also are frequently used in fire protection scenarios, e.g., protection of pulpwood. There is also recent interest in fully autonomous fire suppression systems, where prediction of the trajectory from a fire nozzle is essential for fast targeting. The model developed in this work would prove useful in accessing and reducing fire risk in all of these scenarios.

---

[1]An earlier version of the work in this chapter was published in a conference paper presented at ASME IMECE 2015 [TE15]. This chapter was completely rewritten using the conference paper as an outline to improve the presentation, correct errors, extend the theory, and improve the validation of the theory. Note that much of the notation has changed since then to be more consistent, be easier to understand, and simplify the results. I am the sole author; Prof. Ezekoye was included as an author on the conference paper for his advisory role.

Figure 7.1: Two fire monitors in use by the Portland Fire Department.
Fire monitors can deliver 5000 GPM (~300 L/s) or more through nozzles up to and beyond
3 inches (~7 cm) in diameter, leading to maximum ranges of 200 meters or more.
Photo from https://en.wikipedia.org/wiki/File:Deck_gun_on_American_fire_engine.jpg.

The scenario of interest is fire protection with large water jets, for example, hose streams and fire monitors. Consider a large water jet launched at a speed $\overline{U}_0$ and an angle θ_0 to the horizontal with the center of the nozzle of diameter d_0 at a height h_0. The nozzle outlet is denoted with 0, so, e.g., the nozzle outlet diameter is d_0. See figure 7.2 for an illustration of the problem. This jet gradually breaks up with distance from the nozzle, forming droplets which eventually reach the horizontal plane. The two quantities of interest are the surface water distribution (i.e., wetted area) and the maximum range R that the water jet projects water onto the horizontal plane. As show in figure 2.1, the surface water distribution is often biased towards R.

The basic nomenclature used for liquid jet breakup is shown in schematic in figure 2.1. In this frame the x axis is oriented streamwise. This is not the convention for the frame used in the trajectory models, where x is the distance from the nozzle outlet horizontally. The region of space over which liquid water is continuously connected to the nozzle outlet is called the jet core. The core flow (dark gray) starts being depleted of mass (on average) at
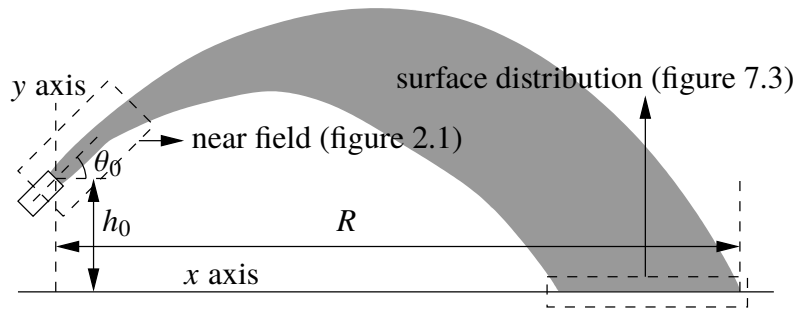
Figure 7.2: Basic trajectory nomenclature with firing angle θ_0, firing height h_0, and maximum range R.

the breakup onset location, $\langle x_i \rangle$. The core ends on average at the breakup length, $\langle x_b \rangle$; b in a subscript also refers to this location. Beyond x_b (the fluctuating breakup length rather than the average breakup length), liquid water exists only as discontinuous slugs and droplets. The lighter gray refers to the region where droplets exist.
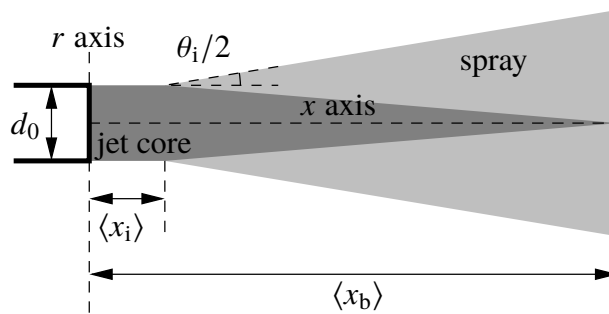
Figure 2.1: Jet breakup variables labeled on a schematic liquid jet. Coordinates are different from figure 7.2. d_0 is the nozzle outlet diameter, $\langle x_i \rangle$ is the average breakup onset location, θ_i is the spray angle, and $\langle x_b \rangle$ is the breakup length.

7.2 What influences the range of a water jet?

Because a variety of different factors influence the range and trajectory of a water jet, a review of these factors and what common models consider is needed. In this review, I emphasize that many previous models neglected important factors like the nozzle design. Selected functional dependencies of the problem studied in this work are shown in figure 1.1.
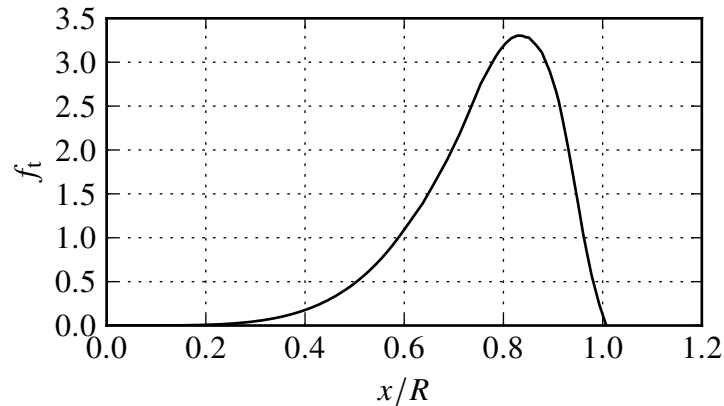
Figure 7.3: Surface water distribution example: probability density of water reaching distance x.

7.2.1 The water jet range anomaly

Water jet range can be estimated by assuming that droplets are emitted directly at the nozzle outlet at the velocity of the jet and that these droplets follow a ballistic trajectory with a known drag coefficient. I refer to this as the *instantaneous breakup* model. This model is known to severely underpredict the range of the jet. For example, Richards and Weatherhead [RW93, p. 284] report that the instantaneous breakup approach suggests that a 30 m/s jet at an angle of 24° producing a 5 mm droplet (presumably the nozzle outlet diameter) with a drag coefficient of 0.45 has a maximum range of 19.5 m, compared against 50 m found experimentally. I call this discrepancy the *range anomaly*.

Another common approach with large water jets is to assume that the jet experiences no drag. This is called the *dragless* approach. This approach over-predicts the range. For example, in the previously mentioned case, the dragless range is estimated to be about 68 m.

There also are empirical approaches to estimate range. The most simple empirical approaches are regression equations, which have been used by Lyshevskii [Lys62a] and Theobald [The81]. There also are computational models which use purely empirical drag models fitted to experimental data [Seg65; HO79; HLO85]. These drag models are inconsistent with known drag models for droplets. Models which select the droplet diameter distribution by matching range or water distribution data are similar, e.g., the model of

166

Fukui, Nakanishi, and Okamura [FNO80]. These models can lead to unrealistically large droplet diameters, as will be explained. Additionally, the accuracy of empirical models is questionable aside from the particular system they were calibrated for. This is particularly true given that some of the drag models used are dimensionally inhomogeneous. Smith et al. [Smi+08, p. 127R] note that empirical models typically require more calibration data than theoretical models for comparable accuracy.

Identifying the cause of the range anomaly is necessary to develop accurate models. I investigate three effects contributing to the range anomaly: air entrainment, jet breakup, and large droplets. Each effect exists in reality, but the relative contributions of each effect are not obvious at present.

7.2.1.1 Effect 1: Reduced drag due to air entrainment

One hypothesis is that the reduction in apparent drag is due primarily to air entrainment, as suggested by Murzabaeb and Yarin [MY85], Richards and Weatherhead [RW93, p. 284], and Grose [Gro99, p. 6]. The reasoning is that a higher entrainment velocity would reduce the velocity difference between the droplets and the surrounding gas flow (ΔU) and then decrease the drag ($F_\mathrm{d} \propto \Delta U^2$) without necessarily changing the drag coefficients of the droplets themselves. The entrainment velocity is created through the coupling between the droplets (or the jet core) and the gas. This momentum coupling is essentially a gas phase momentum source term, much like the source term used to model buoyant plumes that will be discussed in § 7.3.1.5.

Air entrainment is not likely as simple as was just discussed. In contrast to the popular statement of the hypothesis, decreasing air entrainment might lead to an increase in range as suggested by Hoyt and Taylor [HT77a]. The logic here is that the momentum transfer from the jet to the air results in reduced range. The net effect of air entrainment may either be negligible or non-monotonic, i.e., a certain amount of air entrainment is ideal. Too little air entrainment leads to higher drag due to a larger velocity difference, while too much air entrainment requires high drag to occur in the first place.

Further, if increased air entrainment explains the range anomaly, then I might expect higher jet turbulence intensity to increase range. This is because as jet turbulence intensity increases, so does air entrainment [EME80; ME80]. And as air entrainment increases, the relative velocity between the droplets and air decreases, in turn decreasing drag and increasing range. However, increasing jet turbulence intensity is known to decrease range [RHM52; Oeh58]. This could be despite increased air entrainment helping the jet's range, as the jet's turbulence intensity would influence effect 2: increased drag due to jet breakup.

7.2.1.2 Effect 2: Reduced drag before jet breakup

The second hypothesis is that the reduced drag is a consequence of the jet breaking up gradually rather than more abruptly. The hypothesis that preventing breakup leads to increased range in a water jet has a long history [Sch37, p. 513; DiC+68, p. 16; HT77a, p. S253L; TT78, p. A4-56; The81, p. 1], though how jet coherence leads to longer range is not always stated. One possibility is that the "jet core", sometimes called the "intact" or "coherent" part of the jet, experiences less drag than the droplets. This mechanism appears to have been first *recognized* in the efforts of Hatton and Osborne [HO79, p. 38L] to model fire hose streams in 1979, though they made no attempt to *model* the phenomena until 1985 [HLO85], after von Bernuth and Gilley [vBG84, p. 1438L] in 1984 independently developed a model for this effect for irrigation sprinklers. Others using this effect in their later models include Bragg [Bra85], Schottman and Vandergrift [SV86], Augier [Aug96], Kincaid [Kin96], and Zheng, Ryder, and Marshall [ZRM12].

Modeling this effect is much less common than the others, being neglected in the most popular models for jet sprinkler irrigation [CTM01]. This may be due in part to the paper of Seginer, Nir, and von Bernuth [SNvB91, p. 302], which suggested that the calibrated breakup length was negligible for the irrigation sprinklers they measured the trajectories of. Seginer, Nir, and von Bernuth measured neither droplet diameters or breakup lengths, however, so Seginer, Nir, and von Bernuth possibly selected droplet diameters which were unrealistic. This could have led to the incorrect conclusion that the breakup

168

length is negligible in the nozzles tested because the breakup length was calibrated, not measured. Another criticism of the approach is from Richards and Weatherhead [RW93, p. 284], who suggested that the breakup length is "hard to define" without elaborating.[2]

Additionally, this effect is the only one which can explain the long hypothesized effect that delaying the breakup of a water jet (i.e., increasing the breakup length) increases range[3]. The hypothesis that range increases if breakup is prevented has a long history and is the main design goal in fire nozzle design [RHM52; Oeh58; The81]. As evidence of this hypothesis, it is obvious that a fog nozzle would not have as long a range as a smooth bore (i.e., "solid" jet) nozzle. Additionally, the experiments of Theobald [The81] show that the range of a large water jet is roughly ordered by the breakup length, all else equal[4]. Unfortunately, Theobald's experiments are the only I am aware of which quantitatively varied the breakup length independent of other variables, as opposed to qualitatively varying the breakup length by for example changing the nozzle design without measuring the breakup length.

The fog nozzle example also shows that air entrainment and jet breakup are coupled. Air entrainment would obviously be far stronger for a fine spray than an intact jet. As air entrainment is greater for finer sprays than intact jets, this would seem to suggest that longer breakup lengths would tend to reduce air entrainment and consequently increase drag. This highlights the suggestion that air entrainment could both increase or decrease drag depending on the situation.

Further, the earlier mentioned models treat the breakup length as a universal characteristic of water jet systems, neglecting the effects of nozzle geometry and the upstream flow (e.g., the effect of jet turbulence intensity). In other words, it is not sufficient

---

[2]The breakup length is defined clearly in § 2.2, and some additional comments on the definitions are made in § 4.2.

[3]It is likely that more vigorous breakup also leads to smaller average droplet diameters. But the maximum range is controlled primarily by the maximum droplet diameter in ballistic theories, and that does not appear to be influenced strongly by the average droplet diameter. The data is noisy, but it appears that the maximum droplet diameter is not a clear function of anything aside from the nozzle outlet diameter, d_0. See the next subsection.

[4]Or roughly equal, as the droplet size varies in Theobald's experiments.

to make a model with a nonzero breakup length or a nonzero length region where drag is reduced on the jet. Because the breakup length varies greatly between different nozzles and jet systems in general, models need to consider the variation in the breakup length.

Given the disconnect between nozzle design and trajectory models, there is a need to develop models which consider the effect of the nozzle geometry and upstream flow. A reductionist approach, examining the dependencies of specific parts of the problem rather than the whole is needed. Figure 1.1 illustrates the dependencies of each part of the problem and places each chapter of this dissertation in the context of each component of the problem. Previous models were essentially empirical (or at least "postdictive"), and consequently they were tied to the particular system they were calibrated to. A predictive trajectory model would not require calibration, and instead its input quantities could hypothetically be determined without a trajectory test, allowing a true prediction of the trajectory to be made. An example of this is determining the flow coefficient of a valve before implementing it into a flow system, rather than fitting the flow coefficient of the valve to the actual performance of the flow system. And while models can be calibrated to observed trajectories, there is little reason to believe calibrated models are accurate outside the range of the calibration data. I previously mentioned that simply changing the nozzle is likely to make a model inaccurate, as trajectory models typically have no nozzle specific input parameters. As another example, the model of Hatton, Leech, and Osborne [HLO85] is calibrated only for windless conditions. The drag on a cylinder positioned normal to the flow is quite different from that of a droplet or cylinder aligned with the direction of the flow. Consequently, the accuracy of this model should be suspect. A trajectory model based on more fundamental physics (including both nozzle/breakup and aerodynamic effects) would take such a distinction into account. If all of the relevant physics are contained in the trajectory model, and all of the model coefficients can be obtained without conducting a range test, then the model can make predictions.

Finally, it is not ideal to have a parameter which allows for mere *implicit* variation of the breakup length, or variation of the region where drag is reduced in more general. Using as a model input a parameter which can be measured independently of a trajectory test is preferred, as this would allow the model to be independently validated. Another problem is

that if a model uses a coefficient to change the length of a region with lower drag rather than the breakup length, it's not always obvious how that coefficient would change quantitatively if a nozzle geometry parameter were to change, but a breakup length model could handle this situation. Explicitly considering the breakup length avoids these issues.

7.2.1.3 Effect 3: Reduced drag due to large droplet sizes

Larger droplets have relatively less drag because their projected area to volume ratio is lower, increasing their inertia more than the corresponding increase in projected area. Fitting the droplet size distribution to range data is likely to overestimate the droplet sizes without consideration of jet coherence and air entrainment.

As assumption in previous analyses is that the largest droplets formed have a diameter D_{max} equal to the nozzle outlet diameter, d_0. This is not realistic. In both theory and experiment droplets larger than the nozzle can be formed. While the notion of a "droplet diameter" can be hard to define here because large droplets tend to be non-spherical [Haw96, p. 52], some general observations can be made. The diameter of a droplet formed by a laminar inviscid jet as found theoretically by Rayleigh [Ray78] (equation 2.4), about $1.89d_0$, has independently been proposed as the largest by Baljé and Larson [BL49, p. 2] and Dumouchel, Cousin, and Triballier [DCT05, p. 643R]. However, the experiments of Chen and Davis [CD64, p. 196] show the arithmetic average of the droplet diameter at the average breakup point (i.e., $\langle x_b \rangle$) downstream can vary from $1.46d_0$ to $4.30d_0$, clearly contradicting the suggestion that the Rayleigh diameter is the largest. The data of Miesse [Mie55, p. 1695] also has several cases where the droplet diameter was larger than the Rayleigh diameter. However, all D_{max} measurements of Inoue [Ino63, p. 16.111] were less than the Rayleigh diameter. These results are highly variable, so ultimately, the most clear statement is that $D_{max} = O(d_0)$ but larger than d_0, D_{max} varies, and it is unlikely that the D_{max} is greater than $4.5d_0$ in practice.

Unlike the previous two effects, this effect is fairly well established and consequently will receive less attention in this chapter.

7.2.2 Other effects on the trajectory

7.2.2.1 Firing angle

Contrary to popular belief, the range of a large water jet is not typically maximized at a firing angle of $\theta_0 = 45°$. It can be shown that the optimal firing angle is 45° only for dragless projectiles launched at a firing height h_0 of zero.

In practice, the optimal firing angle is typically found to be in the range of 30–35° due largely to the effect of drag. The optimal angle increases to 45° as the pressure drops, which presumably results in less jet breakup and less drag [Fre89, p. 387; RHM52, fig. 20, p. 1171]. The optimal firing angle is a function of the jet Froude number, dimensionless breakup length, wind speed and direction, among other variables, so some inconsistency between studies is expected. The early study of Freeman [Fre89, p. 387] finds the optimal firing angle in still air to be 32°. Rouse, Howe, and Metzler [RHM52, pp. 1168–1171] find the optimal angle to be 30° in still air. Theobald [The81, p. 7L] suggests 35° for turbulent jets, and Comiskey and Yarin [CY18, p. 65] also suggests 35° for laminar jets.

7.2.2.2 Wind

Wind is known to have a strong effect on fire hose streams. Tests typically are done outdoors due to space restrictions. Experimentalists often wait to avoid wind [Fre89, p. 374]. Unfortunately, Rouse, Howe, and Metzler [RHM52, p. 1159] find that the winds are sufficiently calm outdoors only about 1% of the time. Theobald [The81, p. 7R] conducted their experiments in a large hangar to minimize the effects of wind. In a series of outdoor tests, Green [Gre71, p. 3] used two nozzles side-by-side to ensure that the wind conditions are roughly the same for both nozzles. Freeman [Fre89, p. 375] also used the same arrangement to compare two nozzles possibly in the presence of wind, but found this arrangement to be inappropriate for determining the range of a single nozzle due to a roughly equal increase of the range of each jet from the extra air entrainment. (The arrangement of tests into similar groups is called "blocking" in the design of experiments literature.) In the multi-nozzle setup, any differences observed between the jets could be attributed solely to other changes

172

made — Green was interested in the addition of polymers, but it could be a nozzle design change as well.

There is very little research on the effect of wind on the entire trajectory large water jets. There is a very large amount of research on the "jet-in-cross-flow" configuration, and in particular the effect of the cross-flow/wind on the breakup and trajectory of the jet relatively near the nozzle, e.g., see the study and review of Birouk, Nyantekyi-Kwakye, and Popplewell [BNP11] for subsonic cross-flows. The water jet trajectory problem requires examination of areas farther downstream, unfortunately. The jet-in-cross-flow studies also suffer from a problem the trajectory studies suffer from: few (if any) experiments vary the breakup length independent of other variables. This is even more complicated than the windless trajectory case as the wind also changes the breakup length. Improving jet coherence has been hypothesized to improve wind resistance of water jets [Gre71, p. 1].

The jet shape influences how much wind resistance the jet has, with "hollow core" jets produced by a combination nozzle being more susceptible to find than "solid" jets [For91, p. 253], to use terminology from the fire protection literature. This work focuses primarily on "solid" jets. (In principle hollow core jets can be handled in this framework if the breakup length and droplet size distribution are known.)

Because one of the effects of wind is to increase the amount of drag, the optimal firing angle in wind is expected to be lower than that without wind. Cousins and Stewart [CS30, p. 2] observed that the effects of wind were strongest at larger firing angles. The optimal firing angle under windy conditions has been informally observed in practice to be about $10°$ in roughly 15 m/s wind [PG71, p. 2]. Simulations performed by von Bernuth [vBer88] suggest the optimal firing angle can be lower than $5°$ in winds greater than 8 m/s. Another potential cause of the reduction in the optimal firing angle is the existence of the atmospheric boundary layer. The closer the jet is to the ground, the lower the wind velocity it experiences.

7.2.2.3 Firing height

The effect of the firing height h_0 on the trajectory is characterized through the height Froude number, $\mathrm{Fr}_{h_0} \equiv \overline{U}_0^2/(g h_0)$. In still air, the range increases as h_0 increases, or equivalently, as Fr_{h_0} decreases.

If there is no drag, the optimal firing angle can be shown to increase to 45° as Fr_{h_0} increases and decrease to 0° as Fr_{h_0} decreases.

Typically, Fr_{h_0} is small because the velocities involved in the water jet trajectory problem are relatively large. However, the effect of Fr_{h_0} is not always negligible, and as a consequence I'll be including a non-zero firing height in this work.

7.2.2.4 Jet velocity or pressure

The range of a water jet increases as the jet velocity (or equivalently, pressure) is increased, up to a point. After that point, the range will no longer increase as velocity increases [RHM52, p. 1168; Eut57]. The precise reasons for this are unclear, though a change in the regime of the jet from the turbulent surface breakup regime to the atomization regime is a possibility. See chapter 3 for more information on the regimes of a liquid jet.

7.3 Analytical theory and validation

This chapter presents an approximate analytical theory of water jet *maximum range* [TE15] which I call "multi-stage theory". To summarize the theory, a fluid particle travels from the nozzle initially in the "intact" part of the jet. Intact means that the jet has not yet broken into droplets. Jet breakup occurs at a known distance from the nozzle (the breakup length, $\langle x_{\mathrm{b}} \rangle$), after which the fluid particle is a droplet. The model has different drag models for the intact and droplet stages of the jet. Of the effects mentioned in § 7.2.1, the model considers the intact portion of the jet, air entrainment, and droplet size, however, the air entrainment model is rudimentary.

That the nozzle design can strongly affect the range of a water jet is well known.

But until the model presented in this chapter was developed, this fact was not completely reflected in a model beyond the effect of the nozzle design on the droplet size. The droplet size is not a typically discussed effect among nozzle designers. Nozzle designers have an intuitive idea that making breakup occur farther downstream increases range, and it is this effect which I wanted to implement in a model.

It is not sufficient for a model to merely *consider* breakup. One could argue that all instantaneous breakup models consider breakup. Models which consider breakup but assume that the breakup process is universal (e.g., constant breakup length), and not influenced by the nozzle design, are unacceptable.

A related goal of the model is to not require range tests to credibly estimate the range and water distribution. All of the parameters in the model can be measured without measuring range. For example, the breakup length can be measured photographically or through electrical conductivity. The droplet size distribution (and characteristic diameters like $D_{\max}$ and D_{32}) can be measured through many standard techniques. The parameters in the model are not purely for tuning the model. They have physical meanings and ideally will match those measured experimentally. Additionally, leaving these breakup parameters as inputs to the trajectory model allows the use of separate jet breakup models. The trajectory model can use improved jet breakup models developed in the future without modification. This approach also gives confidence to nozzle designers that changes in the breakup parameters (as controlled by the nozzle design) will have the desired effect on the trajectory.[5]

7.3.1 Submodels

7.3.1.1 Drag on the intact jet

For fluid particles before jet breakup occurs, the drag is treated as zero. This is not strictly true, but is the approximation I'll use in this work. For laminar jets

---

[5]While in practice I calibrate the maximum droplet size to the data here, this can be viewed as converting a real non-spherical large "droplet" to a spherical droplet of diameter $D_{\max}$ with equivalent drag.

$(621 \leq \mathrm{Re}_{\ell 0} \leq 1289)$, Comiskey and Yarin [CY18] measured and correlated the (jet length) average skin friction coefficient with the equation $\overline{C}_{\mathrm{f}} = 5\mathrm{Re}_{\ell 0}^{-1/2}$. The cases of interest are turbulent, however, so the applicability of this relationship beyond the Reynolds number limits of the experiment are unknown. The correlation suggests that the drag on high Reynolds number jets is likely low.

Even if the drag in the direction of the jet's motion is negligible, the drag from wind is not. In this model, wind is neglected entirely for simplicity.

7.3.1.2 Jet breakup location

After breakup occurs, droplets are formed. The breakup location can vary greatly for each droplet, from as small as x_{i}, where breakup is first initiated, to as high as x_{b}, where the jet core finally breaks. As a first approximation, the model assumes that all breakup occurs at $\langle x_{\mathrm{b}} \rangle$. As droplet mass flux increases greatly with distance from the nozzle [SDF02, p. 445–446, fig. 10], the droplet volume is expected to mostly come from near the end, x_{b}.

Additionally, the standard deviation of the breakup length, σ_{b}, is a relatively small fraction of the total breakup length. This would indicate that the end of breakup is reasonably well approximated as occurring at the average breakup length, $\langle x_{\mathrm{b}} \rangle$. Defining the coefficient of variation of the breakup length $C_{\sigma_{\mathrm{b}}} \equiv \sigma_{\mathrm{b}}/\langle x_{\mathrm{b}} \rangle$, I find that the available data [Phi73; YO78] is well represented by $C_{\sigma_{\mathrm{b}}} = 0.1291 \pm 0.0019$. This appears to be independent of the nozzle design, but likely applies only for turbulent surface breakup and atomization regimes as the proportionality seems to fail at lower velocities [LDL96, fig. 6–7]. Additionally, the single DNS data point of Agarwal and Trujillo [AT18, fig. 17] returns $C_{\sigma_{\mathrm{b}}} = 0.0847$, which is lower than the experiment, likely because the jet is initially laminar (a different regime; see chapter 3). Figure 7.4 shows a cumulative distribution plot of the instantaneous breakup length x_{b} divided by the average breakup length $\langle x_{\mathrm{b}} \rangle$ for jets produced from converging nozzles, abrupt contraction nozzles, and pipe nozzles. A straight line corresponds to a normal distribution in these coordinates; the available data appears to be well described by normal distributions. The slope determines the standard deviation.
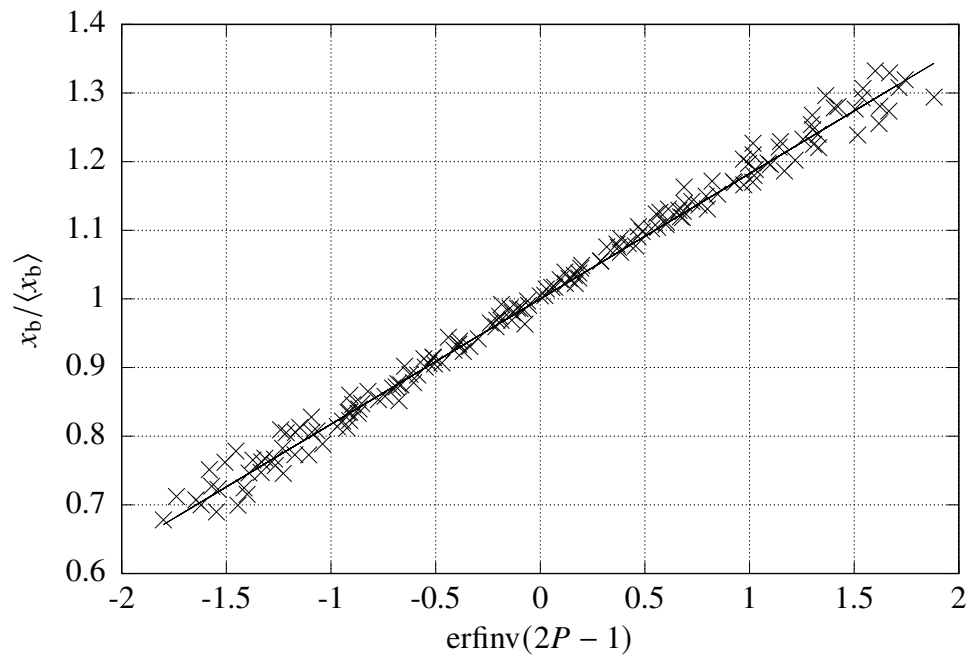
Figure 7.4: A cumulative distribution plot of the instantaneous breakup length normalized by the average breakup length. In these coordinates, a normal distribution is a straight line. Experimental data from Phinney [Phi73] and Yanaida and Ohashi [YO78].

7.3.1.3 Maximum droplet diameter and droplet breakup

The maximum droplet diameter is treated as constant. Breakup of droplets is neglected in this chapter for simplicity. Large droplets are unstable and will break up into smaller droplets [LM17, p. 19], and I believe the neglect of this feature to be the largest source of uncertainty out of those I mentioned. However, existing models for droplet breakup are not known to be particularly accurate and may not improve the accuracy much.

The particle mass does not need to be defined for the jet core in this model, but it does need to be defined for the droplet stage. This requires knowledge of the droplet diameter. As larger droplets travel farther, the maximum range corresponds to the maximum droplet diameter, $D_{\max}$. As mentioned in § 7.2.1.3, the maximum droplet diameter is not very precisely known aside that it's $O(d_0)$. Consequently, the maximum droplet diameter will be chosen to fit the data later in this chapter.

7.3.1.4 Droplet drag

The droplet drag model is standard quadratic drag with a constant drag coefficient, which is a commonly used model. The droplet Reynolds number is approximately (considering the velocity constant and neglecting air entrainment) $D_{\max}\overline{U_0}/\nu_{\mathrm{g}}$ which is $O(10^4)$ in the validation experiments, before the drag crisis typically occurs, where the drag coefficient for a solid sphere is relatively constant [MYO05, p. 526]. Change of the droplet drag coefficient for any reason (Reynolds number variation, droplet shape variation, or other reasons) is neglected in this chapter for simplicity. Loth [Lot08, p. 524L] suggests that $C_{\mathrm{d}} = 0.42$ for a solid spherical particle at high Reynolds number, within 6%, and this is the value used.

7.3.1.5 Air entrainment

The air entrainment model used in this work is simplistic and will only act to increase range, even though there are reasons to believe that air entrainment can decrease range as well — see § 7.2.1.1. In buoyant plume theory [MTT56], an entrainment coefficient

is defined. The entrainment coefficient relates the velocity of the plume centerline to the entrainment velocity. The entrainment coefficient is essentially empirical, and can be viewed as analogous to the (also essentially empirical) turbulent viscosity used in elementary turbulent jet theory [Pop00, pp. 118–122].

Due to differences between the jet and buoyant plume cases, a similar but not identical definition of the entrainment coefficient α was developed:

$$\vec{U}_g \equiv \alpha \vec{U}_d. \tag{7.1}$$

The droplets and gas phase can occupy the same location at different times, so in a time averaged model it could be reasonable to use equation 7.1 along the centerline of the jet.

The experimental measurements of air flow in a spray of Heskestad, Kung, and Todtenkopf [HKT76, figs. 4–6] suggest that $\alpha = 0.1$ is a reasonable approximation to one significant figure at the jet centerline. Given that the spray was much finer in Heskestad, Kung, and Todtenkopf's experiment than the more coherent jets studied in this work, I'd expect the entrainment coefficient to be lower than Heskestad, Kung, and Todtenkopf's, perhaps around 0.05. This is the value used in this work.

A constant entrainment coefficient is a crude approximation. I expect the local entrainment coefficient to vary with the spatial coordinate, Reynolds number, Weber number, and density ratio, if not other variables. However, this approximation is expected to be reasonable enough to roughly determine the sensitivities of the problem. In the future a model for the entrainment coefficient as a function of the droplet drag coefficients and other variables could be developed, generalizing the model further.

7.3.2 Maximum height of a water jet fired vertically

Before focusing on the problem of the full trajectory of a water jet, I'll focus on the simpler problem of the maximum height of a jet fired vertically without wind. Decorative fountains are often fired vertically, and the scenario is also relevant to fighting high-rise fires.

Breakup occurs at a distance $\langle x_b \rangle$ (the breakup length) above the nozzle, which is the origin ($Y = 0$). Before breakup, the jet follows a dragless trajectory. After breakup, the jet is composed of spherical droplets of varying diameters. These droplets are assumed to be not interacting, so they can overlap without collisions or coalescence. As discussed, these droplets have constant drag coefficients. I also only compute the trajectory for a droplet of size D_{max} as I am interested in h, the maximum height. Wind is neglected here. As stated, air entrainment will be handled in a crude fashion with a constant entrainment coefficient.

The vertical coordinate Y_j will be used for the jet centerline. When $Y_j < \langle x_b \rangle$, the equation of motion of the jet is:

$$\frac{\mathrm{d}^2 Y_j}{\mathrm{d}t^2} = \frac{\mathrm{d}V_j}{\mathrm{d}t} = -g, \tag{7.2}$$

where the jet core velocity is V_j.

Equation 7.2 can be solved to obtain the height and velocity as a function of time. These solutions are

$$\frac{\mathrm{d}Y_j}{\mathrm{d}t}(t) = V_j = \overline{U}_0 - gt, \tag{7.3}$$

$$Y_j(t) = \overline{U}_0 t - \tfrac{1}{2}gt^2, \tag{7.4}$$

where $\overline{U}_0$ is the jet bulk velocity[6]. When the breakup length $\langle x_b \rangle$ is less than the maximum possible height H, I'll model the jet as breaking up into droplets instantaneously at $Y_j = \langle x_b \rangle$. At the breakup point the velocity is $V_b = \sqrt{\overline{U}_0^2 - 2g\langle x_b \rangle}$.

For non-dimensionalization, it's useful to normalize by the maximum possible height a jet could obtain to create a "jet efficiency" that is bounded between 0 and 1. This height can be found from equation 7.4, because in the best case no breakup occurs. The

---

[6]Note that in the *water jet trajectory* coordinate system, Y is the vertical coordinate, while in the *jet breakup* coordinate system, x is the nozzle axis coordinate. Consequently, the jet bulk velocity $\overline{U}_0$ in the x direction of the nozzle is also in the Y direction of the trajectory frame. Additionally, as the water jet trajectory computed here is essentially an ensemble-averaged quantity, rather than writing $\langle Y \rangle$, I'll write Y for brevity, using the capitalization as an implied average here. A j subscript will be used for the jet core trajectory, and a d subscript will be used for the droplet trajectory.

maximum possible height is $H = \overline{U}_0^2/(2g)$, assuming a uniform velocity profile. The real height the jet obtains is h. Consequently, the definition of the jet height efficiency is

$$\eta_h \equiv \frac{h}{H} = \frac{2gh}{\overline{U}_0^2}. \tag{7.5}$$

(This definition was first used by Arato, Crow, and Miller [ACM70, p. 2].)

Applying simple Newtonian dynamics, the equation of motion for a particular droplet (after jet breakup, so Y_j changes to Y_d) is

$$m_d \frac{dV_d}{dt} = -m_d g - \frac{1}{2} \rho_g C_d A_d (V_d - V_g)^2, \tag{7.6}$$

where m_d is the mass of the droplet, V_d is the droplet velocity, and V_g is the velocity of the gas immediately around the droplet.

Then, approximating the droplets as spherical, I obtain

$$\frac{\pi}{6} \rho_\ell D^3 \frac{dV_d}{dt} = -\frac{\pi}{6} \rho_\ell D^3 g - \frac{1}{2} \rho_g C_d \frac{\pi}{4} D^2 (V_d - V_g)^2. \tag{7.7}$$

Equation 7.7 can be used to calculate the trajectory for any droplet size D in the entire droplet size distribution $f_D(D)$. My interest in this example is in the maximum height obtained by the jet, which is obtained only for the largest droplets of diameter $D_{\max}$. The equation can be further simplified through the use of a constant entrainment coefficient. If I define the entrainment coefficient α through the equation $V_g = \alpha V_d$, then $V_d - V_g = (1-\alpha)V_d$. With these modifications, equation 7.7 is now

$$\frac{\pi}{6} \rho_\ell D_{\max}^3 \frac{dV_d}{dt} = -\frac{\pi}{6} \rho_\ell D_{\max}^3 g - \frac{1}{2} \rho_g C_d \frac{\pi}{4} D_{\max}^2 (1-\alpha)^2 V_d^2. \tag{7.8}$$

Non-dimensionalizing this result with $\tau \equiv t/(V_b/g)$ and $V_d^* \equiv V_d/V_b$ leads to

$$\frac{dV_d^*}{d\tau} = -1 - \frac{3}{4} \frac{C_d}{\rho_\ell/\rho_g} \frac{(1-\alpha)^2}{D_{\max}/d_0} \mathrm{Fr}_0 (V_b^*)^2 (V_d^*)^2, \tag{7.9}$$

181

where

$$V_b^* \equiv \frac{V_b}{\overline{U_0}} = \sqrt{1 - \frac{2\langle x_b \rangle / d_0}{\mathrm{Fr}_0}}.$$ (7.10)

For simplicity I'll define a reduced drag coefficient:

$$C_d^* \equiv \frac{3}{2} \frac{C_d}{\rho_\ell / \rho_g} \frac{(1-\alpha)^2}{D_{\max}/d_0},$$ (7.11)

so the non-dimensional equation of motion can be written as

$$\frac{dV_d^*}{d\tau} = -1 - \frac{1}{2} C_d^* \mathrm{Fr}_0 (V_b^*)^2 (V_d^*)^2,$$ (7.12)

or after defining $\widehat{C_d} \equiv C_d^* \mathrm{Fr}_0 (V_b^*)^2$,

$$\frac{dV_d^*}{d\tau} = -1 - \frac{1}{2} \widehat{C_d} (V_d^*)^2.$$ (7.13)

Separating variables and integrating equation 7.13 from time τ_b (when the breakup starts, so $V_d(\tau_b) = V_b$) returns

$$\int_{\tau_b}^{\tau} d\widehat{\tau} = \int_1^{V_d^*} \frac{-d\widehat{V_d}^*}{1 + \frac{1}{2}\widehat{C_d}(\widehat{V_d}^*)^2},$$ (7.14)

$$(\tau - \tau_b) = \frac{\mathrm{atan}\left(\sqrt{\widehat{C_d}/2}\right) - \mathrm{atan}\left(V_d^* \sqrt{\widehat{C_d}/2}\right)}{\sqrt{\widehat{C_d}/2}},$$ (7.15)

which can be solved for V_d^*:

$$V_d^* = \frac{\tan\left[\mathrm{atan}\left(\sqrt{\widehat{C_d}/2}\right) - (\tau - \tau_b)\sqrt{\widehat{C_d}/2}\right]}{\sqrt{\widehat{C_d}/2}}.$$ (7.16)

Equation 7.16 can now be integrated to obtain the maximum height. First, it is necessary to determine at what dimensionless time, τ_{top} the maximum height is obtained. The vertical

velocity $V_d^* = 0$ when $\tau = \tau_{\text{top}}$, so equation 7.16 can be solved to find that

$$\tau_{\text{top}} - \tau_b = \frac{\text{atan}\left(\sqrt{\widehat{C_d}/2}\right)}{\sqrt{\widehat{C_d}/2}}. \tag{7.17}$$

Now the maximum height can be found by integrating from the breakup point to the maximum height:

$$h = \langle x_b \rangle + \int_{t_b}^{t_{\text{top}}} V_d \, d\widehat{t} = \langle x_b \rangle + \frac{V_b^2}{g} \int_{\tau_b}^{\tau_{\text{top}}} V_d^* \, d\widehat{\tau}, \tag{7.18}$$

which leads to (after simplifying via trigonometric identities)

$$h = \langle x_b \rangle + \frac{V_b^2}{g} \frac{\ln(\widehat{C_d}/2 + 1)}{\widehat{C_d}}. \tag{7.19}$$

The height efficiency η_h can be obtained from equation 7.19 by applying its definition (equation 7.5) and simplifying using the fact that $\widehat{C_d} \equiv C_d^* \text{Fr}_0 (V_b^*)^2$:

$$\eta_h = \frac{2\langle x_b \rangle / d_0}{\text{Fr}_0} + \frac{2}{C_d^* \text{Fr}_0} \ln \left[\frac{C_d^*}{2} \left(\text{Fr}_0 - \frac{2\langle x_b \rangle}{d_0} \right) + 1 \right]. \tag{7.20}$$

The maximum height in physical coordinates is

$$h = \langle x_b \rangle + \frac{d_0}{C_d^*} \ln \left[\frac{C_d^*}{2} \left(\text{Fr}_0 - \frac{2\langle x_b \rangle}{d_0} \right) + 1 \right]. \tag{7.21}$$

Another possible non-dimensionalization which simplifies some results uses h^* (h-star), defined as

$$h^* \equiv \frac{C_d^* h}{d_0}. \tag{7.22}$$

The h^* equation then is

$$h^* = \frac{C_d^* \langle x_b \rangle}{d_0} + \ln \left[\frac{C_d^*}{2} \left(\text{Fr}_0 - \frac{2\langle x_b \rangle}{d_0} \right) + 1 \right]. \tag{7.23}$$

For convenience, the reduced drag coefficient is

$$C_d^* \equiv \frac{3}{2} \frac{C_d}{\rho_\ell/\rho_g} \frac{(1-\alpha)^2}{D_{\max}/d_0}.$$

(7.11)

As a check on equation 7.20, consider the case where the reduced drag coefficient C_d^* goes to zero, which should cause the jet efficiency to be one. This is not obviously seen in equation 7.20 analytically due to the $2/C_d^*$ term, so I'll use the Taylor series for $\ln(x+1)$,

$$\ln(x+1) = \sum_{n=1}^{\infty} \frac{(-1)^{n+1}}{n} x^n,$$

(7.24)

and compute the limit:

$$\lim_{C_d^* \downarrow 0} \eta_h = \frac{2\langle x_b \rangle/d_0}{\mathrm{Fr}_0} + \lim_{C_d^* \downarrow 0} \sum_{n=1}^{\infty} \frac{(-1)^{n+1}}{n} \left(\frac{C_d^* \mathrm{Fr}_0}{2} \right)^{n-1} \left(1 - \frac{2\langle x_b \rangle/d_0}{\mathrm{Fr}_0} \right)^n,$$

(7.25)

$$= \frac{2\langle x_b \rangle/d_0}{\mathrm{Fr}_0} + 1 - \frac{2\langle x_b \rangle/d_0}{\mathrm{Fr}_0}$$

$$+ \lim_{C_d^* \downarrow 0} \sum_{n=2}^{\infty} \frac{(-1)^{n+1}}{n} \left(\frac{C_d^*}{2} \right)^{n-1} \left(1 - \frac{2\langle x_b \rangle/d_0}{\mathrm{Fr}_0} \right)^n$$

(7.26)

$$= 1.$$

(7.27)

Every term aside from the $n = 1$ term was proportional to C_d^*, so those terms are zero in the limit. The $n = 1$ term does not contain C_d^*, but it does contain some breakup length terms which cancel each other out, returning $\eta_h = 1$ in the limit.

The case where the jet does not break up before reaching its peak ($\langle x_b \rangle = H$) returns $2\langle x_b \rangle/d_0 = \mathrm{Fr}_0$. Then

$$\eta_h(\langle x_b \rangle = H) = 1 + \frac{2}{C_d^*} \ln 1 = 1,$$

(7.28)

as is expected because the jet experiences no drag before breakup in this model.

In the earlier conference paper version of this work [TE15], equation 7.20 was favorably compared against experimental data from Arato, Crow, and Miller [ACM70].

However, Arato, Crow, and Miller's experiments were conducted outdoors, leading to a large spread in the data. Additionally, Arato, Crow, and Miller's data was presented in a way which makes determining details of the nozzles used impossible, requiring making unjustified assumptions. Consequently, new experiments are required to properly validate equation 7.20. Some new vertical jet experiments were conducted indoors for this dissertation but were deemed incomplete and preliminary. These experiments will be published in the future when complete.

7.3.3 Maximum range of a water jet fired approximately horizontally
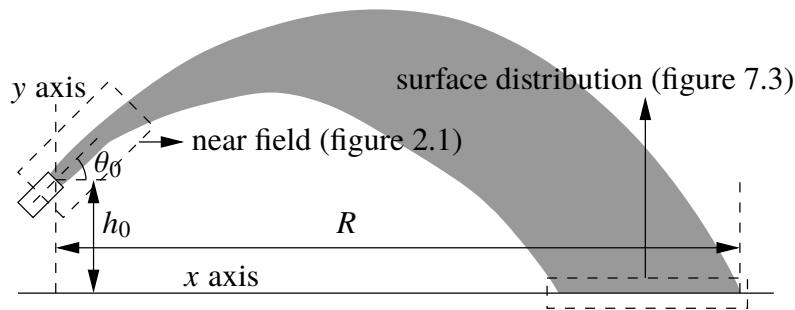
Figure 7.2: Basic trajectory nomenclature with firing angle θ_0, firing height h_0, and maximum range R.

The more general trajectory case is considerably more complex, as can be seen in figure 7.2. The general outline of the analytical solution of the trajectory case is the same as that of the vertical height case. First, the trajectory of the jet's core (X_j and Y_j) is computed without wind, then the trajectory of the droplets after breakup (X_d and Y_d) is computed. As in figure 7.2, X is horizontal and Y is vertical.

7.3.3.1 Dragless jet core trajectory

The equations of motion and initial conditions for the jet's core (dragless) are

$$\frac{\mathrm{d}^2 X_j}{\mathrm{d}t^2} = \frac{\mathrm{d}U_j}{\mathrm{d}t} = 0, \qquad\qquad \frac{\mathrm{d}^2 Y_j}{\mathrm{d}t^2} = \frac{\mathrm{d}V_j}{\mathrm{d}t} = -g,$$

$$X_j(0) = 0, \qquad\qquad\qquad Y_j(0) = h_0,$$

185

$$\frac{\mathrm{d}X_\mathrm{j}}{\mathrm{d}t}(0) = U_\mathrm{j} = \overline{U}_0 \cos\theta_0, \qquad\qquad \frac{\mathrm{d}Y_\mathrm{j}}{\mathrm{d}t}(0) = V_\mathrm{j} = \overline{U}_0 \sin\theta_0, \qquad (7.29)$$

where θ_0 is the firing angle, h_0 is the firing height, and, as before, g is the acceleration due to gravity and $\overline{U}_0$ is the jet bulk velocity. These equations have the solutions

$$X_\mathrm{j}(t) = \overline{U}_0 \cos(\theta_0)\, t, \qquad (7.30)$$

$$Y_\mathrm{j}(t) = \overline{U}_0 \sin(\theta_0)\, t - \frac{1}{2}gt^2 + h_0. \qquad (7.31)$$

To non-dimensionalize the range as an efficiency like in the vertical jet case, it is necessary to first find the maximum possible range in the dragless case given a fixed firing height h_0 (setting the firing angle θ_0 to the optimal value). This derivation is tedious and omitted for brevity[7]. Using the maximum possible range, the range efficiency is

$$\eta_R \equiv \frac{R}{R_\mathrm{opt}} = \frac{Rg}{\overline{U}_0^2}\sqrt{\frac{\mathrm{Fr}_{h_0}}{\mathrm{Fr}_{h_0} + 2}}. \qquad (7.32)$$

7.3.3.2 Droplet trajectory after breakup

The breakup length in the trajectory case needs to be generalized to consider the curvature of the trajectory. There are two main options: breakup occurs where the arclength of the jet equals the breakup length $\langle x_\mathrm{b}\rangle$, or that breakup occurs at the breakup time $\langle t_\mathrm{b}\rangle \equiv \langle x_\mathrm{b}\rangle/\overline{U}_0$. Both of these reduce to breakup occurring a distance $\langle x_\mathrm{b}\rangle$ along the nozzle if the trajectory is straight. However, the breakup time specification is mathematically simpler and will be chosen for that reason.

The breakup locations X_b and Y_b can be computed from equations 7.30 and 7.31:

$$X_\mathrm{b} \equiv X_\mathrm{j}(\langle t_\mathrm{b}\rangle) = \cancel{\overline{U}_0} \cos\theta_0 \frac{\langle x_\mathrm{b}\rangle}{\cancel{\overline{U}_0}} = \langle x_\mathrm{b}\rangle \cos\theta_0, \qquad (7.33)$$

$$Y_\mathrm{b} \equiv Y_\mathrm{j}(\langle t_\mathrm{b}\rangle) = \cancel{\overline{U}_0} \sin\theta_0 \frac{\langle x_\mathrm{b}\rangle}{\cancel{\overline{U}_0}} - \frac{1}{2}g\left(\frac{\langle x_\mathrm{b}\rangle}{\overline{U}_0}\right)^2 + h_0,$$

[7]Part of the proof can be found in a Mathematics Stack Exchange post [Pic15].

$$= \langle x_b \rangle \sin \theta_0 - \frac{g}{2} \left(\frac{\langle x_b \rangle}{\overline{U}_0} \right)^2 + h_0. \tag{7.34}$$

And the velocities at breakup are

$$U_b \equiv U_j(\langle t_b \rangle) = \overline{U}_0 \cos \theta_0, \tag{7.35}$$

$$V_b \equiv V_j(\langle t_b \rangle) = \overline{U}_0 \sin \theta_0 - \frac{g \langle x_b \rangle}{\overline{U}_0}. \tag{7.36}$$

The position and velocity of the jet at breakup will be used as the initial conditions for the droplets after breakup. Similar to the vertical height case, the droplet stage of the trajectory has the equation of motion

$$m_d \frac{d\vec{U}_d}{dt} = -m_d \vec{g} - \frac{1}{2} \rho_g C_d A_d \left\| \vec{U}_d - \vec{U}_g \right\| (\vec{U}_d - \vec{U}_g), \tag{7.37}$$

where $\vec{U}_d = U_d \hat{i} + V_d \hat{j}$ is the droplet velocity vector, $\vec{U}_g$ is the air velocity vector, and the remainder of the terms are the same as in the vertical jet case. The air entrainment model $\vec{U}_g \equiv \alpha \vec{U}_d$ can be applied to this case as before.

In the trajectory case it is more convenient to non-dimensionalize by the jet bulk velocity $\overline{U}_0$ instead of the breakup velocity $|\vec{U}_b|$, as was done in the vertical jet case. Consequently, here I define

$$\tau \equiv \frac{t}{\overline{U}_0 / g}, \tag{7.38}$$

$$\vec{U}_d^* \equiv \frac{\vec{U}_d}{\overline{U}_0}, \text{ and} \tag{7.39}$$

$$\vec{X}_d^* \equiv \frac{\vec{X}_d}{\overline{U}_0^2 / g}, \tag{7.40}$$

then non-dimensionalize the equation of motion to obtain

$$\frac{d\vec{U}_d^*}{d\tau} = -\hat{j} - \frac{3}{4} \frac{C_d}{\rho_\ell / \rho_g} \frac{(1 - \alpha)^2}{D_{max} / d_0} \mathrm{Fr}_0 \left\| \vec{U}_d^* \right\| \vec{U}_d^*, \tag{7.41}$$

which, after introducing the reduced drag coefficient (equation 7.11) is simplified to

$$\frac{d\vec{U}_d^*}{d\tau} = -\hat{j} - \frac{1}{2}C_d^*\mathrm{Fr}_0\left\|\vec{U}_d^*\right\|\vec{U}_d^*. \tag{7.42}$$

Now, for simplicity, let's define

$$C_d^\circ \equiv C_d^*\mathrm{Fr}_0 \tag{7.43}$$

so that

$$\frac{d\vec{U}_d^*}{d\tau} = -\hat{j} - \frac{1}{2}C_d^\circ\left\|\vec{U}_d^*\right\|\vec{U}_d^*. \tag{7.44}$$

The equations of motion of a particle experiencing quadratic drag in two dimensions (like equation 7.44) are not known to have analytical solutions[8]. Fortunately, a small firing angle approximation called the "flat fire" approximation (found in this work to be accurate for firing angles less than $35°$) can be applied. This approximation is well known in the ballistics literature [McC12, § 5.3], but has not been applied to the trajectory of water jets before this work. In the flat fire approximation the droplet velocity magnitude $\left\|\vec{U}_d\right\|$ is assumed equal to U_d because if the firing angle θ_0 is small then V_d is small. Consequently, the approximate system of ODEs is

$$\frac{dU_d^*}{d\tau} = -\frac{1}{2}C_d^\circ(U_d^*)^2, \tag{7.45}$$

$$\frac{dV_d^*}{d\tau} = -1 - \frac{1}{2}C_d^\circ U_d^*V_d^*. \tag{7.46}$$

As the drag force in the flat fire approximation is smaller than reality, this approximation will overpredict the range of the jet, with larger errors for larger firing angles. Note

---

[8]There is a subtle math error which has allowed some water jet trajectory researchers to develop what they believe to be exact solutions to the quadratic drag equations. Kawakami [Kaw71, p. 178L] and Lorenzini [Lor04, p. 3] demonstrate this error. Using Lorenzini's notation, the drag law can be written as $\vec{F}_d = -k\vec{U}_d^2$. This notation is ambiguous as the vector product is not defined clearly. Unfortunately this ambiguity leads the author to write the drag laws for each direction incorrectly. The vector drag law would be more correctly written as $\vec{F}_d = -k\left\|\vec{U}_d\right\|\vec{U}_d = -k\sqrt{U_d^2 + V_d^2}(U_d\hat{i} + V_d\hat{j})$. This notation is unambiguous and shows that the x and y directions are coupled. Instead, Lorenzini uses $\vec{U}_d^2 = U_d^2\hat{i} + V_d^2\hat{j}$, which is false. If this error is instead viewed as an approximation, this is still not acceptable as if the x velocity were large, then the y term would also need to be at least that large, but Lorenzini's specification does not allow that.

that because this is an approximation, it can not be used for quantitative verification of CFD software packages, though it may be useful as a qualitative check that the CFD software is close to the flat fire solution when expected to be.

Initial conditions are needed to solve the non-dimensional equations of motion (equations 7.45 and 7.46). The non-dimensional initial conditions are

$$X_b^* \equiv X_d^*(\tau_b) = \frac{g\langle x_b \rangle}{\overline{U}_0^2} \cos\theta_0 = \frac{\langle x_b \rangle / d_0}{\mathrm{Fr}_0} \cos\theta_0, \tag{7.47}$$

$$Y_b^* \equiv Y_d^*(\tau_b) = \frac{\langle x_b \rangle / d_0}{\mathrm{Fr}_0} \sin\theta_0 - \frac{1}{2}\left(\frac{\langle x_b \rangle / d_0}{\mathrm{Fr}_0}\right)^2 + \frac{1}{\mathrm{Fr}_{h_0}}, \tag{7.48}$$

$$U_b^* \equiv U_d^*(\tau_b) = \cos\theta_0, \tag{7.49}$$

$$V_b^* \equiv V_d^*(\tau_b) = \sin\theta_0 - \frac{\langle x_b \rangle / d_0}{\mathrm{Fr}_0}. \tag{7.50}$$

Using these initial conditions, the solutions are

$$U_d^* = \frac{U_b^*}{\frac{1}{2}C_d^\circ U_b^* \tau + 1}, \tag{7.51}$$

$$V_d^* = -\left(\frac{\frac{1}{2}C_d^\circ U_b^* \tau + 1}{C_d^\circ U_b^*}\right) + \frac{1}{\frac{1}{2}C_d^\circ U_b^* \tau + 1}\left(V_b^* + \frac{1}{C_d^\circ U_b^*}\right), \tag{7.52}$$

$$X_d^* = \frac{2\ln\left(\frac{1}{2}C_d^\circ U_b^* \tau + 1\right)}{C_d^\circ} + X_b^*, \tag{7.53}$$

$$Y_d^* = -\left(\frac{\frac{1}{2}C_d^\circ U_b^* \tau + 1}{C_d^\circ U_b^*}\right)^2 + \frac{2}{C_d^\circ U_b^*}\left(V_b^* + \frac{1}{C_d^\circ U_b^*}\right)\ln\left(\frac{1}{2}C_d^\circ U_b^* \tau + 1\right)$$
$$+ \frac{1}{(C_d^\circ U_b^*)^2} + Y_b^*. \tag{7.54}$$

A sketch of the solution procedure will be provided for brevity. Equation 7.45 is a first-order autonomous ODE which can readily be solved by separation of variables and direct integration. Once equation 7.45 is solved, the result can be substituted into equation 7.46. Then equation 7.46 can be solved after applying the change of variables $\xi \equiv \ln\left(\frac{1}{2}C_d^\circ U_b^* \tau + 1\right)$. This new variable ξ can be though of as a measure of how far the

trajectory has progressed, as can be seen by rearranging the solution for X_d^* to state

$$\tfrac{1}{2}C_d^\circ(X_d^* - X_b^*) = \ln\left(\tfrac{1}{2}C_d^\circ U_b^*\tau + 1\right). \tag{7.55}$$

As ξ is proportional to a dimensionless distance from breakup and simplifies the equations of motion, it is of fundamental importance to the water jet trajectory problem. Define the time when the droplets impact the ground as $\tau_{\max}$, corresponding to when the maximum range R is obtained. Then

$$X_d^*(\tau_{\max}) = \frac{Rg}{\overline{U}_0^2} = \eta_R\sqrt{1 + \frac{2}{\mathrm{Fr}_{h_0}}} \tag{7.56}$$

using the definitions of X_d^* (equation 7.40) and η_R (equation 7.32). Now equation 7.54 at $\tau_{\max}$ can be written

$$Y_d^*(\tau_{\max}) = 0 = -\left(\frac{\tfrac{1}{2}C_d^\circ U_b^*\tau_{\max} + 1}{C_d^\circ U_b^*}\right)^2 + \frac{2}{C_d^\circ U_b^*}\left(V_b^* + \frac{1}{C_d^\circ U_b^*}\right)\underbrace{\ln\left(\tfrac{1}{2}C_d^\circ U_b^*\tau_{\max} + 1\right)}_{\text{equation 7.55}}$$

$$+ \frac{1}{(C_d^\circ U_b^*)^2} + Y_b^*. \tag{7.57}$$

After substituting in equation 7.55 at time $\tau_{\max}$ and solving this result for $\tfrac{1}{2}C_d^\circ U_b^*\tau_{\max} + 1$, I obtain

$$\tfrac{1}{2}C_d^\circ U_b^*\tau_{\max} + 1 = [(C_d^\circ U_b^* V_b^* + 1)C_d^\circ(X_d^*(\tau_{\max}) - X_b^*)$$

$$+ 1 + (C_d^\circ U_b^*)^2 Y_b^*]^{1/2}. \tag{7.58}$$

Substituting this result into equation 7.55 at time $\tau_{\max}$ returns an implicit equation for $X_d^*(\tau_{\max})$,

$$C_d^\circ(X_d^*(\tau_{\max}) - X_b^*) = \ln[(C_d^\circ U_b^* V_b^* + 1)C_d^\circ(X_d^*(\tau_{\max}) - X_b^*)$$

$$+ 1 + (C_d^\circ U_b^*)^2 Y_b^*], \tag{7.59}$$

which can be written in terms of η_R using equation 7.56. After writing the above in terms of η_R and substituting in the definitions of X_b^* (equation 7.53), U_b^* (equation 7.51), V_b^* (equation 7.52), and Y_b^* (equation 7.54), I obtain:

$$
\begin{aligned}
C_d^{\circ} &\left(\eta_R \sqrt{1 + \frac{2}{\mathrm{Fr}_{h_0}}} - \frac{\langle x_b \rangle / d_0}{\mathrm{Fr}_0} \cos \theta_0 \right) \\
&= \ln \left[\left(C_d^{\circ} \left(\sin \theta_0 - \frac{\langle x_b \rangle / d_0}{\mathrm{Fr}_0} \right) \cos \theta_0 + 1 \right) C_d^{\circ} \left(\eta_R \sqrt{1 + \frac{2}{\mathrm{Fr}_{h_0}}} - \frac{\langle x_b \rangle / d_0}{\mathrm{Fr}_0} \cos \theta_0 \right) \right. \\
&\quad \left. + 1 + \left(\frac{\langle x_b \rangle / d_0}{\mathrm{Fr}_0} \sin \theta_0 - \frac{1}{2} \left(\frac{\langle x_b \rangle / d_0}{\mathrm{Fr}_0} \right)^2 + \frac{1}{\mathrm{Fr}_{h_0}} \right) \left(C_d^{\circ} \cos \theta_0 \right)^2 \right].
\end{aligned}
\tag{7.60}
$$

Now, for convenience, I define

$$
\widehat{\eta} \equiv C_d^{\circ} \left(\eta_R \sqrt{1 + \frac{2}{\mathrm{Fr}_{h_0}}} - \frac{\langle x_b \rangle / d_0}{\mathrm{Fr}_0} \cos \theta_0 \right)
\tag{7.61}
$$

$$
a \equiv 1 + \left(\frac{\langle x_b \rangle / d_0}{\mathrm{Fr}_0} \sin \theta_0 - \frac{1}{2} \left(\frac{\langle x_b \rangle / d_0}{\mathrm{Fr}_0} \right)^2 + \frac{1}{\mathrm{Fr}_{h_0}} \right) \left(C_d^{\circ} \cos \theta_0 \right)^2,
\tag{7.62}
$$

$$
b \equiv 1 + C_d^{\circ} \left(\sin \theta_0 - \frac{\langle x_b \rangle / d_0}{\mathrm{Fr}_0} \right) \cos \theta_0,
\tag{7.63}
$$

so equation 7.60 can be written as

$$
\widehat{\eta} = \ln(a + b \widehat{\eta}).
\tag{7.64}
$$

In principle equation 7.60 can be solved with an implicit solver. However, I desire an explicit solution to make analysis easier. The range efficiency η_R can be found explicitly in terms of the Lambert W function, which is defined through the equation

$$
z = W(z) e^{W(z)}.
\tag{7.65}
$$

This function is multiple valued as can be seen in figure 7.5. The two real branches are conventionally denoted 0 and -1.
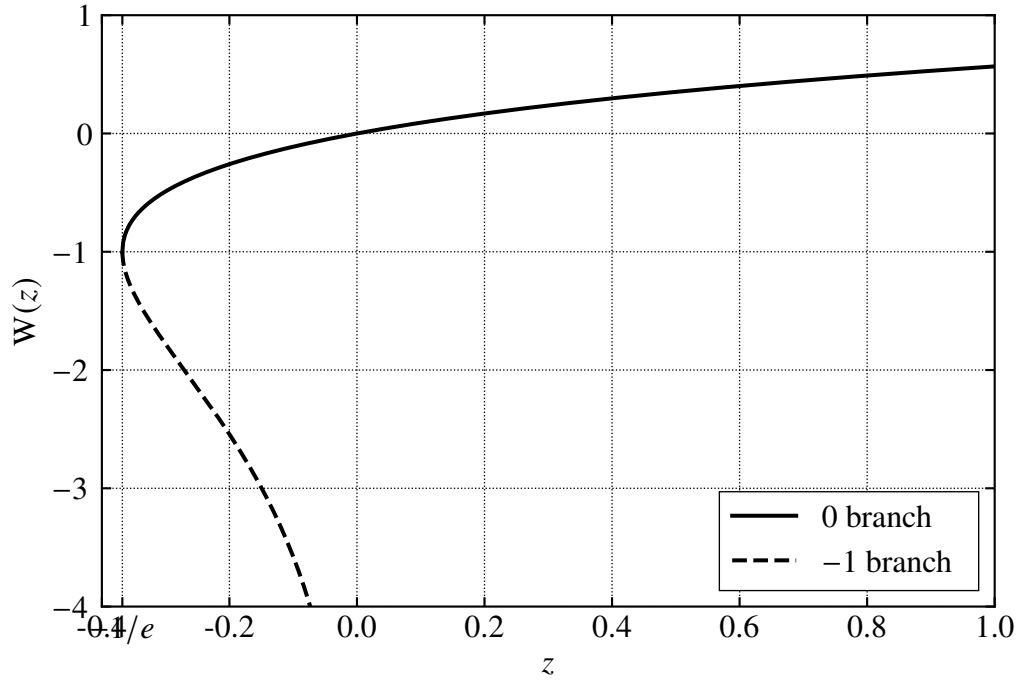
Figure 7.5: The Lambert W function and its two real branches.

One can rearrange equation 7.60 into this form. First, take the exponential of equation 7.64 and factor out b on the right hand side:

$$\exp(\widehat{\eta}) = a + b\widehat{\eta} = b(a/b + \widehat{\eta}). \tag{7.66}$$

Multiply by $\exp(a/b)$:

$$\exp(a/b)\exp(\widehat{\eta}) = b\exp(a/b)(a/b + \widehat{\eta}). \tag{7.67}$$

Take the result to the -1st power:

$$\exp[-(a/b + \widehat{\eta})] = \frac{b^{-1}\exp(-a/b)}{a/b + \widehat{\eta}}, \tag{7.68}$$

which can be rearranged into a form like the definition of the Lambert W function:

$$-(a/b + \widehat{\eta})\exp[-(a/b + \widehat{\eta})] = \frac{-\exp(-a/b)}{b}. \tag{7.69}$$

From equation 7.69 and the definition of the Lambert W function (equation 7.65) one can write

$$W\left[\frac{-\exp(-a/b)}{b}\right] = -\frac{a}{b} - \widehat{\eta} \tag{7.70}$$

or rearranged in terms or $\widehat{\eta}$, the variable which contains η_R:

$$\widehat{\eta} = -\frac{a}{b} - W_{-1}\left[\frac{-\exp(-a/b)}{b}\right] \tag{7.71}$$

The correct branch is the -1 branch of the Lambert W function, which is specified with the subscript in W_{-1}. Using the definition of $\widehat{\eta}$ (equation 7.61), the result can be written explicitly in terms of η_R. I repeat all the functional dependencies (C_d^*, a, and b) and conversion to physical range below for convenience.

$$C_d^* \equiv \frac{3}{2}\frac{C_d}{\rho_\ell/\rho_g}\frac{(1-\alpha)^2}{D_{max}/d_0}, \tag{7.11}$$

$$a \equiv 1 + (C_d^* \cos\theta_0)^2\left[\left(\frac{\langle x_b \rangle}{d_0}\sin\theta_0 + \frac{h_0}{d_0}\right)Fr_0 - \frac{1}{2}\left(\frac{\langle x_b \rangle}{d_0}\right)^2\right], \tag{7.72}$$

$$b \equiv 1 + C_d^* \cos\theta_0\left(Fr_0 \sin\theta_0 - \frac{\langle x_b \rangle}{d_0}\right), \tag{7.73}$$

$$\eta_R = \frac{1}{Fr_0}\sqrt{\frac{Fr_{h_0}}{Fr_{h_0} + 2}}\left(\frac{\langle x_b \rangle}{d_0}\cos\theta_0 - \frac{a}{bC_d^*} - \frac{1}{C_d^*}W_{-1}\left(-\frac{\exp(-a/b)}{b}\right)\right), \tag{7.74}$$

$$R = d_0\left(\frac{\langle x_b \rangle}{d_0}\cos\theta_0 - \frac{a}{bC_d^*} - \frac{1}{C_d^*}W_{-1}\left(-\frac{\exp(-a/b)}{b}\right)\right). \tag{7.75}$$

where (as before) C_d^* is a reduced drag coefficient, ρ_ℓ is the liquid (water) mass density, ρ_g is the gas (air) mass density, $Fr_0 \equiv \overline{U_0^2}/(g d_0)$ is the Froude number, g is gravitational acceleration, D_{max} is the largest droplet diameter of the spray (assumed constant), and $Fr_{h_0} \equiv \overline{U_0^2}/(g h_0)$ is the height Froude number. a and b are model intermediary variables which are used in equation 7.74.

193

As before for h^* (equation 7.22), R^* (R-star) can be defined, offering a simplifying alternative non-dimensionalization:

$$R^* \equiv \frac{C_d^* R}{d_0} \tag{7.76}$$

so that

$$R^* = \frac{C_d^* \langle x_b \rangle}{d_0} \cos \theta_0 - \frac{a}{b} - W_{-1}\left(-\frac{\exp(-a/b)}{b}\right). \tag{7.77}$$

7.3.3.3 Lambert W function implementations and approximations

The Lambert W function has been implemented in many software packages. In Matlab and Octave, the function `lambertw(-1, z)` computes the value of the -1 branch of the Lambert W function at z. In Python, after importing the `lambertw` function from `scipy.special`, the -1 branch of the Lambert W function can be computed with `lambertw(z, -1)`. The GNU Scientific Library has an implementation[9]. A JavaScript implementation based on the GNU Scientific Library is also available[10].

However, for cases where an implementation is not available (e.g., Excel), an approximation developed in this work could be used:

$$W_{-1}(z) \approx -2 - e^2(z - z_0) - \frac{e^6}{6}(z - z_0)^3, \tag{7.78}$$

where $z_0 = -2e^{-2}$.

The typical series approximations to the Lambert W function are only for the 0 branch, which is not applicable to this case. The 3 term approximation I developed (equation 7.78) is within 1% accuracy for the cases of interest. This approximation is based on a Taylor series centered at the single inflection point of the -1 branch. Approximating the function here is convenient because it reduces the number of terms in the series and the coefficients of the series can be expressed as elementary functions at this location.

---

[9]https://www.gnu.org/software/gsl/manual/html_node/Lambert-W-Functions.html
[10]https://github.com/protobi/lambertw
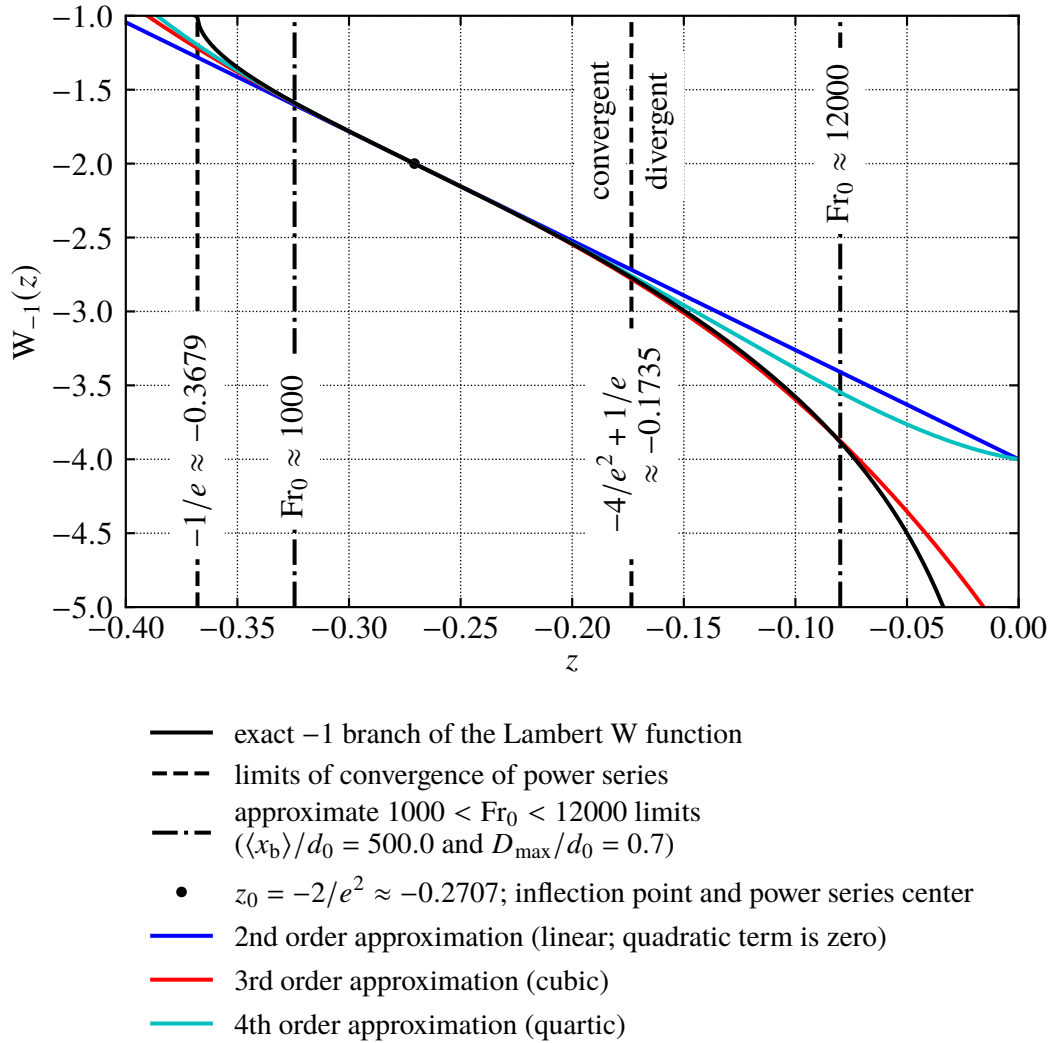
Figure 7.6: The −1 branch of the Lambert W function and Taylor series approximations center at the inflection point.

The legend for the figure reads:

- exact −1 branch of the Lambert W function
- limits of convergence of power series
- approximate $1000 < Fr_0 < 12000$ limits ($\langle x_b \rangle / d_0 = 500.0$ and $D_{max}/d_0 = 0.7$)
- $z_0 = -2/e^2 \approx -0.2707$; inflection point and power series center
- 2nd order approximation (linear; quadratic term is zero)
- 3rd order approximation (cubic)
- 4th order approximation (quartic)

First, the location of the inflection point must be found. Applying implicit differentiation to the definition of the Lambert W function (equation 7.65) returns

$$\frac{\mathrm{d}z}{\mathrm{d}z} = \frac{\mathrm{d}}{\mathrm{d}z} \left(W_{-1}(z) e^{W_{-1}(z)} \right), \tag{7.79}$$

$$1 = e^{W_{-1}(z)} W'(z) (W_{-1}(z) + 1), \tag{7.80}$$

$$W'_{-1}(z) = \frac{1}{e^{W_{-1}(z)} (W_{-1}(z) + 1)}. \tag{7.81}$$

Taking the derivative of equation 7.80, returns

$$0 = e^{W_{-1}(z)} (W_{-1}(z) + 1) W''_{-1}(z) + e^{W_{-1}(z)} (W_{-1}(z) + 2)(W'_{-1}(z))^2. \tag{7.82}$$

The second derivative can be solved for, leading to

$$W''(z) = \frac{-(W_{-1}(z) + 2)}{e^{W_{-1}(z)} (W_{-1}(z) + 1)^2}. \tag{7.83}$$

I'll call the inflection point z_0. Setting $W''_{-1}(z_0)$ to zero and rearranging returns $W_{-1}(z_0) = -2$, so by using the definition of the Lambert W function (equation 7.65) I find that $z_0 = -2e^{-2}$.

Standard computations of the first, third, and fourth derivatives of the Lambert W function at z_0 return that $W'_{-1}(z_0) = -e^2$, $W'''_{-1}(z_0) = -e^6$, and $W^{(4)}_{-1}(z_0) = 2e^8$. Then the Taylor series approximation to $W_{-1}(z)$ centered at z_0 is

$$W_{-1}(z) = -2 - e^2(z - z_0) - \frac{e^6}{6}(z - z_0)^3 + \frac{e^8}{12}(z - z_0)^4 + O\left[(z - z_0)^5 \right]. \tag{7.84}$$

The -1 branch starts at the branch point, $z = -1/e \approx -0.3679$, where the slope is vertical and the Lambert W function switches from the -1 branch to the 0 branch. Unfortunately, the radius of convergence of the full power series is bounded by the location of the nearest singularity, which is at the branch point, $z = -1/e$. So the power series is divergent for $z > -4/e^2 + 1/e \approx -0.1735$, which is within the range of the argument z expected. See figure 7.6 for an illustration of the Lambert W function, the series

approximations to the Lambert W function, the expected span of the argument of the Lambert W function, and the region of convergence of the series approximations. The quartic approximation barely performs any better than the linear approximation for this reason. But, purely by coincidence, the third order approximation follows the exact curve closely up to $z \approx -0.07$, beyond the upper limit of where the series converges. This means that the third order approximation is within 1% up to an approximate Froude number of 12000.

Consequently, the following approximation is recommended:

$$W_{-1}(z) \approx -2 - e^2(z - z_0) - \frac{e^6}{6}(z - z_0)^3, \tag{7.78}$$

where again, $z_0 = -2e^{-2}$.

7.3.3.4 Model validation and analysis

Model validation. The analytical model was compared against experimental data from Theobald [The81], the only source for which breakup length ($\langle x_b \rangle$) measurements were available for all data points, or could be reasonably estimated. Theobald also has the only measurements of water jet trajectories made indoors, eliminating the effect of wind. Some additional lower angle data (without known breakup length) comes from the outdoor experiments of Hickey [Hic73] — the breakup length in this case was estimated from equation 3.28 with the turbulence intensity assumed to be 10%.

Note that there is appreciable uncertainty in most of this data. Even using data without the influence of wind, this uncertainty is appreciable. Experiments not completed in time for this dissertation suggest that pressure variations between shots are the largest contributor to the uncertainties. Higher precision pressure regulation is necessary for proper scientific study of water jet trajectories. With these limitations in mind, the model can still be evaluated, but will require comparison against better data in the future.

Theobald's provided breakup length curves did not cover the highest Weber numbers. When the Weber numbers were too high, the highest value of the breakup length available

was chosen. The breakup length measurements are shown in figure 7.7 as a function of Weber number ($We_{\ell 0} \equiv \rho_\ell \overline{U}_0^2 d_0 / \sigma$). Also included is an approximate laminar trend (for $Re_{\ell 0} \gg We_{\ell 0}$, where $Re_{\ell 0} \equiv \overline{U}_0 d_0 / \nu_\ell$) and an empirical regression for the turbulent surface breakup regime from § 3.4.10. Theobald was British and his nozzles were smaller than typical US nozzles, leading to smaller Weber and Reynolds numbers and a regime change (downstream transition regime) compared against US water jets. From the perspective of the trajectory model, this is acceptable as long as the breakup length is known, but it means that the empirical regression for $\langle x_b \rangle$ (equation 3.28) is not applicable for Theobald's data.

The maximum droplet diameter, $D_{\max}$, was the only variable available for calibration. These large droplets are unstable and will break up on their own. The analytical model does not have a droplet breakup model, and consequently the maximum droplet diameter is an *effective* maximum droplet diameter in the analytical model. This is expected to be smaller than the actual maximum, but on the same order of magnitude. I chose $D_{\max}/d_0 = 0.8$ as this best fit the available data. This is consistent with the available experimental data for the maximum droplet diameter.

See figure 7.8 for the comparisons of range efficiency as calculated by the analytical model and experimentally measured. The model is not perfect, but it reasonably collapses the data for the three different nozzles tested. Note that this model is still reasonably accurate despite the fact that Theobald has many cases with firing angles larger than those acceptable in the flat fire approximation.

Sensitivity analysis. While severe jet breakup is well accepted to be detrimental to the performance of water jet trajectory systems, figure 7.9 makes it clear that the majority of the problems of jet breakup would come from reduced droplet size rather than reduced breakup length. While doubling the breakup length and disabling air entrainment entirely ($\alpha = 0$) lead to only modest changes in jet efficiency, reducing the maximum droplet diameter from $3d_0$ to d_0 massively reduces jet efficiency. Also visible in this plot that the jet efficiency decreases appreciably as the Froude number increases.
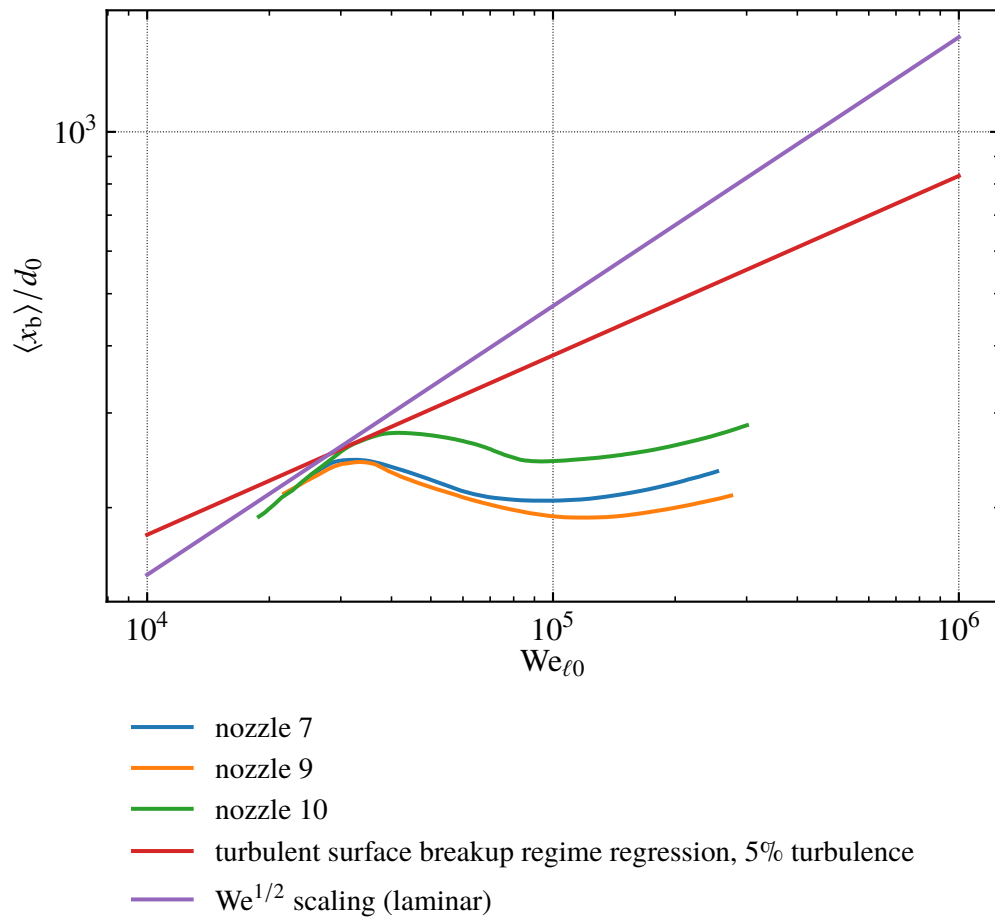
Figure 7.7: Breakup length curves from Theobald [The81] for three different nozzles along with a regression for the turbulent surface breakup regime (equation 3.28) and the expected laminar trends.
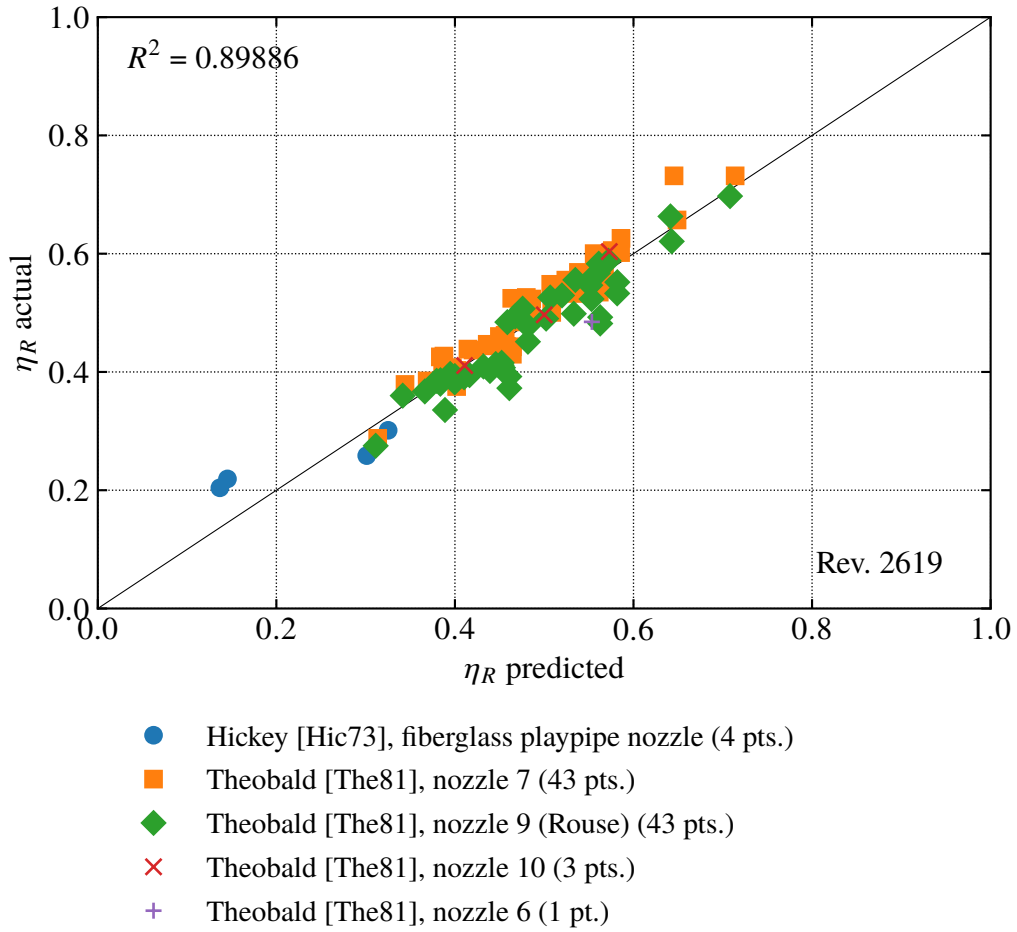
Figure 7.8: Comparison of R predictions (equation 7.74) to experimental measurements.
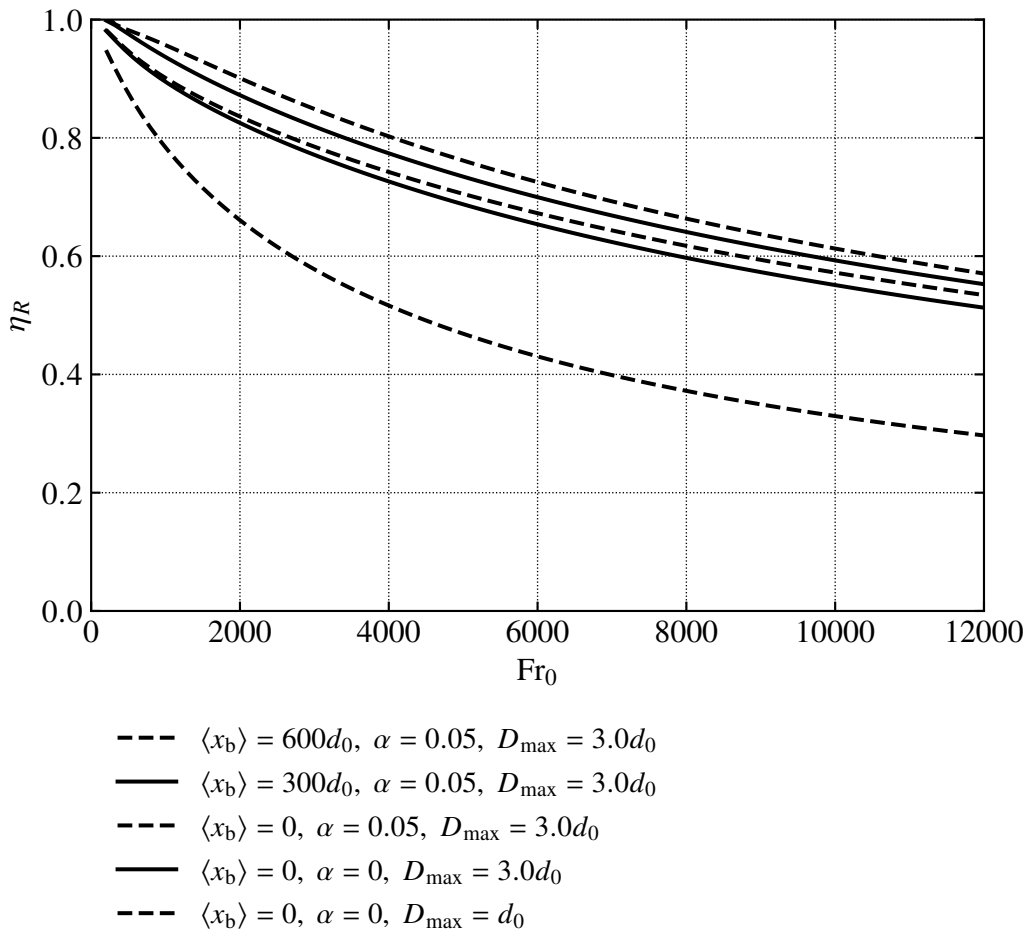
Figure 7.9: General trends of range efficiency η_R as a function of Fr_0 for various examples. The lines are ordered as written in the legend, i.e., the lowest line in the legend is the lowest line in the plot

Why the flat fire approximation is accurate at larger angles than one might expect.
The flat-fire approximation is known to be reasonably accurate up through angles as large as $45°$, as shown by Warburton, Wang, and Burgdörfer [WWB10, p. 99].

A small contribution to this comes from the breakup process. The initial firing angle the flat-fired equations see is not θ_0. Instead the appropriate angle is the angle the jet makes when breakup occurs, θ_b. The tangent of this angle is

$$\tan \theta_b = \tan \theta_0 - \frac{\langle x_b \rangle / d_0}{\mathrm{Fr}_0 \cos \theta_0}. \tag{7.85}$$

Thus, θ_b is always smaller than θ_0. However, it is not much smaller; the deviation is on the order of a single degree in a typical case. Thus, this effect does not entirely explain the success of the flat-fired approximation.

7.4 Conclusions

Typical models of water jet trajectories treat the jet as a collection of non-interacting droplets exiting the nozzle. This implicitly assumes that the breakup length of the jet is zero. However, conventional fire hose nozzle design guidelines emphasize reducing breakup (increasing the breakup length) as a way to improve the range of water jets. This effect can not be reproduced in typical models. Models also frequently neglect air entrainment effects. To address these shortcomings, a new analytical model of the trajectory of a water jet was developed using a small angle approximation called the flat fire approximation. This model considers both the breakup length and air entrainment. The model was validated against existing data from the literature, most of which was conducted indoors (improving the reliability of the experiments) and most of which had measured breakup lengths (in contrast to typical experiments).

Chapter 8

Summary of new results

As a convenience to the reader, important new results in this dissertation are summarized and reproduced in this chapter. How each result fits into the overall water jet trajectory problem can be seen in the trajectory flow chart reproduced here as well (figure 1.1).

8.1 Regime diagram

The schematic regime diagram in chapter 3 is reproduced here (figure 3.3). Again, note that this diagram is merely a schematic, applicable only to the special case of pipe nozzles at low ambient densities. For a particular case, equations in chapter 3 for the boundaries of the regimes are provided which should generalize fairly well to other cases, though additional research on regime boundaries is needed to reduce uncertainties in some cases like the atomization regime boundary.

8.2 Transition to the downstream transition regime from the laminar Rayleigh regime

The boundary between the laminar Rayleigh and downstream transition regimes is modeled with the following equation in this work:

$$\text{Re}_{\ell 0,\text{crit}} = \frac{\text{Re}_{\ell x,\text{trans}} - 3C_{\text{LR}}\text{We}_{\ell 0}}{C_{\text{LR}}\text{We}_{\ell 0}^{1/2}}. \tag{3.14}$$
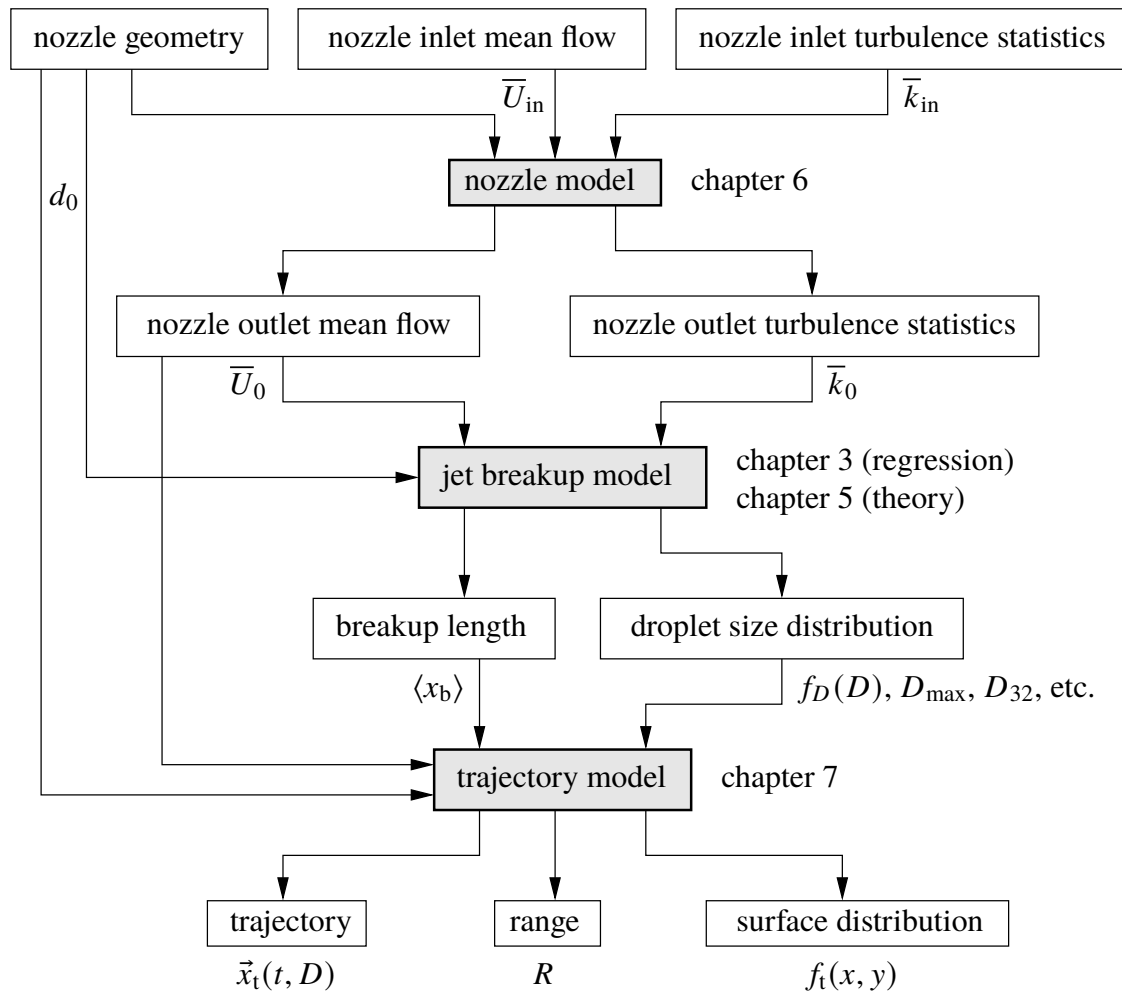
Figure 1.1: Flow chart showing the main variables involved in the trajectory problem as a whole, and the chapters which cover each part. "Variables" which are essentially constant in the water jet trajectory problem such as the fluid properties are neglected here.
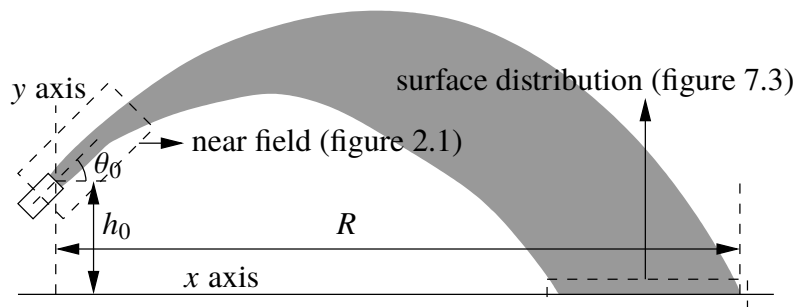
Figure 7.2: Basic trajectory nomenclature with firing angle θ_0, firing height h_0, and maximum range R.
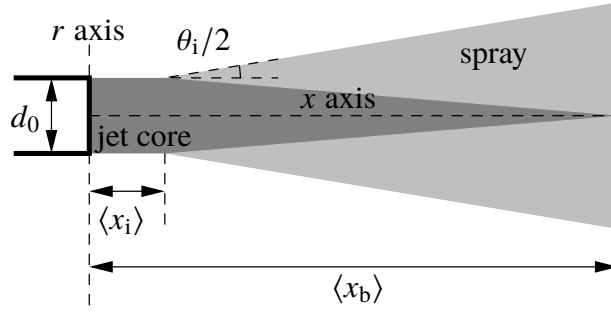
Figure 2.1: Jet breakup variables labeled on a schematic liquid jet. Coordinates are different from figure 7.2. d_0 is the nozzle outlet diameter, $\langle x_i \rangle$ is the average breakup onset location, θ_i is the spray angle, and $\langle x_b \rangle$ is the breakup length.

The values $\mathrm{Re}_{\ell x,\mathrm{trans}} = 1.75 \times 10^5$ and $C_{\mathrm{LR}} = 8.51$ fit the available data reasonably well. This regime boundary differs significantly from the status quo as described in § 3.4.5. Convention states that this regime transition is caused by the onset of ambient density effects. In contrast, equation 3.14 is based on the idea that turbulence transition on the jet causes the regime transition, which does not preclude the possibility that ambient density effects influence the transition, but also does not require ambient density effects.

8.3 Turbulent Rayleigh regime breakup length

As shown in § 3.4.8, the breakup length in the turbulent Rayleigh regime is best modeled with the equation

$$\frac{\langle x_b \rangle}{d_0} = \mathrm{arccsch}\left(C_v \overline{\mathrm{Tu}}_0 \mathrm{We}_{\ell 0}^{1/2} \right) \mathrm{We}_{\ell 0}^{1/2}, \tag{8.1}$$

where $C_v = 0.0615$ (31 points, $R^2 = 0.961$).

Note that this is significantly different from the previous theory applied to this regime, which actually applies only for the laminar Rayleigh regime:

$$\frac{\langle x_b \rangle}{d_0} = C_{\mathrm{LR}} \left(\mathrm{We}_{\ell 0}^{1/2} + 3\frac{\mathrm{We}_{\ell 0}}{\mathrm{Re}_{\ell 0}} \right). \tag{2.12}$$

The former equation is derived using an *initial disturbance velocity* rather than an *initial*

Figure 3.3: Schematic regime diagram at low ambient densities *for illustration purposes only*. Do not use this plot to determine the regime. Regime boundaries are very approximate and apply only for a special case. More general regime boundary equations are given in the text. The nozzle critical Reynolds number will typically be an order of magnitude or more higher than in this plot, which is based on long pipe nozzles (fully developed pipe flow) that have atypically low critical Reynolds numbers — see table 3.2. Constant high density ratio ($\rho_\ell/\rho_g = 1000/1.2$) corresponding approximately to water-air at standard temperature and pressure. The dripping boundary is also for water-air systems. Turbulence intensity is 5%. Turbulent regime boundaries should vary with Reynolds number in a smooth pipe due to variation of turbulence intensity with the Reynolds number — see figure 3.4.

disturbance amplitude, with the initial disturbance velocity being related to the turbulence intensity of the jet.

8.4 Transition to the turbulent surface breakup regime from the turbulent Rayleigh regime

An estimate for the boundary between the the turbulent Rayleigh and turbulent surface breakup regimes can be derived by combining theory for both regimes. The derivation is in § 3.4.9; the final result for the boundary is

$$\mathrm{We}_{\ell 0,\mathrm{crit}} = 8\overline{\mathrm{Tu}_0}^{-2}. \tag{3.27}$$

8.5 Turbulent surface breakup regime quantities of interest

Many quantities of interest relevant to the turbulent surface breakup regime are shown in figure 2.1. In chapter 3, empirical regressions were developed for these quantities of interest. In chapter 5, theoretical models were developed for the same quantities of interest. In this section, I summarize both the regressions and theories. Note that if a prediction of a quantity of interest in this regime is desired, the regressions would typically be preferred as they are more accurate.

The regression for the breakup length is (193 points, $R^2 = 0.958$)

$$\frac{\langle x_\mathrm{b} \rangle}{d_0} = 3.61\overline{\mathrm{Tu}_0}^{-0.275}\mathrm{We}_{\ell 0}^{0.334}. \tag{3.28}$$

The corresponding theory for the breakup length is

$$\frac{\langle x_\mathrm{b} \rangle}{d_0} = C_{x_\mathrm{b}}\overline{\mathrm{Tu}_0}^{-3/5}\left(\mathrm{We}_{\ell 0}\frac{\Lambda_0}{d_0}\right)^{1/5}. \tag{5.16}$$

For the spray angle, the regression is (5 points, $R^2 = 0.983$)

$$\tan\left(\frac{\theta_i}{2}\right) = 4.73 \times 10^{-4} \overline{\text{Tu}}_0^{0.827} \text{We}_{\ell 0}^{0.621}, \tag{3.29}$$

and the theory is

$$\tan\left(\frac{\theta_i}{2}\right) = C_{\theta_i} \overline{\text{Tu}}_0^{3/5} \left(\text{We}_{\ell 0} \frac{\Lambda_0}{d_0}\right)^{-1/5}. \tag{5.17}$$

Note that to my knowledge *all* theories for the spray angle tend to perform poorly, as can be seen in table 2.2.

For the breakup onset location, the regression is (52 points, $R^2 = 0.758$)

$$\frac{\langle x_i \rangle}{d_0} = 13.0 \left(\overline{\text{Tu}}_0^3 \text{We}_{\ell 0}\right)^{-0.915}, \tag{3.30}$$

which is quite similar to the theory:

$$\frac{\langle x_i \rangle}{d_0} = C_{x_i} \overline{\text{Tu}}_0^{-3} \text{We}_{\ell 0}^{-1}. \tag{5.11}$$

For the Sauter mean diameter, the regression is (29 points, $R^2 = 0.712$)

$$\frac{D_{32}}{d_0} = 0.564 \left(\overline{\text{Tu}}_0^2 \text{We}_{\ell 0}\right)^{-0.644}, \tag{3.31}$$

which also compares favorably against the theory:

$$\frac{D_{32}}{d_0} = C_{D_{32}} \overline{\text{Tu}}_0^{-6/5} \text{We}_{\ell 0}^{-3/5} \left(\frac{\Lambda_0}{d_0}\right)^{2/5}. \tag{5.9}$$

For the average droplet radial velocity at formation, the regression is (17 points, $R^2 = -0.0131$)

$$\frac{\langle v_d \rangle}{v_0'} = 0.0582 \left(\overline{\text{Tu}}_0^2 \text{We}_{\ell 0}\right)^{0.0322}, \tag{3.32}$$

which compares poorly against the data. This is likely due to the large error in the measurements; high-accuracy is not possible. The theory for this quantity may be more

credible in this case:

$$\frac{\langle v_\mathrm{d}\rangle}{\overline{v'_0}} = C_{v_\mathrm{d}}\overline{\mathrm{Tu}}_0^{-2/5}\left(\mathrm{We}_{\ell 0}\frac{\Lambda_0}{d_0}\right)^{-1/5}. \tag{5.10}$$

8.6 Transition to the atomization regime from the turbulent surface breakup regime

Based on the intersection between the equations for the breakup length in the turbulent surface breakup and atomization regimes, a boundary between those two regimes can be developed. A simple approximation to this boundary is

$$\mathrm{We}_{\mathrm{g0,crit}} = 3.17\overline{\mathrm{Tu}}_0^{-0.876}. \tag{3.35}$$

8.7 Atomization regime breakup length

Like in the turbulent surface breakup regime, a regression was constructed for the breakup length in the atomization regime (11 points, $R^2 = 0.602$):

$$\frac{\langle x_\mathrm{b}\rangle}{d_0} = 5.31\overline{\mathrm{Tu}}_0^{-0.568}\left(\frac{\rho_\ell}{\rho_\mathrm{g}}\right)^{0.335}, \tag{3.33}$$

This regression has far larger error than the corresponding regression for the turbulent surface breakup regime.

8.8 Turbulent Bernoulli equation for a streamtube

In engineering practice, semi-empirical modifications to the Bernoulli equation for a streamtube are used, where an empirical "loss" term accounts for energy lost from the mean flow. This is often called the "mechanical energy balance" or the "engineering Bernoulli equation". Attempts have been made to relate this equation to the Navier-Stokes equations, but no efforts have been complete successes so far. In this work, I offer a complete derivation showing precisely what "loss" is. Starting from the Reynolds-averaged equations, one can

derive the following for a streamtube:

$$0 = \dot{m} \left[\frac{\alpha \overline{U}^2}{2} + \frac{\overline{P}}{\rho} + \overline{k} \right]_1^2 + \rho \int_{CS} \int_s \left[\varepsilon_m + \varepsilon - \nu \frac{\partial}{\partial x_j} \left(U_i \frac{\partial U_i}{\partial x_j} \right) \right.$$

$$\left. + \frac{1}{2} \frac{\partial \langle u_j u_i u_i \rangle}{\partial x_j} - \nu \frac{\partial^2 k}{\partial x_i \partial x_i} + \frac{\partial U_i \langle u_i u_j \rangle}{\partial x_j} - \frac{1}{\rho} \frac{\partial \langle u_i p \rangle}{\partial x_i} \right] d\Psi. \qquad (6.15)$$

This result is similar to the engineering Bernoulli equation. If some terms in the result above are approximated as zero, then what is commonly called "loss" can be found to be approximately

$$\text{loss} = \sum \zeta \cdot \tfrac{1}{2} \overline{U}^2 = \Delta \overline{k} + \frac{\rho}{\dot{m}} \int_\Psi (\varepsilon_m + \varepsilon) \, d\Psi. \qquad (6.17)$$

This result can be used to develop simple analytical models for turbulence quantities in internal flows using the same empirical loss coefficients used to calculate mean flow quantities.

8.9 Model of the turbulence intensity at the outlet of a nozzle
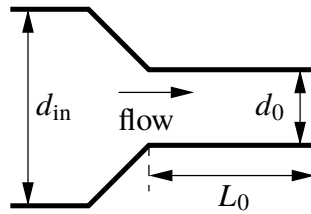
Figure 6.1: Schematic nozzle geometry.

Equation 6.17 is not useful for our purposes as-is. We want a model for the turbulence intensity at the outlet of a nozzle, and equation 6.17 is only a tool that can be used to construct such a model. A schematic nozzle is shown in figure 6.1.

Using rapid distortion theory, one can derive an estimate for the turbulence intensity at the end of a contraction, e.g., a contraction in a nozzle. Considering all 3 components of

the turbulent kinetic energy, one can obtain the following:

$$\overline{Tu_c^2} = \frac{3}{4}\left(\frac{\overline{Tu_{in}}}{c}\right)^2 \left[\frac{\left(\frac{1}{3} - 2b\right)[\ln(4c^3) - 1]}{c^2} + 2\left(b + \frac{1}{3}\right)c\right], \tag{6.24}$$

Then using equation 6.17, one can derive an estimate of the turbulence intensity at the outlet of a nozzle using the previous estimate:

$$\overline{Tu_0^2} = \overline{Tu_{FD}^2} + \left(\overline{Tu_c^2} - \overline{Tu_{FD}^2}\right)\exp\left(-\frac{3\overline{Tu_{FD}^2}}{f}\frac{L_0 - x_{trans}}{d_0}\right), \tag{6.26}$$

Above, x_{trans} is the length needed for turbulence transition. Even if the flow is turbulent entering a contraction (e.g., a nozzle), it can relaminarize and will to transition to turbulence again downstream.

8.10 Vertical jet height

Consider a water jet fired vertically. This jet reaches a maximum height h. We can define a height efficiency,

$$\eta_h \equiv \frac{h}{H} = \frac{2gh}{\overline{U_0^2}}, \tag{7.5}$$

which is bounded between 0 and 1.

Then, to predict the height of water jets, a model for the height efficiency was developed:

$$C_d^* \equiv \frac{3}{2}\frac{C_d}{\rho_\ell/\rho_g}\frac{(1-\alpha)^2}{D_{max}/d_0}, \tag{7.11}$$

$$\eta_h = \frac{2\langle x_b\rangle/d_0}{Fr_0} + \frac{2}{C_d^* Fr_0}\ln\left[\frac{C_d^*}{2}\left(Fr_0 - \frac{2\langle x_b\rangle}{d_0}\right) + 1\right]. \tag{7.20}$$

In physical coordinates, the maximum height is

$$h = \langle x_b \rangle + \frac{d_0}{C_d^*} \ln \left[\frac{C_d^*}{2} \left(Fr_0 - \frac{2\langle x_b \rangle}{d_0} \right) + 1 \right]. \tag{7.21}$$

8.11 Horizontal jet range

Consider a water jet fired approximately horizontally as shown in figure 7.2, with a small firing angle θ_0. We are interested in predicting the maximum range R of the jet. Like in the vertical height case, we can define a range efficiency,

$$\eta_R \equiv \frac{R}{R_{opt}} = \frac{Rg}{\overline{U}_0^2} \sqrt{\frac{Fr_{h_0}}{Fr_{h_0} + 2}}, \tag{7.32}$$

which is bounded between 0 and 1.

Then, as before, we can develop a model for the range efficiency:

$$C_d^* \equiv \frac{3}{2} \frac{C_d}{\rho_\ell / \rho_g} \frac{(1 - \alpha)^2}{D_{max}/d_0}, \tag{7.11}$$

$$a \equiv 1 + (C_d^* \cos \theta_0)^2 \left[\left(\frac{\langle x_b \rangle}{d_0} \sin \theta_0 + \frac{h_0}{d_0} \right) Fr_0 - \frac{1}{2} \left(\frac{\langle x_b \rangle}{d_0} \right)^2 \right], \tag{7.72}$$

$$b \equiv 1 + C_d^* \cos \theta_0 \left(Fr_0 \sin \theta_0 - \frac{\langle x_b \rangle}{d_0} \right), \tag{7.73}$$

$$\eta_R = \frac{1}{Fr_0} \sqrt{\frac{Fr_{h_0}}{Fr_{h_0} + 2}} \left(\frac{\langle x_b \rangle}{d_0} \cos \theta_0 - \frac{a}{bC_d^*} - \frac{1}{C_d^*} W_{-1} \left(-\frac{\exp(-a/b)}{b} \right) \right). \tag{7.74}$$

In physical coordinates, the range is

$$R = d_0 \left(\frac{\langle x_b \rangle}{d_0} \cos \theta_0 - \frac{a}{bC_d^*} - \frac{1}{C_d^*} W_{-1} \left(-\frac{\exp(-a/b)}{b} \right) \right). \tag{7.75}$$

Chapter 9

Future work

This chapter briefly describes some planned future extensions of this work which may be undertaken by myself or others.

9.1   Spectral stability theory

While the present state-of-the-art for stability theory as described in chapter 2 has been overall unsuccessful, I believe the problems can be corrected. The turbulent Rayleigh theory developed in § 3.4.8 shows that *in principle* turbulent jet breakup can be modeled accurately with a relatively simple model, if one is careful in the development of the model. Previous approximations like reducing the problem to the "most unstable mode" are unacceptable; an approach that considers all scales is needed. Presently, I am developing a theory somewhat analogous to classical spectral turbulence theories. The current plan is to start with the relatively simpler temporal planar interface case as has been studied through DNS by McCaslin and Desjardins [MD15]. A 2D version of this problem was studied theoretically by Borodin and Dityakin [BD51a], however, there apparently are serious mathematical errors in that work.

In this case, the turbulence is homogeneous and isotropic in the directions parallel to the free surface, but obviously inhomogeneous in the direction normal to the free surface. As with Weber's theory, the "jet" does not convect downstream; conversion between time and position is made through the bulk velocity, $\overline{U}_0$. By taking the Fourier transform of the Navier-Stokes equations in planes parallel to the free surface, one can develop evolution equations for the Fourier spectra of slices of the flow. The use of the continuous Fourier transform rather than a discrete series eases the conversion into a continuous droplet

diameter spectra.

The question now is how to handle the direction of inhomogeneity. There are multiple possible avenues that I am presently exploring. At first I am planning a linear theory, however, this approach offers the possibility of applying turbulence models in spectral space to handle the non-linear convective term. The non-linear boundary condition can be handled in ways previously done in the literature if deemed necessary. It is likely that the linear theory can be analytical, but the non-linear theory likely would require a computational implementation, hopefully one which is computationally inexpensive.

9.2 New experiments and DNS with varying turbulence properties

There is very little turbulent jet breakup data available with varying turbulence intensity. The main source of data in this dissertation comes from Kusui [Kus69]. Unfortunately, as discussed in footnote 15 on page 110, Kusui's experiments had a moderate length smooth section after the rough section, and it is possible this reduced the turbulence intensity from that of a completely rough pipe nozzle. Additionally, Kusui only measured breakup lengths. New experiments with pipes of varying roughness can address the data quality issue with Kusui's experiments and discover the effect of turbulence intensity on other quantities of interest (like the droplet size) in turbulent jet breakup. The friction factor of each tube used should be reported to easily convert this to an estimate of the turbulence intensity through equation 4.1.

Similarly, experiments examining the downstream evolution of turbulence in jet breakup are lacking. The experiments of Mansour and Chigier [MC94b] were in the turbulent Rayleigh regime, which is not typically of interest; the conclusions may not generalize to other regimes. The experiments of Wolf, Incropera, and Viskanta [WIV95] used square jets which were likely in the turbulent surface breakup or atomization regime. The shape of the jet could change the evolution of the turbulence downstream, so it is unclear how well this study will generalize to cases more typically of interest.

Alternatively, for the non-cavitating case one can use large-scale models of nozzles

to measure turbulence quantities at the nozzle outlet, and then conduct spray experiments on small-scale nozzles [Bog48; Vli75; Leb19; KB83; KF93; HR95]. This idea is quite old, dating back to 1948 in the work of Bogdanovich, but has not been used to its full potential.

Direct numerical simulation offers the ability to independently vary the turbulence intensity and other variables that would be difficult to change experimentally, like the integral scales. To date there have been few studies to do this [SW08; Sal+18; Tor+20], and of the existing studies, only one measured droplet sizes and none measured breakup lengths. More direct numerical simulations are needed studying quantities of interest which can be predicted by theories and used in practice.

9.3   Optimal design of water jet trajectory systems

Conventional design guidelines for water jet trajectory systems emphasize reducing jet breakup. However, reducing jet breakup alone is insufficient for optimal performance. From equations developed in chapter 7, one can derive simple criteria to determine the optimal nozzle diameter given a desired range. Different objective functions may be used, for example, minimizing the flow rate or minimizing the pump power. Theoretically, these criteria can greatly increase the performance of water jet trajectory systems when compared against typical naive selection of the nozzle diameter. At present, the theory for this work has been developed, but the experiments needed to validate the theory are incomplete.

9.4   Water jet trajectory experiments

Some water jet trajectory experiments were conducted in 2019, mostly outdoors. These experiments had repeatability issues due mainly (but not solely) to wind. Some of the data collected is in appendix A, but this neglects the water distributions measured. We found that outdoor experiments are completely unacceptable in terms of repeatability, which is unfortunately as most previous water jet trajectory tests had only one trial per configuration. Consequently, the repeatability error is unknown in most experiments. In October 2019, Sam Matthews and I conducted some indoor experiments at gaspedal in

Austin, TX. Unfortunately, these tests were very time consuming and still had repeatability issues. Later, smaller scale tests narrowed the cause of the repeatability issues to the pressure regulator used. A high precision pressure regularly is necessary to obtain repeatable results, and a new series of indoor experiments is planned when time and space is available.

Appendix A

Tabulated jet breakup regime data

Table A.1 summarizes the results of some water jet trajectory experiments done in 2019. Raw data collected in these experiments is available from GitHub [Tre20b]. Long smooth brass tubes were used as nozzles. The nozzle aspect ratio (L_0/d_0) ranges from 30.3 to 181.8, so all tests have fully developed turbulent flow. The tests were conducted at ambient pressures and temperatures. The ambient temperature ranged from 75 °F to 92 °F. The working fluid was water. All experiments were outdoors aside from the 2019-10-26 series.

The original goal of these experiments was to measure the surface water distribution of water jets under controlled conditions to use for model validation in chapter 7. However, wind caused the repeatability of the range and water distribution measurements to be extremely poor. The experiments conducted, however, are perfectly suitable to classify the jet regime visually, and provide a modest amount of data for the turbulent Rayleigh regime at higher Ohnesorge numbers than any previous experiment. New indoor experiments are planned and will not be complete in time for this dissertation's publication.

The experimental apparatus was a vertical pressure chamber with an inlet for air and water at the top and an outlet for water at the bottom. Because water is heavier than air, the water sat at the bottom of the chamber. The experimental setup is shown in figure A.1. In this figure a small nozzle at low pressure is being used; the jet is not easy to see. The approximate range can be seen from the puddle on the ground. If a larger jet and higher pressure were used then the range would easily exceed the distance the camera can cover in this shot.

The essentials of the experimental procedure are relatively simple: Close the water

Figure A.1: Outdoor test setup without troughs.

outlet valve. Disconnect the air compressor so that the water chamber is not under pressure. Adjust the angle of the nozzle on the experimental apparatus until the desired firing angle is obtained. Open the water inlet valve at the top. Pour in a known amount of water. Close the water inlet. Reconnect the air compressor. Set the pressure regulator to desired pressure. Turn on the video camera. Open the water outlet valve to fire the jet. When the water runs out, turn off the camera and disconnect the air compressor.

The video camera is used to determine the duration of the shot, so that the bulk velocity may be determined. The video is clear enough to determine the regime, e.g., figure A.3 shows a still frame where the jet is clearly in the turbulent surface breakup regime. (The still frame is less clear than the video.)

Earlier tests used the puddle formed on the ground to measure range with a tape measure. This was found to an unreliable indicator of where the water landed originally due to droplet rebounds off the ground. Later tests used troughs to measure range to avoid the droplet rebound problem. The volume of water in each trough was measured to construct a distribution function.

date	trial	$\mathrm{We}_{\ell 0}$	$\mathrm{Re}_{\ell 0}$	regime
2019-06-04	1	228	6240	TR
2019-06-04	2	1020	13200	TR
2019-06-04	3	1860	17800	TR
2019-06-04	4	2130	19100	TR
2019-06-04	5	4620	28100	TR/TSB
2019-06-06	1	8970	100000	TSB
2019-06-06	2	11400	113000	TSB
2019-06-12	1	4160	66100	TR/TSB
2019-06-12	2	8640	95300	TSB
2019-06-12	3	1210	26500	TR
2019-06-12	4	2510	38100	TR
2019-06-12	5	4280	49700	TR/TSB
2019-06-13	1	14700	95100	TSB
2019-08-05	1	19700	10400	TSB
2019-08-06	1	8550	77300	TSB
2019-10-26	1	24600	137000	TSB
2019-10-26	2	27300	144000	TSB
2019-10-26	3	6930	53900	TSB

Table A.1: Trajectory experiments conducted during this dissertation, used only for chapter 3. TR = turbulent Rayleigh and TSB = turbulent surface breakup. Transitional data marked as two different regimes.

Figure A.2: Troughs for water distribution measurements.

Figure A.3: Still frame from video of 2019-08-06 experiment.

Appendix B

Relevant variables in turbulent jet breakup and dimensional analysis

The purpose of this appendix is to explain which variables are relevant to the problem of turbulent jet breakup and perform a dimension analysis of the problem. While many readers would consider what's stated in this appendix to be obvious, it is clear while reading the literature that many researchers do not understand these basic issues and make avoidable mistakes because of that.

B.1 Nozzle frame vs. jet frame
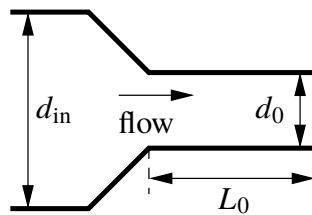
Figure 6.1: Schematic nozzle geometry.

It is necessary to select the reference frame for the jet breakup problem, as this determines which variables are relevant. Two different references frames have been used in the literature, and sometimes the two have been confused with each other[1]. One is the

---

[1]For example, the relatively recent review of liquid jet breakup by Birouk and Lekic [BL09] discusses nozzle geometric factors extensively. On p. 506, Birouk and Lekic mention both nozzle internal flow and the nozzle outlet turbulence as if the two are independent factors, but as is discussed here, one is redundant given the other. However, the nozzle frame is not fully characterized, as is typical. Nozzle inlet factors are not mentioned beyond "supply line pressure vibrations". Nozzle inlet turbulence conditions are not mentioned at all.

nozzle frame, which views the problem as a function of the nozzle geometry and nozzle *inlet* conditions. For example, in figure 6.1, the left side of the figure is the inlet to the nozzle. By continuity, it is equivalent to use either the nozzle outlet (jet) bulk velocity $\overline{U}_0$ or the nozzle inlet bulk velocity $\overline{U}_{in}$ to characterize the bulk velocity in the nozzle, though the jet bulk velocity is almost universally used.

The other reference frame is the *jet* frame, which uses quantities at the nozzle *outlet* plane (bulk velocity, turbulence statistics, etc.) as the boundary conditions. Again, in figure 6.1, the right side of the figure is the outlet of the nozzle, which is the inlet to the jet domain. The shape of the nozzle does not need to be known here. It is redundant to specify the nozzle inlet conditions and nozzle geometry (and roughness) along with the nozzle outlet conditions. The turbulence statistics are determined by the nozzle inlet conditions and nozzle geometry.

Consequently, "nozzle geometry effects" are the effects the nozzle geometry has on the nozzle outlet mean velocity profile and nozzle outlet turbulence statistics, and the subsequent effect these have on the jet breakup. The jet perspective is preferred, as it fully describes the flow state, allows generalization to nozzle geometries not tested, is simpler (the nozzle perspective has more dependent variables, e.g., the nozzle geometry), and allows the development of separate models for internal flow and jet breakup which can be validated separately, allowing problems to be identified more easily (see § 4.5).

For the nozzle frame, it is rare that all important variables are known, in particular, the upstream conditions are rarely characterized or discussed. Bogdanovich [Bog48, p. 43] stated that in the cases he tested, the nozzle inlet was not found to be a factor, however, this is merely an assertion with no supporting data. In contrast, Oehler [Oeh58, pp. 8-9] states that "All disturbances of the flow which reach the nozzle entrance are passed on to the jet — although in a different form — and affect its quality and range." Reitz and Bracco [RB82, p. 1714L] discussed how nozzle upstream conditions could possibly affect jet stability. Of the studies I am aware of which measured spray nozzle turbulence intensity at the nozzle outlet [Bog48; KB83; KF93; HR95], only two [KF93; HR95] measured turbulence intensity at the nozzle inlet. This leads to, for example, not all nozzles with an

222

aspect ratio $L_0/d_0 = 4$ performing identically. The nozzle inlet conditions affect the outlet conditions. Consequently, the jet perspective is superior for developing jet breakup models. One model determines the effects of the nozzle on the flow through it, and the jet breakup model determines the effect of the nozzle outlet flow on the breakup.

Fully developed flows are an exception to the general rule that the nozzle inlet turbulence is important. If the nozzle orifice is long enough, a universal turbulent state will be reached that is independent of the nozzle inlet turbulence. The development length may be affected by the nozzle inlet turbulence, however.

The use of a nozzle frame combined with the view that nozzle inlet turbulence is unimportant is sometimes used to justify omitting the turbulence intensity as a variable. The problems associated with omitting variables will be discussed in § 4.3.

B.2 Dimensional analysis fundamentals

Dimensional analysis [Lan51] can help us understand the functional dependency of the jet breakup process. There have been many dimensional analyses of turbulent jet breakup, several of which come to divergent conclusions. See table B.1 for a summary of selected studies in chronological order[2]. Some of the divergence is caused by a difference in variables considered, others by ad-hoc assumptions independent of dimensional analysis. One author considers dimensional analysis to have failed to provide useful information [Ham94, pp. 271–272], but it is worth analyzing why dimensional analysis has failed so far.

The easiest failure mode for dimensional analysis is the neglect of an important variable. Few dimensional analyses have considered the turbulence intensity directly. There

---

[2]Table B.1 is not comprehensive, as the more I looked, the more dimensional analyses I found. The table also was limited to what can fit on one page for brevity; I am aware of additional studies, but have neglected those which are lesser known and essentially duplicate better known work. Studies before 1954 were neglected in the table because the jet breakup problem was generally poorly understood then. 31 studies were neglected from the table for brevity. A list of these studies is available from the author to the interested researcher. These studies tended to neglect the effect of nozzle geometry; none included a turbulent RMS velocity. I focused on identifying studies which considered a turbulent RMS velocity specifically. Given the focus on identifying studies with the turbulent RMS velocity, and the removal of studies which neglected it, studies with the turbulent RMS velocity are overrepresented in table B.1.

has been a trend in the past several decades to include parameters for nozzle geometry effects, which influence turbulence intensity, though they also change the velocity profile, making identifying the relative contributions of each factor impossible ("confounding", which will be discussed in chapter 4). As discussed previously, jet inlet based analyses are preferred to nozzle based analyses (§ B.1). Dimensional analyses which explicitly considered the turbulence intensity (or something exactly equivalent) are denoted with • in the $\overline{v'_0}$ column of table B.1, while studies which used an inexact proxy like nozzle geometry are denoted with ∘.

The neglect of some variables is acceptable and uncontroversial. For example, ambient pressure is often neglected. The jet is a free jet at low Mach number with a practically homogeneous pressure field, so a single value is acceptable in the typical case. And if the flow is not cavitating, so only the ambient density is a factor in the problem, there is no reason to include the ambient pressure as a variable.

There are several observations to highlight from table B.1. The first is that the majority of these dimensional analyses are essentially the same, considering only the independent variables d_0, $\overline{U}_0$, ν_g, ν_ℓ, ρ_g, ρ_ℓ, and σ, possibly neglecting the gas viscosity ν_g. If dimensional analysis is unsuccessful, then the most obvious path forward would be to expand the independent variables considered. The second is that turbulence quantities like $\overline{v'_0}$ and Λ_0 do not appear more likely to be included more recently than in the past. The importance of these quantities still needs to be communicated.

B.3 Ad-hoc arguments in dimensional analysis

Not visible in the table but worth noting are the various ad-hoc arguments about which variables are relevant and the functional forms of the equations. These arguments often end up being in error. The assumption that the quantities of interest are a function of mainly the Reynolds number is common [Sch37, p. 521R; Hal+52, p. 1187; Sha72], and probably the most egregious of these assumptions. The logic appears to be that turbulence causes breakup and is a function of the Reynolds number (or equivalently,

viscosity), therefore turbulent jet breakup quantities of interest are necessarily functions of the Reynolds number. A related argument is that turbulent dissipation is important, therefore viscosity is important [SM00b], however, this misses the fact that turbulent dissipation is often independent of viscosity at high Reynolds numbers.

In the turbulent surface breakup regime it can be shown that the breakup length[3] is insensitive to the Reynolds number if one is careful to account for the confounding between the Weber number, the Reynolds numbers, and the turbulence intensity[4]. See § 4.4.2 for the justification based on regression analysis of experimental data. The theory developed in this dissertation, CDRSV theory (chapter 5), can explain this observation by noting that these jets are influenced by the minimum scale, and the minimum scale in the turbulent surface breakup regime (absent atmospheric gas effects) is the Hinze scale, which is not a function of viscosity.

There are other examples. Oguey, Mamin, and Baatard [OMB59; Hal+52] neglect surface tension because "the jet surface [is] very irregular" [Hal+52, p. 1181]. But that is precisely when surface tension becomes more important because a more irregular surface has larger surface area and consequently more energy is stored in the surface. As yet another example, Baron [Bar49, p. A-8] assumes that the breakup length $\langle x_\mathrm{b} \rangle / d_0$ is proportional to the Weber number $\mathrm{We}_{\ell 0}^{1/2}$ based on a questionable argument suggesting that the breakup length $\langle x_\mathrm{b} \rangle / d_0$ is proportional to "the size of the eddies" that cause the initial deformation of the jet. Baron argues that these eddies scale with the jet bulk velocity $\overline{U}_0$, which could imply $\langle x_\mathrm{b} \rangle / d_0 \propto \mathrm{We}_{\ell 0}^{1/2}$. However, as Baron also considers the Reynolds number $\mathrm{Re}_{\ell 0}$ a relevant factor, it's not clear why $\langle x_\mathrm{b} \rangle / d_0 \propto \mathrm{Re}_{\ell 0}$ or something more complex involving both the Reynolds and Weber numbers is any less plausible. Of course, that assumes that Baron's argument about the size of eddies makes sense, and it does not as a spectrum of eddies contributes, and there's no reason to believe that reducing a characteristic eddy size is likely to reduce breakup length (if anything, as argued later in this dissertation, eddies

---

[3]And presumably other quantities of interest.
[4]This, of course, assumes that the Reynolds number is high enough to establish turbulent flow. If that is satisfied then the sensitivity to the Reynolds number appears to be small if extant.

smaller than a certain size do not contribute to breakup). As a final example, Bataev [Bat78, p. 4] suggests that the breakup onset location $\langle x_i \rangle$ can be found from a critical ratio of a Reynolds number using $\langle x_i \rangle$ as a length scale and the Weber number $\mathrm{We}_{\ell 0}$. This is justified based on a vague argument about how the air boundary layer scales with a distance Reynolds number and the strength of the surface scales with a Weber number. Ultimately the result is incorrect when compared against experimental data.

These arguments are often called "dimensional analysis" in the literature, but they are entirely separate. Including all known variables and letting the data answer the questions of which variables are relevant would often be more productive. If there is too little data to answer whether a particular variable is relevant, allow theory based on first principles (even if approximate) rather than ad hoc arguments to justify the omission of a variable or a functional form. This is the approach I will be taking.

B.4   Similarity criteria for turbulent flows

Many researchers seem to believe (even if they do not state so explicitly) that merely matching the Reynolds number is sufficient to maintain similarity of the turbulence. More careful reflection indicates that this is not true, as even in single phase flows, the integral scale and Reynolds stress tensor are not necessarily controlled solely by the Reynolds number or geometric factors. This topic is discussed surprisingly little in the literature outside of atmospheric physics [MLS67, chapter IV; Cer71; Sny72]. However, it has been recognized that it is necessary to match the turbulence intensity for drag measurements at Reynolds numbers where the "drag crisis" can occur [Gol65, vol. 2, p. 501]. However, matching the turbulence intensity alone is not sufficient as there are other factors like the surface roughness [Bir60, p. 41].

Analysis of the governing equations can lead one astray here. Dimensional analyses are often performed naively on the steady (laminar) equations, not realizing that this might miss important criteria. To my knowledge this has not been discussed much in the literature. Typically the quantities of interest are actually averages, so one needs to analyze governing

equations for the averages. Analysis of these governing equations is valid, but it also requires a *closed model* in practice. Without a turbulence model, the turbulence closure problem leads to an infinite sequence of closure equations, which in turn presumably leads to an infinite number of similarity criteria to model turbulence [Obe+15]. So the choice of the variables which characterize the turbulence could be seen as depending on which turbulence model is selected, and this has to be viewed as an approximation of the true dynamics.

In this dissertation, the integral scale and turbulent RMS velocity have been selected as the important criteria defining the turbulence aside from the Reynolds number[5]. That this choice is sufficient for similarity is not established, but it is believed to be a reasonable approximation. The regression analysis in § 3.4.10 suggests that if the integral scale and velocity profile are roughly constant, the turbulence intensity alone is sufficient to produce accurate regressions. As an approximation, a single turbulent RMS velocity has been chosen, which could be interpreted as an isotropic turbulence assumption or a statement about which direction (i.e., the radial direction) matters in turbulent jet breakup. Plane average values of the integral scale and turbulent RMS velocity are used for simplicity as well, and may be physically justified by noting that initial inhomogeneities often are eliminated downstream through turbulent diffusion.

B.5   Dimensional analysis results

For the dimensional analysis, I consider all independent variables in table B.1 and only the characteristic droplet diameter D_{ij} (for any values of i and j) as the dependent variable. The other dependent variables can be substituted without loss of generality. The variables are D_{ij} (dependent variable, L), nozzle outlet diameter d_0 (L), radial (liquid jet) turbulent RMS velocity $\overline{v_0'}$ (L/T), jet bulk velocity $\overline{U}_0$ (L/T), nozzle boundary layer thickness δ_0 (L)[6], the integral length scale Λ_0 (L), liquid kinematic viscosity ν_ℓ (L^2/T), gas kinematic viscosity ν_g (L^2/T), liquid mass density ρ_ℓ (M/L^3), gas mass density ρ_g (M/L^3), and surface

---

[5]The Reynolds stress $\langle uv \rangle$ can be a minor factor in CDRSV theory in the spray angle θ_i or the breakup onset location $\langle x_i \rangle$, but does not appear elsewhere in the present theory, so it is being neglected.

[6]Alternatively, the liquid surface velocity gradient $\partial U/\partial r|_{0s}$ (1/T) can be used.

tension σ (M/T^2). L, M, and T refer to the fundamental dimensions of length, mass, and time respectively. There are 11 variables and 3 dimensions. The rank of the dimensional matrix is $k = 3$, so there are $n = N - k = 11 - 3 = 8$ dimensionless groups. The following are chosen in this work:

$$\frac{D_{ij}}{d_0} \qquad \text{(relative characteristic droplet size)}, \qquad \text{(B.1)}$$

$$\frac{\langle x_\text{i} \rangle}{d_0} \qquad \text{(dimensionless breakup onset location)}, \qquad \text{(B.2)}$$

$$\frac{\langle x_\text{b} \rangle}{d_0} \qquad \text{(dimensionless breakup length)}, \qquad \text{(B.3)}$$

$$\theta_\text{i} \qquad \text{(spray angle)}, \qquad \text{(B.4)}$$

$$\text{We}_{\ell 0} \equiv \frac{\rho_\ell d_0 \overline{U}_0^2}{\sigma} \qquad \text{(liquid Weber number)}, \qquad \text{(B.5)}$$

$$\overline{\text{Tu}_0} \equiv \frac{\overline{v'_0}}{\overline{U}_0} \qquad \text{(liquid turbulence intensity)}, \qquad \text{(B.6)}$$

$$\frac{\rho_\ell}{\rho_\text{g}} \qquad \text{(density ratio)}, \qquad \text{(B.7)}$$

$$\text{Re}_{\ell 0} \equiv \frac{\overline{U}_0 d_0}{\nu_\ell} \qquad \text{(liquid Reynolds number)}, \qquad \text{(B.8)}$$

$$\frac{\nu_\ell}{\nu_\text{g}} \qquad \text{((kinematic) viscosity ratio)}, \qquad \text{(B.9)}$$

$$\frac{\Lambda_0}{d_0} \qquad \text{(dimensionless integral length scale), and} \qquad \text{(B.10)}$$

$$\frac{\delta_0}{d_0} \qquad \text{(dimensionless boundary layer thickness)}. \qquad \text{(B.11)}$$

Nozzle geometry effects. Many models take into account a nozzle geometric feature, e.g., usually the nozzle aspect ratio L_0/d_0. These approaches tend to neglect the nozzle inlet and other geometry parameters, unfortunately. See § B.1 for details about why it's better to use nozzle outlet quantities rather than nozzle geometry.

Dundurs and Hamilton [DH54, p. 59] correctly note that $\overline{v'_0}$, Λ_0, and δ_0 are affected by the nozzle geometry. So I could mark each of these parameters with open circles ($\circ$) instead of the typical filled circles ($\bullet$). However, this would tend to give the impression that

those dimensional analyses were more complete than they actually were. For that reason, I've marked only the $\overline{v_0'}$ column with open circles, simply to indicate that these models have some sort of nozzle geometry effect factored in that does not get specific about which variables the nozzle geometry changes.

This dissertation discusses $\overline{\text{Tu}}_0$ effects in detail, however, Λ_0/d_0 and δ_0/d_0 effects are largely neglected.

Factors neglected in the table include unsteadiness, secondary flows/swirl, gravity, cavitation, vibration, anisotropy, Reynolds stress, asymmetry, evaporation/vaporization, nozzle imperfections, compressibility (an infinite speed of sound is assumed), mean radial flow, continuum effects (e.g., the mean free path and Knudsen number), buoyancy, and the co-flow/entrainment velocity.

	dependent variables				independent variables									
	D_{ij}	$\langle x_i \rangle$	$\langle x_b \rangle$	θ_i	d_0	$\overline{v'_0}$	$\overline{U}_0$	δ_0	Λ_0	ν_g	ν_ℓ	ρ_g	ρ_ℓ	σ
Dundurs and Hamilton [DH54]	•				•	•	•	•	•	•	•	•	•	•
Lyshevskiy [Lys60; Lys62b; Lys63; Lys71]	•		•	•	•		•				•	•	•	•
Ranz [Ran56; Ran58]	•			•	•		•				•	•	•	•
Dodu [Dod60]				•	•	○	•						•	•
Inoue [Ino63]	•				•	•	•				•		•	•
Chen and Davis [Che62; CD64]	•		•		•		•				•		•	•
Smirnov [Smi65]			•		•	○	•				•	•	•	•
Isaev [Isa66; Isa67; Isa73]	•				•	•	•				•		•	•
Lapple, Henry, and Blake [LHB67]	•				•	○	•			•		•	•	•
Bataev [Bat78]		•		•	•		•			•	•	•	•	•
Phinney [PH70; Phi73; Phi75]			•		•	•	•				•		•	•
Yanaida [Yan74]			•		•	○	•				•		•	•
Walzel [Wal80; Wal82]	•				•	○	•			•	•	•	•	•
Petrillo [Pet88]			•		•	•	•			•			•	•
Ruiz and Chigier [RC87; RC90; RC91]				•	•	○	•			•	•	•	•	•
Sauerwein [Sau20]			•		•	•	•			•	•	•	•	•
Cavanaugh and Peterson [CP94]			•		•	•	•			•		•	•	•
Lin and Reitz [LR98]			•		•	○	•			•	•	•	•	•
Rantanen et al. [RVC99]	•			•	•	○	•			•	•	•	•	•
Sirignano and Mehring [SM00a]	•				•		•			•	•	•	•	•
Lin [Lin03]	•		•	•	•		•			•	•	•	•	•
Gorokhovski and Herrmann [GH08]	•				•	•	•		•	•		•	•	•
Sander and Weigand [SW08]				•	•	•	•	•	•	•	•	•	•	•
Petit et al. [Pet+15; Man+12]	•				•		•			•	•	•	•	•

Table B.1: Variables considered in previous dimensional analyses of turbulent jet breakup. See text for details.

•, explicit; ○, implicit, e.g., $\overline{v'_0}$ might be taken into account implicitly with a nozzle geometry parameter

B.6 Characterizing velocity profile effects[7]

If a liquid jet exits a nozzle with a non-uniform velocity profile, at low ambient densities the velocity profile would tend to flatten out. This process is called velocity profile relaxation, and its affect on jet breakup has been the subject of much speculation. Velocity profile relaxation has been proposed as a cause of jet breakup since the early work of Schweitzer [Sch37] in 1937, and independently a few years later by Littaye [Lit42] in 1942. One generally accepted explanation is that non-uniform velocity profiles have excess energy, which can accelerate the breakup process [EH58; Rup62; MM74; BL09; LM17], though the details of the physical mechanism remain vague. This effect could alternatively be called a boundary layer or shear instability [HT85; WMF95].

McCarthy and Molloy [MM74, p. 7] proposed the velocity profile kinetic energy coefficient as a measure of the tendency for velocity profile relaxation to cause breakup:

$$\alpha \equiv \frac{\int_{A_0} U_0^3 \, dA}{\overline{U}_0^3 A_0}. \tag{B.12}$$

Above, U_0 is the (local) mean axial velocity at the nozzle outlet and A_0 is the nozzle outlet area ($A_0 = \pi d_0^2/4$).

The larger the kinetic energy coefficient is, the stronger breakup due to velocity profile relaxation is according to McCarthy and Molloy. The kinetic energy coefficient α is smallest ($\alpha = 1$) for a uniform/flat velocity profile, and largest for a parabolic profile ($\alpha = 2$). For a fully developed turbulent pipe velocity profile $\alpha \approx 1.06$ [Ben80, p. 219][8], which, if the criteria is true, suggests that fully developed turbulent pipe flows are not likely to see major velocity profile relaxation effects. (Note that this does mean that turbulent flows in general won't see velocity profile relaxation effects.) McCarthy and Molloy justified

---

[7]This section is adapted from the introduction of of Trettel [Tre19b]. In that paper I proposed a theory for how velocity profile relaxation affects turbulent jet breakup. I am no longer confident in the specific model I developed in that paper and have not included it in this dissertation for that reason. However, the problems identified in the introduction remain unchanged.

[8]McCarthy and Molloy [MM74, p. 7L] incorrectly suggest that α is in the range of 1.1 to 1.2, but direct computation indicates lower. This suggests that α barely changes at all with nozzle length in the turbulent case.

this with figure B.1, which shows jets which are identical aside from changing the nozzle length, which changes the velocity profile from relatively flat to more parabolic as the flow develops. The jet is initially laminar in each case shown, though it likely would be turbulent for the fully developed case as the Reynolds number is 4750.

Instead of the kinetic energy coefficient, the effect of velocity profile relaxation could also be characterized with the dimensionless boundary layer thickness, equation B.11, as was done previously. However, the dimensionless boundary layer thickness is less frequently used in the literature.

To avoid velocity profile relaxation and consequently enhance the stability of turbulent liquid jets, special nozzles have been designed to produce flat velocity profiles [The81; HT85], and these efforts appear to produce more stable jets. Additionally, some of the longest breakup lengths I am aware of, $\langle x_b \rangle = O(1000)$, were obtained with short nozzles (nozzle orifice length $L_0 = d_0$) [ASH85, fig. 4] which produce relatively flat velocity profiles [Qui06, fig. 4, p. 283]. However, there are flaws in this narrative.

McCarthy and Molloy's photographs are qualitative at best. Objective measurements of the breakup length are necessary to validate the theory. The apparent worst-case-scenario, a parabolic velocity profile, appears to be more stable than previously thought. Linear stability analysis for laminar jets shows that parabolic velocity profiles are actually *more stable than uniform* [LG86; DY88; IM00]. Indeed, the experimental data shows that for laminar jets, as the orifice (development) length increases (again, changing the velocity profile from roughly flat to parabolic), the breakup length increases by 30%[9], qualitatively consistent with linear stability theory. See figure B.2. For this plot I compiled data from Arai, Shimizu, and Hiroyasu [ASH85] for breakup length as a function of nozzle length, and interpolated the data to get lines of constant Weber number. Each line is also a constant, but

---

[9]The difference appears to be statistically significant. Arai, Shimizu, and Hiroyasu [ASH85] provide no uncertainty estimates, but assuming the statistical uncertainty is negligible for electrical conductivity measurements (as they are essentially a large number of pulses), the main source of uncertainty is the precision of the length measurement. If the experimental setup of Arai, Shimizu, and Hiroyasu was similar to that of Phinney and Humphries [PH70, p. 9], the measurement was within $2\,\text{mm}$. Then for $L_0/d_0 = 1$, $\langle x_b \rangle / d_0 = 72.4 \pm 6.7$, and for $L_0/d_0 = 50$, $\langle x_b \rangle / d_0 = 93.8 \pm 6.7$.
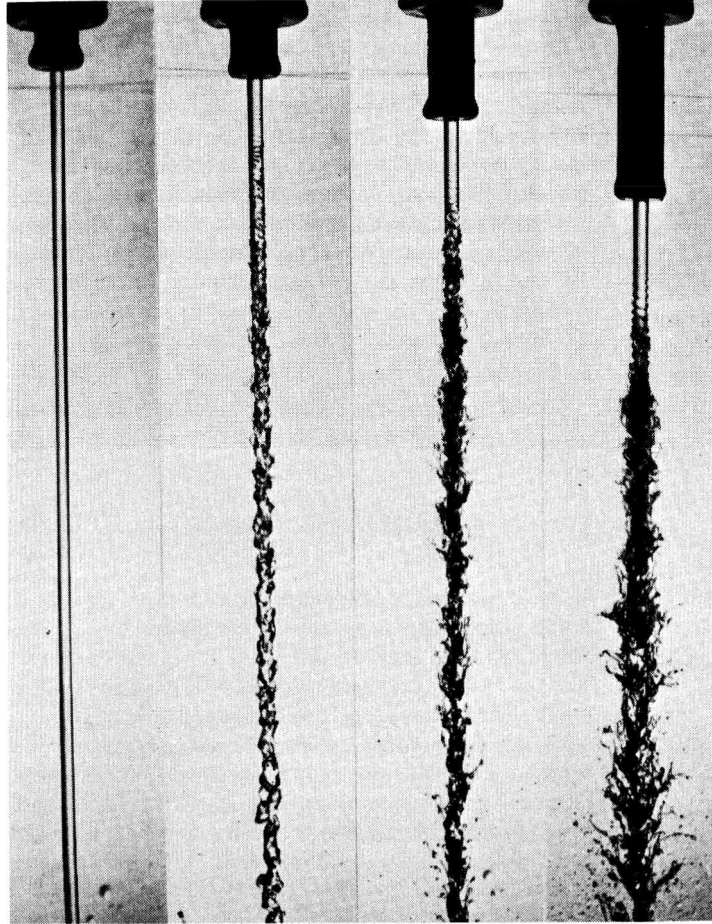
Figure B.1: Figure 5 from McCarthy and Molloy [MM74]: Effect of nozzle design on the stability of glycerol-water jets.

Jet viscosity	11 cP
Jet velocity	20 m/s (approx.)
Nozzle diameter	2.54 mm
Jet Reynolds no.	4750
Jet Ohnesorge no.	0.026
Exposure	30 μs
Nozzle aspect ratio	$L_0/d_0 = 0, 1, 5$ and 10 (left to right)
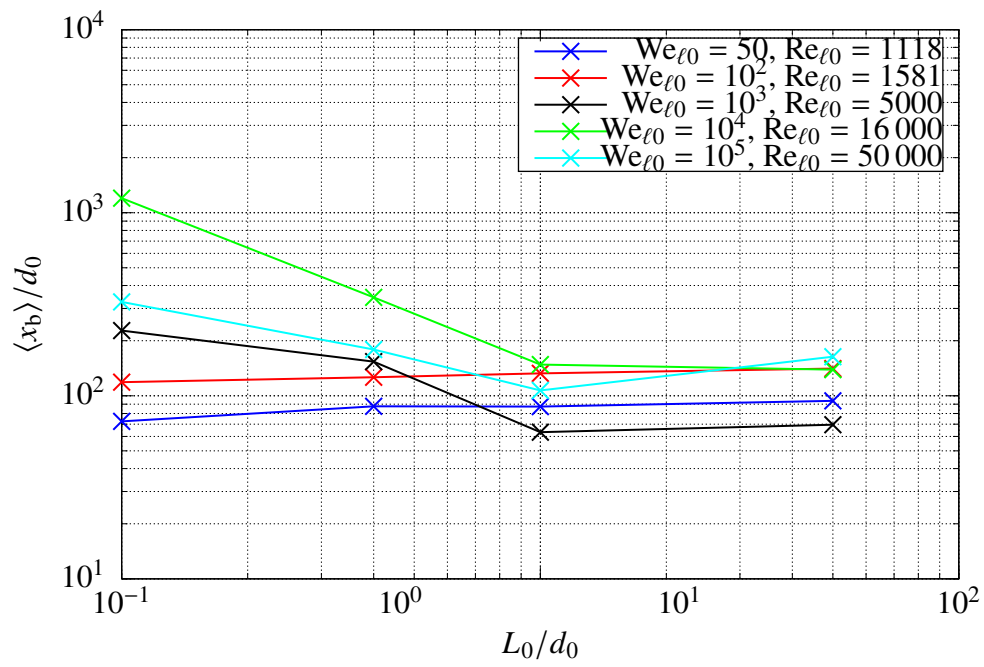
Figure B.2: Effect of nozzle aspect ratio (L_0/d_0) on dimensionless breakup length ($\langle x_b \rangle / d_0$) from the data of Arai, Shimizu, and Hiroyasu [ASH85].

different, Reynolds number[10]. The trend is not as expected for the two laminar cases — the breakup length is roughly constant as the nozzle aspect ratio L_0/d_0 increases, and slightly increasing for the lowest Reynolds number case. Here, L_0 is the length of the nozzle orifice. A longer nozzle aspect ratio for the laminar case would indicate that the velocity profile is closer to parabolic. If velocity profile relaxation were so catastrophic for laminar jets as McCarthy and Molloy [MM74] claim, then why is the this not observed in this experiment?

Clues come from the nozzle aspect ratios and hydrodynamic regime in the example used by McCarthy and Molloy [MM74, fig. 5]. The example of McCarthy and Molloy is for an initially laminar but transitional jet at high Weber number ($We_{\ell 0} \approx 1.5 \times 10^4$), which is close to the $We_{\ell 0} = 1 \times 10^4$ case in figure B.2[11]. For this case, as the nozzle aspect ratio increased, the breakup length decreases through $L_0/d_0 \approx 10$, which is the longest aspect ratio considered by McCarthy and Molloy. The trend McCarthy and Molloy observed applies only for high Weber number liquid jets with $L_0/d_0 \lesssim 10$. The breakup length trend at higher nozzle aspect ratios is slightly increasing, contrary to what one might expect from reading McCarthy and Molloy. Indeed, Debler and Yu [DY88] examine only $L_0/d_0 \gtrsim 10$ and come to the opposite conclusion as McCarthy and Molloy at lower Reynolds numbers.

An alternative mechanism can explain the observed trends. The transitional and turbulent data of McCarthy and Molloy [MM74] and Arai, Shimizu, and Hiroyasu [ASH85] both suffer from *confounding* between the turbulence intensity and velocity profile[12]. I discuss confounding in detail in § 4.4. Essentially, both the turbulence intensity and velocity profile are changing when the nozzle length changes [Kle81]. McCarthy and Molloy [MM74, p. 10] do not seem to be aware of this given that they state that "these jets, on issuing from the nozzles, differ from each other *only* in the value of α" (the emphasis is my own). An increase in disturbances in the flow as measured by turbulence intensity would

---

[10]See the caption of figure B.2 for the precise Reynolds numbers.

[11]Also compare the Reynolds numbers: $Re_{\ell 0} = 4750$ for McCarthy and Molloy [MM74, fig. 5], 16 000 in figure B.2.

[12]Jets which will remain laminar even in the fully developed state, e.g., the cases for which $Re_{\ell 0} < 2000$ in figure B.2 do not suffer from this confounding problem because the disturbances introduced from the wall are damped by viscosity. Hence the low Reynolds number (always laminar regardless of L_0/d_0) case mentioned earlier does not suffer from this confounding.

obviously affect the stability of the jet and its transition to turbulence. Others agree on this point — at higher Reynolds numbers Debler and Yu attribute McCarthy and Molloy's observations to the onset of turbulence. To be clear, both the turbulence intensity and velocity profile are factors, but the relative contributions of each can not be determined based on the experiments of McCarthy and Molloy and Arai, Shimizu, and Hiroyasu.

The case where the breakup length $\langle x_b \rangle$ in Arai, Shimizu, and Hiroyasu [ASH85] was $O(1000)$ likely had low turbulence intensity as the diameter contraction ratio was $d_{in}/d_0 = 10$. Large contractions tend to reduce the turbulence intensity [HR76]. As the nozzle length increases, the turbulence intensity at the nozzle outlet increases due to the effects of the shear at the walls[13]. The increase in breakup length as the nozzle length increases from $L_0/d_0 = 10$ to 50 could be explained by turbulence transition moving to inside the nozzle as nozzle becomes basically a fully developed pipe flow. Turbulence transition inside the nozzle appears to stabilize jets, as will be discussed more below and in § 3.4.6.

An unambiguous test would try to maintain the turbulence intensity as close as possible between the two velocity profiles tested to isolate the effect of the velocity profile. Likely the breakup lengths were much longer for shorter nozzle aspect ratios in the data of Arai, Shimizu, and Hiroyasu due to the low turbulence intensity for their short nozzles. Including other studies, the data for short nozzle aspect ratios seems to vary greatly, likely due to the turbulence intensity being a strong function of the inflow. See, for example, that the breakup lengths reported by Chen and Davis [CD64] for their short nozzles are much lower than those of Arai, Shimizu, and Hiroyasu [ASH85].

A qualitative unambiguous test was conducted by Wu, Miranda, and Faeth [WMF95]. The turbulence intensity was low in this case, but not quantified. While breakup lengths were not measured, the photographs show that breakup was suppressed when the boundary

---

[13]The nozzle design approach of Theobald [The81] came from Whitehead, Wu, and Waters [WWW51], and suffers from a similar problem. In addition to having a flat velocity profile, Whitehead, Wu, and Waters also avoid boundary layer separation to keep the turbulence intensity low. Consequently, the apparent success of Theobald's nozzle design is not necessarily due to the velocity profile relaxation effects discussed in Theobald [The81].

layer was thinner. The DNS study of Sander and Weigand [SW08, fig. 11], and it makes clear that breakup at least qualitatively is influenced by the velocity profile.

The early studies of Eisenklam and Hooper [EH58] (at $\mathrm{Re}_{\ell 0} \approx 3000$ to $12\,000$) and Rupe [Rup62, fig. 4, p. 12] (at $\mathrm{Re}_{\ell 0} \approx 2100$) have photos showing initially laminar jets with near complete breakup occurring over a short distance. While these researchers suggested that the parabolic velocity profile was responsible for this observation, as was previously detailed, laminar jets with parabolic velocity profiles show no particular inclination towards instability at Reynolds numbers below the critical Reynolds number. Instead, I hypothesize that turbulence transition outside of the nozzle causes the strong breakup, and that turbulence transition is sensitive to the velocity profile. The Reynolds numbers where this form of breakup occurs coincides well with where transition to turbulence occurs in fully developed pipe flows[14]. This idea is consistent with the observations of Hoyt and Taylor [HT85, p. 96L] who suggest that when a liquid jet transitions to turbulence after it has exited the nozzle, the transition is more violent than if the jet were already turbulent. Further, Hoyt and Taylor propose that reducing boundary layer thickness at the nozzle outlet can reduce these effects, which again, is consistent with the idea that the velocity profile influences turbulence transition. The earlier mentioned DNS study of Sander and Weigand [SW08] showed a clear sensitivity to the velocity profile. Sander and Weigand used low Reynolds numbers from 3000 to 7000, which are roughly in the transitional range for fully developed pipe flows, ultimately consistent with the idea that turbulence transition can cause strong breakup and also can be influenced by the velocity profile.

The reader is referred to Portillo, Collicott, and Blaisdell [PCB11] and Umemura [Ume14] for the latest experimental and theoretical research on transitional liquid jets, including detailed explanations of the transition mechanism which may be useful for nozzle design in this regime. More research is needed to explain why transitional liquid jets appear so unstable.

---

[14]Some readers may believe that a Reynolds number of $12\,000$ is far too high to be transitional for pipe flow, but laminar fully developed pipe flows have been maintained at Reynolds numbers as high as $100\,000$ depending on the quality of the experimental setup [Mul11, p. 7]. Indeed, Reynolds himself was able to establish laminar pipe flow at a Reynolds number of $13\,000$.

Note that many of the trends discussed previously seem to apply only at low ambient densities, i.e., density ratios $\rho_\ell/\rho_g > 500$. The data of Arai, Shimizu, and Hiroyasu [ASH85, fig. 7] seems to suggest that at high ambient densities and moderate jet velocities, nozzle length has little effect, but at higher jet velocities, longer nozzles have much longer breakup lengths than shorter nozzles. At present I can not explain these trends. This section focuses only on the low ambient density case.

Bibliography

Unless otherwise stated, I have at least partial copies of all documents cited. I've attempted to provide the interested reader with adequate information to locate harder to find documents, and would be happy to answer any questions about locating any of the documents cited.

All abstracts mentioned are written in English. If a LCCN is included, the document is available at the Library of Congress. For the TT field, the parentheses indicate which collection the translation was held in: SLA for the Special Libraries Association collection (now at the British Library and the NRC Canada National Science Library; see https://www.loc.gov/rr/scitech/trs/trstt.html), LC for Library of Congress Technical Reports and Standards collection, and OTS for Office of Technical Services (now NTIS). I will typically cite translations of foreign language papers and mention the original afterward. However, for certain papers which I am aware of a translation that I do not have a copy of, I will cite the original and mention the translation.

[AB51]   G. M. Asset and P. D. Bales. *Hydraulic Jets at Low Reynolds Number and Constant Weber Number*. Medical Laboratories Research Report 69. Army Chemical Center, Maryland: Chemical Corps Medical Laboratories, June 1951. 24 pp. DTIC: ADB219700. NTIS: PB105506. (In the Library of Congress Technical Reports & Standards collection under the report number NP-3466.) (Cit. on pp. 52, 57, 60, 61, 99, 100, 111).

[ACM70]   E. G. Arato, D. A. Crow, and D. S. Miller. *Investigations of a High Performance Water Nozzle*. Research Report 1058. Cranfield, Bedford, UK: British Hydromechanics Research Association, June 1970. 32 pp. OCLC: 29652590 (cit. on pp. vii, 181, 184, 185).

[AKY06]   K. Ahn, J. Kim, and Y. Yoon. "Effects of Orifice Internal Flow on Transverse Injection into Subsonic Crossflows: Cavitation and Hydraulic Flip". *Atomization and Sprays* 16(1) (2006), pp. 15–34. ISSN: 1044-5110. DOI: 10.1615/AtomizSpr.v16.i1.20 (cit. on p. 90).

[Als78] K. M. M. Alshamani. "Correlations among Turbulent Shear Stress, Turbulent Kinetic Energy, and Axial Turbulence Intensity". *AIAA Journal* 16(8) (1978), pp. 859–861. ISSN: 0001-1452. DOI: 10.2514/3.7594 (cit. on p. 150).

[And93] M. J. Andrews. "The Large-Scale Fragmentation of the Intact Liquid Core of a Spray Jet". *Atomization and Sprays* 3(1) (1993), pp. 29–54. ISSN: 1044-5110. DOI: 10.1615/AtomizSpr.v3.i1.20 (cit. on p. 21).

[Ara12] M. Arai. "Physics behind Diesel Sprays". *ICLASS 2012*. Ed. by C. Tropea and E. Gutheil. Heidelberg, Germany, Sept. 5, 2012. URL: http://www.ilasseurope.org/ICLASS/iclass2012_Heidelberg/Contributions/Paper-pdfs/Contribution1419_b.pdf. Archived at https://perma.cc/U58B-28FQ on Mar. 18, 2019. (Cit. on p. 101).

[AS68] D. W. Appel and F. R. Swenson. "Measurement of Surface Roughness of Turbulent Water Jets". *Tappi* 51(3) (1968), pp. 132–141. ISSN: 0039-8241 (cit. on p. 26).

[ASH85] M. Arai, M. Shimizu, and H. Hiroyasu. "Break-up Length and Spray Angle of High Speed Jet". *Proceedings of the 3rd International Conference on Liquid Atomisation and Spray Systems*. Ed. by P. Eisenklam and A. Yule. Imperial College, London, UK: Institute of Energy, July 1985, IB/4/1–IB/4/10. OCLC: 18600142 (cit. on pp. 67, 70, 72, 85, 90, 99, 102, 114, 115, 143, 150, 232, 234–236, 238).

[AT18] A. Agarwal and M. F. Trujillo. "A Closer Look at Linear Stability Theory in Modeling Spray Atomization". *International Journal of Multiphase Flow* 109 (Dec. 1, 2018), pp. 1–13. ISSN: 0301-9322. DOI: 10.1016/j.ijmultiphaseflow.2018.06.021 (cit. on pp. 26, 27, 73, 176).

[Aug96] P. Augier. "Contribution à l'étude et à la modélisation mécaniste-statistique de la distribution spatiale des apports d'eau sous un canon d'irrigation: application à la caractérisation des effets du vent sur l'uniformité d'arrosage [Contribution to the study and mechnistical-statistical simulation of the water distributed from an irrigation gun: application to characterize the effects of wind on water application uniformity]". PhD thesis. Paris, France: ENGREF, 1996. 248 pp. OCLC: 945572944 (Includes English abstract.) (Cit. on p. 168).

[Baf77] V. E. Baftalovsky. "Vliyaniye kachestva obrabotki nasadki na kompaktnost' vodyanykh struy v avtomodel'nom rezhime istecheniya [Effect of nozzle pro-

cessing quality on the compactness of water jets in a self-similar flow regime]". *Nauchnye soobshcheniia (Institut gornogo dela im. A.A. Skochinskogo)* 150 (1977), pp. 97–105. ISSN: 0540-939X (cit. on pp. 99, 124).

[Baf82]   V. E. Baftalovsky. "O porogovykh znacheniyakh skorosti istecheniya vodyanykh struy v avtomodel'nom rezhime [On the threshold values of the velocity of the water jets in the self-similar regime]". *Nauchnye soobshcheniia (Institut gornogo dela im. A.A. Skochinskogo)* 207 (1982), pp. 84–92. ISSN: 0540-939X (cit. on pp. 99, 124).

[Bal10]   B. S. Balewski. "Experimental Investigation of the Influence of Nozzle-Flow Properties on the Primary Spray Breakup". Dr.-Ing. dissertation. Darmstadt, Germany: TU Darmstadt, 2010. 144 pp. OCLC: 642949628 (cit. on p. 101).

[Bar49]   T. Baron. *Atomization of Liquid Jets and Droplets*. Technical Report 4. Urbana, IL: Engineering Experiment Station, University of Illinois, Feb. 15, 1949. 28 pp. URL: https://apps.dtic.mil/docs/citations/AD1066215 (cit. on pp. 104, 225).

[Bat78]   O. V. Bataev. *Dispersion of the Water Jet in a Pelton Turbine*. Translation 1484. Denver, CO: U.S. Dept. of the Interior, Bureau of Reclamation, Engineering and Research Center, Division of Design, Engineering Services Branch, 1978. 6 pp. TT: 79-14217 (SLA). OCLC: 6387347. (Changed ownership after I obtained a copy. Should be available from Linda Hall Library as of this writing.) (Cit. on pp. 226, 230). Trans. of "K voprosu o rasseivanii vodyanoy strui kovshovoy gidroturbiny [To the question of the dispersion of a water jet in a Pelton turbine]". *Trudy VNIIGidromash* (42) (1971), pp. 43–48.

[BC55]   R. Betchov and D. W. Clutter. *On The Breakup Of Liquid Jets*. Summary progress report 1. Washington, DC: George Washington University, Sept. 1955. 79 pp. DTIC: CBRNIAC-CB-115627 (cit. on pp. 57, 99, 122).

[BD51a]   V. A. Borodin and Y. F. Dityakin. *Unstable Capillary Waves on Surface of Separation of Two Viscous Fluids*. Technical memorandum 1281. Washington, DC: National Advisory Committee for Aeronautics, Apr. 1951. 20 pp. URL: http://ntrs.nasa.gov/search.jsp?R=19930093959. ISSN: 0096-7602. PB: 103505. Also see the corrections noted by: [Mey+53] (cit. on p. 213). Trans. of V. A. Borodin and Y. F. Dityakin. "Neustoychivyye kapillyarnyye volny na poverkhnosti razdela dvukh vyazkikh zhidkostey [Unstable capillary waves

on surface of separation of two viscous fluids]". *Prikladnaia matematika i mekhanika* XIII(3) (1949), pp. 267–276. ISSN: 0032-8235.

[BD51b]   I. G. Bowen and G. P. Davies. *Particle Size Distribution and the Estimation of Sauter Mean Diameter*. Technical Report ICT/28. London, UK: Shell Petroleum Co. Ltd., 1951. DTIC: ADB183499 (cit. on p. 101).

[Bea99]   J. C. Beale. "Modeling Fuel Injection Using Kelvin-Helmholtz/Rayleigh-Taylor Hybrid Atomization Model in KIVA-3V". MS thesis. Madison, WI: University of Wisconsin, 1999. 105 pp. OCLC: 42012813 (cit. on p. 19).

[Ben80]   R. P. Benedict. *Fundamentals of Pipe Flow*. New York, NY: Wiley, 1980. 531 pp. ISBN: 978-0-471-03375-2 (cit. on pp. 155, 231).

[Ber59]   W. Bergwerk. "Flow Pattern in Diesel Nozzle Spray Holes". *Proceedings of the Institution of Mechanical Engineers* 173(1) (June 1, 1959), pp. 655–660. ISSN: 0020-3483, DOI: 10.1243/PIME_PROC_1959_173_054_02. Abstract: [DeJ64, p. 52] (cit. on p. 105).

[BGK89]   M. A. Brutyan, V. N. Golubkin, and P. L. Krapivskiy. "Bernoulli's Equation for the Axisymmetric Flow of a Viscous Fluid". *Fluid mechanics: Soviet research* 18(3) (1989), pp. 118–121. ISSN: 0096-0764 (cit. on p. 146). Trans. of "Ob uravnenii Bernulli dlya osesimmetrichnykh techeniy vyazkoy zhidkosti [On the Bernoulli equation for the axisymmetric flow of a viscous fluid]". *Uchenye zapiski TsAGI* 19(2) (1988), pp. 98–100. ISSN: 0321-3439. URL: https://cyberleninka.ru/article/n/ob-uravnenii-bernulli-dlya-osesimmetrichnyh-techeniy-vyazkoy-zhidkosti.

[Bir60]   G. Birkhoff. *Hydrodynamics: A Study in Logic, Fact, and Similitude*. Revised. Princeton, NJ: Princeton University Press, 1960. 184 pp. ISBN: 978-0-313-20118-9 (cit. on p. 226).

[Bir64]   G. Birkhoff. "Averaged Conservation Laws in Pipes". *Journal of Mathematical Analysis and Applications* 8(1) (Feb. 1, 1964), pp. 66–77. ISSN: 0022-247X. DOI: 10.1016/0022-247X(64)90084-8 (cit. on p. 148).

[BL09]   M. Birouk and N. Lekic. "Liquid Jet Breakup in Quiescent Atmosphere: A Review". *Atomization and Sprays* 19(6) (2009), pp. 501–528. ISSN: 1044-5110. DOI: 10.1615/AtomizSpr.v19.i6.20 (cit. on pp. 38, 40, 102, 221, 231).

[BL49]   O. E. Baljé and L. V. Larson. *The Mechanism of Jet Disintegration*. Memorandum Report MCREXE-664-531B. Wright-Patterson AFB, Ohio: AAF

Air Materiel Command, Engineering Division, Aug. 29, 1949. 48 pp. URL: https://apps.dtic.mil/docs/citations/ADB817993. NTIS: PB159576. DTIC ATI: 64810 (cit. on p. 171).

[BL94]   S. K. Bhunia and J. H. Lienhard. "Splattering During Turbulent Liquid Jet Impingement on Solid Targets". *Journal of Fluids Engineering* 116(2) (June 1, 1994), pp. 338–344. ISSN: 0098-2202. DOI: 10.1115/1.2910277 (cit. on p. 107).

[BLS02]   R. B. Bird, E. N. Lightfoot, and W. E. Stewart. *Transport Phenomena*. New York, NY: Wiley, 2002. ISBN: 978-0-471-41077-5 (cit. on pp. 147, 156).

[BNP11]   M. Birouk, B. Nyantekyi-Kwakye, and N. Popplewell. "Effect of Nozzle Geometry on Breakup Length and Trajectory of Liquid Jet in Subsonic Crossflow". *Atomization and Sprays* 21(10) (2011), pp. 847–865. ISSN: 1044-5110. DOI: 10.1615/AtomizSpr.2012004338 (cit. on p. 173).

[Bog48]   I. I. Bogdanovich. "Vliyaniye podgotovki topliva v forsunke na tonkost' raspyla [Influence of fuel preparation in the nozzle on the fineness of the spray]". Candidate of Technical Sciences dissertation. Moscow, USSR: Zhukovsky Air Force Engineering Academy, 1948. 136 pp. Russian State Library: https://search.rsl.ru/en/record/01000176055 (Partial English translation available from Ben Trettel upon request.) (Cit. on pp. 9, 11, 23, 30, 32, 103, 119, 121, 215, 222).

[Bor96]   R. Borghi. "The Links between Turbulent Combustion and Spray Combustion and Their Modelling". *Transport Phenomena in Combustion: Proceedings of the Eighth International Symposium on Transport Phenomena in Combustion (ISTP-VIII) Held in San Francisco, California, July 16-20, 1995*. Vol. 1. Washington, DC: Taylor & Francis, 1996, pp. 1–18. ISBN: 978-1-56032-456-0 (cit. on p. 31).

[Bou+68]   P. J. Bourke, D. T. Pulling, L. E. Gill, and W. H. Dentin. "The Measurement of Turbulent Velocity Fluctuations and Turbulent Temperature Fluctuations in the Supercritical Region by a Hot-Wire Anemometer and a Cold Wire Resistance Thermometer". *Heat Transfer and Fluid Dynamics of near Critical Fluids*. London: Institution of Mechanical Engineers, Mar. 27, 1968, pp. 58–67. ISBN: 978-0-85298-000-2 (cit. on p. 107).

[BP51]   W. D. Baines and E. G. Petersen. "An Investigation of Flow through Screens". *Transactions of the American Society of Mechanical Engineers* 73 (1951), pp. 467–480. ISSN: 0097-6822 (cit. on pp. 147, 148).

[BP54]   G. K. Batchelor and I. Proudman. "The Effect of Rapid Distortion of a Fluid in Turbulent Motion". *The Quarterly Journal of Mechanics and Applied Mathematics* 7(1) (Jan. 1, 1954), pp. 83–103. ISSN: 0033-5614. DOI: 10.1093/qjmam/7.1.83 (cit. on pp. 49, 150, 158).

[BR99]   J. C. Beale and R. D. Reitz. "Modeling Spray Atomization with the Kelvin-Helmholtz/Rayleigh-Taylor Hybrid Model". *Atomization and Sprays* 9(6) (1999), pp. 623–650. ISSN: 1044-5110. DOI: 10.1615/AtomizSpr.v9.i6.40 (cit. on pp. 11, 12, 19, 33).

[Bra85]   S. L. Bragg. "An Evaluation of Sprinkler Jet Breakup as a Function of Pressure". MS thesis. Athens, GA: University of Georgia, 1985. 85 pp. OCLC: 12756956 (cit. on p. 168).

[BS02]   E. Babinsky and P. E. Sojka. "Modeling Drop Size Distributions". *Progress in Energy and Combustion Science* 28(4) (2002), pp. 303–329. ISSN: 0360-1285. DOI: 10.1016/S0360-1285(02)00004-7 (cit. on p. 24).

[BS20]   G. Brenn and M. Stelter. "A Generalized Ohnesorge Nomogram for Liquid Jet Breakup Regimes". *Atomization and Sprays* (2020). ISSN: 1044-5110. DOI: 10.1615/AtomizSpr.2020034267 (cit. on p. 37).

[Bus74]   W. Buschulte. "Liquid Propellant Atomization by Injector Elements and Its Effect on Combustion Chamber Efficiency". *Israel Journal of Technology* 12(1) (1974), pp. 57–68. ISSN: 0021-2202 (cit. on p. 101).

[CD64]   T.-F. Chen and J. R. Davis. "Disintegration of a Turbulent Water Jet". *Journal of the Hydraulics Division* 90(1) (Jan. 1964), pp. 175–206. ISSN: 0044-796X. Errata: "Disintegration of a Turbulent Jet: Errata". *Journal of the Hydraulics Division* 90(6) (Nov. 1964), p. 273. ISSN: 0044-796X (cit. on pp. 20, 26, 57, 85, 99, 100, 102, 109, 114, 115, 143, 171, 230, 236).

[CD96]   J. Cousin and C. Dumouchel. "Coupling of Classical Linear Theory and Maximum Entropy Formalism for Prediction of Drop Size Distribution in Sprays: Application to Pressure-Swirl Atomizers". *Atomization and Sprays* 6(5) (1996), pp. 601–622. ISSN: 1044-5110. DOI: 10.1615/AtomizSpr.v6.i5.50 (cit. on p. 30).

[Cer71]   J. E. Cermak. "Laboratory Simulation of the Atmospheric Boundary Layer". *AIAA Journal* 9(9) (1971), pp. 1746–1754. ISSN: 0001-1452. DOI: 10.2514/3.49977 (cit. on p. 226).

[Che62]   T.-F. Chen. "The Mechanics of Disintegration of a Water Jet". PhD dissertation. Davis, CA: University of California, Davis, 1962. 84 pp. OCLC: 6970717 (cit. on p. 230).

[CL99]   C. Clanet and J. C. Lasheras. "Transition from Dripping to Jetting". *Journal of Fluid Mechanics* 383 (Mar. 1999), pp. 307–326. ISSN: 0022-1120. DOI: 10.1017/S0022112098004066 (cit. on pp. 67, 68).

[Coo75]   W. C. Cooley. *Appendix C: References and Bibliography with Abstracts*. Vol. IV. Survey of Underground Hydraulic Coal Mining Technology. Rockville, MD: Terraspace, Inc., 1975. 279 pp. OCLC: 2084540. NTIS: PB251496 (cit. on p. 271).

[CP94]   C. J. Cavanaugh and P. F. Peterson. "Scale Modeling of Oscillating Sheet Jets for the HYLIFE-II Inertial Confinement Fusion Reactor". *Fusion Technology* 26 (3P2 Nov. 1, 1994), pp. 917–921. ISSN: 0748-1896. DOI: 10.13182/FST94-A40271 (cit. on p. 230).

[CR96]   N. Chigier and R. D. Reitz. "Regimes of Jet Breakup and Breakup Mechanisms (Physical Aspects)". *Recent Advances in Spray Combustion: Spray Atomization and Drop Burning Phenomena*. American Institute of Aeronautics and Astronautics, 1996, pp. 109–135. ISBN: 978-1-56347-175-9. DOI: 10.2514/5.9781600866418.0109.0135 (cit. on pp. 40, 46).

[CS30]   E. W. Cousins and H. B. Stewart. *Investigation of the Range of Monitor Nozzle Streams*. Report 9749. Factory Mutual Laboratories, Dec. 31, 1930. 11 pp. (Available from FM Global Research.) (Cit. on pp. vii, 173).

[CTM01]   P. Carrión, J. Tarjuelo, and J. Montero. "SIRIAS: A Simulation Model for Sprinkler Irrigation. I. Description of Model". *Irrigation Science* 20(2) (May 3, 2001), pp. 73–84. ISSN: 0342-7188. DOI: 10.1007/s002710000031 (cit. on p. 168).

[CY18]   P. M. Comiskey and A. L. Yarin. "Friction Coefficient of an Intact Free Liquid Jet Moving in Air". *Experiments in Fluids* 59(4) (Apr. 1, 2018), p. 65. ISSN: 0723-4864. DOI: 10.1007/s00348-018-2519-y (cit. on pp. vi, 172, 176).

[DCT05]   C. Dumouchel, J. Cousin, and K. Triballier. "On the Role of the Liquid Flow Characteristics on Low-Weber-Number Atomization Processes". *Experiments in Fluids* 38(5) (Mar. 19, 2005), pp. 637–647. ISSN: 0723-4864. DOI: 10.1007/s00348-005-0944-1 (cit. on pp. 9, 23, 119, 121, 171).

[DeJ59]   K. J. DeJuhasz. *Spray Literature Abstracts*. In collab. with E. A. Scicchitano. Vol. 1. 4 vols. New York, NY: American Society of Mechanical Engineers, 1959. 384 pp. URL: https://hdl.handle.net/2027/uc1.b3688902. OCLC: 1704784, 7414497. LCCN: 59004809 (cit. on pp. 248, 250, 252, 257, 259, 260, 264, 270, 275, 282).

[DeJ64]   K. J. DeJuhasz. *Spray Literature Abstracts*. Vol. 2. 4 vols. Heidelberg, Germany: Druckerei Winter, 1964. 384 pp. OCLC: 1704784, 7414497. LCCN: 59004809 (cit. on pp. 242, 276).

[DeJ67]   K. J. DeJuhasz. *Spray Literature Abstracts*. Vol. 3. 4 vols. Heidelberg, Germany: Universitäts-Druckerei Winter, 1967. 384 pp. URL: https://hdl.handle.net/2027/uc1.b4599834. OCLC: 1704784, 7414497. LCCN: 59004809 (cit. on pp. 249, 267).

[Dem+07] F.-X. Demoulin, P.-A. Beau, G. Blokkeel, A. Mura, and R. Borghi. "A New Model for Turbulent Flows with Large Density Fluctuations: Application to Liquid Atomization". *Atomization and Sprays* 17(4) (2007), pp. 315–345. ISSN: 1044-5110. DOI: 10.1615/AtomizSpr.v17.i4.20 (cit. on p. 12).

[DH54]   J. Dundurs and W. S. Hamilton. *Liquid Jet Disintegration*. Evanston, IL: Northwestern University Hydraulics Laboratory, Jan. 1954. 67 pp. OCLC: 30307233. DTIC: AD0224665 (cit. on pp. 228, 230).

[DI85]   G. De Jarlais and M. Ishii. *Inverted Annular Flow Experimental Study*. Washington, DC; Springfield, VA: Division of Accident Evaluation, Office of Nuclear Regulatory Research, U.S. Nuclear Regulatory Commission : Available from Supt. of Docs., U.S. G.P.O. ; National Technical Information Service, 1985 (cit. on p. 99).

[DiC+68] V. DiCamillo, D. Quigg, V. Neradka, and R. McMichael. *Jet Delivery Optimization*. Final Report R-4-23-68. Silver Spring, MD: Bowles Engineering Corporation, Apr. 1968. 120 pp. URL: https://ntrl.ntis.gov/NTRL/dashboard/searchResults/titleDetail/PB178437.xhtml (cit. on p. 168).

[DIL86]   G. De Jarlais, M. Ishii, and J. Linehan. "Hydrodynamic Stability of Inverted Annular Flow in an Adiabatic Simulation". *Journal of Heat Transfer* 108(1) (Feb. 1, 1986), pp. 84–92. ISSN: 0022-1481. DOI: 10.1115/1.3246909 (cit. on pp. 99, 117).

[DM53]   J. A. Duffie and W. R. Marshall. "Factors Influencing the Properties of Spray-Dried Materials". *Chemical engineering progress* 49(8) (1953), pp. 417–423. ISSN: 0360-7275 (cit. on p. 99).

[Dod59]   J. Dodu. "Influence des nombres de Weber et de Reynolds sur la dispersion des jets liquides à grand vitesse [The influence of the Weber and Reynolds numbers on the dispersion of high-speed liquid jet]". *Comptes rendus hebdomadaires des séances de l'Académie des sciences* 249(4) (July 27, 1959), pp. 499–501. ISSN: 0001-4036. URL: http://gallica.bnf.fr/ark:/12148/bpt6k3201c/f515. item. Abstract: [LHB67, abstract D-43, p. 133R] (cit. on p. 111).

[Dod60]   J. Dodu. "Similitude des jets liquides à grande vitesse [Similarity of high-speed liquid jets]". *Recherches sur les turbines hydrauliques*. Nice, France: La Houille Blanche, Sept. 1960, C.1-1 to C.1–6. OCLC: 2160883 (Includes English abstract.) (Cit. on pp. 111, 230).

[DP10a]   O. Desjardins and H. Pitsch. "Detailed Numerical Investigation of Turbulent Atomization of Liquid Jets". *Atomization and Sprays* 20(4) (2010), pp. 311–336. ISSN: 1044-5110. DOI: 10.1615/AtomizSpr.v20.i4.40 (cit. on p. 30).

[DP10b]   P. A. Durbin and B. A. Pettersson Reif. *Statistical Theory and Modeling for Turbulent Flows*. 2nd ed. Chichester, UK: Wiley, Oct. 25, 2010. 372 pp. ISBN: 978-0-470-68931-8 (cit. on pp. 150, 152).

[Dum08]   C. Dumouchel. "On the Experimental Investigation on Primary Atomization of Liquid Streams". *Experiments in Fluids* 45(3) (Sept. 1, 2008), pp. 371–422. ISSN: 1432-1114. DOI: 10.1007/s00348-008-0526-0 (cit. on pp. 47, 53, 67, 69).

[Dum09]   C. Dumouchel. "The Maximum Entropy Formalism and the Prediction of Liquid Spray Drop-Size Distribution". *Entropy* 11(4) (Nov. 2, 2009), pp. 713–747. DOI: 10.3390/e11040713 (cit. on p. 30).

[DY88]   W. Debler and D. Yu. "The Break-Up of Laminar Liquid Jets". *Proceedings of the Royal Society of London A: Mathematical, Physical and Engineering*

Sciences 415(1848) (Jan. 8, 1988), pp. 107–119. ISSN: 1364-5021. DOI: 10.1098/rspa.1988.0005 (cit. on pp. 99, 100, 232, 235, 236).

[EF87] D. A. Ervine and H. T. Falvey. "Behaviour of Turbulent Water Jets in the Atmosphere and in Plunge Pools". *Proceedings of the Institution of Civil Engineers* 83(1) (Jan. 3, 1987), pp. 295–314. ISSN: 1753-7789. DOI: 10.1680/iicep.1987.353. Discussion: [Hoy+88] (cit. on p. 9).

[EFW97] D. A. Ervine, H. T. Falvey, and W. Withers. "Pressure Fluctuations on Plunge Pool Floors". *Journal of Hydraulic Research* 35(2) (Mar. 1, 1997), pp. 257–279. ISSN: 0022-1686. DOI: 10.1080/00221689709498430 (cit. on p. 104).

[EH58] P. Eisenklam and P. C. Hooper. *Flow Characteristics of Laminar and Turbulent Jets of Liquid*. Report J.R.L. 42. London, UK: Imperial College of Science and Technology, Sept. 1958. 55 pp. URL: http://naca.central.cranfield.ac.uk/ reports/arc/20914.pdf. Archived at https://perma.cc/4DM9-HPU3 on Feb. 15, 2019 (cit. on pp. 49, 54, 57, 59, 99, 123, 231, 237).

[EME80] D. A. Ervine, E. McKeogh, and E. M. Elsawy. "Effect of Turbulence Intensity on the Rate of Air Entrainment by Plunging Water Jets". *Proceedings of the Institution of Civil Engineers* 69(2) (June 1, 1980), pp. 425–445. ISSN: 1753-7789. DOI: 10.1680/iicep.1980.2545 (cit. on pp. 9, 83, 86, 149, 168).

[Etz+18] M. Etzold, A. Deswal, L. Chen, and F. Durst. "Break-up Length of Liquid Jets Produced by Short Nozzles". *International Journal of Multiphase Flow* 99 (Feb. 1, 2018), pp. 397–407. ISSN: 0301-9322. DOI: 10.1016/j.ijmultiphaseflow.2017.11.006 (cit. on p. 75).

[Etz19] M. Etzold. "Zeitmodulierte, monodisperse Tropfengenerierung zur Herstellung von Feinstsprays [Time-modulated, monodisperse droplet generation for the production of ultra-fine sprays]". Dr.-Ing. dissertation. Erlangen, Germany: Friedrich-Alexander-Universität Erlangen-Nürnberg, Mar. 25, 2019. 235 pp. DOI: 10.25593/978-3-96147-224-6 (cit. on p. 46).

[Eut57] G. A. Euteneuer. "Druckabhängigkeit von Tropfengröße und Wurfweite bei Sprühstrahlen [Drop size and throw distance of jet sprays as functions of pressure]". *VFDB Zeitschrift* 6(3) (Aug. 1957), pp. 124–128. OCLC: 3170116. Abstracts: [DeJ59, p. 90], [LHB67, abstract E-16, p. 140L] (cit. on p. 174).

[Fae91] G. M. Faeth. "Structure and Atomization Properties of Dense Turbulent Sprays". *Symposium (International) on Combustion*. Twenty-Third Sympo-

sium (International) on Combustion 23(1) (1991), pp. 1345–1352. ISSN: 0082-0784. DOI: 10.1016/S0082-0784(06)80399-1 (cit. on p. 40).

[FNO80] Y. Fukui, K. Nakanishi, and S. Okamura. "Computer Evaluation of Sprinkler Irrigation Uniformity". *Irrigation Science* 2(1) (Oct. 1980), pp. 23–32. ISSN: 0342-7188. DOI: 10.1007/BF00285427 (cit. on p. 167).

[For91] D. P. Fornell. *Fire Stream Management Handbook*. Saddle Brook, N.J.: Fire Engineering, 1991. ISBN: 978-0-87814-927-8 (cit. on p. 173).

[Fre89] J. R. Freeman. "Experiments Relating to Hydraulics of Fire Streams". *Transactions of the American Society of Civil Engineers* XXI(2) (Nov. 1889), pp. 303–482. ISSN: 0066-0604. URL: https://hdl.handle.net/2027/uc1.31210023545690?urlappend=%3Bseq=479. Abstract: [DeJ67, p. 110] (cit. on p. 172).

[Fri65] A. Fritzsche. *Über den Zusammenhang von Strahlzerfall und turbulentem Stoffaustausch, untersucht am Beispiel des runden Strahles [On the relation of jet disintegration and turbulent mass transfer, using the example of the circular beam]*. Fortschritt-Berichte der VDI-Zeitschriften. Reihe 7: Strömungstechnik 2. Verlag des Vereins Deutscher Ingenieure, 1965. 99 pp. ISSN: 0341-1753. OCLC: 9022319 (cit. on p. 30).

[GG08] F. J. García and H. González. "Normal-Mode Linear Analysis and Initial Conditions of Capillary Jets". *Journal of Fluid Mechanics* 602 (May 2008), pp. 81–117. ISSN: 0022-1120. DOI: 10.1017/S0022112008000724 (cit. on p. 77).

[GH08] M. Gorokhovski and M. Herrmann. "Modeling Primary Atomization". *Annual Review of Fluid Mechanics* 40(1) (2008), pp. 343–366. ISSN: 0066-4189. DOI: 10.1146/annurev.fluid.40.111406.102200 (cit. on pp. 103, 230).

[GJ88] J. Groth and A. V. Johansson. "Turbulence Reduction by Screens". *Journal of Fluid Mechanics* 197 (Dec. 1988), pp. 139–155. ISSN: 0022-1120. DOI: 10.1017/S0022112088003209 (cit. on p. 147).

[GM66] R. P. Grant and S. Middleman. "Newtonian Jet Stability". *AIChE Journal* 12(4) (July 1, 1966), pp. 669–678. ISSN: 1547-5905. DOI: 10.1002/aic.690120411 (cit. on pp. 41, 44, 47, 57, 67, 69, 70, 85, 99, 100, 114–117, 143).

[Gol65]   S. Goldstein. *Modern Developments in Fluid Dynamics: An Account of Theory and Experiment Relating to Boundary Layers Turbulent Motion and Wakes.* 2 vols. New York: Dover, 1965. ISBN: 978-0-486-61358-1 (cit. on p. 226).

[Gor01]   M. Gorokhovski. "The Stochastic Lagrangian Model of Drop Breakup in the Computation of Liquid Sprays". *Atomization and Sprays* 11(5) (2001), pp. 505–519. ISSN: 1044-5110. DOI: 10.1615/AtomizSpr.v11.i5.20 (cit. on pp. 120, 121, 124, 125).

[Gow69]   J. L. Gow. "Fully-Developed Turbulent Flow in Smooth and Rough-Walled Pipe". MS thesis. Bozeman, MT: Montana State University, Mar. 1969. 89 pp. URL: http://scholarworks.montana.edu/xmlui/handle/1/5237 (cit. on pp. 107, 158).

[Gra65]   R. P. Grant. "Newtonian Jet Stability". PhD dissertation. Rochester, NY: University of Rochester, 1965. 272 pp. URL: https://search.proquest.com/docview/302310692 (cit. on pp. 51, 71, 72, 102).

[Gre71]   J. H. Green. *Effect of Polymer Additives on Nozzle Stream Coherence: A Preliminary Study.* Technical Note 504. San Diego, CA: Naval Undersea Research and Development Center, Mar. 1971. 18 pp. URL: https://apps.dtic.mil/docs/citations/AD1068484 (cit. on pp. 172, 173).

[Gro83]   R. D. Grose. "Orifice Flow at Low Reynolds Number". *Journal of pipelines* 3 (1983), pp. 207–214. ISSN: 0166-5324 (cit. on p. 146).

[Gro99]   D. Grose. "Mathematical Modelling and Simulation of Irrigation Sprinklers". PhD thesis. Cranfield, UK: Cranfield University, Oct. 16, 1999. 80 pp. URL: http://dspace.lib.cranfield.ac.uk/handle/1826/9603 (cit. on p. 167).

[HA90]   H. Hiroyasu and M. Arai. *Structures of Fuel Sprays in Diesel Engines.* Technical Paper 900475. Society of Automotive Engineers, Feb. 1990. DOI: 10.4271/900475. ISSN: 0148-7191 (cit. on p. 99).

[Hae32]   A. Haenlein. *Disintegration of a Liquid Jet.* Technical memorandum 659. Washington, DC: National Advisory Committee for Aeronautics, Feb. 1932. 27 pp. URL: http://ntrs.nasa.gov/search.jsp?R=19930094757. ISSN: 0096-7602 (cit. on pp. 39, 44, 69). Trans. of "Über den Zerfall eines Flüssigkeitsstrahles [About the disintegration of a liquid jet]". *Forschung auf dem Gebiet des Ingenieurwesens A* 2(4) (Apr. 1931), pp. 139–149. ISSN: 0015-7899. DOI: 10.1007/BF02584624. Abstract: [DeJ59, p. 135].

[Hal+52]   G. Halbronn, P. Oguey, M. Mamin, F. Baatard, J. H. Arnold, H. Rouse, D. E. Metzler, and J. W. Howe. "Discussion of "Experimental Investigation of Fire Monitors and Nozzles"". *Transactions of the American Society of Civil Engineers* 117(1) (Jan. 1952), pp. 1176–1188. ISSN: 0066-0604 (cit. on pp. 224, 225, 267, 271).

[Ham94]   W. B. Hammerschlag. "A Better Description of Liquid Jet Breakup Using a Spatial Model Including Viscous Effects". PhD dissertation. Arlington, TX: The University of Texas at Arlington, 1994. 316 pp. URL: http://search.proquest.com/docview/304156061. OCLC: 840037536 (cit. on p. 223).

[Har53]   D. B. Harmon. "Prediction of the Mean Drop Size in a Spray from a Cylindrical Nozzle with Flow at High Reynolds Moduli". PhD thesis. University of California, Los Angeles, July 1953. 164 pp. OCLC: 15310442 (cit. on pp. iv, 148).

[Haw96]   R. D. Hawkes. "A Quantitative Method for In-Flight Characterization of Sprinkler Jet Breakup". MS thesis. Lincoln, NE: University of Nebraska, 1996. 91 pp. OCLC: 36267986 (cit. on p. 171).

[Hei62]   M. F. Heidmann. "Photography and Analysis of Time Variation in Drop Size Distribution of a Liquid Spray". *Journal of the SMPTE* 71 (1A Jan. 1962), pp. 519–524. ISSN: 0361-4573. DOI: 10.5594/J18190XY (cit. on p. 101).

[Hel68]   H. von Helmholtz. "On Discontinuous Movements of Fluids". *The London, Edinburgh, and Dublin Philosophical Magazine and Journal of Science* 36(244) (Nov. 1, 1868), pp. 337–346. ISSN: 1941-5982. DOI: 10.1080/14786446808640073 (cit. on p. 14). Trans. of H. von Helmholtz. "Über diskontinuierliche Flüssigkeitsbewegungen [On the discontinuous movements of fluids]". *Monatsberichte der Königlichen Preussische Akademie der Wissenschaften zu Berlin* 23 (Apr. 1868), pp. 215–228. OCLC: 884529906.

[HG91]   K. Y. Huh and A. D. Gosman. "A Phenomenological Model of Diesel Spray Atomization". *Proceedings of the International Conference on Multiphase Flows*. Ed. by G. Matsui. Vol. 2. Tsukuba, Japan, 1991, pp. 515–518. OCLC: 831380048 (See the citation for Huh, Lee, and Koo [HLK98] for a note about an error in this paper.) (Cit. on pp. 11, 148).

[HGH05]   Y. Han, W. George, and J. Hjarne. "Effect of a Contraction on Turbulence. Part 1: Experiment". *43rd AIAA Aerospace Sciences Meeting and Exhibit*. American

Institute of Aeronautics and Astronautics, 2005. DOI: 10.2514/6.2005-1119 (cit. on p. 150).

[Hic73]   H. E. Hickey. *Evaluation of Discharge Stream Projections from Two Selected Nozzles at Minimum Angle Elevations*. MP 73-1. Boston, MA: National Fire Protection Association, 1973. 12 pp. OCLC: 22039979 (cit. on pp. 197, 200).

[Hin55]   J. O. Hinze. "Fundamentals of the Hydrodynamic Mechanism of Splitting in Dispersion Processes". *AIChE Journal* 1(3) (Sept. 1, 1955), pp. 289–295. ISSN: 1547-5905. DOI: 10.1002/aic.690010303. Abstract: [DeJ59, p. 153] (cit. on p. 133).

[Hin75]   J. O. Hinze. *Turbulence*. New York, NY: McGraw-Hill, 1975. 790 pp. ISBN: 978-0-07-029037-2 (cit. on p. 133).

[Hir00]   H. Hiroyasu. "Spray Breakup Mechanism from the Hole-Type Nozzle and Its Applications". *Atomization and Sprays* 10(3-5) (2000). ISSN: 1044-5110. DOI: 10.1615/AtomizSpr.v10.i3-5.130 (cit. on p. 5).

[HKT76]   G. Heskestad, H. C. Kung, and N. F. Todtenkopf. *Air Entrainment in Water Sprays and Spray Curtains*. ASME paper 76-WA/FE-40. 1976. 12 pp. OCLC: 43272637 (cit. on p. 179).

[HLK98]   K. Y. Huh, E. Lee, and J. Koo. "Diesel Spray Atomization Model Considering Nozzle Exit Turbulence Conditions". *Atomization and Sprays* 8(4) (1998), pp. 453–469. ISSN: 1044-5110. DOI: 10.1615/AtomizSpr.v8.i4.60. PubPeer: 95455FA4147A9CBD5EAA5185D21DAC (The nozzle outlet turbulent kinetic energy model in this paper is in error, as has been discussed in chapter 6.) (Cit. on pp. 11, 14, 34, 35, 105, 119, 129, 130, 142, 144, 148–150, 251).

[HLO85]   A. P. Hatton, C. M. Leech, and M. J. Osborne. "Computer Simulation of the Trajectories of Large Water Jets". *International Journal of Heat and Fluid Flow* 6(2) (June 1985), pp. 137–141. ISSN: 0142-727X. DOI: 10.1016/0142-727X(85)90051-7 (cit. on pp. 166, 168, 170).

[HO79]   A. P. Hatton and M. J. Osborne. "The Trajectories of Large Fire Fighting Jets". *International Journal of Heat and Fluid Flow* 1(1) (Mar. 1979), pp. 37–41. ISSN: 0142-727X. DOI: 10.1016/0142-727X(79)90023-7 (cit. on pp. 166, 168).

[Hos+16]   S. M. Hosseinalipour, H. Karimaei, E. Movahednejad, and F. Ommi. "Application of Maximum Entropy Principle for Estimation of Droplet-Size

Distribution Using Internal Flow Analysis of a Swirl Injector". *International Journal of Spray and Combustion Dynamics* 8(3) (Sept. 1, 2016), pp. 205–216. ISSN: 1756-8277. DOI: 10.1177/1756827716654647 (cit. on p. 30).

[Hoy+88]   J. W. Hoyt, J. J. Taylor, D. A. Ervine, and H. T. Halvey. "Behaviour of Turbulent Water Jets in the Atmosphere and in Plunge Pools. Discussion on Paper 9136". *Proceedings of the Institution of Civil Engineers* 85(2) (June 1, 1988), pp. 359–363. DOI: 10.1680/iicep.1988.142 (cit. on pp. 30, 248).

[HR76]   A. K. M. F. Hussain and V. Ramjee. "Effects of the Axisymmetric Contraction Shape on Incompressible Turbulent Flow". *Journal of Fluids Engineering* 98(1) (Mar. 1, 1976), pp. 58–68. ISSN: 0098-2202. DOI: 10.1115/1.3448210 (cit. on p. 236).

[HR95]   L. He and F. Ruiz. "Effect of Cavitation on Flow and Turbulence in Plain Orifices for High-Speed Atomization". *Atomization and Sprays* 5(6) (1995). ISSN: 1044-5110. DOI: 10.1615/AtomizSpr.v5.i6.30 (cit. on pp. 215, 222).

[HSA82]   H. Hiroyasu, M. Shimizu, and M. Arai. "The Breakup of High Speed Liquid Jet in a High Pressure Gaseous Atmosphere". *Proceedings of the 2nd International Conference on Liquid Atomization and Spray Systems*. Madison, WI: Dept. of Chemical Engineering, University of Wisconsi, Madison, June 1982, pp. 69–74. OCLC: 10261204 (cit. on p. 99).

[HT77a]   J. W. Hoyt and J. J. Taylor. "Turbulence Structure in a Water Jet Discharging in Air". *Physics of Fluids* 20(10) (1977), S253–S257. ISSN: 0031-9171. DOI: 10.1063/1.861738 (cit. on pp. 167, 168).

[HT77b]   J. W. Hoyt and J. J. Taylor. "Waves on Water Jets". *Journal of Fluid Mechanics* 83(1) (Nov. 1977), pp. 119–127. ISSN: 0022-1120. DOI: 10.1017/S0022112077001074 (cit. on pp. 48, 51, 120, 121).

[HT79]   J. W. Hoyt and J. J. Taylor. "Effect of Nozzle Shape and Polymer Additives on Water Jet Appearance". *Journal of Fluids Engineering* 101(3) (Sept. 1, 1979), pp. 304–308. ISSN: 0098-2202. DOI: 10.1115/1.3448966 (cit. on p. 51).

[HT80]   J. W. Hoyt and J. J. Taylor. "Pipe-Exit Flow Photography". *Cavitation and Polyphase Flow Forum — 1980*. Joint Meeting of the Fluids Engineering Division and the Gas Turbine Division. New Orleans, LA: ASME, Mar. 1980, pp. 42–44 (cit. on pp. 62, 67, 99, 122).

[HT82]   J. W. Hoyt and J. J. Taylor. "Water-Jet Photography". *Naval research reviews* XXXIV(4) (1982), pp. 3–9. ISSN: 0028-145X. URL: https://apps.dtic.mil/docs/citations/ADA123226 (cit. on p. 61).

[HT85]   J. W. Hoyt and J. J. Taylor. "Effect of Nozzle Boundary Layer on Water Jets Discharging in Air". *Jets and Cavities: International Symposium*. Winter Annual Meeting of the American Society of Mechanical Engineers. Ed. by J. H. Kim, O. Furuya, and B. R. Parkin. Vol. 31. FED. Miami Beach, FL: ASME, Nov. 1985, pp. 93–100. OCLC: 13104157 (cit. on pp. 9, 54, 67, 73, 75, 231, 232, 237).

[Hua+94]   Z. Huang, Y. M. Shao, S. Shiga, H. Nakamura, and T. Karasawa. "The Role of Orifice Flow Pattern in Fuel Atomization". *Proceedings of the Sixth International Conference on Liquid Atomization and Spray Systems, July 18-22, 1994, Palais Des Congrès, Rouen, France*. ICLASS 94. New York, NY: Begell House, 1994, pp. 86–93. ISBN: 978-1-56700-019-1 (cit. on p. 99).

[Ici82]   J. Iciek. "The Hydrodynamics of a Free, Liquid Jet and Their Influence on Direct Contact Heat Transfer — I Hydrodynamics of a Free, Cylindrical Liquid Jet". *International Journal of Multiphase Flow* 8(3) (June 1982), pp. 239–249. ISSN: 0301-9322. DOI: 10.1016/0301-9322(82)90033-7 (cit. on p. 99).

[IM00]   E. A. Ibrahim and S. O. Marshall. "Instability of a Liquid Jet of Parabolic Velocity Profile". *Chemical Engineering Journal* 76(1) (Jan. 2000), pp. 17–21. ISSN: 1385-8947. DOI: 10.1016/S1385-8947(99)00110-2 (cit. on p. 232).

[Inc+06]   F. P. Incropera, D. P. DeWitt, T. L. Bergman, and A. S. Lavine. *Fundamentals of Heat and Mass Transfer*. 6th ed. John Wiley & Sons, Mar. 10, 2006. 1024 pp. ISBN: 978-0-471-45728-2 (cit. on p. 107).

[Ino63]   H. Inoue. "Mean Drop Size and Maximum Drop Size of Sprays Emitted by the Sprinkler". *Transactions, Congress on Irrigation and Drainage* 4 (1963), pp. 16.99–16.114. ISSN: 0589-3127 (cit. on pp. 11, 30, 171, 230).

[Isa66]   A. P. Isaev. "Optimal'nyye rezhimy raboty dal'nostruynykh dozhdeval'nykh mashin [Optimal operating conditions of long-range sprinklers]". *Mekhanizatsiya i elektrifikatsiya sotsialisticheskogo sel'skogo khozyaystva* 24(9) (1966), pp. 4–9. ISSN: 0206-572X. (English translation available from Ben Trettel upon request.) (Cit. on p. 230).

[Isa67]   A. P. Isaev. "Raschet parametrov dal'nestuynykh mashin i apparatov [Dimensioning long-range jet machines and devices]". *Traktory i sel'khozmashiny* (3) (1967), pp. 29–32. OCLC: 8520694 (cit. on p. 230).

[Isa73]   A. P. Isaev. *Gidravlika dozhdeval'nykh mashin [Hydraulics of sprinklers]*. Moscow, USSR: Mashinostroenie, 1973. 214 pp. OCLC: 1044502. LCCN: 74303368 (cit. on p. 230).

[Jac83]   M. K. Jackson. "Two-Phase Characteristics of Turbulent Water Jets". PhD thesis. Exeter, UK: University of Exeter, 1983. 374 pp. URL: http://ethos.bl.uk/OrderDetails.do?uin=uk.bl.ethos.633045. OCLC: 731729141 (cit. on p. 148).

[Kar+92]   T. Karasawa, M. Tanaka, K. Abe, S. Shiga, and T. Kurabayashi. "Effect of Nozzle Configuration on the Atomization of a Steady Spray". *Atomization and Sprays* 2(4) (1992), pp. 411–426. ISSN: 1044-5110. DOI: 10.1615/AtomizSpr.v2.i4.30 (cit. on p. 99).

[Kas+17]   A. Kastengren, J. Ilavsky, J. P. Viera, R. Payri, D. J. Duke, A. Swantek, F. Z. Tilocco, N. Sovis, and C. F. Powell. "Measurements of Droplet Size in Shear-Driven Atomization Using Ultra-Small Angle x-Ray Scattering". *International Journal of Multiphase Flow* 92 (June 1, 2017), pp. 131–139. ISSN: 0301-9322. DOI: 10.1016/j.ijmultiphaseflow.2017.03.005 (cit. on p. 118).

[Kaw71]   K. Kawakami. "Study on the Computation of Horizontal Distance of Jet Issued from Nozzle". *Proceedings of the Japan Society of Civil Engineers* 1971(191) (1971), pp. 83–89. ISSN: 0385-5392. DOI: 10.2208/jscej1969.1971.191_83. (This paper has a major error which invalidates its model as noted in footnote 8 on page 188.) (Cit. on p. 188).

[KB83]   J. C. Kent and G. M. Brown. "Nozzle Exit Flow Characteristics for Square-Edged and Rounded Inlet Geometries". *Combustion Science and Technology* 30(1-6) (Jan. 1, 1983), pp. 121–132. ISSN: 0010-2202. DOI: 10.1080/00102208308923615 (cit. on pp. 51, 103, 215, 222).

[KF93]   A. L. Knox-Kelecy and P. V. Farrell. *Spectral Characteristics of Turbulent Flow in a Scale Model of a Diesel Fuel Injector Nozzle*. Technical Paper 930924. Society of Automotive Engineers, Mar. 1993. DOI: 10.4271/930924. ISSN: 0148-7191 (cit. on pp. 215, 222).

[Kim+03]   W. T. Kim, S. K. Mitra, X. Li, L. A. Prociw, and T. C. J. Hu. "A Predictive Model for the Initial Droplet Size and Velocity Distributions in Sprays and Comparison with Experiments". *Particle & Particle Systems Characterization* 20(2) (May 1, 2003), pp. 135–149. ISSN: 1521-4117. DOI: 10.1002/ppsc.200390011 (cit. on p. 30).

[Kim83]   S. Kim. "An Investigation of Heat and Mass Transport in Turbulent Liquid Jets". PhD dissertation. Los Angeles, CA: University of California, Los Angeles, 1983. 204 pp. OCLC: 11440592. NTIS: DE84011174. (Cit. on pp. iv, 99, 108, 129).

[Kin96]   D. C. Kincaid. "Spraydrop Kinetic Energy from Irrigation Sprinklers". *Transactions of the American Society of Agricultural Engineers* 39(3) (1996), pp. 847–853. ISSN: 0001-2351. DOI: 10.13031/2013.27569 (cit. on p. 168).

[Kle81]   A. Klein. "Review: Turbulent Developing Pipe Flow". *Journal of Fluids Engineering* 103(2) (June 1, 1981), pp. 243–249. ISSN: 0098-2202. DOI: 10.1115/1.3241726 (cit. on pp. 149, 159, 160, 235).

[KM00]   J.-H. Kim and B.-S. Moon. "Spray Cone Angles of Port Fuel Injectors by Different Measuring Techniques". *ICLASS 2000*. Pasadena, CA, July 2000, pp. 501–508. URL: http://ilasseurope.org/events/8th-iclass/. Archived at https://perma.cc/7HM6-YBXP on Mar. 18, 2019. (Cit. on p. 101).

[KM69]   F. W. Kroesser and S. Middleman. "Viscoelastic Jet Stability". *AIChE Journal* 15(3) (1969), pp. 383–386. ISSN: 1547-5905. DOI: 10.1002/aic.690150316 (cit. on p. 69).

[KM89a]   S. Kim and A. F. Mills. "Condensation on Coherent Turbulent Jets: Part II — A Theoretical Study". *Journal of Heat Transfer* 111(4) (Nov. 1, 1989), pp. 1075–1082. ISSN: 0022-1481. DOI: 10.1115/1.3250770 (cit. on p. 107).

[KM89b]   S. Kim and A. F. Mills. "Condensation on Coherent Turbulent Liquid Jets: Part I — Experimental Study". *Journal of Heat Transfer* 111(4) (Nov. 1, 1989), pp. 1068–1074. ISSN: 0022-1481. DOI: 10.1115/1.3250769 (cit. on p. 67).

[KMO17]   A. R. Kerstein, A. Movaghar, and M. Oevermann. "Parameter Dependences of the Onset of Turbulent Liquid-Jet Breakup". *Journal of Fluid Mechanics* 811(R5) (Jan. 2017). ISSN: 0022-1120. DOI: 10.1017/jfm.2016.806 (cit. on pp. 11, 35, 36, 139).

256

[Kol91]   A. N. Kolmogorov. "On the Breakage of Drops in a Turbulent Flow". *Selected Works of A. N. Kolmogorov*. Ed. and trans. by V. M. Tikhomirov. Mathematics and Its Applications (Soviet Series) 25. Springer, 1991, pp. 339–343. ISBN: 978-94-011-3030-1. DOI: 10.1007/978-94-011-3030-1_50 (cit. on p. 133). Trans. of "O droblenii kapel' v turbulentnom potoke [On the breakage of drops in a turbulent flow]". *Doklady Akademii Nauk SSSR* 66(5) (1949), pp. 825–828. ISSN: 0002-3264. Abstract: [DeJ59, p. 183].

[KT78]   Y. Kitamura and T. Takahashi. "Influence of Nozzle Length on Breakup of a Liquid Jet". Proceedings of the 1st International Conference on Liquid Atomization and Spray Systems. Tokyo, Japan: The Fuel Society of Japan, Aug. 1978. OCLC: 5329335 (cit. on p. 99).

[Kus68]   T. Kusui. "Liquid Jet Flow into Still Gas : 3rd Report, The Effect of Nozzle Loss Coefficient and Area Coefficient on the Core Length of the Jet". *Transactions of the Japan Society of Mechanical Engineers* 34(260) (1968), pp. 670–677. DOI: 10.1299/kikai1938.34.670 (cit. on p. 99).

[Kus69]   T. Kusui. "Liquid Jet Flow into Still Gas: Jet Flow by Circular Rough Tube". *Bulletin of JSME* 12(53) (1969), pp. 1062–1071. ISSN: 0021-3764. DOI: 10.1299/jsme1958.12.1062 (cit. on pp. 9, 41, 44, 55, 57, 82, 85, 90, 92, 99, 102, 108–110, 114–116, 123, 143, 214).

[Laf+74]   P. Lafrance, G. Aiello, R. C. Ritter, and J. S. Trefil. "Drop Spectrometry of Laminar and Turbulent Jets". *Physics of Fluids* 17(7) (July 1, 1974), pp. 1469–1470. ISSN: 0031-9171. DOI: 10.1063/1.1694917 (cit. on p. 52).

[Laf77]   P. Lafrance. "The Breakup Length of Turbulent Liquid Jets". *Journal of Fluids Engineering* 99(2) (June 1, 1977), pp. 414–415. ISSN: 0098-2202. DOI: 10.1115/1.3448776. Also see: P. Lafrance. *The Response of Linear Unstable Systems to Stationary Gaussian Excitation*. Memorandum Report 2700. Aberdeen Proving Ground, MD: Ballistic Research Labs, Nov. 1976. 18 pp. URL: https://apps.dtic.mil/docs/citations/ADA032955 (cit. on pp. 24, 25, 104).

[Lan51]   H. L. Langhaar. *Dimensional Analysis and Theory of Models*. New York, NY: Wiley, 1951. 166 pp. ISBN: 978-0-88275-682-0. MR: 39675. (Cit. on p. 223).

[Lau54]   J. Laufer. *The Structure of Turbulence in Fully Developed Pipe Flow*. Technical report 1174. Washington, DC: National Advisory Committee for Aeronautics,

1954. 18 pp. URL: http://ntrs.nasa.gov/search.jsp?R=19930092199. ISSN: 0096-7599 (cit. on pp. 107, 158).

[Law70]   C. J. Lawn. *Application of the Turbulence Energy Equation to Fully Developed Flow in Simple Ducts*. Research report RD/B/R1575 parts A, B and C. Berkeley, Gloucestershire, UK: Central Electricity Generating Board, Feb. 1970. 228 pp. OCLC: 499600590 (Available from the author: c.j.lawn@qmul.ac.uk.) (Cit. on pp. v, 258).

[Law71]   C. J. Lawn. "The Determination of the Rate of Dissipation in Turbulent Pipe Flow". *Journal of Fluid Mechanics* 48(3) (Aug. 1971), pp. 477–505. ISSN: 0022-1120. DOI: 10.1017/S002211207100171X. Also see: [Law70] (cit. on pp. 107, 158).

[LDL96]   S. Leroux, C. Dumouchel, and M. Ledoux. "The Stability Curve of Newtonian Liquid Jets". *Atomization and Sprays* 6(6) (1996), pp. 623–647. ISSN: 1044-5110. DOI: 10.1615/AtomizSpr.v6.i6.10 (cit. on p. 176).

[Leb19]   O. N. Lebedev. *On the Issue of Atomizing Fuel with Diesel Injectors*. Translation. University of Texas at Austin, Mar. 26, 2019. 8 pp. DOI: 10.26153/tsw/878 (cit. on pp. 10, 11, 30–32, 48, 51, 103, 112, 124, 215). Trans. of "K voprosu o raspylivanii topliva dizel'nymi forsunkami [On the issue of atomizing fuel with diesel injectors]". *Izvestiia Sibirskogo otdeleniia Akademii nauk SSSR, Seriia tekhnicheskikh nauk* 3(1) (1977), pp. 40–44. ISSN: 0002-3434.

[Len67]   H. P. Lenz. *Zur Berechnung des Zerfalles von Fluessigkeitsstrahlen niedriger Austrittsgeschwindigkeiten [For calculating the breakup of liquid jets at low exit velocities]*. Fortschritt-Berichte der VDI-Zeitschriften. Reihe 3: Verfahrenstechnik 20. Verlag des Vereins Deutscher Ingenieure, 1967. 18 pp. ISSN: 0506-3108 (cit. on p. 21).

[LF73]   V. B. Lemberskii and M. B. Ferber. "The Dispersivity of a Sprayed Liquid". *Fluid Dynamics* 8(1) (Jan. 1, 1973), pp. 145–148. ISSN: 1573-8507. DOI: 10.1007/BF01017650 (cit. on p. 27).

[LG86]   S. J. Leib and M. E. Goldstein. "The Generation of Capillary Instabilities on a Liquid Jet". *Journal of Fluid Mechanics* 168 (July 1986), pp. 479–500. ISSN: 0022-1120. DOI: 10.1017/S0022112086000472 (cit. on p. 232).

[LHB67]   C. E. Lapple, J. P. Henry, and D. E. Blake. *Atomization — a Survey and Critique of the Literature*. Technical Report 6. Menlo Park, CA: Stanford

Research Institute, Apr. 1967. 268 pp. URL: https://apps.dtic.mil/docs/citations/AD0821314. OCLC: 643256034 (cit. on pp. 103, 230, 247, 248, 261, 270).

[LHL75]   R. C. D. Lissenburg, J. O. Hinze, and H. Leijdens. "An Experimental Investigation of the Effect of a Constriction on Turbulent Pipe Flow". *Applied Scientific Research* 31(5) (Dec. 1, 1975), pp. 343–362. ISSN: 0003-6994, 1573-1987. DOI: 10.1007/BF00418046 (cit. on pp. 51, 79).

[Lig09]   M. Lightfoot. "Fundamental Classification of Atomization Processes". *Atomization and Sprays* 19(11) (2009), pp. 1065–1104. ISSN: 1044-5110. DOI: 10.1615/AtomizSpr.v19.i11.50 (cit. on p. 47).

[Lin+19]   Y. Ling, D. Fuster, G. Tryggvason, and S. Zaleski. "A Two-Phase Mixing Layer between Parallel Gas and Liquid Streams: Multiphase Turbulence Statistics and Influence of Interfacial Instability". *Journal of Fluid Mechanics* 859 (Jan. 2019), pp. 268–307. ISSN: 0022-1120. DOI: 10.1017/jfm.2018.825 (cit. on p. 134).

[Lin03]   S. P. Lin. *Breakup of Liquid Sheets and Jets*. Cambridge University Press, Aug. 21, 2003. 287 pp. ISBN: 978-1-139-43978-7 (cit. on p. 230).

[Lit42]   G. Littaye. *Contribution à l'étude des jets liquides [Contribution to the study of liquid jets]*. Publications scientifiques et techniques du Secrétariat d'etat à l'Aviation 181. Paris, France, 1942. 102 pp. OCLC: 6719427 (cit. on pp. 44, 99, 124, 231).

[Lit44]   G. Littaye. "On a Theory for the Pulverisation of Liquid Jets [Review 45]". *Bulletin, International Institute of Refrigeration* 25(II) (1944), pp. 57–58. OCLC: 243888541 (cit. on p. 45). Trans. of "Sur une théorie de la pulvérisation des jets liquides [On a theory of the pulverization of liquid jets]". *Comptes rendus hebdomadaires des séances de l'Académie des sciences* 217(4) (July 26, 1943), pp. 99–100. ISSN: 0001-4036. URL: http://gallica.bnf.fr/ark:/12148/bpt6k31698/f99.item. Abstract: [DeJ59, p. 207].

[LM17]   A. H. Lefebvre and V. G. McDonell. *Atomization and Sprays*. 2nd ed. Boca Raton, FL: CRC Press, 2017. 300 pp. ISBN: 978-1-4987-3625-1 (cit. on pp. 16, 17, 38–40, 48, 67, 102, 178, 231).

[LN72]   R. I. Loehrke and H. M. Nagib. *Experiments on Management of Free-Stream Turbulence*. Report 598. AGARD, Sept. 1972. 113 pp. URL: https://apps.dtic.mil/docs/citations/AD0749891 (cit. on p. 147).

[Lor04]   G. Lorenzini. "Simplified Modelling of Sprinkler Droplet Dynamics". *Biosystems Engineering* 87(1) (Jan. 2004), pp. 1–11. ISSN: 1537-5110. DOI: 10.1016/j.biosystemseng.2003.08.015. (This paper has a major error which invalidates its model as noted in footnote 8 on page 188.) (Cit. on p. 188).

[Lot08]   E. Loth. "Quasi-Steady Shape and Drag of Deformable Bubbles and Drops". *International Journal of Multiphase Flow* 34(6) (June 2008), pp. 523–546. ISSN: 0301-9322. DOI: 10.1016/j.ijmultiphaseflow.2007.08.010 (cit. on p. 178).

[Lou+97]   P. Loulou, R. D. Moser, N. N. Mansour, and B. J. Cantwell. *Direct Numerical Simulation of Incompressible Pipe Flow Using a B-Spline Spectral Method*. Technical Memorandum 110436. Moffett Field, CA: National Aeronautics and Space Administration, Ames Research Center, Feb. 1997, p. 157. URL: http://ntrs.nasa.gov/search.jsp?R=19970011270 (cit. on p. 79).

[LR98]   S. P. Lin and R. D. Reitz. "Drop and Spray Formation from a Liquid Jet". *Annual Review of Fluid Mechanics* 30(1) (1998), pp. 85–105. ISSN: 0066-4189. DOI: 10.1146/annurev.fluid.30.1.85 (cit. on pp. 20, 27, 28, 38–40, 47, 54, 55, 230).

[LS33]   D. W. Lee and R. C. Spencer. *Photomicrographic Studies of Fuel Sprays*. Technical Report 454. Langley Field, VA: National Advisory Committee for Aeronautics, Langley Aeronautical Lab, 1933. 30 pp. URL: http://ntrs.nasa.gov/search.jsp?R=19930091529. ISSN: 0096-7599. Abstract: [DeJ59, p. 202] (cit. on p. 120).

[LXF13]   S.-h. Liu, J. Xue, and M. Fan. "The Calculation of Mechanical Energy Loss for Incompressible Steady Pipe Flow of Homogeneous Fluid". *Journal of Hydrodynamics* 25(6) (Dec. 1, 2013), pp. 912–918. ISSN: 1878-0342. DOI: 10.1016/S1001-6058(13)60440-0 (cit. on p. 148).

[Lys60]   A. S. Lyshevskiy. *On the Influence of Turbulence Upon the Disintegration of Liquid Jets*. Miscellaneous translation M1366. British Library Lending Division, 1960. 11 pp. OCLC: 499759447. TT: 60-17199 (LC, SLA) (In the Library of Congress Technical Reports & Standards collection under

the TT number.) (Cit. on p. 230). Trans. of A. S. Lyshevskii. "O vliyanii turbulentnosti na raspad zhidkoy strui [The influence of turbulence on the disintegration of a fluid jet]". *Trudy, Novocherkasskii politekhnicheskii institut* 39(53) (1957), pp. 81–86. Abstract: [LHB67, abstract L-55, pp. 183R-184L] (To my knowledge the Russian original is only available from a Russian library like the National Library of Russia.)

[Lys62a] A. S. Lyshevskii. "Dal'nost' poleta gidromonitornykh struy [Range of hydraulic monitor jets]". *Izvestiia vysshikh uchebnykh zavedenii, Energetika* 5(6) (June 1962), pp. 113–118. ISSN: 0579-2983 (cit. on p. 166).

[Lys62b] A. S. Lyshevskii. "O nekotorykh zakonomernostyakh rezaniya gornykh porod struyey zhidkosti sverkhvysokogo davleniya [Some laws governing the cutting of rock with a liquid jet of ultrahigh pressure]". *Ugol' Ukrainy* (9) (Sept. 1962), pp. 28–29. ISSN: 0041-5804 (cit. on p. 230). *Some Laws Governing the Cutting of Rock with a Liquid Jet of Ultra-High Pressure*. SMRE-Trans 5017. 1964.

[Lys63] A. S. Lyshevskii. "K raschetu sopel mekhanicheskikh forsunok [Design of jets for mechanical sprayers]". *Izvestiia vysshikh uchebnykh zavedenii, Khimiia i khimicheskaia tekhnologiia* 6(5) (1963), pp. 865–873. ISSN: 0579-2991. Chemical Abstracts: 60-11628h (cit. on p. 230). A. S. Lyshevskiy. *Design of Jets for Mechanical Sprayer*. USAMIIA-K-9143. Fort Detrick, MD: Army Medical Intelligence and Information Agency, Aug. 16, 1979. 13 pp. DTIC: ADB055179.

[Lys71] A. S. Lyshevskii. *Raspylivanie topliva v sudovykh dizeliakh [Spraying of fuel in marine diesel engines]*. Leningrad, USSR: Sudostroenie, 1971. 248 pp. LCCN: 72321343 (cit. on p. 230).

[MA66] R. R. Mikatarian and R. G. Anderson. "An Experimental Investigation of a Liquid Jet Expelled into a Vacuum." *Journal of Spacecraft and Rockets* 3(2) (1966), pp. 267–268. ISSN: 0022-4650. DOI: 10.2514/3.28432 (cit. on pp. 99, 122).

[Mac77] L. M. Mack. "Transition Prediction and Linear Stability Theory". *Fluid Dynamics Panel Symposium*. Laminar-Turbulent Transition. AGARD Conference Proceedings. Technical University of Denmark, Lyngby, Denmark: AGARD,

1977. ISBN: 978-92-835-0204-3. URL: http://ntrs.nasa.gov/search.jsp?R= 19780006374 (cit. on p. 21).

[Mag+17] G. M. Magnotti, K. E. Matusik, D. J. Duke, B. W. Knox, G. L. Martinez, C. F. Powell, A. L. Kastengren, and C. L. Genzale. "Modeling the Influence of Nozzle-Generated Turbulence on Diesel Sprays". ILASS-Americas 2017. May 2017. URL: http://www.ilass.org/2/database/Detail.aspx?AbstractID=1121. Archived at https://perma.cc/C3GJ-54ZE on Mar. 18, 2019. (Cit. on pp. 11, 33, 104).

[Mag17] G. M. Magnotti. "Modeling the Influence of Nozzle-Generated Turbulence on Diesel Sprays". PhD dissertation. Atlanta, GA: Georgia Institute of Technology, July 19, 2017. 212 pp. URL: https://smartech.gatech.edu/handle/1853/59024 (cit. on pp. 11, 12, 33, 34, 55).

[Man+12] S. Mandato, E. Rondet, G. Delaplace, A. Barkouti, L. Galet, P. Accart, T. Ruiz, and B. Cuq. "Liquids' Atomization with Two Different Nozzles: Modeling of the Effects of Some Processing and Formulation Conditions by Dimensional Analysis". *Powder Technology* 224 (July 1, 2012), pp. 323–330. ISSN: 0032-5910. DOI: 10.1016/j.powtec.2012.03.014 (cit. on p. 230).

[Man94] A. B. Mansour. "The Effects of Non-Newtonian Rheology and Liquid Turbulence on Twin-Fluid Atomization". PhD dissertation. Pittsburgh, PA: Carnegie Mellon University, 1994. 251 pp. URL: https://search.proquest.com/docview/ 304089037 (cit. on pp. 99, 101).

[MB04] W. O. H. Mayer and R. Branam. "Atomization Characteristics on the Surface of a Round Liquid Jet". *Experiments in Fluids* 36(4) (Apr. 1, 2004), pp. 528–539. ISSN: 1432-1114. DOI: 10.1007/s00348-003-0675-0 (cit. on p. 99).

[MC94a] A. Mansour and N. Chigier. "Effect of Turbulence on the Stability of Liquid Jets and the Resulting Droplet Size Distribution". *Atomization and Sprays* 4(5) (1994), pp. 583–604. ISSN: 1044-5110 (cit. on pp. 52, 67, 70, 75, 79, 81).

[MC94b] A. Mansour and N. Chigier. "Turbulence Characteristics in Cylindrical Liquid Jets". *Physics of Fluids* 6(10) (Oct. 1, 1994), pp. 3380–3391. ISSN: 1070-6631. DOI: 10.1063/1.868396 (cit. on pp. 77, 129, 214).

[McC12] R. L. McCoy. *Modern Exterior Ballistics: The Launch and Flight Dynamics of Symmetric Projectiles*. Revised 2nd ed. Atglen, PA: Schiffer Publishing,

2012. 328 pp. ISBN: 978-0-7643-3825-0. Errata for the first edition: http://www.dexadine.com/mccoy.html. Archived at https://perma.cc/BXR6-J43K on Oct. 27, 2018 (cit. on p. 188).

[McC15]   J. McCaslin. "Development And Application Of Numerical Methods For Interfacial Dynamics In Turbulent Liquid-Gas Flows". PhD dissertation. Ithaca, NY: Cornell University, Jan. 26, 2015. 233 pp. URL: http://hdl.handle.net/1813/39359. OCLC: 919488480 (cit. on p. 263).

[MD01]   H. Malot and C. Dumouchel. "Experimental Investigation of the Drop Size Distribution of Sprays Produced by a Low-Velocity Newtonian Cylindrical Liquid Jet". *Atomization and Sprays* 11(3) (2001), pp. 227–254. ISSN: 1044-5110. DOI: 10.1615/AtomizSpr.v11.i3.20 (cit. on pp. 41, 44, 69).

[MD15]   J. O. McCaslin and O. Desjardins. "Direct Numerical Simulation of Surface Tension Effects on Interface Dynamics in Turbulence". *ILASS-Americas 2015*. Rayleigh, NC, May 2015. URL: http://www.ilass.org/2/database/Detail.aspx?AbstractID=1025. Archived at https://perma.cc/A8AG-9L45 on Oct. 26, 2018. (Also see the author's dissertation [McC15] which covers the same topic.) (Cit. on pp. 134, 213).

[ME80]   E. J. McKeogh and E. M. Elsawy. "Air Retained in Pool by Plunging Water Jet". *Journal of the Hydraulics Division* 106(10) (Oct. 1980), pp. 1577–1593. ISSN: 0044-796X (cit. on pp. 9, 83, 86, 149, 168).

[Mer98]   R. N. Meroney. "Spurious or Virtual Correlation Errors Commonly Encountered in Reduction of Scientific Data". *Journal of Wind Engineering and Industrial Aerodynamics* 77-78 (Sept. 1, 1998), pp. 543–553. ISSN: 0167-6105. DOI: 10.1016/S0167-6105(98)00171-8 (cit. on p. 112).

[Mey+53] W. E. Meyer, T. C. Benton, S. I. Plotnick, S. G. Turley, W. D. Brooks, and J. R. Bartoo. *A Basic Study of the Physics of Aerosol Formation*. Quarterly technical report 7. University Park, PA: Pennsylvania State College, Apr. 1953. 78 pp. DTIC: CBRNIAC-CB-112197. PB: 150130. (In the Library of Congress Technical Reports & Standards collection under the PB number.) (Cit. on p. 241).

[MG17]   G. M. Magnotti and C. L. Genzale. "Detailed Assessment of Diesel Spray Atomization Models Using Visible and X-Ray Extinction Measurements". *International Journal of Multiphase Flow* 97 (Dec. 2017), pp. 33–45. ISSN:

0301-9322. DOI: 10.1016/j.ijmultiphaseflow.2017.08.002 (cit. on pp. 20, 104, 105, 118).

[Mie55]   C. C. Miesse. "Correlation of Experimental Data on the Disintegration of Liquid Jets". *Industrial & Engineering Chemistry* 47(9) (Sept. 1, 1955), pp. 1690–1701. ISSN: 0019-7866. DOI: 10.1021/ie50549a013. Abstract: [DeJ59, p. 228] (cit. on pp. 41, 44–46, 104, 116, 171).

[Min52]   E. M. Minskii. *Turbulentnost' ruslovogo potoka [Turbulence of channel flow]*. Leningrad, USSR: Gidrometeoizdat, 1952. 164 pp. (Available at the Library of Congress: https://lccn.loc.gov/54017672.) (Cit. on p. 107).

[ML99]   S. K. Mitra and X. Li. "A Predictive Model for Droplet Size Distribution in Sprays". *Atomization and Sprays* 9(1) (1999). ISSN: 1044-5110. DOI: 10.1615/AtomizSpr.v9.i1.20 (cit. on p. 30).

[MLM16]   N. Moallemi, R. Li, and K. Mehravaran. "Breakup of Capillary Jets with Different Disturbances". *Physics of Fluids* 28(1) (Jan. 1, 2016), p. 012101. ISSN: 1070-6631. DOI: 10.1063/1.4938095 (cit. on p. 21).

[MLS67]   G. McVehil, G. Ludwig, and T. Sundaram. *On the Feasibility of Modeling Small Scale Atmospheric Motions*. CAL Report ZB-2328-P-1. Buffalo, NY: Cornell Aeronautical Laboratory, Apr. 22, 1967. 182 pp. DOI: 10.2172/12518811. OCLC: 10203238, 957122162 (cit. on p. 226).

[MM74]   M. J. McCarthy and N. A. Molloy. "Review of Stability of Liquid Jets and the Influence of Nozzle Design". *The Chemical Engineering Journal* 7(1) (1974), pp. 1–20. ISSN: 0300-9467. DOI: 10.1016/0300-9467(74)80021-3 (cit. on pp. 9, 16, 17, 67, 102, 117, 231–233, 235, 236).

[MO16]   R. D. Moser and T. A. Oliver. "Validation of Physical Models in the Presence of Uncertainty". *Handbook of Uncertainty Quantification*. Ed. by R. Ghanem, D. Higdon, and H. Owhadi. Cham: Springer International Publishing, 2016, pp. 1–28. ISBN: 978-3-319-11259-6. DOI: 10.1007/978-3-319-11259-6_2-1 (cit. on p. 98).

[Mov+11]   E. Movahednejad, F. Ommi, S. M. Hosseinalipour, C. P. Chen, and S. A. Mahdavi. "Application of Maximum Entropy Method for Droplet Size Distribution Prediction Using Instability Analysis of Liquid Sheet". *Heat and Mass Transfer* 47(12) (June 2, 2011), p. 1591. ISSN: 0947-7411, 1432-1181. DOI: 10.1007/s00231-011-0797-5 (cit. on p. 30).

[Mov+17]   A. Movaghar, M. Linne, M. Oevermann, F. Meiselbach, H. Schmidt, and A. R. Kerstein. "Numerical Investigation of Turbulent-Jet Primary Breakup Using One-Dimensional Turbulence". *International Journal of Multiphase Flow* 89 (Mar. 2017), pp. 241–254. ISSN: 0301-9322. DOI: 10.1016/j.ijmultiphaseflow.2016.09.023 (cit. on pp. 11, 33, 121, 125).

[MTT56]   B. R. Morton, G. Taylor, and J. S. Turner. "Turbulent Gravitational Convection from Maintained and Instantaneous Sources". *Proceedings of the Royal Society of London. Series A. Mathematical and Physical Sciences* 234(1196) (Jan. 24, 1956), pp. 1–23. ISSN: 1364-5021, 1471-2946. DOI: 10.1098/rspa.1956.0011 (cit. on p. 178).

[MTZ86]   S. Malloggi, L. Tognotti, and S. Zanelli. "An Experimental Study on the Mechanism of Jet Breakup". *Proceedings of the Two-Day Meeting on Sprays and Their Applications*. Milan, Italy, 1986, pp. 24–29. OCLC: 247131494 (cit. on pp. 99, 123).

[Müh52]   E. Mühlemann. "[Review 868: "Theoretical and Experimental Study of the Dispersion of the Jet in Pelton Turbines" by P. Oguey, M. Mamin, and F. Baatard]". *Applied Mechanics Reviews* 5(3) (Mar. 1952), p. 133. ISSN: 0003-6900 (cit. on p. 267).

[Mul11]   T. Mullin. "Experimental Studies of Transition to Turbulence in a Pipe". *Annual Review of Fluid Mechanics* 43(1) (2011), pp. 1–24. ISSN: 0066-4189. DOI: 10.1146/annurev-fluid-122109-160652 (cit. on pp. 48, 50, 237).

[MY85]   M. T. Murzabaeb and A. L. Yarin. "Dynamics of Sprinkler Jets". *Fluid Dynamics* 20(5) (Sept. 1985), pp. 715–722. ISSN: 1573-8507. DOI: 10.1007/BF01050084 (cit. on p. 167). Trans. of "Dinamika dozhdeval'nykh struy [Dynamics of sprinkler jets]". *Izvestiia Akademii nauk SSSR, Mekhanika zhidkosti i gaza* (5) (September-October, 1985), pp. 60–67. ISSN: 0568-5281.

[MYO05]   B. R. Munson, D. F. Young, and T. H. Okiishi. *Fundamentals of Fluid Mechanics*. 5th ed. Wiley, Mar. 11, 2005. ISBN: 978-0-471-67582-2 (cit. on p. 178).

[Nat18]   V. Y. Natanzon. *On the Atomization of Fuel in Diesel Engines*. Translation. University of Texas at Austin, Sept. 22, 2018. 60 pp. DOI: 10.15781/T2XP6VN8B (cit. on pp. 11, 30, 31, 33–35, 103, 124, 130, 142, 148). Trans. of "O raspylivanii topliva v dvigatelyakh dizelya [On the atomization of fuel in diesel

engines]". *Dizelestroenie* (3) (1938), pp. 3–10. OCLC: 145405221. LCCN: sv91018992.

"O raspylivanii topliva v dvigatelyakh dizelya. Kharakter techniya topliva v otverstii forsunki [On the atomization of fuel in diesel engines. The nature of the flow of fuel in the nozzle orifice]". *Dizelestroenie* (4) (1938), pp. 6–11. OCLC: 145405221. LCCN: sv91018992.

"O raspylivanii topliva v dvigatelyakh dizelya. Stolknovenie kapel' i rost ikh razmera [On the atomization of fuel in diesel engines. The collision of the droplets and the growth of their size]". *Dizelestroenie* (5) (1938), pp. 19–23. OCLC: 145405221. LCCN: sv91018992.

[Nin07]   W. Ning. "Development of a Next-Generation Spray and Atomization Model Using an Eulerian-Lagrangian Methodology". PhD dissertation. Madison, WI: University of Wisconsin-Madison, 2007. 186 pp. URL: https://search.proquest.com/docview/304780393 (cit. on p. 20).

[NN80]   I. K. Nikitin and F. A. Nikitina. "Turbulent Pressure Fluctuations in Pressure Systems with Local Resistances, and a Method for Their Computation". *Fluid mechanics: Soviet research* 9(4) (1980), pp. 86–95. ISSN: 0096-0764 (cit. on pp. 147, 148). Trans. of "Turbulentnyye pul'satsii davleniya v napornykh sistemakh s mestnymi soprotivleniyami i metod ikh rascheta [Turbulent pressure fluctuations in pressure systems with local resistances, and a method for their computation]". *Stratifitsirovannye i turbulentnye techeniia: Sb. nauch. tr. [Stratified and turbulent flows: Collection of scientific proceedings].* Kiev, Ukraine: Naukova Dumka, 1979, pp. 10–18. OCLC: 7671395.

[NS79]   R. Narasimha and K. R. Sreenivasan. "Relaminarization of Fluid Flows". *Advances in Applied Mechanics* 19 (Jan. 1, 1979), pp. 221–309. ISSN: 0065-2156. DOI: 10.1016/S0065-2156(08)70311-9 (cit. on p. 49).

[Obe+15]   M. Oberlack, M. Wacławczyk, A. Rosteck, and V. Avsarkisov. "Symmetries and Their Importance for Statistical Turbulence Theory". *Mechanical Engineering Reviews* 2(2) (2015), pp. 15-00157-15–00157. DOI: 10.1299/mer.15-00157 (cit. on p. 227).

[Obe01]   W. L. Oberkampf. "What Are Validation Experiments?" *Experimental Techniques* 25(3) (May 1, 2001), pp. 35–40. ISSN: 1747-1567. DOI: 10.1111/j.1747-1567.2001.tb00023.x (cit. on pp. 118, 124).

[Oeh58]   T. Oehler. *Characteristics, Operational Conditions and Limits of the Performance of Rotary Rainers / 2. Effects of the Design of Rainer and Nozzle on the Quality and Range of the Water Jet*. Translation 42. Silsoe, Bedfordshire, UK: National Institute of Agricultural Engineering, 1958. 13 pp. OCLC: 220878007 (cit. on pp. 9, 168, 169, 222). Trans. of "Merkmale, Bedingung und Grenzen der Leistungsfähigkeit von Drehstrahlregnern / II. Auswirkungen der Dimensionierung und Formgebung von Regner und Düse auf die Güte und Wurfweite des Wasserstrahls". *Landtechnische Forschung* 7(6) (1957), pp. 162–167. ISSN: 0458-712X.

[Ohn19]   W. von Ohnesorge. *The Formation of Drops by Nozzles and the Breakup of Liquid Jets*. Translation. University of Texas at Austin, Oct. 20, 2019. 5 pp. DOI: 10.26153/tsw/3391 (cit. on pp. 39, 40, 42, 44, 49, 51, 73). Trans. of "Die Bildung von Tropfen an Düsen und die Auflösung flüssiger Strahlen [The formation of drops by nozzles and the breakup of liquid jets]". *Zeitschrift für Angewandte Mathematik und Mechanik* 16(6) (Jan. 1, 1936), pp. 355–358. ISSN: 1521-4001. DOI: 10.1002/zamm.19360160611. Also see: G. H. McKinley and M. Renardy. "Wolfgang von Ohnesorge". *Physics of Fluids* 23(12) (Dec. 1, 2011), p. 127101. ISSN: 1070-6631. DOI: 10.1063/1.3663616. Alternative URL: http://hdl.handle.net/1721.1/79098.

[OMB59]   P. Oguey, M. Mamin, and F. Baatard. *Theoretical and Experimental Study of Jet Dispersion of Pelton Wheels*. Translation 211. Whetstone, UK: English Electric Co. Ltd., 1959. 48 pp. British Library: BLL01018486049 (cit. on pp. iv, 225). Trans. of "Étude théoretique et expérimentale de la dispersion du jet dans la turbine Pelton". *Bulletin technique de la Suisse romande* 77(4) (1951), pp. 37–47. ISSN: 0007-5744. DOI: 10.5169/seals-58145. Abstracts: [Müh52], [Hal+52, pp. 1179–1185], [DeJ67, p. 254].

[OS10]   A. R. Osta and K. A. Sallam. "Nozzle-Geometry Effects on Upwind-Surface Properties of Turbulent Liquid Jets in Gaseous Crossflow". *Journal of Propulsion and Power* 26(5) (Sept. 1, 2010), pp. 936–946. ISSN: 0748-4658. DOI: 10.2514/1.49737 (cit. on p. 103).

[Ost+12]   A. R. Osta, J. Lee, K. A. Sallam, and K. Fezzaa. "Study of the Effects of the Injector Length/Diameter Ratio on the Surface Properties of Turbulent Liquid Jets in Still Air Using X-Ray Imaging". *International Journal of*

Multiphase Flow 38(1) (Jan. 2012), pp. 87–98. ISSN: 0301-9322. DOI: 10.1016/j.ijmultiphaseflow.2011.08.011 (cit. on p. 106).

[Ost10]   A. R. Osta. "Effect of Nozzle Length-to-Diameter Ratio on Atomization of Turbulent Liquid Jets". Stillwater, OK: University of Oklahoma, Dec. 1, 2010. URL: https://shareok.org/handle/11244/7816 (cit. on pp. 99, 101).

[Pal62]   R. S. Palmer. "Water Jet Breakup from Stainless Steel Tubes". *Agricultural engineering* 43 (Aug. 1962), pp. 456–457. ISSN: 0002-1458 (cit. on pp. 99, 123).

[Pan13]   R. L. Panton. *Incompressible Flow*. 4th ed. Hoboken, NJ: Wiley, 2013. 878 pp. ISBN: 978-1-118-01343-4 (cit. on pp. 147, 156).

[Pat68]   R. P. Patel. *Reynolds Stresses in Fully Developed Turbulent Flow down a Circular Pipe*. Mechanical Engineering Research Laboratories Report 68-7. Montreal, Canada: McGill University, Oct. 1968. 64 pp. ISSN: 0076-1966. Alternative OCLC: 837022837 (cit. on pp. 107, 158).

[PCB11]   J. E. Portillo, S. H. Collicott, and G. A. Blaisdell. "Measurements of Axial Instability Waves in the near Exit Region of a High Speed Liquid Jet". *Physics of Fluids* 23(12) (Dec. 1, 2011), p. 124105. ISSN: 1070-6631, 1089-7666. DOI: 10.1063/1.3671733 (cit. on p. 237).

[Pet+15]   J. Petit, S. Méjean, P. Accart, L. Galet, P. Schuck, C. Le Floch-Fouéré, G. Delaplace, and R. Jeantet. "A Dimensional Analysis Approach for Modelling the Size of Droplets Formed by Bi-Fluid Atomisation". *Journal of Food Engineering* 149 (Mar. 1, 2015), pp. 237–247. ISSN: 0260-8774. DOI: 10.1016/j.jfoodeng.2014.10.022 (cit. on p. 230).

[Pet88]   A. Petrillo. "Diffusione di getti d'acqua circolari turbolenti in aria [Diffusion of circular turbulent water jets in air]". *L'Energia elettrica* 65(5) (May 1988), pp. 197–207. ISSN: 0013-7308 (cit. on p. 230).

[Pfe61]   W. Pfenninger. "Transition in the Inlet Length of Tubes at High Reynolds Numbers". *Boundary Layer and Flow Control*. Ed. by G. V. Lachmann. New York, NY: Pergamon, 1961, pp. 970–980. ISBN: 978-1-4832-2666-8. OCLC: 34608520 (cit. on pp. 50, 51).

[PG71]   H. B. Peterson and R. L. Gipe. *Flush-Deck Nozzles (Navy Type S) for Fire Suppresion. Part 1. Discharge Pattern Studies*. Memorandum Report 2322. Washington, DC: Naval Research Laboratory, Aug. 1971. 25 pp. URL:

https://apps.dtic.mil/docs/citations/AD0730023. ISSN: 0502-3378 (cit. on p. 173).

[PH70]   R. E. Phinney and W. Humphries. *Stability of a Viscous Jet — Newtonian Liquids*. NOLTR 70-5. White Oak, MD: Naval Ordnance Lab, Jan. 7, 1970. 64 pp. URL: https://ntrl.ntis.gov/NTRL/dashboard/searchResults/titleDetail/AD707320.xhtml. OCLC: 227592065, 23116695 (cit. on pp. 57, 70, 72, 99, 100, 109, 230, 232).

[Phi72]   R. E. Phinney. "Stability of a Laminar Viscous Jet — the Influence of the Initial Disturbance Level". *AIChE Journal* 18(2) (Mar. 1, 1972), pp. 432–434. ISSN: 1547-5905. DOI: 10.1002/aic.690180229 (cit. on p. 20).

[Phi73]   R. E. Phinney. "The Breakup of a Turbulent Liquid Jet in a Gaseous Atmosphere". *Journal of Fluid Mechanics* 60(4) (Oct. 1973), pp. 689–701. ISSN: 0022-1120. DOI: 10.1017/S0022112073000418 (cit. on pp. 24, 52, 53, 57, 72, 78, 80, 99–101, 123, 176, 177, 230).

[Phi75]   R. E. Phinney. "Breakup of a Turbulent Liquid Jet in a Low-Pressure Atmosphere". *AIChE Journal* 21(5) (Sept. 1, 1975), pp. 996–999. ISSN: 1547-5905. DOI: 10.1002/aic.690210523 (cit. on pp. 52, 67, 78, 80, 85, 99, 100, 114, 115, 143, 230).

[Pic15]   T. Piccolo. *Calculus - Derivation of the Optimal Firing Angle of a Dragless Projectile with an Initial Height*. Oct. 16, 2015. URL: https://math.stackexchange.com/a/1483034/22048 (cit. on p. 186).

[Pop00]   S. B. Pope. *Turbulent Flows*. New York, NY: Cambridge University Press, 2000. 802 pp. ISBN: 978-0-521-59886-6 (cit. on pp. 6, 133–135, 147, 150, 151, 154–157, 159, 179).

[Pow70]   R. E. Powe. "Turbulence Structure in Smooth and Rough Pipes". PhD thesis. Bozeman, MT: Montana State University, 1970. 559 pp. URL: http://scholarworks.montana.edu/xmlui/handle/1/4513. OCLC: 41730748 (cit. on pp. 7, 107, 109, 158).

[Qui06]   W. R. Quinn. "Upstream Nozzle Shaping Effects on near Field Flow in Round Turbulent Free Jets". *European Journal of Mechanics - B/Fluids* 25(3) (May 1, 2006), pp. 279–301. ISSN: 0997-7546. DOI: 10.1016/j.euromechflu.2005.10.002 (cit. on p. 232).

[Ran56]   W. E. Ranz. *On Sprays and Spraying; a Survey of Spray Technology for Research and Development Engineers*. Bulletin 65. University Park, PA: Pennsylvania State University, Department of Engineering Research, 1956. 81 pp. URL: https://catalog.hathitrust.org/Record/100714886. OCLC: 6149967. DTIC: ADB184382. Abstract: [DeJ59, p. 285] (cit. on pp. 44–46, 230).

[Ran58]   W. E. Ranz. "Some Experiments on Orifice Sprays". *The Canadian Journal of Chemical Engineering* 36(4) (Aug. 1, 1958), pp. 175–181. ISSN: 1939-019X. DOI: 10.1002/cjce.5450360405. Abstract: [DeJ59, p. 286], [LHB67, abstract R-11, p. 209L] (cit. on pp. 11, 18, 230).

[Ray78]   J. W. S. Rayleigh. "On The Instability Of Jets". *Proceedings of the London Mathematical Society* 10(1) (Nov. 14, 1878), pp. 4–13. ISSN: 1460-244X. DOI: 10.1112/plms/s1-10.1.4. Abstract: [DeJ59, pp. 289–290] (cit. on pp. 11, 12, 16, 24, 171).

[RB82]   R. D. Reitz and F. V. Bracco. "Mechanism of Atomization of a Liquid Jet". *Physics of Fluids* 25(10) (Oct. 1, 1982), pp. 1730–1742. ISSN: 0031-9171. DOI: 10.1063/1.863650 (cit. on pp. 15, 20, 106, 222).

[RB86]   R. D. Reitz and F. V. Bracco. "Mechanisms of Breakup of Round Liquid Jets". *Encyclopedia of Fluid Mechanics*. Vol. 3. 10 vols. Houston, TX: Gulf Pub. Co., Book Division, 1986, pp. 233–249. ISBN: 978-0-87201-514-2 (cit. on pp. 8, 15, 54).

[RBM65]   J. M. Robertson, T. H. Burkhart, and J. D. Martin. *A Study of Turbulent Flow in Rough Pipes*. T.&A.M. report 279. Urbana, IL: University of Illinois, 1965. 142 pp. URL: https://catalog.hathitrust.org/Record/102273122. OCLC: 11063056 (cit. on pp. 7, 107, 158).

[RC87]   F. Ruiz and N. A. Chigier. *The Effects of Design and Operating Conditions of Fuel Injectors on Flow and Atomization*. Technical Paper 870100. Warrendale, PA: Society of Automotive Engineers, Feb. 1987. DOI: 10.4271/870100. ISSN: 0148-7191 (cit. on pp. 113, 230).

[RC90]   F. Ruiz and N. A. Chigier. "Design and Uncertainty Analysis of a Series of Atomization Experiments in Seven Variables". *Journal of Fluids Engineering* 112(1) (Mar. 1, 1990), pp. 96–106. ISSN: 0098-2202. DOI: 10.1115/1.2909375 (cit. on pp. 113, 230).

[RC91]   F. Ruiz and N. A. Chigier. "Parametric Experiments on Liquid Jet Atomization Spray Angle". *Atomization and Sprays* 1(1) (1991), pp. 23–45. ISSN: 1044-5110. DOI: 10.1615/AtomizSpr.v1.i1.30 (cit. on pp. 113, 230).

[RD64]   W. E. Ranz and W. M. Dreier. "Initial Instability of a Viscous Fluid Interface". *Industrial & Engineering Chemistry Fundamentals* 3(1) (Feb. 1, 1964), pp. 53–60. ISSN: 0196-4313. DOI: 10.1021/i160009a010 (cit. on pp. 11, 18).

[Reb66]   I. Reba. "Applications of the Coanda Effect". *Scientific American* 214 (June 1, 1966), pp. 84–92. ISSN: 0036-8733. DOI: 10.1038/scientificamerican0666-84 (cit. on p. 39).

[Rei78]   R. D. Reitz. "Atomization and Other Breakup Regimes of a Liquid Jet". PhD dissertation. Princeton, NJ: Princeton University, 1978. 336 pp. URL: https://search.proquest.com/docview/302918755. Alternative URL: https://uwmadison.box.com/s/38y5hz57xzzphkux7p4t. OCLC: 989608825 (cit. on pp. 18, 20, 39, 40, 44, 46, 47, 50, 53, 55, 91, 99, 100, 123).

[Rei87]   R. D. Reitz. "Modeling Atomization Processes in High-Pressure Vaporizing Sprays". *Atomisation and Spray Technology* 3(4) (1987), pp. 309–337. ISSN: 0266-3481. URL: https://uwmadison.box.com/AandS (cit. on p. 18).

[RGP18]   I. d. C. Ruiz-Rodriguez, L. Ganippa, and R. Pos. "Evaluation of Different Methodologies Used for Diesel Spray Angle Detection". *ICLASS 2018*. Chicago, IL, July 2018. URL: http://ilasseurope.org/events/iclass-2018/ (cit. on p. 101).

[RH76]   V. Ramjee and A. K. M. F. Hussain. "Influence of the Axisymmetric Contraction Ratio on Free-Stream Turbulence". *Journal of Fluids Engineering* 98(3) (Sept. 1, 1976), pp. 506–515. ISSN: 0098-2202. DOI: 10.1115/1.3448386 (cit. on p. 150).

[RHM52]   H. Rouse, J. W. Howe, and D. E. Metzler. "Experimental Investigation of Fire Monitors and Nozzles". *Transactions of the American Society of Civil Engineers* 117(1) (Jan. 1952), pp. 1147–1175. ISSN: 0066-0604. Paper no. 2529. Discussion: [Hal+52]. Abstracts: [Rob52], [Coo75, abstract 89, p. 28] (cit. on pp. 9, 109, 168, 169, 172, 174).

[Rid09]   W. J. Rider. "A Rogue's Gallery of V&V Practice". MeV Summer School Lunch Talk. July 22, 2009. URL: https://www.osti.gov/biblio/1141709. SAND2009-4667C (cit. on p. 99).

[RN94]   K. Ramamurthi and K. Nandakumar. "Effect of Injector Orifice Configurations on Atomization". *Proceedings of the Sixth International Conference on Liquid Atomization and Spray Systems, July 18-22, 1994, Palais Des Congrès, Rouen, France*. ICLASS 94. New York, NY: Begell House, 1994, pp. 342–349. ISBN: 978-1-56700-019-1 (cit. on p. 99).

[RO19]   C. Rubel and M. Owkes. "Extraction of Droplet Genealogies from High-Fidelity Atomization Simulations". *ILASS-Americas 2019*. Ed. by M. Owkes. Tempe, AZ, May 2019. URL: http://www.ilass.org/2/database/Detail.aspx? AbstractID=1265 (cit. on p. 119).

[Rob52]   J. M. Robertson. "[Review 1766: "Experimental Investigation of Fire Monitors and Nozzles" by H. Rouse, J. W. Howe, and D. E. Metzler]". *Applied Mechanics Reviews* 5(6) (June 1952), pp. 268–269. ISSN: 0003-6900 (cit. on p. 271).

[Rou62]   H. Rouse. "On the Bernoulli Theorem for Turbulent Flow". *Miszellaneen Der Angewandten Mechanik*. Berlin: Akademie-Verlag, 1962, pp. 267–272. LCCN: 67057747. OCLC: 1087321363, 1074265098, 216816386, 875880500 (cit. on p. 148).

[RP68]   R. S. Rosler and H. R. Prieto. "Investigation of the Exactness of Reynolds Similarity". *Chemical Engineering Science* 23(10) (Oct. 1, 1968), pp. 1219–1224. ISSN: 0009-2509. DOI: 10.1016/0009-2509(68)89031-1 (cit. on p. 107).

[RT73]   C. A. Richardson and W. A. Thornton. *Jet Cutting Technology: A Bibliography*. Bedford: BHRA Fluid Engineering, 1973. ISBN: 978-0-900983-22-1 (cit. on p. 275).

[Ruf90]   G. A. Ruff. "Structure and Mixing Properties of the Near-Injector Region of Nonevaporating Pressure-Atomized Sprays". PhD dissertation. Ann Arbor, MI: University of Michigan, 1990. 229 pp. URL: https://search.proquest.com/docview/303861313. OCLC: 68788712 (cit. on pp. 67, 84, 99, 144).

[Rup62]   J. H. Rupe. *On the Dynamic Characteristics of Free-Liquid Jets and a Partial Correlation with Orifice Geometry*. Technical Report 32-207. Pasadena, CA: Jet Propulsion Laboratory, Jan. 15, 1962. 34 pp. URL: https://ntrs.nasa.gov/search.jsp?R=19620000813. DTIC: AD0272819. OCLC: 773206091 (cit. on pp. 57, 60, 61, 71, 99, 122, 231, 237).

[RVC99]   P. Rantanen, A. Valkonen, and A. Cronhjort. "Measurements of a Diesel Spray with a Normal Size Nozzle and a Large-Scale Model". *International Journal*

of Heat and Fluid Flow 20(5) (Oct. 1, 1999), pp. 545–551. ISSN: 0142-727X. DOI: 10.1016/S0142-727X(99)00046-6 (cit. on p. 230).

[RW93]   P. J. Richards and E. K. Weatherhead. "Prediction of Raingun Application Patterns in Windy Conditions". *Journal of Agricultural Engineering Research* 54(4) (Apr. 1993), pp. 281–291. ISSN: 0021-8634. DOI: 10.1006/jaer.1993.1021 (cit. on pp. 166, 167, 169).

[SA10]   S. Som and S. K. Aggarwal. "Effects of Primary Breakup Modeling on Spray and Combustion Characteristics of Compression Ignition Engines". *Combustion and Flame* 157(6) (June 2010), pp. 1179–1193. ISSN: 0010-2180. DOI: 10.1016/j.combustflame.2010.02.018 (cit. on pp. 11, 12, 34).

[SA81]   A. M. Sterling and W. T. Abbott. "Mechanisms of Water Jet Instability". *Proceedings of the First U.S. Water Jet Symposium*. Golden, CO: Colorado School of Mines Press, Apr. 1981, I-4.1 to I–4.6. ISBN: 978-0-918062-48-2 (cit. on pp. 52, 81).

[SAH84]   M. Shimizu, M. Arai, and H. Hiroyasu. "Measurements of Breakup Length in High Speed Jet". *Bulletin of JSME* 27(230) (1984), pp. 1709–1715. DOI: 10.1299/jsme1958.27.1709 (cit. on pp. 67, 85, 90, 92, 114, 115, 143).

[Sal+18]   F. J. Salvador, S. Ruiz, M. Crialesi-Esposito, and I. Blanquer. "Analysis on the Effects of Turbulent Inflow Conditions on Spray Primary Atomization in the Near-Field by Direct Numerical Simulation". *International Journal of Multiphase Flow* 102 (May 1, 2018), pp. 49–63. ISSN: 0301-9322. DOI: 10.1016/j.ijmultiphaseflow.2018.01.019 (cit. on pp. 122, 215).

[Sal02]   K. A. Sallam. "Properties of Spray Formation by Turbulent Primary Breakup". PhD dissertation. Ann Arbor, MI: University of Michigan, 2002. 156 pp. URL: https://search.proquest.com/docview/276490767. OCLC: 715536061 (cit. on pp. 11, 47, 80, 84, 85, 87, 90, 92, 101, 114, 115, 140, 143, 144).

[Sal10]   B. E. Salyers. "Spray Characteristics From Fire Hose Nozzles". MS thesis. College Park, MD: University of Maryland, 2010. 46 pp. URL: http://drum.lib.umd.edu/handle/1903/10486 (cit. on p. 99).

[San55]   V. A. Sandborn. *Experimental Evaluation of Momentum Terms in Turbulent Pipe Flow*. Technical note 3266. Cleveland, OH: National Advisory Committee for Aeronautics, Jan. 1955. URL: http://ntrs.nasa.gov/search.jsp?R=19930084016. ISSN: 0097-2177 (cit. on pp. 107, 108, 158).

[Sau20]   U. K. Sauerwein. *Theoretical Investigation of the Instability of Turbulent Capillary Jets*. Translation. University of Texas at Austin, 2020. 57 pp. DOI: 10.26153/tsw/9412 (cit. on pp. 26, 230). Trans. of "Theoretischer Teil". *Theoretische und experimentelle Untersuchung der Instabilität turbulenter Kapillarstrahlen [Theoretical and experimental investigation of the instability of turbulent capillary jets]*. Darmstadt, Germany: TU Darmstadt, 1992, pp. 16–68. OCLC: 841713740.

[SB81]   J. Scheiman and J. D. Brooks. "Comparison of Experimental and Theoretical Turbulence Reduction from Screens, Honeycomb, and Honeycomb-Screen Combinations". *Journal of Aircraft* 18(8) (1981), pp. 638–643. ISSN: 0021-8669. DOI: 10.2514/3.57538. Also see: J. Scheiman. *Comparison of Experimental and Theoretical Turbulence Reduction Characteristics for Screens, Honeycomb, and Honeycomb-Screen Combinations*. Technical Paper 1958. Hampton, VA: National Aeronautics and Space Administration, Dec. 1981. 55 pp. URL: http://ntrs.nasa.gov/search.jsp?R=19820006182 (cit. on p. 147).

[SB89]   C. E. Synolakis and H. S. Badeer. "On Combining the Bernoulli and Poiseuille Equation — A Plea to Authors of College Physics Texts". *American Journal of Physics* 57(11) (Nov. 1, 1989), pp. 1013–1019. ISSN: 0002-9505. DOI: 10.1119/1.15812 (cit. on p. 146).

[SC96]   U. Shavit and N. Chigier. "Development and Evaluation of a New Turbulence Generator for Atomization Research". *Experiments in Fluids* 20(4) (Feb. 1996), pp. 291–301. ISSN: 0723-4864. DOI: 10.1007/BF00192674 (cit. on p. 109).

[Sch+19]   E. Schillaci, O. Antepara, N. Balcázar, J. R. Serrano, and A. Oliva. "A Numerical Study of Liquid Atomization Regimes by Means of Conservative Level-Set Simulations". *Computers & Fluids* 179 (Jan. 30, 2019), pp. 137–149. ISSN: 0045-7930. DOI: 10.1016/j.compfluid.2018.10.017 (cit. on p. 44).

[Sch07]   P. J. Schmid. "Nonmodal Stability Theory". *Annual Review of Fluid Mechanics* 39(1) (2007), pp. 129–162. DOI: 10.1146/annurev.fluid.38.050304.092139 (cit. on p. 25).

[Sch11]   C. Schmitz. "A Turbulence-Based Model for the Primary Breakup of Pressure Atomized Liquid Jets". MS thesis. Ames, IA: Iowa State University, Jan. 1,

2011. 77 pp. URL: http://lib.dr.iastate.edu/etd/10296 (cit. on pp. 11, 33, 34, 145).

[Sch37]   P. H. Schweitzer. "Mechanism of Disintegration of Liquid Jets". *Journal of Applied Physics* 8(8) (Aug. 1, 1937), pp. 513–521. ISSN: 0021-8979. DOI: 10.1063/1.1710333. Abstracts: [DeJ59, p. 316], [RT73, abstract 1.3, p. 3L] (cit. on pp. 29, 168, 224, 231).

[SDF02]   K. A. Sallam, Z. Dai, and G. M. Faeth. "Liquid Breakup at the Surface of Turbulent Round Liquid Jets in Still Gases". *International Journal of Multiphase Flow* 28(3) (Mar. 2002), pp. 427–449. ISSN: 0301-9322. DOI: 10.1016/S0301-9322(01)00067-2. Zbl: 1136.76629 (cit. on pp. 52, 55, 62, 63, 67, 78, 99, 101, 141, 142, 176).

[Seg65]   I. Seginer. "Tangential Velocity of Sprinkler Drops". *Transactions of the ASAE* 8(1) (1965), pp. 90–93. ISSN: 0001-2351. DOI: 10.13031/2013.40437 (cit. on p. 166).

[Sel85]   R. W. Sellens. "A Prediction of the Droplet Size and Velocity Distribution in a Spray from First Principles". MS thesis. Waterloo, Canada: University of Waterloo, 1985. 147 pp. URL: http://hdl.handle.net/10012/10836. OCLC: 258553527 (cit. on p. 30).

[Sel87]   R. W. Sellens. "Drop Size and Velocity Distributions in Sprays: A New Approach Based on the Maximum Entropy Formalism". PhD thesis. Waterloo, Canada: University of Waterloo, 1987. URL: http://hdl.handle.net/10012/10842. OCLC: 632839637 (cit. on p. 30).

[Sha72]   S. S. Shavlovsky. "Hydrodynamics of High Pressure Fine Continuous Jets". *First International Symposium on Jet Cutting Technology*. Ed. by T. E. Brock and C. A. Richardson. University of Warwick, Coventry, UK: British Hydromechanics Research Association, 1972, A6.81–A6.92. ISBN: 978-0-900983-20-7 (cit. on pp. 117, 224).

[Sit63]   G. Sitkei. *Contribution to the Theory of Jet Atomization*. Technical translation F-129. Washington, DC: National Aeronautics and Space Administration, Oct. 1963. 32 pp. URL: https://hdl.handle.net/2027/uiug.30112106740126. ISSN: 0499-9355. NASA: N63-22948. TT: 63-11730 (OTS). Alternative URL: https://ntrs.nasa.gov/search.jsp?R=19630013068 (The w' term in equation 3 likely should be u'.) (Cit. on pp. 11, 30, 31). Trans. of "Beitrag

zur Theorie der Strahlzerstäubung [To the theory of jet atomization]". *Acta technica, Academiae Scientiarum Hungaricae* 25(1-2) (1959), pp. 87–117. ISSN: 0001-7035. Abstract: [DeJ64, p. 342].

[SJA06]   E. Shirani, A. Jafari, and N. Ashgriz. "Turbulence Models for Flows with Free Surfaces and Interfaces". *AIAA Journal* 44(7) (2006), pp. 1454–1462. ISSN: 0001-1452. DOI: 10.2514/1.16647 (cit. on p. 104).

[Skr66]   G. P. Skrebkov. "Turbulent Pulsations in a Liquid Jet, and Its Atomization". *Journal of Applied Mechanics and Technical Physics (Foreign Technology Division)* (3) (Feb. 16, 1966), pp. 142–151. URL: https://apps.dtic.mil/ docs/citations/AD0635269 (cit. on pp. iv, 9, 11, 34, 35, 84, 99, 103, 107, 108, 121, 142, 144). Trans. of "Turbulentnyye pul'satsii v zhidkoy struye i yeye raspylivaniye [Turbulent pulsations in a liquid jet and its atomization]". *Prikladnaya mekhanika i tekhnicheskaya fizika* (3) (May 1963), pp. 79–83. ISSN: 0869-5032. URL: http://www.sibran.ru/journals/issue.php?ID= 160175&ARTICLE_ID=160248. Archived at https://perma.cc/2DQJ-N68G on Oct. 26, 2018.

[SM00a]   W. A. Sirignano and C. Mehring. "Review of Theory of Distortion and Disintegration of Liquid Streams". *Progress in Energy and Combustion Science* 26(4-6) (Aug. 2000), pp. 609–655. ISSN: 0360-1285. DOI: 10.1016/S0360-1285(00)00014-9 (cit. on p. 230).

[SM00b]   W. A. Sirignano and C. A. Mehring. "Comments on Energy Conservation in Liquid-Stream Disintegration". *ICLASS 2000*. Pasadena, CA, July 2000, pp. 1249–1256. URL: http://ilasseurope.org/events/8th-iclass/. OCLC: 55714733, 248376666, 59540956 (cit. on p. 225).

[Smi+08]   R. J. Smith, M. H. Gillies, G. Newell, and J. P. Foley. "A Decision Support Model for Travelling Gun Irrigation Machines". *Biosystems Engineering* 100(1) (May 2008), pp. 126–136. ISSN: 1537-5110. DOI: 10.1016/j.biosystemseng.2008.01.004 (cit. on p. 167).

[Smi65]   V. I. Smirnov. "The effect of the geometric characteristic l/d of the nozzle on the solid portion of the jet". *Technology of the textile industry, U.S.S.R.* (1) (1965), pp. 121–124. ISSN: 0040-1684 (cit. on p. 230). Trans. of "O vliyanii geometricheskoy kharakteristiki l/d sopla na dlinu sploshiogo uchastka strui [The effect of the geometric characteristic l/d of the nozzle on the solid

portion of the jet]". *Izvestiia vysshikh uchebnykh zavedenii. Tekhnologiia tekstil'noi promyshlennosti* (1) (1965), pp. 123–126. ISSN: 0021-3497.

[Smi71]   V. I. Smirnov. "The Confidence Volume of the Samples for Determining the Droplet Size of an Atomized Liquid". *Technology of the textile industry, U.S.S.R.* (1) (1971), pp. 113–116. ISSN: 0040-1684 (cit. on p. 101).

[SNvB91]   I. Seginer, D. Nir, and R. D. von Bernuth. "Simulation of Wind-Distorted Sprinkler Patterns". *Journal of Irrigation and Drainage Engineering* 117(2) (1991), pp. 285–306. ISSN: 0733-9437. DOI: 10.1061/(ASCE)0733-9437(1991)117:2(285) (cit. on p. 168).

[Sny72]   W. H. Snyder. "Similarity Criteria for the Application of Fluid Models to the Study of Air Pollution Meteorology". *Boundary-Layer Meteorology* 3(1) (Sept. 1, 1972), pp. 113–134. ISSN: 1573-1472. DOI: 10.1007/BF00769111 (cit. on p. 226).

[SS75]   A. M. Sterling and C. A. Sleicher. "The Instability of Capillary Jets". *Journal of Fluid Mechanics* 68(3) (Apr. 1975), pp. 477–495. ISSN: 0022-1120. DOI: 10.1017/S0022112075001772 (cit. on pp. 41, 44, 49, 59, 67, 69, 70, 99).

[SSS99]   S. D. Sovani, P. E. Sojka, and Y. R. Sivathanu. "Prediction of Drop Size Distributions from First Principles: The Influence of Fluctuations in Relative Velocity and Liquid Physical Properties". *Atomization and Sprays* 9(2) (1999), pp. 133–152. ISSN: 1044-5110. DOI: 10.1615/AtomizSpr.v9.i2.20 (cit. on pp. 24, 25).

[Sta+05]   M. Stahl, M. Gnirß, N. Damaschke, and C. Tropea. "Laser Doppler Measurements of Nozzle Flow and Optical Characterisation of the Generated Spray". *ILASS-Europe 2005*. Ed. by C. Chauveau and J. Pagé. Orléans, France, 2005. URL: http://ilasseurope.org/events/20th-ilass-europe/. OCLC: 500578955, 255275024. Archived at https://perma.cc/SA5Q-WD5N on Nov. 15, 2018 (cit. on p. 5).

[SV86]   R. W. Schottman and S. B. Vandergrift. "Sprinkler Jet Breakup as a Function of Pressure". *1986 Summer Meeting of the American Society of Agricultural Engineers*. San Luis Obispo, CA, 1986. Paper no. 86-2102. OCLC: 15097193 (cit. on p. 168).

[SW08]   W. Sander and B. Weigand. "Direct Numerical Simulation and Analysis of Instability Enhancing Parameters in Liquid Sheets at Moderate Reynolds

Numbers". *Physics of Fluids* 20(5) (May 1, 2008), pp. 053301.1–053301.18. ISSN: 1070-6631. DOI: 10.1063/1.2909661 (cit. on pp. 215, 230, 237).

[Tat64]   T. Tate. "On the Magnitude of a Drop of Liquid Formed under Different Circumstances". *The London, Edinburgh, and Dublin Philosophical Magazine and Journal of Science* 27(181) (Mar. 1, 1864), pp. 176–180. ISSN: 1941-5982. DOI: 10.1080/14786446408643645 (cit. on p. 67).

[Tay58]   G. I. Taylor. "Generation of Ripples by Wind Blowing over a Viscous Fluid". *Aerodynamics and the Mechanics of Projectiles and Explosions*. Ed. by G. K. Batchelor. Vol. 3. The Scientific Papers of Sir Geoffrey Ingram Taylor. Cambridge University Press, 1958, pp. 244–254. ISBN: 978-0-521-15904-3 (cit. on pp. 11, 18, 19). Repr. of *Generation of Ripples by Wind Blowing over a Viscous Fluid*. ARC Research Item 19. Chemical Defence Research Department, Ministry of Supply, 1940.

[TE15]   B. Trettel and O. A. Ezekoye. "Theoretical Range and Trajectory of a Water Jet". *Proceedings of ASME 2015 International Mechanical Engineering Congress and Exposition*. Vol. 7A. Houston, TX, Nov. 2015. ISBN: 978-0-7918-5746-5. DOI: 10.1115/IMECE2015-52103. (Chapter 7 is a complete rewrite of this paper.) (Cit. on pp. 163, 174, 184).

[The81]   C. Theobald. "The Effect of Nozzle Design on the Stability and Performance of Turbulent Water Jets". *Fire Safety Journal* 4(1) (Aug. 1981), pp. 1–13. ISSN: 0379-7112. DOI: 10.1016/0379-7112(81)90002-3 (cit. on pp. 4, 166, 168, 169, 172, 197–200, 232, 236).

[Tho71]   S. W. Thomson. "Hydrokinetic Solutions and Observations". *Philosophical Magazine Series 4* 42(281) (Nov. 1, 1871), pp. 362–377. ISSN: 1941-5982. DOI: 10.1080/14786447108640585 (cit. on p. 14).

[Thr09]   P. N. Threlfall-Holmes. "Spray Dryer Modelling". PhD thesis. Heriot-Watt University, Oct. 2009. URL: https://www.ros.hw.ac.uk/handle/10399/2292 (cit. on p. 42).

[TM03]   L. Tang and S. M. Masutani. "Laminar to Turbulent Flow Liquid-Liquid Jet Instability and Breakup". The Thirteenth International Offshore and Polar Engineering Conference. International Society of Offshore and Polar Engineers, Jan. 1, 2003, pp. 317–324. ISBN: 978-1-880653-60-9. URL: https://www.onepetro.org/conference-paper/ISOPE-I-03-128 (cit. on p. 44).

[Ton+90]   Y. L. Tonkonogiy, V. N. Buz, A. A. Garbuz, and A. I. Kalinchak. "Effect of Roughness on the Transition Reynolds Number". *Fluid mechanics: Soviet research* 19(4) (1990), pp. 13–19. ISSN: 0096-0764 (cit. on pp. 48, 51).

[Tor+20]   A. J. Torregrosa, R. Payri, F. Javier Salvador, and M. Crialesi-Esposito. "Study of Turbulence in Atomizing Liquid Jets". *International Journal of Multiphase Flow* (May 1, 2020), p. 103328. ISSN: 0301-9322. DOI: 10.1016/j.ijmultiphaseflow.2020.103328 (cit. on p. 215).

[Tor73]   T. P. Torda. "Evaporation of Drops and Breakup of Sprays". *Astronautica Acta* 18 (1973), pp. 383–393. ISSN: 0004-6205 (cit. on p. 44).

[TP03]   H. V. Tafreshi and B. Pourdeyhimi. "The Effects of Nozzle Geometry on Water-jet Breakup at High Reynolds Numbers". *Experiments in Fluids* 35(4) (Oct. 1, 2003), pp. 364–371. ISSN: 0723-4864, 1432-1114. DOI: 10.1007/s00348-003-0685-y (cit. on p. 50).

[Tre18]   B. Trettel. "Estimating Turbulent Kinetic Energy and Dissipation from Internal Flow Loss Coefficients". *ICLASS 2018*. Ed. by M. Herrmann and O. Desjardins. Paper no. 328. Chicago, IL, July 2018. DOI: 10.31224/osf.io/qsfp7 (cit. on p. 146).

[Tre19a]   B. Trettel. "Improving the Validation of Turbulent Jet Breakup Models". *ILASS-Americas 2019*. Ed. by M. Owkes. Paper no. 18. Tempe, AZ, May 2019. DOI: 10.31224/osf.io/k2fnm (cit. on p. 98).

[Tre19b]   B. Trettel. "Turbulent Theory of Velocity-Profile-Induced Jet Breakup". *ILASS-Americas 2019*. Ed. by M. Owkes. Paper no. 19. Tempe, AZ, May 2019. DOI: 10.31224/osf.io/486jh (cit. on p. 231).

[Tre20a]   B. Trettel. "Conditional Damped Random Surface Velocity Theory of Turbulent Jet Breakup". *Atomization and Sprays* 31 (2020). (Accepted.) ISSN: 1044-5110. DOI: 10.1615/AtomizSpr.2020033172. Preprint DOI: 10.31224/osf.io/35u7g (cit. on pp. 5, 121, 128).

[Tre20b]   B. Trettel. "pipe-jet-breakup-data". 2020. URL: https://github.com/btrettel/pipe-jet-breakup-data (cit. on pp. 57, 217).

[Tre20c]   B. Trettel. "Reevaluating the Jet Breakup Regime Diagram". *Atomization and Sprays* 31 (2020). (Accepted.) ISSN: 1044-5110. DOI: 10.1615/AtomizSpr.2020033171. Preprint DOI: 10.31224/osf.io/nqhs5 (Note that regime diagram has been improved since the preprint.) (Cit. on p. 37).

[TRF92]   L.-K. Tseng, G. A. Ruff, and G. M. Faeth. "Effects of Gas Density on the Structure of Liquid Jets in Still Gases". *AIAA Journal* 30(6) (1992), pp. 1537–1544. ISSN: 0001-1452. DOI: 10.2514/3.11098 (cit. on pp. 99, 100).

[Tru+18]   M. F. Trujillo, S. Gurjar, M. Mason, and A. Agarwal. "Global Characterization of the Spray Formation Process". *Atomization and Sprays* 28(9) (2018), pp. 811–835. ISSN: 1044-5110. DOI: 10.1615/AtomizSpr.2018027169 (cit. on p. 73).

[Tsy19a]   N. F. Tsyapko. *On the Causes of Expansion of a Hydromonitor Water Jet*. Translation. University of Texas at Austin, Apr. 4, 2019. 4 pp. DOI: 10.26153/tsw/1271 (cit. on pp. 35, 124, 144, 148). Trans. of "O prichinakh rasshireniya gidromonitornoy strui vody [On the causes of expansion of a hydromonitor water jet]". *Voprosy gidravlicheskoy dobychi uglya: Trudy VNIIGidrouglya* 13 (1968), pp. 18–19.

[Tsy19b]   N. F. Tsyapko. *Some Questions on the Theory of Hydromonitor Water Jets*. Translation. University of Texas at Austin, Apr. 4, 2019. 10 pp. DOI: 10.26153/tsw/1270 (cit. on pp. 35, 124). Trans. of "Nekotoryye voprosy teorii gidromonitornoy strui vody [Some questions of the theory of hydromonitor water jets]". *Voprosy gidravlicheskoy dobychi uglya: Trudy VNIIGidrouglya* 13 (1968), pp. 12–18.

[TT78]   P. F. Thorne and C. R. Theobald. "The Effect of Nozzle Geometry on the Turbulent Structure of Water Jets — a Photographic Study". *Papers Presented at the Fourth International Symposium on Jet Cutting Technology*. Ed. by H. S. Stephens, J. Clarke, and C. A. Stapleton. Vol. 1. University of Kent at Canterbury, England: BHRA Fluid Engineering, 1978, A4-55 to A4–64. ISBN: 978-0-900983-79-5 (cit. on p. 168).

[Ume14]   A. Umemura. "Model for the Initiation of Atomization in a High-Speed Laminar Liquid Jet". *Journal of Fluid Mechanics* 757 (Oct. 2014), pp. 665–700. ISSN: 0022-1120. DOI: 10.1017/jfm.2014.511 (cit. on p. 237).

[vBer88]   R. D. von Bernuth. "Effect of Trajectory Angle on Performance of Sprinklers in Wind". *Journal of Irrigation and Drainage Engineering* 114(4) (1988), pp. 579–587. ISSN: 0733-9437. DOI: 10.1061/(ASCE)0733-9437(1988)114:4(579) (cit. on p. 173).

[vBG84]   R. D. von Bernuth and J. R. Gilley. "Sprinkler Droplet Size Distribution Estimation from Single Leg Data". *Transactions of the American Society of Agricultural Engineers* 27(5) (1984), pp. 1435–1441. ISSN: 0001-2351. DOI: 10.13031/2013.32984 (cit. on p. 168).

[vdSan74] E. van de Sande. "Air Entrainment by Plunging Water Jets". PhD thesis. Delft, Netherlands: TU Delft, 1974. 123 pp. URL: http://resolver.tudelft.nl/uuid: 312a587e-29f7-4d1d-a1f2-68c786f800c7 (cit. on p. 99).

[vdSS76]   E. van de Sande and J. M. Smith. "Jet Break-up and Air Entrainment by Low Velocity Turbulent Water Jets". *Chemical Engineering Science* 31(3) (Jan. 1, 1976), pp. 219–224. ISSN: 0009-2509. DOI: 10.1016/0009-2509(76)85060-9 (cit. on pp. 48, 49, 51, 52).

[Vel46]   M. A. Velikanov. "Kinematicheskaya struktura turbulentnogo ruslovogo potoka [Kinematic structure of turbulent channel flow]". *Izvestiia Akademii nauk SSSR. Seriia geograficheskaia i geofizicheskaia* 10(4) (1946), pp. 331–340. OCLC: 26627963] (cit. on p. 107).

[Vli75]   H. Vliem. "The Influence of Restrictions on the Breakup Pattern of Turbulent Water Jets; a Simple Model of the External Urinary Stream of the Human Male". MS thesis. Delft, Netherlands: Technische Hogeschool Delft, May 1975. 76 pp. URL: https://archive.org/details/vliem_influence_1975 (cit. on pp. v, 79, 81, 215).

[VS73]   E. Van de Sande and J. M. Smith. "Surface Entrainment of Air by High Velocity Water Jets". *Chemical Engineering Science* 28(5) (May 1, 1973), pp. 1161–1168. ISSN: 0009-2509. DOI: 10.1016/0009-2509(73)85025-0 (cit. on p. 122).

[Wal80]   P. Walzel. "Turbulenter Zerfall von Flüssigkeitsstrahlen aus der Sicht der Ähnlichkeitstheorie [Turbulent breakup of liquid jets from the perspective of similarity theory]". *Chemie Ingenieur Technik* 52(6) (Jan. 1, 1980), pp. 525–526. ISSN: 1522-2640. DOI: 10.1002/cite.330520609 (cit. on p. 230).

[Wal82]   P. Walzel. "Advantages and Limits in Large Scale Modeling of Atomizers". *Proceedings of the 2nd International Conference on Liquid Atomization and Spray Systems*. Madison, WI, June 1982, pp. 187–194. OCLC: 10261204 (cit. on p. 230).

[Wan68]   D. P. Wang. "Finite Amplitude Effect on the Stability of a Jet of Circular Cross-Section". *Journal of Fluid Mechanics* 34(2) (Nov. 1968), pp. 299–313. ISSN: 0022-1120. DOI: 10.1017/S0022112068001904 (cit. on p. 23).

[Web19]   C. Weber. *Breakup of a Liquid Jet*. Translation. University of Texas at Austin, Oct. 20, 2019. 38 pp. DOI: 10.26153/tsw/3371 (cit. on pp. 11, 17, 21, 23, 26, 34, 68, 69, 74, 76, 81, 213). Trans. of "Zum Zerfall eines Flüssigkeitsstrahles [On the disintegration of a liquid jet]". *Zeitschrift für Angewandte Mathematik und Mechanik* 11(2) (Jan. 1, 1931), pp. 136–154. ISSN: 0044-2267. DOI: 10.1002/zamm.19310110207. Abstract: [DeJ59, p. 366].

[WF93]   P.-K. Wu and G. M. Faeth. "Aerodynamic Effects on Primary Breakup of Turbulent Liquids". *Atomization and Sprays* 3(3) (1993), pp. 265–289. ISSN: 1044-5110. DOI: 10.1615/AtomizSpr.v3.i3.20 (cit. on pp. 55, 87, 88, 93, 99, 101, 119, 137, 138, 140).

[WF95]   P.-K. Wu and G. M. Faeth. "Onset and End of Drop Formation along the Surface of Turbulent Liquid Jets in Still Gases". *Physics of Fluids* 7(11) (Nov. 1, 1995), pp. 2915–2917. ISSN: 1089-7666. DOI: 10.1063/1.868667 (cit. on pp. 9, 11, 34, 35, 87, 99, 101, 117, 121, 135, 140).

[WIV95]   D. H. Wolf, F. P. Incropera, and R. Viskanta. "Measurement of the Turbulent Flow Field in a Free-Surface Jet of Water". *Experiments in Fluids* 18(6) (Apr. 1, 1995), pp. 397–408. ISSN: 0723-4864. DOI: 10.1007/BF00208462 (cit. on pp. 129, 214).

[WMF95]   P.-K. Wu, R. F. Miranda, and G. M. Faeth. "Effects of Initial Flow Conditions on Primary Breakup of Nonturbulent and Turbulent Round Liquid Jets". *Atomization and Sprays* 5(2) (1995), pp. 175–196. ISSN: 1044-5110. DOI: 10.1615/AtomizSpr.v5.i2.40 (cit. on pp. 44, 49, 51, 87, 88, 119, 137, 138, 140, 231, 236).

[WTF92]   P.-K. Wu, L.-K. Tseng, and G. M. Faeth. "Primary Breakup in Gas/Liquid Mixing Layers for Turbulent Liquids". *Atomization and Sprays* 2(3) (1992), pp. 295–317. ISSN: 1044-5110. DOI: 10.1615/AtomizSpr.v2.i3.60 (cit. on pp. 11, 28, 30–35, 67, 99, 101, 119, 129, 130, 134–137).

[Wu+83]   K.-J. Wu, C.-C. Su, R. L. Steinberger, D. A. Santavicca, and F. V. Bracco. "Measurements of the Spray Angle of Atomizing Jets". *Journal of Fluids*

Engineering 105(4) (Dec. 1, 1983), pp. 406–413. ISSN: 0098-2202. DOI: 10.1115/1.3241019 (cit. on pp. 67, 99, 100).

[Wu83]   K.-J. Wu. "Atomizing Round Jets". PhD dissertation. Princeton, NJ: Princeton University, 1983. 301 pp. OCLC: 82865393 (cit. on p. 133).

[Wu92]   P.-K. Wu. "Liquid Surface Breakup of Nonturbulent and Turbulent Liquids". PhD dissertation. Ann Arbor, MI: University of Michigan, 1992. 157 pp. URL: https://search.proquest.com/docview/304013956. OCLC: 753326265 (cit. on pp. 87–89, 101, 104, 137, 138, 140).

[WWB10]   R. D. H. Warburton, J. Wang, and J. Burgdörfer. "Analytic Approximations of Projectile Motion with Quadratic Air Resistance". *Journal of Service Science and Management* 3(1) (2010), pp. 98–105. DOI: 10.4236/jssm.2010.31012 (cit. on p. 202).

[WWW51]   L. G. Whitehead, L. Y. Wu, and M. H. L. Waters. "Contracting Ducts of Finite Length". *The Aeronautical Quarterly* 2(4) (Feb. 1951), pp. 254–271. ISSN: 0001-9259. DOI: 10.1017/S0001925900000469 (cit. on p. 236).

[Yan74]   K. Yanaida. "Flow Characteristics of Water Jets". *Proceedings of the Second International Symposium on Jet Cutting Technology*. Ed. by N. G. Coles and S. J. Barratt. Cambridge, UK: BHRA Fluid Engineering, Apr. 1974, A2.19–A2.32. ISBN: 978-0-900983-37-5 (cit. on pp. 99, 230).

[Yan92]   H. Q. Yang. "Asymmetric Instability of a Liquid Jet". *Physics of Fluids A: Fluid Dynamics* 4(4) (Apr. 1, 1992), pp. 681–689. ISSN: 0899-8213. DOI: 10.1063/1.858287 (cit. on p. 27).

[YBS10]   V. Yakhot, S. C. C. Bailey, and A. J. Smits. "Scaling of Global Properties of Turbulence and Skin Friction in Pipe and Channel Flows". *Journal of Fluid Mechanics* 652 (June 2010), pp. 65–73. ISSN: 0022-1120. DOI: 10.1017/S0022112010001497 (cit. on p. 107).

[YO78]   K. Yanaida and A. Ohashi. "Flow Characteristics of Water Jets in Air". *Papers Presented at the Fourth International Symposium on Jet Cutting Technology*. Ed. by H. S. Stephens, J. Clarke, and C. A. Stapleton. Vol. 1. University of Kent at Canterbury, England: BHRA Fluid Engineering, 1978, A3.39–A3.53. ISBN: 978-0-900983-79-5 (cit. on pp. 101, 176, 177).

[YR04]   Y. Yi and R. D. Reitz. "Modeling the Primary Breakup of High-Speed Jets". *Atomization and Sprays* 14(1) (2004), pp. 53–80. ISSN: 1044-5110. DOI: 10.1615/AtomizSpr.v14.i1.40 (cit. on p. 27).

[ZRM12]   Y. Zheng, N. Ryder, and A. W. Marshall. "Model Development for Predicting Fire Hose Stream Characteristics". *2012 Suppression, Detection and Signaling Research and Applications Symposium (SUPDET 2012)*. Phoenix, Arizona, Mar. 2012. URL: https://www.nfpa.org/-/media/Files/News-and-Research/Archived-proceedings/2012-SUPDET/29Zheng-et-al-extended-abstract.ashx?la=en. Archived at https://perma.cc/CB9W-PZ4R on Nov. 26, 2018. Slides at: https://www.nfpa.org/-/media/Files/News-and-Research/Archived-proceedings/2012-SUPDET/29Zheng-et-al-presentation.ashx?la=en. Slides archived at https://perma.cc/Q28M-S5DY on Nov. 26, 2018 (cit. on p. 168).